

**Programs Towards Tetrahydropyran Containing Small Macrolides of Cyanobacterial Origins: Synthetic Methodology Development and Total Synthesis**

**Rendy Kartika**

**Publication Date**

12-09-2008

**License**

This work is made available under a All Rights Reserved license and should only be used in accordance with that license.

**Citation for this work (American Psychological Association 7th edition)**

Kartika, R. (2008). *Programs Towards Tetrahydropyran Containing Small Macrolides of Cyanobacterial Origins: Synthetic Methodology Development and Total Synthesis* (Version 1). University of Notre Dame. <https://doi.org/10.7274/08612n51m2b>

This work was downloaded from CurateND, the University of Notre Dame's institutional repository.

For more information about this work, to report or an issue, or to preserve and share your original work, please contact the CurateND team for assistance at [curate@nd.edu](mailto:curate@nd.edu).

PROGRAMS TOWARDS TETRAHYDROPYRAN CONTAINING  
SMALL MACROLIDES OF CYANOBACTERIAL ORIGINS:  
SYNTHETIC METHODOLOGY DEVELOPMENT AND TOTAL SYNTHESIS

VOLUME ONE

A Dissertation

Submitted to the Graduate School of  
the University of Notre Dame  
in Partial Fulfillment of the Requirements  
for the Degree of

Doctor of Philosophy

by

Rendy Kartika

---

Richard E. Taylor, Director

Graduate Program in Chemistry and Biochemistry

Notre Dame, Indiana

September 2008

PROGRAMS TOWARDS TETRAHYDROPYRAN CONTAINING  
SMALL MACROLIDES OF CYANOBACTERIAL ORIGINS:  
SYNTHETIC METHODOLOGY DEVELOPMENT AND TOTAL SYNTHESIS

Abstract

by

Rendy Kartika

This dissertation comprises two major components that sequentially describe literature reviews pertinent to tetrahydropyran-containing small macrolides of cyanobacterial origins and research in the field of synthetic organic chemistry that demonstrates synthetic methodology development directed for stereoselective production of highly functionalized oxacycles and their applications in complex molecule synthesis.

The research discussion commences with a systematic study towards the total synthesis of (+)-acutiphycin, a highly cytotoxic macrolide with an unknown mode of action. Our convergent route was highlighted by an extensive utilization of the vinylogous Mukaiyama aldol reactions for the construction of both southern and northern

hemispheres of the macrolide. The acutiphycin study concluded with a thorough investigation of aldol-mediated advanced fragments coupling strategy.

Our research continues with the development of electrophile-induced ether transfer reaction. This novel synthetic method readily generated 1,3-*syn* diol monoether, a common functionality in polyketide that presents a significant synthetic challenge. This transformation was accomplished by simply exposing homoallylic alkoxymethyl ether to iodine monochloride. The reaction mechanism was proposed via an intermediacy of chloromethyl ether as observed by *in situ* NMR experiments.

The ability to quench the chloromethyl ether intermediate with various nucleophiles, such as cyanide or thiophenol, showcased the versatility of the ether transfer reaction. This strategy readily yielded precursors for the production of six-membered oxygen heterocycles via a general three-step sequence: ether transfer, cyclization, and functionalization reactions. Depending upon the functionalization step, a robust production of stereocomplementary 4-alkoxy-2,6-*cis*- and *trans*-disubstituted tetrahydropyrans and *trans*-2,6-disubstituted-3,4-dihydropyrans was successfully achieved in a stereoselective fashion. These methods were then successfully applied to an efficient construction of the oxacycle core of phorboxazole A and swinholide A.

Our final research project describes a concise enantioselective total synthesis of neopeltolide macrolactone. The successful synthetic approach was highlighted by sequential utilization of the ether transfer methodology, functionalization, and radical cyclization to directly install the requisite stereochemistry embedded within neopeltolide's tetrahydropyran ring. Our synthesis only required 14 steps in the longest linear sequence, 15 steps overall. More importantly, it was free of discreet installation

steps for protecting groups, thus representing a rare example in complex polyketide synthesis.

*This dissertation is dedicated in loving memory of my grandparents:*

*“Kung Kung” Lukiman Lianto and “Bo Bo” Erna Rahayu*

*for their unconditional love and teaching me that education is the key to a bright future.*

## TABLE OF CONTENTS

### VOLUME ONE

LIST OF FIGURES .....	xv
LIST OF SCHEMES .....	xviii
LIST OF TABLES .....	xxviii
LIST OF ABBREVIATIONS .....	xxix
ACKNOWLEDGMENTS .....	xxxvii

CHAPTER ONE	TETRAHYDROPYRAN CONTAINING SMALL MACROLIDES OF CYANOBACTERIAL ORIGIN .....	1
1.1.	Purpose .....	1
1.2.	Cyanobacteria .....	1
1.2.1.	Cyanobacterial Secondary Metabolites .....	2
1.3.	Tetrahydropyran Containing Macrolides .....	5
1.4.	Macrolides from Cyanobacteria <i>Oscillatoria Acutissima</i> .....	6
1.5.	Macrolides from Cyanobacteria <i>Lyngbya bouillonii</i> .....	6
1.5.1.	Lyngbyaloside .....	8

1.5.2.	Lyngbouilloside .....	8
1.5.3.	Lyngbyaloside B .....	9
1.6.	Macrolides from Marine Sponge <i>Callipelta</i> sp. ....	9
1.7.	Macrolides from Marine Sponge <i>Phorbas</i> sp. ....	12
1.8.	Macrolides from Sea Hare <i>Dolabella auricularia</i> .....	14
1.8.1.	Aurisides A and B .....	15
1.8.1.1.	Paterson's Approach .....	16
1.8.1.1.1.	Preparation of Aldehyde <b>1.21</b> .....	17
1.8.1.1.2.	Preparation of Enol Silane <b>1.22</b> .....	18
1.8.1.1.3.	Preparation of Fluorosugars <b>1.23</b> and <b>1.24</b> .....	19
1.8.1.1.4.	Construction of Aurisides Aglycon .....	21
1.8.1.1.5.	Mukaiyama Glycosylation to Aurisides A and B .....	22
1.8.1.2.	Yamada's Approach .....	23
1.8.1.2.1.	Preparation of Aldehyde <b>1.44</b> .....	25
1.8.1.2.2.	Preparation of Vinyl Iodide <b>1.45</b> .....	26
1.8.1.2.3.	Construction of Aurisides Aglycon .....	27
1.8.1.2.4.	Mukaiyama Glycosylation to Aurisides A and B .....	28
1.8.1.3.	Olivo's Approach .....	30
1.8.1.3.1.	Construction of Methyl Pyranoside <b>1.62</b> .....	31
1.8.1.3.2.	Preparation of Acetylene <b>1.63</b> .....	32
1.8.1.3.3.	Preparation of Alkyne <b>1.63</b> .....	33
1.8.2.	Dolastatin 19 .....	34
1.8.2.1.	Structural Revision .....	35



1.8.2.2.	Paterson's Approach .....	37
1.8.2.2.1.	The First Aldol Reaction .....	38
1.8.2.2.2.	The Second Aldol Reaction .....	40
1.8.2.2.3.	Macrolactonization and Glycosylation .....	41
1.9.	Macrolides from Calcareous Sponge <i>Leucascandra caveolata</i> .....	42
1.10.	Macrolide from Marine Sponges Related to <i>Daedalopelta sollas</i> .....	46
1.10.1.	Panek's Approach .....	48
1.10.1.1.	Preparation of Aldehyde <b>1.96</b> .....	49
1.10.1.2.	[4+2] Annulation .....	51
1.10.1.3.	Endgame Strategy .....	52
1.10.2.	Scheidt's Approach .....	53
1.10.2.1.	Preparation of Dioxinone <b>1.110</b> .....	54
1.10.2.2.	Preparation of Alcohol <b>1.111</b> .....	55
1.10.2.3.	Novel Prins Macrolactonization .....	57
1.10.2.4.	Endgame Strategy .....	58
1.10.3.	Lee's Approach .....	59
1.10.3.1.	Preparation of Common Intermediate <b>1.130</b> .....	60
1.10.3.2.	Much Improved Prins Macrolactonization .....	62
1.10.3.3.	Alternative Prins Macrolactonization .....	63
1.10.3.4.	Endgame Strategy .....	65
1.10.4.	Maier's Approach .....	65
1.10.4.1.	Preparation of Aldehyde <b>1.149</b> .....	66

1.10.4.2.	Completion to Neopeltolide Macrolide Core .....	68
1.10.5.	Sasaki's Approach .....	69
1.10.5.1.	Preparation of Enol Phosphate <b>1.163</b> .....	70
1.10.5.2.	Preparation of Alkyl Iodide <b>1.164</b> .....	71
1.10.5.3.	Construction of 2,4,6-Trisubstituted Tetrahydropyran .....	72
1.10.5.4.	Endgame Strategy .....	73
1.10.6.	Kozmin's Approach .....	74
1.10.6.1.	Macrolactone Construction .....	75
1.10.6.2.	Stereochemical Elaboration and Endgame Strategy .....	76
1.11.	Macrolides from Red Alga <i>Polycavernosa tsudai</i> and <i>Acanthophora specifera</i> .....	77
1.12.	Conclusion .....	82
CHAPTER TWO	(+)-ACUTIPHYCIN: ISOLATION AND TOTAL SYNTHESES .....	84
2.1.	Purpose .....	84
2.2.	Isolation and Biological Activity .....	84
2.3.	Structural Elucidation .....	85
2.3.1.	NMR Experiments .....	85
2.3.2.	Chemical Degradation Studies .....	86
2.3.3.	NOE-Based Conformational Analysis .....	89
2.4.	Previous Total Syntheses .....	90
2.4.1.	Smith's Approach .....	90

2.4.1.1.	Preparation of Fragment <b>2.13</b> .....	91
2.4.1.2.	Preparation of Fragment <b>2.14</b> .....	92
2.4.1.3.	Fragments Coupling and Endgame Strategy .....	95
2.4.1.4.	Endgame Strategy .....	97
2.4.2.	Kiyooka's Approach .....	98
2.4.2.1.	The First Aldol Reaction .....	100
2.4.2.2.	The Second Aldol Reaction .....	101
2.4.2.3.	The Third Aldol Reaction .....	102
2.4.2.4.	The Fourth Aldol Reaction .....	107
2.4.2.5.	The Fifth Aldol Reaction .....	108
2.4.3.	Jamison's Approach .....	109
2.4.3.1.	Concise Five-Fragment Coupling .....	110
2.4.3.2.	A Novel Macrolactonization Strategy .....	113
2.5.	Conclusion .....	114

## CHAPTER THREE

## SYNTHETIC STUDIES TOWARDS

	(+)-ACUTIPHYCIN .....	116
3.1.	Purpose .....	116
3.2.	The Role of Natural Products as Anticancer Drugs .....	116
3.3.	Taylor Group Interests in Polyketide Natural Products .....	119
3.4.	(+)-Acutiphycin as an Attractive Target .....	122
3.5.	Retrosynthetic Analysis .....	123

3.6.	Preparation of Fragment <b>3.13</b> .....	124
3.6.1.	Acetate Aldol via Homoaldol Methodology .....	125
3.6.1.1.	Peter Beak's Homoaldol Reactions .....	128
3.6.1.2.	Homoaldol Reactions with Beak's Auxiliary <b>3.21</b> .....	132
3.6.1.3.	Ozonolysis Study .....	134
3.6.1.4.	Study with Redesigned TBS Auxiliary .....	137
3.6.2.	Acetate Aldol via Asymmetric Allylation .....	141
3.6.3.	The Horner-Wadsworth-Emmons Reaction .....	143
3.6.4.	The Vinylogous Mukaiyama Aldol Reaction with <i>N,O</i> -Ketene Acetal .....	144
3.7.	Preparation of Fragment <b>3.14</b> .....	147
3.7.1.	Preparation of Aldehyde <b>3.74</b> .....	148
3.7.2.	<i>Four Plus Two</i> Carbon Atoms Addition .....	150
3.7.2.1.	Preparation of Chan's Diene <b>3.81</b> .....	151
3.7.2.2.	Titanium(IV)-BINOL Promoted Asymmetric Aldol Reaction .....	153
3.7.2.3.	Directed Reduction, Enolate Addition, and Cyclization .....	154
3.7.3.	<i>Two Plus Four</i> Carbon Atom Addition .....	159
3.7.3.1.	Soderquist Allylation and Acetate Aldol .....	159
3.7.3.2.	Evans Polar Induction Model .....	161
3.7.3.3.	Cyclization and Mitsunobu Inversion .....	169
3.8.	Fragments <b>3.13</b> and <b>3.14</b> Coupling Studies .....	171
3.8.1.	Enolization Study .....	171
3.8.2.	Mukaiyama Aldol Approach .....	174

3.8.3.	House Aldol Approach .....	176
3.8.4.	TBAF-Mediated Aldol Approach .....	178
3.8.5.	Coupling With Truncated Aldehyde <b>3.138</b> .....	179
3.9.	Revised Strategy .....	180
3.10.	Preparation of Vinyl Iodide <b>3.140</b> .....	181
3.11.	Preparation of Aldehyde <b>3.142</b> .....	182
3.12.	Construction of C9 – C13 Region .....	183
3.13.	Future Directions .....	184
3.13.1.	Construction of Acutiphycin Carbon Framework .....	184
3.13.2.	Jamison Macrolactonization Strategy .....	186
3.13.3.	Boeckman Macrolactonization Strategy .....	188
3.13.4.	Endgame Strategy .....	190
3.14.	Conclusion .....	191
CHAPTER FOUR	PELORUSIDE A AND ELECTROPHILE-INDUCED	
	ETHER TRANSFER .....	193
4.1.	Purpose .....	193
4.2.	Peloruside A .....	193
4.2.1.	Peloruside A as a Polyketide Natural Product .....	195
4.3.	Peloruside A and 1,3- <i>syn</i> Diol Monoether .....	196
4.3.1.	Carbonate Cyclization .....	197
4.3.2.	Chiral Auxiliary Promoted Aldol Reactions .....	198

4.3.2.1.	Taylor's Approach .....	198
4.3.2.2.	Roush's Approach .....	199
4.3.3.	Chiral Reagents .....	200
4.3.3.1.	Brown's Allyl(Ipc) <sub>2</sub> borane .....	200
4.3.3.1.1.	Zhou's Approach .....	201
4.3.3.1.2.	De Brabander's Approach .....	201
4.3.3.2.	Ketone Reduction with the CBS Reagent .....	202
4.3.4.	Substrate Controlled .....	203
4.3.4.1.	Epoxidation – Ring Opening .....	203
4.3.4.2.	Allylation – Tetrahydropyran Ring Opening .....	204
4.3.4.3.	Mitsunobu Inversion .....	205
4.3.4.4.	Evans-Tishchenko Reduction .....	206
4.4.	Electrophile-Induced Ether Transfer .....	207
4.4.1.	The Proof of Concept .....	208
4.4.2.	Mechanistic Insights .....	210
4.5.	Ether transfer and Structural Diversity .....	216
4.6.	Conclusion .....	218

CHAPTER FIVE	STEREOSELECTIVE SYNTHESIS OF OXYGEN HETEROCYCLES VIA ELECTROPHILE-INDUCED ETHER TRANSFER .....	220
5.1.	Purpose .....	220

5.2.	Ether Transfer and Oxacycle Methodology .....	221
5.3.	An Expedient Route to 2-Cyano Tetrahydropyran .....	225
5.3.1.	Functional Group Interconversions .....	231
5.3.2.	Reductive Decyanation Study .....	232
5.4.	Preparation of Highly Versatile 2-Sulfone Tetrahydropyran .....	236
5.5.	Stereoselective Synthesis of 2,4,6-Trisubstituted Tetrahydropyrans .....	238
5.5.1.	4-Alkoxy-2,6- <i>trans</i> -Disubstituted Tetrahydropyran .....	239
5.5.2.	4-Alkoxy-2,6- <i>cis</i> -Disubstituted Tetrahydropyran .....	242
5.5.3.	4-Hydroxy-2,6-Disubstituted Tetrahydropyrans .....	246
5.5.4.	Stereoselective Synthesis of C3 – C17 Fragment of Phorboxazole A .....	247
5.5.4.1.	Optimizing the Alkylation Step .....	253
5.6.	Stereoselective Synthesis of 2,6- <i>trans</i> -Disubstituted 3,4- Dihydropyran .....	256
5.6.1.	Stereoselective Synthesis of C7-C17 Fragment of Swinholide A .....	260
5.7.	Conclusion .....	263

CHAPTER SIX	CONCISE ENANTIOSELECTIVE TOTAL SYNTHESIS OF NEOPELTOLIDE MACROLACTONE .....	265
-------------	--	-----

6.1.	Purpose .....	265
6.2.	Neopeltolide .....	266
6.2.1.	Mode of Action .....	267

6.2.2.	Structural Resemblance to Leucascandrolide A .....	267
6.2.3.	Molecular Compartments Responsible for the Observed Biological Activities .....	268
6.2.4.	Neopeltolide C5-Epimer .....	270
6.3.	Limitation of Sulfonylpyran-Based Methodology .....	271
6.3.1.	Alternative Sequence to 2,6- <i>cis</i> -Tetrahydropyran .....	272
6.4.	Retrosynthesis .....	273
6.5.	Preparation of $\beta$ -Hydroxy Sulfide <b>6.18</b> .....	275
6.6.	Preparation of Aldehyde <b>6.19</b> .....	276
6.7.	Segments Coupling .....	277
6.8.	Construction of 2,4,6-Trisubstituted-Tetrahydropyran Core .....	279
6.9.	Endgame Strategy .....	283
6.10.	Spectroscopic Comparison .....	284
6.11.	Conclusion .....	287
CHAPTER SEVEN	FUTURE DIRECTIONS .....	288
7.1.	Purpose .....	288
7.2.	Synopsis of Previous Chapters .....	288
7.3.	Structure – Activity Relationship Study .....	290
7.3.1.	Conformation – Activity Relationship in Epothilones .....	290
7.3.2.	Conformation – Activity Relationship in (+)-Acutiphycin .....	295
7.3.2.1.	Conformational Analysis about C5 – C13 Region .....	295



7.3.2.2.	Conformational Analysis about C14 – C1 Region .....	297
7.4.	Electrophile-Induced Ether Transfer: Stereoselective Synthesis of Spiroketal .....	299
7.4.1.	Preparation of Milbemycin $\beta_3$ Spiroketal Core .....	301
7.4.1.1.	A Model Study in the Alkylation Reaction .....	303
7.4.1.2.	Alkylation via Vinyl Lithium .....	304
7.4.1.3.	Coupling via the Suzuki-Miyaura Reaction .....	305
7.4.1.4.	Acid Promoted Spiroketalization .....	306
7.4.1.5.	Alternative Route via Barton-McCombie Deoxygenation .....	307
7.4.2.	Total Synthesis of (+)-Aigialospirol .....	309
7.4.2.1.	Preparation of Fragments <b>7.54</b> and <b>7.55</b> .....	310
7.4.2.2.	Ferrier-Like Spiroketalization .....	312
7.4.2.3.	Endgame Strategy .....	313
7.5.	More Structural Novelty from the Ether Transfer Reactions .....	313
7.5.1.	Novel Approach to 2,4,6-Trisubstituted Oxepane .....	314
7.5.2.	A Unique Access to 2,4,6-Trisubstituted Oxepanone .....	317
7.5.3.	Preparation of Post-PKS Modified-Like Polyketide Synthetic Fragments .....	319
7.6.	Conclusion .....	322

## VOLUME TWO

CHAPTER EIGHT	SUPPORTING INFORMATION: EXPERIMENTAL .....	324
8.1.	General Information .....	324
8.2.	Experimental Procedures for Chapter Three .....	325
8.3.	Experimental Procedures for Chapter Four .....	352
8.4.	Experimental Procedures for Chapter Five .....	354
8.5.	Experimental Procedures for Chapter Six .....	446
CHAPTER NINE	SUPPORTING INFORMATION: NMR SPECTRA .....	466
9.1.	General Information .....	466
REFERENCES	.....	569

## LIST OF FIGURES

Figure 1.1 .....	4
Figure 1.2 .....	6
Figure 1.3 .....	7
Figure 1.4 .....	11
Figure 1.5 .....	13
Figure 1.6 .....	15
Figure 1.7 .....	35
Figure 1.8 .....	37
Figure 1.9 .....	43
Figure 1.10 .....	47
Figure 1.11 .....	79
Figure 1.12 .....	81
Figure 1.13 .....	82
Figure 2.1 .....	85
Figure 2.2 .....	90
Figure 2.3 .....	104
Figure 2.4 .....	105
Figure 3.1 .....	118

Figure 3.2 .....	120
Figure 3.3 .....	121
Figure 3.4 .....	126
Figure 3.5 .....	143
Figure 3.6 .....	146
Figure 3.7 .....	153
Figure 3.8 .....	161
Figure 3.9 .....	162
Figure 3.10 .....	165
Figure 3.11 .....	170
Figure 4.1 .....	194
Figure 4.2 .....	196
Figure 4.3 .....	214
Figure 5.1 .....	224
Figure 5.2 .....	225
Figure 5.3 .....	229
Figure 5.4 .....	243
Figure 5.5 .....	255
Figure 6.1 .....	266
Figure 6.2 .....	268
Figure 6.3 .....	269
Figure 6.4 .....	269
Figure 6.5 .....	281

Figure 6.6 .....	285
Figure 6.7 .....	286
Figure 7.1 .....	290
Figure 7.2 .....	291
Figure 7.3 .....	292
Figure 7.4 .....	293
Figure 7.5 .....	295
Figure 7.6 .....	296
Figure 7.7 .....	297
Figure 7.8 .....	298
Figure 7.9 .....	299
Figure 7.10 .....	300
Figure 7.11 .....	322

## LIST OF SCHEMES

Scheme 1.1 .....	17
Scheme 1.2 .....	18
Scheme 1.3 .....	19
Scheme 1.4 .....	20
Scheme 1.5 .....	22
Scheme 1.6 .....	23
Scheme 1.7 .....	24
Scheme 1.8 .....	26
Scheme 1.9 .....	27
Scheme 1.10 .....	28
Scheme 1.11 .....	29
Scheme 1.12 .....	30
Scheme 1.13 .....	32
Scheme 1.14 .....	33
Scheme 1.15 .....	34
Scheme 1.16 .....	38
Scheme 1.17 .....	39
Scheme 1.18 .....	41

Scheme 1.19 .....	42
Scheme 1.20 .....	45
Scheme 1.21 .....	49
Scheme 1.22 .....	50
Scheme 1.23 .....	51
Scheme 1.24 .....	53
Scheme 1.25 .....	54
Scheme 1.26 .....	55
Scheme 1.27 .....	56
Scheme 1.28 .....	57
Scheme 1.29 .....	58
Scheme 1.30 .....	59
Scheme 1.31 .....	60
Scheme 1.32 .....	61
Scheme 1.33 .....	63
Scheme 1.34 .....	64
Scheme 1.35 .....	65
Scheme 1.36 .....	66
Scheme 1.37 .....	67
Scheme 1.38 .....	69
Scheme 1.39 .....	70
Scheme 1.40 .....	71
Scheme 1.41 .....	72

Scheme 1.42 .....	73
Scheme 1.43 .....	74
Scheme 1.44 .....	75
Scheme 1.45 .....	76
Scheme 1.46 .....	77
Scheme 2.1 .....	87
Scheme 2.2 .....	88
Scheme 2.3 .....	89
Scheme 2.4 .....	91
Scheme 2.5 .....	92
Scheme 2.6 .....	93
Scheme 2.7 .....	94
Scheme 2.8 .....	95
Scheme 2.9 .....	96
Scheme 2.10 .....	97
Scheme 2.11 .....	98
Scheme 2.12 .....	100
Scheme 2.13 .....	101
Scheme 2.14 .....	102
Scheme 2.15 .....	103
Scheme 2.16 .....	106
Scheme 2.17 .....	107
Scheme 2.18 .....	108



Scheme 2.19 .....	109
Scheme 2.20 .....	110
Scheme 2.21 .....	111
Scheme 2.22 .....	112
Scheme 2.23 .....	113
Scheme 2.24 .....	114
Scheme 3.1 .....	124
Scheme 3.2 .....	125
Scheme 3.3 .....	128
Scheme 3.4 .....	129
Scheme 3.5 .....	131
Scheme 3.6 .....	132
Scheme 3.7 .....	133
Scheme 3.8 .....	134
Scheme 3.9 .....	134
Scheme 3.10 .....	135
Scheme 3.11 .....	136
Scheme 3.12 .....	137
Scheme 3.13 .....	138
Scheme 3.14 .....	139
Scheme 3.15 .....	139
Scheme 3.16 .....	141
Scheme 3.17 .....	142

Scheme 3.18 .....	143
Scheme 3.19 .....	144
Scheme 3.20 .....	145
Scheme 3.21 .....	146
Scheme 3.22 .....	147
Scheme 3.23 .....	148
Scheme 3.24 .....	150
Scheme 3.25 .....	150
Scheme 3.26 .....	151
Scheme 3.27 .....	151
Scheme 3.28 .....	152
Scheme 3.29 .....	154
Scheme 3.30 .....	155
Scheme 3.31 .....	156
Scheme 3.32 .....	157
Scheme 3.33 .....	158
Scheme 3.34 .....	158
Scheme 3.35 .....	159
Scheme 3.36 .....	160
Scheme 3.37 .....	162
Scheme 3.38 .....	163
Scheme 3.39 .....	164
Scheme 3.40 .....	167

Scheme 3.41 .....	168
Scheme 3.42 .....	169
Scheme 3.43 .....	170
Scheme 3.44 .....	171
Scheme 3.45 .....	172
Scheme 3.46 .....	175
Scheme 3.47 .....	175
Scheme 3.48 .....	176
Scheme 3.49 .....	177
Scheme 3.50 .....	178
Scheme 3.51 .....	179
Scheme 3.52 .....	180
Scheme 3.53 .....	181
Scheme 3.54 .....	182
Scheme 3.55 .....	183
Scheme 3.56 .....	184
Scheme 3.57 .....	185
Scheme 3.58 .....	186
Scheme 3.59 .....	187
Scheme 3.60 .....	188
Scheme 3.61 .....	190
Scheme 3.62 .....	191
Scheme 4.1 .....	198

Scheme 4.2 .....	199
Scheme 4.3 .....	200
Scheme 4.4 .....	201
Scheme 4.5 .....	202
Scheme 4.6 .....	203
Scheme 4.7 .....	204
Scheme 4.8 .....	205
Scheme 4.9 .....	206
Scheme 4.10 .....	207
Scheme 4.11 .....	207
Scheme 4.12 .....	208
Scheme 4.13 .....	209
Scheme 4.14 .....	210
Scheme 4.15 .....	214
Scheme 4.16 .....	215
Scheme 5.1 .....	222
Scheme 5.2 .....	223
Scheme 5.3 .....	226
Scheme 5.4 .....	231
Scheme 5.5 .....	232
Scheme 5.6 .....	233
Scheme 5.7 .....	236
Scheme 5.8 .....	237

Scheme 5.9 .....	238
Scheme 5.10 .....	238
Scheme 5.11 .....	242
Scheme 5.12 .....	246
Scheme 5.13 .....	247
Scheme 5.14 .....	249
Scheme 5.15 .....	250
Scheme 5.16 .....	251
Scheme 5.17 .....	252
Scheme 5.18 .....	253
Scheme 5.19 .....	256
Scheme 5.20 .....	260
Scheme 5.21 .....	261
Scheme 5.22 .....	262
Scheme 5.23 .....	263
Scheme 6.1 .....	270
Scheme 6.2 .....	271
Scheme 6.3 .....	272
Scheme 6.4 .....	273
Scheme 6.5 .....	274
Scheme 6.6 .....	275
Scheme 6.7 .....	276
Scheme 6.8 .....	278

Scheme 6.9 .....	279
Scheme 6.10 .....	280
Scheme 6.11 .....	284
Scheme 7.1 .....	301
Scheme 7.2 .....	302
Scheme 7.3 .....	303
Scheme 7.4 .....	303
Scheme 7.5 .....	304
Scheme 7.6 .....	305
Scheme 7.7 .....	306
Scheme 7.8 .....	307
Scheme 7.9 .....	308
Scheme 7.10 .....	308
Scheme 7.11 .....	309
Scheme 7.12 .....	310
Scheme 7.13 .....	311
Scheme 7.14 .....	311
Scheme 7.15 .....	312
Scheme 7.16 .....	313
Scheme 7.17 .....	314
Scheme 7.18 .....	315
Scheme 7.19 .....	316
Scheme 7.20 .....	317

Scheme 7.21 .....	318
Scheme 7.22 .....	319
Scheme 7.23 .....	320
Scheme 7.24 .....	321

## LIST OF TABLES

Table 3.1 .....	140
Table 3.2 .....	173
Table 4.1 .....	213
Table 4.2 .....	217
Table 5.1 .....	228
Table 5.2 .....	230
Table 5.3 .....	234
Table 5.4 .....	240
Table 5.5 .....	245
Table 5.6 .....	254
Table 5.7 .....	258
Table 6.1 .....	282
Table 7.1 .....	294



## LIST OF ABBREVIATIONS

$[\alpha]^{20}_D$ .....	absolute optical rotation
$^{13}\text{C}$ .....	carbon 13
$^1\text{H}$ .....	proton
2,2-DMP .....	2,2-dimethoxypropane
9-BBN .....	9-borabicyclo[3.3.1]nonane
Å .....	angstrom
$A_{1,3}$ .....	allylic 1,3
Ac .....	acetate, acetic
AD-mix .....	asymmetric dihydroxylation mixture
AIBN .....	azobisisobutyronitrile
ATP .....	adenosine-5'-triphosphate
b .....	broad
BINAP .....	2,2'-bis(diphenylphosphino)-1,1'-binaphthyl
BINOL .....	1,1'-binaphthalene-2,2'-diol
Bn .....	benzyl
Boc .....	<i>tert</i> -butoxycarbonyl
Boc-ON .....	2-( <i>tert</i> -butoxycarbonyloxyimino)-2-phenylacetonitrile
BOM .....	benzyloxymethyl

BPS	<i>tert</i> -butyldiphenylsilyl
Bu	butyl
Bz	benzoate
c	concentration
CBS	Corey-Bakshi-Shibata
CD	circular dichroism
<i>c</i> -Hex	cyclohexyl
cm	centimeter
Cp	cyclopentadienyl
CSA	camphorsulfonic acid
Cy	cyclohexyl
$\delta$	chemical shift
d	doublet
DABCO	1,4-diazabicyclo[2.2.2]octane
DAST	diethylaminosulfur trifluoride
DBB	4,4'-di- <i>tert</i> -butyl-biphenyl
DCC	dicyclohexylcarbodiimide
DDQ	2,3-dicyano-5,6-dichloro-parabenzoquinone
DEAD	diethyl azodicarboxylate
DET	diethyl tartrate
DHP	2,3-dihydropyran
DI	deionized
DIAD	diisopropyl azodicarboxylate

DIBAL .....	diisobutylaluminium hydride
DIPA .....	diisopropylamine
DIPEA .....	<i>N,N</i> -diisopropylethylamine
DIPT .....	diisopropyl tartrate
DMAP .....	4-dimethylaminopyridine
DMB .....	3,4-dimethoxybenzyl
DME .....	dimethoxyethane
DMF .....	dimethylformamide
DMP .....	Dess-Martin periodinane
DMPU .....	1,3-dimethyl-3,4,5,6-tetrahydro-2(1H)-pyrimidinone
DMS .....	dimethylsulfide
DMSO .....	dimethylsulfoxide
dppf .....	1,1'- <i>bis</i> (diphenylphosphino)ferrocene
dr .....	diastereomeric ratio
DTBMP .....	2,6-di- <i>tert</i> -butyl-4-methylpyridine
DTBP .....	2,6-di- <i>tert</i> -butylpyridine
<i>E</i> .....	<i>Entgegen</i>
E .....	electrophile
ED <sub>50</sub> .....	half maximal effective concentration
EDCI .....	1-ethyl-3-(3-dimethylaminopropyl)carbodiimide hydrochloride
ee .....	enantiomeric excess
EPHP .....	1-ethylpiperidine hypophosphite
eq .....	equivalent

er	enantiomeric ratio
Et	ethyl
FAB	fast atomic bombardment
FT-IR	Fourier transform infrared
g	gram
GI <sub>50</sub>	half maximal growth inhibition concentration
h	heptet
HMDS	hexamethyldisilazane
HMPA	hexamethylphosphoramide
HOBT	hydroxybenzotriazole
HPLC	high-performance liquid chromatography
HRMS	high resolution mass spectrometry
HWE	Horner-Wadsworth-Emmons
Hz	Hertz
IC <sub>50</sub>	half maximal inhibitory concentration
imid	imidazole
Ipc	isopinocampheyl
<i>i</i> -Pr	isopropyl
J	coupling constant
kg	kilogram
LAH	lithium aluminum hydride
LD <sub>99</sub>	dosage required to kill 99% of population
LDA	lithium diisopropylamide

M	.....	molar
m	.....	meter, multiplet
mCPBA	.....	<i>meta</i> -chloroperoxybenzoic acid
Me	.....	methyl
MEM	.....	methoxyethoxymethyl
Mes	.....	mesityl
mg	.....	milligram
μg	.....	microgram
MHz	.....	megaHertz
MIC	.....	minimum inhibitory concentration
mL	.....	milliliter
mM	.....	millimolar
μM	.....	micromolar
mmol	.....	millimol
MOM	.....	methoxymethyl
Ms	.....	mesyl, mesylate
NBS	.....	<i>N</i> -bromosuccinimide
<i>n</i> -Bu	.....	<i>normal</i> -butyl
NHK	.....	Nozaki-Hiyama-Kishi
NIS	.....	<i>N</i> -iodosuccinimide
nM	.....	nanomolar
NMO	.....	<i>N</i> -methylmorpholine <i>N</i> -oxide
NMR	.....	nuclear magnetic resonance

NOE	nuclear Overhauser effect
Nuc	nucleophile
p	pentet
PCC	pyridinium chlorochromate
PDC	pyridinium dichromate
Ph	phenyl
Piv	pivalate, pivaloyl
PKS	polyketide synthase
PLE	porcine liver esterase
PMB	<i>para</i> -methoxybenzyl
PMP	<i>para</i> -methoxyphenyl
PNBA	<i>para</i> -nitrobenzoic acid
ppm	part per million
PPTS	pyridinium <i>para</i> -toluenesulfonate
py	pyridine
q	quartet
<i>R</i>	<i>Rectus</i>
Red-Al	sodium <i>bis</i> (2-methoxyethoxy)aluminumhydride
<i>S</i>	<i>Sinister</i>
s	singlet
SAR	structure-activity-relationship
<i>s</i> -Bu	<i>sec</i> -butyl
t	triplet

T/C .....	test/control
TASF .....	tris(dimethylamino)sulfonium difluorotrimethylsilicate
TBAF .....	tetra- <i>n</i> -butylammonium fluoride
TBAI .....	tetra- <i>n</i> -butylammonium iodide
TBHP .....	<i>tert</i> -butyl hydrogen peroxide
TBS .....	<i>tert</i> -butyldimethylsilyl
<i>t</i> -Bu .....	<i>tert</i> -butyl
TCBCl .....	2,4,6-trichlorobenzoyl chloride
TCICA .....	trichloroisocyanuric acid
TEA .....	triethylamine
temp .....	temperature
TEMPO .....	2,2,6,6-tetramethylpiperidine-1-oxyl
TES .....	triethylsilyl
TFA .....	trifluoroacetic acid
Tf .....	triflate, triflic
THF .....	tetrahydrofuran
THP .....	tetrahydropyranyl
TIPS .....	triisopropylsilyl
TLC .....	thin layer chromatography
TMS .....	trimethylsilyl
tol .....	toluene, toluyl
Tos .....	tosyl, tosylate
TPAP .....	tetrapropylammonium perruthenate

Tr .....	trityl
Ts .....	tosyl, tosylate
UV .....	ultraviolet
x .....	sextet
<i>Z</i> .....	<i>Zusammen</i>



## ACKNOWLEDGMENT

Five years have gone by too quickly, and it seemed only yesterday when I first stepped my foot in this great university and began my journey as a graduate student in the Department of Chemistry and Biochemistry. My experience has been fulfilling both professionally and personally, and there are so many people who have contributed for the success of this dissertation. Without them, none of this research would have been possible.

First and foremost, my utmost gratitude lies upon my advisor, Professor Richard E. Taylor. Rich was the perfect advisor that I could ask for. His hands-off method helped the development of my problem solving skills, but his door was always open anytime I needed guidance. Rich's broad knowledge of chemistry and science made him a role model as a researcher. His constant questions of "why" and "how" made me learn to understand the ever-growing problems in chemical science and be able to creatively come up with reasonable solutions for them. Rich was also an excellent teacher. Early in my graduate career, I had the opportunity to enroll in two of his advanced organic chemistry courses. His thoroughness and approachable personality made learning fun, interactive, and rewarding.

Rich, thank you very much for your confidence in me and giving me big break with the ether transfer projects. I will always remember your advice to always take pride

in my work, and never be content but always move forward and pursue something better. I have learned so much, and yet, still not enough from you. I hope one day I can make you proud as much as I am very proud to say that you were (still are and will always be) my mentor.

My committee members, Professors Marvin Miller, Paul Helquist, and Kenneth Henderson, were fantastic. Their challenge, guidance, and helpful discussions during my graduate career were invaluable. I thank them for writing numerous letters of recommendation on my behalf and also for reading and reviewing this dissertation. My teaching mentors, Professors DeeAnne Goodenough-Lashua and Bradley Smith, were influential in my decision to pursue an academic career. Their enthusiasm and creativity as professors are truly inspirational, and they showed me that teaching is a very rewarding profession.

The help that I received from the professional specialists in the Department of Chemistry and Biochemistry is greatly appreciated: Dr. Jaroslav Zajicek for helping me with my NMR quests; I truly admire your ability to solve any 1D or 2D NMR problems, Dr. Igor Veretennikov for maintaining the NMR's, and also Nonka Sevov for running my countless number of high resolution mass-spec samples. I also thank the staff in the Department of Chemistry and Biochemistry office: Debbie Bennett, Cheryl Copley, Rosemary Patti, and Rita Egendoerfer for making sure that the needs of graduate students were always met. I will miss Joseph Wilk in the stockroom. His genuine care and attention for our lab supplies was phenomenal.

I acknowledge the Department of Chemistry and Biochemistry and the University of Notre Dame for providing me with the opportunity to pursue my Ph.D. and especially

for the financial supports through the teaching assistantship in the 2003 – 2005 academic years and the Reilly Fellowship award in the 2007 – 2008 academic year. I am also honored to have received several graduate teaching awards, such as the 2004 and 2006 Kaneb Center Outstanding Teaching Assistants and the prestigious departmental Rudolph S. Bottei Graduate Teaching Award in 2005.

Prior to Notre Dame, I was educated by extraordinary teachers. California State Polytechnic University at Pomona (Cal Poly Pomona) has an excellent group of organic chemistry faculty. I was first introduced to organic chemistry in a formal one-year junior course taught by Professor David Brown. I was so enthused by the subject that I changed my major to chemistry. Subsequently, I took several advanced organic chemistry courses independently taught by Professors Phillip Beauchamp, Francis Flores, and Laurie Starkey. My undergraduate research advisor, Professor Douglas Klumpp was influential in shaping my interests in organic chemistry research. He patiently trained me to be an independent undergraduate researcher. He also recognized my potential and eventually encouraged me to continue my education and pursue an advanced degree. I am also thankful for Mrs. Elizabeth Aning, my counselor and mentor at Kolese Santo Yusup High School in Malang, Indonesia. She somehow managed to help me focused on my education through those difficult and rebellious teenage years.

My family both in Indonesia and Los Angeles has been a great anchor in my life. They brought me up to become the person I am, and they have done a fantastic job. Although unfortunately we do not get to see each other very often, I always know that their unconditional love, support, and prayers always help me get through even my toughest times. I grew up in a fairly large and yet close extended family whom I really

love. I owe my success to my late grandparents “Kung Kung” and “Bo Bo” particularly for teaching me since I was very young that education is the key to a bright future. My mom is a strong woman, and she has always been there for me even just to chat for hours about our daily lives. I am grateful for my wonderful siblings: Patricia, Robert, and Raymond. My life is also enriched with my cousins, Shelly and Revian. Additionally, I would like to express a special gratitude to my aunt, Mommy Mineke L. Bates. She took me into her house from Indonesia, sent me to college, and treated me as if I were her own son. For these unparalleled kindness and generosity, I am forever grateful. Without her, I would not be writing this dissertation.

The 2003 – 2008 “Taylorites” are a bunch of amazing people who made my daily life in the lab enjoyable. I do thank all of them for putting up with my unmatched personality and for the beautiful friendships we have developed throughout these five years. I will honestly miss our daily conversations, i.e. arguments, not only about reaction mechanisms and irreproducible literature precedents, but also topics in general: college football (including how much Colin Cowherd and Mark May actually resented Notre Dame), politics, world religions, food, and so much more. I also appreciate the precious time they spent proofreading my thesis.

I am grateful for having the current inhabitants of lab 358 as my lab mates, as these guys had to endure seeing me and hearing me yapping everyday. Jeff, many thanks for the constant chemistry challenge and for preparing my starting material of both enantiomers (oops!). You are a good buddy, and I need more mechanism questions, please.

I am offering a special thank you to my mentors: Christina Risatti, Bill Paquette, Jim Tung, and Dave Guisella. They demonstrated true leadership. They taught me how to be a responsible group member, and I will always look up to them. Tina, let's say that you have successfully created a clone of yourself in the Taylor lab in terms of producing high quality experimental and NMR analyses. Bill and Jim, thanks so much for showing me a bunch of lab tricks (no pun intended). Dave, you made me realize that great chemists not only know how to use their hands to run reactions in a hood but also to fix common lab instruments when they are not working. I learned that staring at a faulty instrument alone would not fix it.

Myriam Roy and Kai Liu are not only my great lab mates, but they are my best friends. They have always been there for me in good or bad times in these past five years, and I greatly appreciated their supports and friendships. I will surely miss our regular hangouts in and out of the lab as well as the many road-trips we had either for conferences or just simply for sightseeing. I believe that our friendship will ever flourish and last for our lifetime. Myriam, we have been close friends since the first day we met in the new graduate student orientation, and thank you for letting me confide in you. I also thank Kai and his wife, Xiangning Li, for often inviting me to their home and cooking marvelous dinners.

Finally, I was blessed to have had the privilege of mentoring and working closely with three extremely talented undergraduate researchers: Michael Johnson (BS 2005), Tanner Freeman (BS 2007), and Thomas Gruffi (Class of 2009). Their enthusiasm always kept me feeling youthful. Not only did these guys become my good friends, but they also really taught me how to be patient when dealing with research students. I

worked with Tanner for two years. Tanner was one of the smartest kids I've ever known in my life, and working with him really made me learn how to efficiently plan, design, and execute his research plans. Obviously, this is a skill that I will ultimately need when I begin my career in academia. I also commended his patience and coolness when dealing with my frustration. Also, I owe Tommy for the success of the neopeltolide project. His dedication and hard work in the tetrahydropyran methodology really paid off, and his important result eventually became the foundation for our successful total synthesis of the neopeltolide macrolactone.

My heart is very much attached to Notre Dame, and I am leaving this special place with a heavy heart. The beautiful campus, the famed Golden Dome, the Basilica of the Sacred Heart, the "Touchdown Jesus" Hesburgh Library, the Grotto, the traditions, the football games, the marching band, and everything that breathes the Notre Dame spirit will always be missed and never forgotten. I have naturally grown to become a die-hard Notre Dame Football fan, and I am proud to say that in these past five years, I have never missed a single home game (including spring games). I will definitely come back to the Notre Dame campus in the future as often as I can either for visiting old colleagues or for football games, but this time as a proud alumnus. I will always bleed gold and blue, through and through. GO IRISH!

## CHAPTER ONE

### TETRAHYDROPYRAN CONTAINING SMALL MACROLIDES OF CYANOBACTERIAL ORIGIN

#### **1.1. Purpose**

The purpose of this chapter is to detail literature reviews pertinent to small macrolides of cyanobacterial origin, particularly those with C3 – C7 tetrahydropyran moieties embedded within the macrolactone ring. This review will cover several aspects regarding these macrolides, including brief discussions on the isolation and biological evaluation of the macrolides. Selected total syntheses of these macrolides also will be presented.

#### **1.2. Cyanobacteria**

Cyanobacteria, also known as blue-green alga, are a phylum of bacteria that utilize photosynthesis to acquire their energy and to manufacture their food. Although they are typically found in warm water, cyanobacteria can survive in any conceivable moist environment. Cyanobacteria are unicellular, but they readily aggregate to form

larger, macroscopically visible colonial species, such as filaments, sheets, or hollow balls. Cyanobacterial photosynthetic pigments include chlorophyll *a* and phycobiliproteins, which account for their blue-green appearance. Another common coloration to cyanobacteria, the brownish red, is mainly caused by carotenoids and phycoerythrins. Due to the lack of flagella, cyanobacteria move about by gliding along surfaces or floating by forming internal gas vesicles. Cyanobacteria also may exist as endosymbionts with other organisms, such as lichens, protists, sponges, and plants.

Cyanobacteria are often credited with shaping the evolution and the ecological course in the history of earth.<sup>1</sup> Due to their photosynthetic capabilities, ancient cyanobacteria generated the oxygen atmosphere in the present day earth during the Archaean and Proterozoic Eras. Through an endosymbiotic evolutionary process, chloroplasts found in eukaryotic cells are most likely originated from cyanobacteria. Purportedly, some time in the late Proterozoic or the early Cambrian eras, cyanobacteria began to reside within certain eukaryotic cells and produce food for the host through photosynthesis in return. Equipped with enzyme nitrogenase, certain species of cyanobacteria are capable to fix nitrogen in aerobic conditions to ammonia, nitrites, and nitrates which are readily absorbed by plants and converted to protein and nucleic acids.

### **1.2.1. Cyanobacterial Secondary Metabolites**

The secondary metabolites produced by cyanobacteria often exhibit a broad spectrum of biological activities which include antifungal, antiviral, antibiotic, anticancerous, and protein synthesis inhibition.<sup>2, 3</sup> In fact, both freshwater<sup>4</sup> and marine<sup>5</sup>



cyanobacteria are recognized as one of the most promising groups of microorganisms from which numerous biologically active natural products have been isolated and characterized. Cyanobacterial natural products are extremely diverse in their structural motifs and are categorized into a multiple class of natural products, such as lipopeptides, alkaloids, cyclopeptides, cyclodepsipeptides, glycolipids, oligosaccharides, aromatics, nucleosides, terpenoids, polyketides, and many others. Most likely, these secondary metabolites are derived from a complex combination of non-ribosomal peptide synthase, polyketide synthase, and fatty acid biosynthetic machineries.

Cyanobacterial natural products are often extremely toxic, thereby presenting serious health hazards towards living organisms, including human beings. For example, in 1991, Haddock and Cruz reported 15 accidental human poisoning cases which resulted in three deaths in Guam after these victims consumed red algae *Polycavernosa tsudai*, a common local dietary component.<sup>6</sup> The causative toxin was identified as polycavernoside A **1.1**. Additionally, in the year of 2002 – 2003, Yoshu-Yamashita and co-workers reported that 36 people became sick, eight of whom did not survive, after ingesting the red alga *Acanthophora specifera* in the Philippines.<sup>7</sup> Research found that polycavernoside A also was the toxin responsible for these horrific food poisoning incidents. Although polycavernoside A was isolated from red algae, as described in detail in the later parts of this chapter, the biogenesis of this natural product can be traced from that of cyanobacteria.

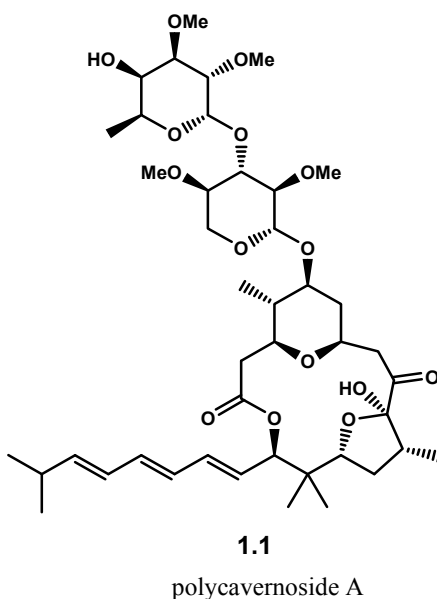


**Figure 1.1**

Cyanobacteria typically lack functional immune systems, and therefore, these microorganisms spend a significant amount of energy producing secondary metabolites as a means for their defensive systems against attacks from predators.<sup>8</sup> Carmichael and co-workers reported that cyanobacterial toxins may be lethal to marine zooplankton or readily affect their reproductive capability.<sup>9</sup> DeMott and co-workers also noted that typically zooplankton choose not to eat cyanobacteria when given the opportunity.<sup>10</sup> However, in case when food is scarce, these creatures will modulate the amount of cyanobacteria they consume to avoid deadly dosages.

Research on the isolation, characterization, and biological assays of cyanobacterial natural products did not really peak until 1980's. Some of the notable groups that have undertaken these daunting investigations included those of the late Richard Moore from the University of Hawaii, William Gerwick from the Oregon State University, and William Fenical from the University of California in San Diego. An

assessment in 2001 suggested that more than 4000 strains of cyanobacteria have been screened for these purposes.<sup>5</sup> Interestingly, about 6% of these natural products possess some degrees of anticancer activity, a fact that strongly suggests that cyanobacteria are an extremely rich source of compounds with significant medicinal values.<sup>11</sup>

### **1.3. Tetrahydropyran Containing Macrolides**

Tetrahydropyrans are the most common ring system found in polyketides. Their presence adds a significant degree of conformational rigidity and is likely to be critical to the pharmacophore of biologically active natural products. Given the vast structural diversity of cyanobacterial tetrahydropyran-containing natural products, to narrow the literature research parameters, this review will only discuss macrolides that share the following structural characteristics. First, the size of the macrolide ring will be limited to 18-membered or less. Second, the macrolide must be constructed from a single monomeric seco acid subunit. Third, the macrolide must feature an internal pyran moiety embedded within the C3 – C7 segment of the macrolactone ring. Lastly, the macrolide must possess a pendant non-oxygenated hydrophobic side chain at the site of macrolactonization.

This present chapter will summarize literature precedents on the isolation and initial biological data for all macrolides that satisfy the aforementioned criteria. However, the discussion regarding the synthetic studies on these macrolides will be limited to selected macrolides whose total syntheses have not yet appeared in any published review articles as of June 2008.

#### 1.4. Macrolides from Cyanobacteria *Oscillatoria Acutissima*

The first series of tetrahydropyran-containing natural products that fits the outlined literature research parameters are macrolides isolated from cyanobacteria *Oscillatoria acutissima*: acutiphycin **1.2** and 20,21-didehydroacutiphycin **1.3**.<sup>12</sup> As a significant portion of this dissertation is dedicated to the synthetic studies towards acutiphycin, Chapter Two will be dedicated exclusively for detailed assessment of these macrolides, which includes their isolation, characterization, solution conformation, and previous total syntheses.

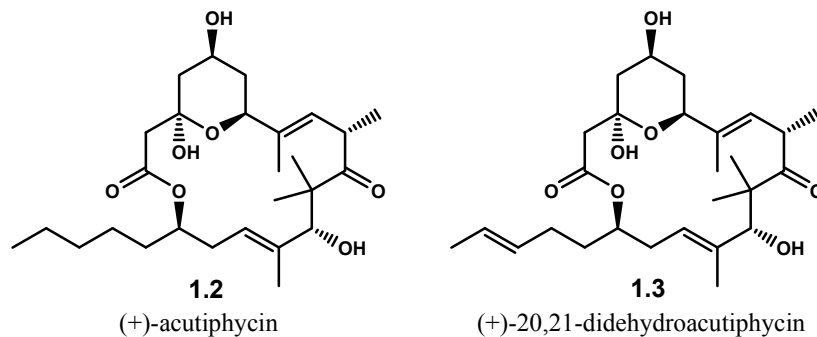
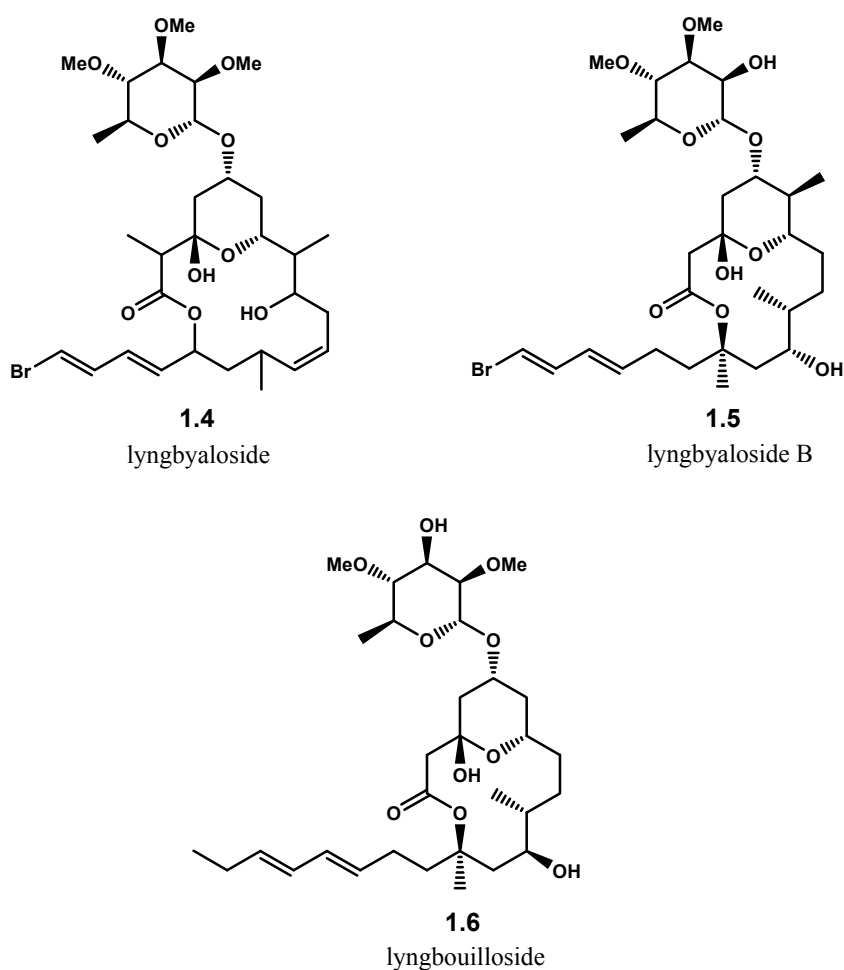


Figure 1.2

#### 1.5. Macrolides from Cyanobacteria *Lyngbya bouillonii*

Cyanobacteria *Lyngbya bouillonii* proved to be a prolific source of tetrahydropyran-containing macrolides such as lyngbyaloside **1.4**,<sup>13</sup> lyngbyaloside B **1.5**,<sup>14</sup> and lyngbouilloside **1.6**,<sup>15</sup> Figure 1.3. *L. bouillonii* is filamentous, non-heterocystous cyanobacteria that potentially grow up to 50  $\mu\text{m}$  wide and can be found in

coral reefs as dark reddish, tenacious plant masses. Often, this species is misidentified as *L. majuscula*, which is cyanobacteria responsible for a dermatitis condition known as swimmer's itch. In addition to acutiphycins, these secondary metabolites of *L. bouillonii* are the only known macrolide glycosides isolated *directly* from marine cyanobacteria that are not coexisting as symbionts. To date, efforts towards their total synthesis have not been reported.



**Figure 1.3**

### 1.5.1. Lyngbyaloside

The discovery of natural products from *L. bouillonii* began with a report in 1997 wherein Daloze and co-workers described the isolation of lyngbyaloside **1.4** from specimens collected at Laing Island in Papua New Guinea.<sup>13</sup> After extraction and purification, lyngbyaloside was isolated in 0.96 mg as an amorphous solid from 11.9 grams of the dried algae. The gross structure of lyngbyaloside was assigned as a 16-membered macrolide with the glycosidic residue identified as 2,3,4-tri-*O*-methyl-6-deoxy- $\alpha$ -mannopyranose. The aglycon moiety was found to contain eight stereogenic centers and an embedded tetrahydropyran ring which compasses the C3 – C7 region. Due to the flexibility of the macrolide ring, stereochemistry of the five stereocenters unfortunately remained unassigned. Also, a biological evaluation of lyngbyaloside was not performed due to the limited natural availability of the material.

### 1.5.2. Lyngbouilloside

Five years later, Gerwick and co-workers reported their finding of macrolide lyngbouilloside **1.6**. The natural product was isolated from *L. bouillonii* collected at the north coast of New Britain in Papua New Guinea.<sup>15</sup> From two grams of cyanobacterial lipid extract, 4.5 mg of the macrolide was obtained. Detailed spectroscopic analyses revealed that lyngbouilloside is a 14-membered macrolide glycoside that contains a C3 – C7 hemiketalpyran segment. The sugar portion was identified as 2,4-di-*O*-methylrhamnopyranoside. Initial biological assays of this compound suggested moderate

cytotoxicity against neuro-2a neuroblastoma cells with  $IC_{50} = 17 \mu M$ . Interestingly, the C13 of lyngbouilloside was assigned as a tertiary macrolactone center, which is rather unusual functionality for cyclic polyketides particularly from the perspective of biosynthesis. Although, its total synthesis has not been reported, Cossy and co-workers recently published their efforts towards the synthesis of the C1 – C13 fragment of Lyngbouilloside.<sup>16</sup>

### 1.5.3. Lyngbyaloside B

Shortly after Gerwick's report, Moore and co-workers published their isolation of the third macrolide glycosides isolated from cyanobacteria *L. Bouillonii*, which was collected from Ulong Channel in Palau.<sup>14</sup> The isolated natural product, Lyngbyaloside B **1.5**, appears to be a structural homologue to lyngbouilloside **1.6**. In addition to the requisite C3 – C7 tetrahydropyran segment, this 14-membered macrolide also contains a pendant sugar residue, characterized as 3,4-di-*O*-methylrhamnopyranoside. Only 0.6 mg of material was isolated from the crude extract, and its corresponding biological evaluation showed weak cytotoxicity against KB cells and LoVo cells with  $IC_{50}$  values of 4.3  $\mu M$  and 15  $\mu M$  respectively.

### 1.6. Macrolides from Marine Sponge *Callipelta* sp.

Marine sponges from the order Lithistida have proven to be an exceptionally rich source of secondary metabolites. In 1996, Minale and co-workers reported the isolation

and the characterization of structurally unique macrolide glycoside callipeltoside A **1.7** from shallow water lithistid sponge, *Callipelta* sp., which was collected in the waters off the east coast of New Caledonia.<sup>17</sup> 3.5 mg of callipeltoside A was isolated from 2.5 kg of the freeze-dried sponge. The initial biological evaluation of this extract showed moderate cytotoxicity against the NSCLC-N6 human bronchopulmonary non-small-cell-lung carcinoma and P388 with IC<sub>50</sub> value of 11.26 and 15.26 µg/mL respectively. Further analyses have indicated that callipeltoside A inhibits cell proliferation *in vitro* at the level of the G1 phase either via enzyme inhibition or by inducing terminal cell differentiation. Additionally, callipeltoside A was found to protect *in vitro* cells infected by the HIV virus.

As shown in Figure 1.4, callipeltoside A **1.7** is a 14-membered macrolide with an embedded 2-hydroxypyran moiety at the C3 – C7 segment. In addition to the unusual sugar residue, which was assigned as 4-amino-4,6-dideoxy-3-C-2-*O*-dimethyl- $\alpha$ -talopyranosyl, callipeltoside A also contains the hydrophobic side chain constructed by a structurally unique chlorocyclopropyl dienyne moiety. Other callipeltoside variants, such as callipeltosides B **1.8** and C **1.9**, have been isolated also from the same marine sponge species, and interestingly, the carbohydrate moieties of callipeltosides B and C were assigned in opposite enantiomeric series to that found on callipeltoside A.<sup>18</sup> Recently, MacMillan and co-workers found that this stereochemical assignment was found incorrect through total synthesis and subsequently revised its structure to **1.10**.<sup>19</sup> Despite the fact that callipeltosides are secondary metabolites of a marine sponge, their biogenesis may be classified as cyanobacterial. Given that cyanobacteria are known to coexist in an endosymbiotic relationship with marine sponges, the profound structural



resemblance of callipeltosides to lyngbyaloside B **1.5** and lyngbouilloside **1.6**, macrolides directly produced by cyanobacteria, significantly support this hypothesis.

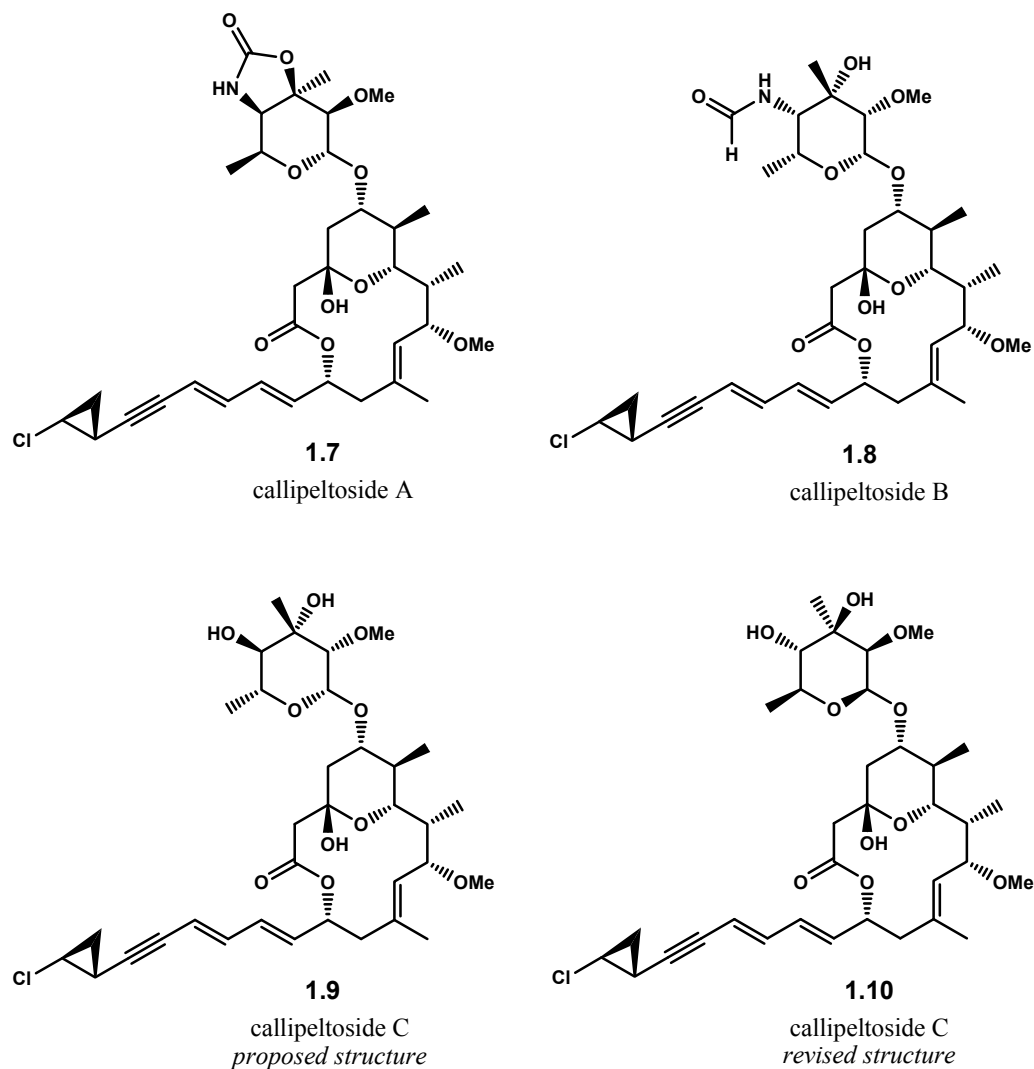


**Figure 1.4**

Due to the structural complexity and interesting biological activities of callipeltoside A **1.7**, the natural product has become a popular target among synthetic chemists. Numerous strategies to access a variety of callipeltoside A synthetic fragments

have been reported.<sup>20-29</sup> Furthermore, the total synthesis of this molecule has been achieved by several research groups, including those of Paterson,<sup>30, 31</sup> Trost,<sup>32-34</sup> Evans,<sup>35, 36</sup> Panek,<sup>37</sup> and Marshall.<sup>38</sup> Their synthetic endeavors are highlighted in reviews recently published by Kalesse<sup>39</sup> and Paterson,<sup>40</sup> and thus further discussion will not ensue.

### 1.7. Macrolides from Marine Sponge *Phorbas* sp.

In a report published in 2007, Molinski and co-workers reexamined the minor fractions of their previously extracted marine sponge *Phorbas* sp., which was harvested near Muiron Island, Western Australia, in 1993.<sup>41</sup> This investigation led to the discovery of phorbasides A – E **1.11** – **1.12** which were isolated in 1.29 mg, 1.30 mg, 1.40 mg, 0.78 mg, and 0.84 mg respectively from 236 grams of the dried specimen.<sup>42, 43</sup> The phorbasides appear to be structural homologues of callipeltosides **1.7** – **1.10**, as these natural products feature a 14-membered macrolactone ring elaborated with the requisite 2-hydroxypyran moiety residing in the C3 – C7 segment as well as the chlorocyclopropyl dienyne hydrophobic side residue, Figure 1.5. However, the differences between the aglycon of phorbasides and that of callipeltosides are apparent. In addition to the C2 methylation, which is absent in callipeltosides, phorbasides are distinguished by the stereochemistry of the chlorocyclopropane group, which is opposite to that of callipeltosides.

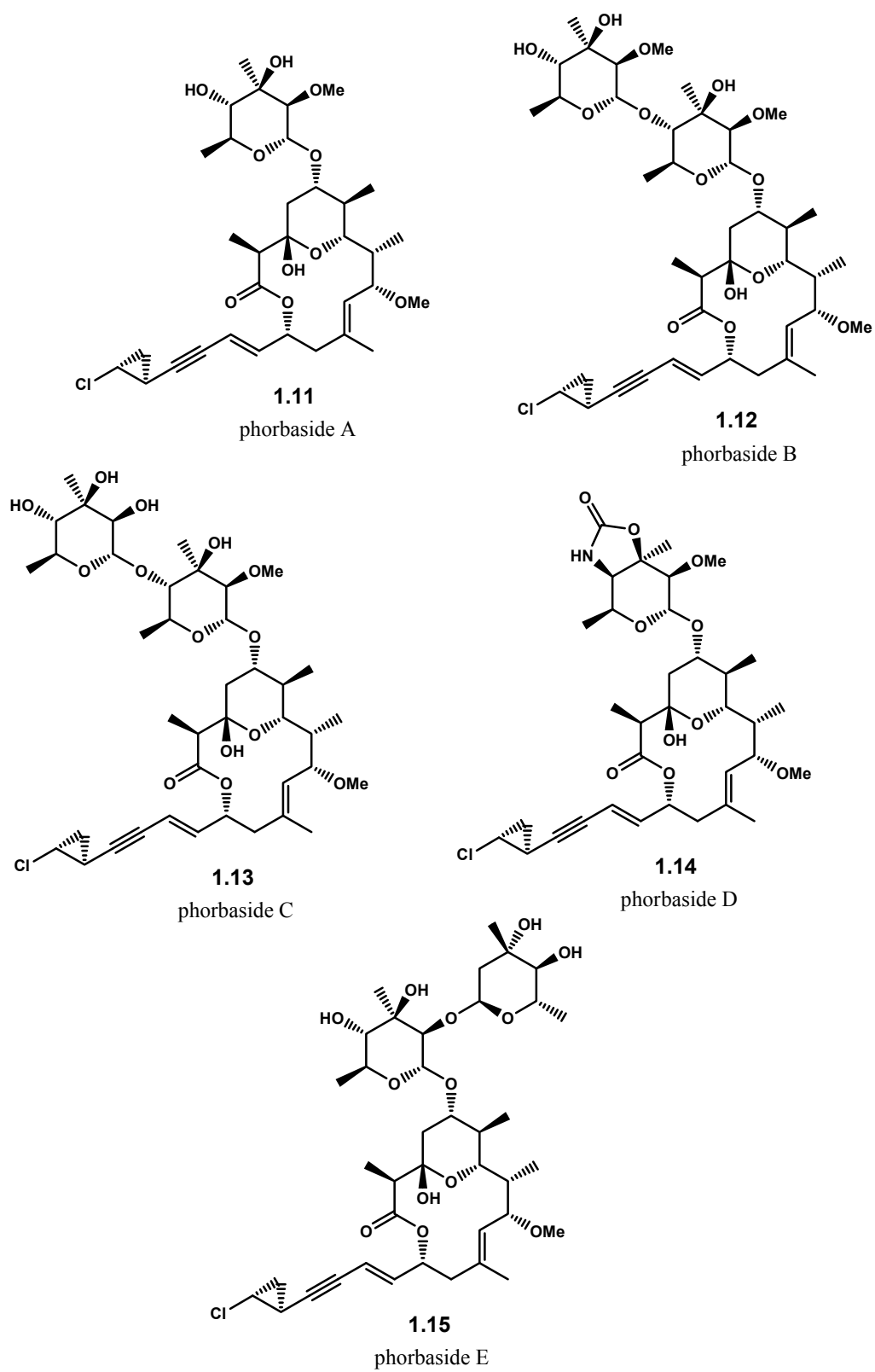


**Figure 1.5**

Phorbasides exhibit moderate to potent cytotoxicity against cultured human colon cancer HCT-116 cells. Phorbaside C appears the most potent with an  $IC_{50}$  value of 2.0  $\mu$ M. Phorbaside E is somewhat less active ( $IC_{50}$  = 10.2  $\mu$ M), and phorbasides A and D are substantially less active with  $IC_{50}$  values of 30 and 61.9  $\mu$ M respectively. Efforts towards the total syntheses of phorbasides have not yet appeared in any published articles at the time this thesis was submitted.

### **1.8. Macrolides from Sea Hare *Dolabella auricularia***

The next series of natural products structurally satisfy the research parameters are macrolide glycosides aurisides A **1.16** and B **1.17**<sup>44</sup> and dolastatin 19 **1.18**.<sup>45</sup> These polyketides are secondary metabolites extracted from Japanese sea hare *Dolabella auricularia*. In addition to the C3 – C7 hemiketalpyran moiety embedded within the 14-membered macrolide ring and their respective sugar residues, aurisides A and B as well as dolastatin 19 contain a structurally unique pendant hydrophobic bromine-substituted conjugated diene moiety. In fact, these compounds seem to be structural analogs of lyngbyalose B **1.5** and lyngbouillose **1.6**, which strongly suggests their cyanobacterial origin, most likely from the dietary intake of the marine invertebrate.

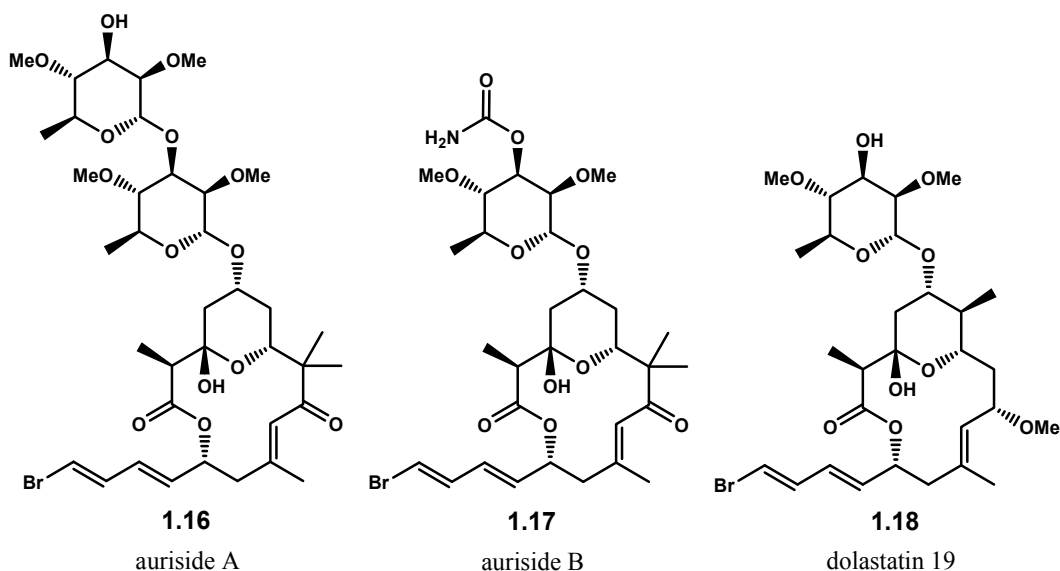


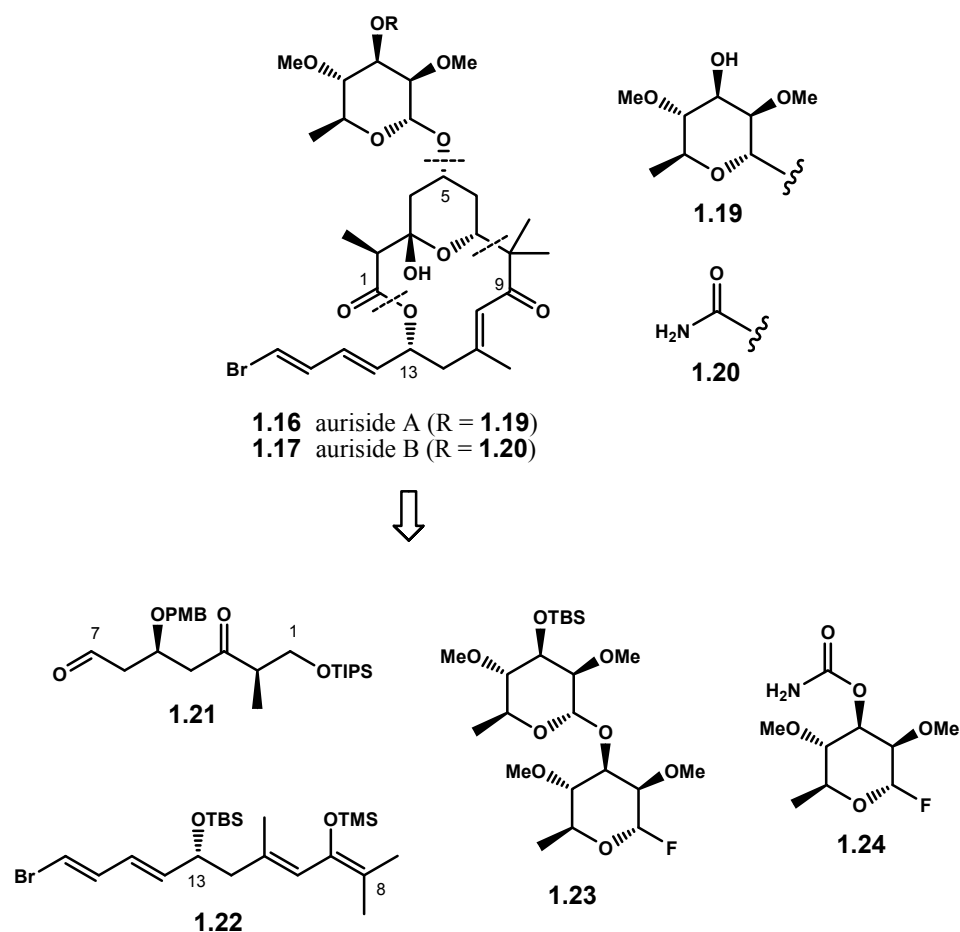
**Figure 1.6**

### 1.8.1. Aurisides A and B

The isolation of aurisides A **1.16** and B **1.17** was reported by Yamada and co-workers in 1996.<sup>44</sup> Aurisides A and B were isolated as amorphous solids in 0.8 mg and 0.7 mg respectively from 138 kg of the internal organs harvested from 278 kg of Japanese sea hare *D. auricularia* collected in Mie Prefecture, Japan. The biological evaluations of these natural products indicated cytotoxicity against HeLa S<sub>3</sub> cervical cancer cells with IC<sub>50</sub> values of 0.17 and 1.2 µg/mL, respectively. Due to their interesting biological properties and extremely low natural abundance, aurisides have aroused significant interests among the synthetic community. Two total syntheses of the natural products have been reported independently by Paterson<sup>46</sup> and Yamada.<sup>47, 48</sup> Furthermore, Olivo and co-workers also have reported their efforts towards the construction of aurisides synthetic fragments<sup>22, 49, 50</sup> and more recently the macrolactone of auriside.<sup>51</sup>

#### 1.8.1.1. Paterson's Approach

Despite the fact that Yamada and co-workers reported the total synthesis of the aurisides aglycon in 1998,<sup>48</sup> the total syntheses of aurisides A and B did not appear in literature until 2005 when Paterson and co-workers published their convergent approach to these natural products.<sup>46</sup> Scheme 1.1 demonstrates the retrosynthesis undertaken by the Paterson group. As depicted, the bond disconnections would provide three synthetic fragments: aldehyde **1.21**, enol silane **1.22**, and fluorosugars **1.23** and **1.24** respectively for aurisides A and B. A Mukaiyama aldol reaction was envisioned to bring together these fragments and thereby set up the C7 – C8 connectivity. Late stage macrolactonization and glycosylation reactions then would complete the synthesis.

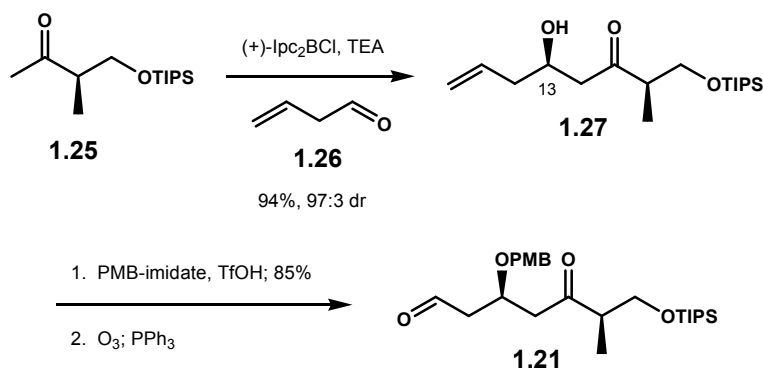


Scheme 1.1

#### 1.8.1.1.1. Preparation of Aldehyde 1.21

The synthesis of aldehyde **1.21** commenced with a boron-mediated aldol reaction between methyl ketone **1.25**<sup>52</sup> and aldehyde **1.26**. Soft enolization of readily accessible ketone **1.25** with chiral isopinocampheyl (Ipc)-based boron reagent followed by addition of freshly prepared aldehyde **1.26** furnished  $\beta$ -hydroxy ketone **1.27** in 94% yield almost as a single diastereomer.<sup>53, 54</sup> The newly generated C13 hydroxyl was then protected as a

PMB ether,<sup>55</sup> and subsequent ozonolysis treatment oxidatively cleaved the terminal olefin to complete the short synthetic sequence to aldehyde **1.21**, Scheme 1.2.



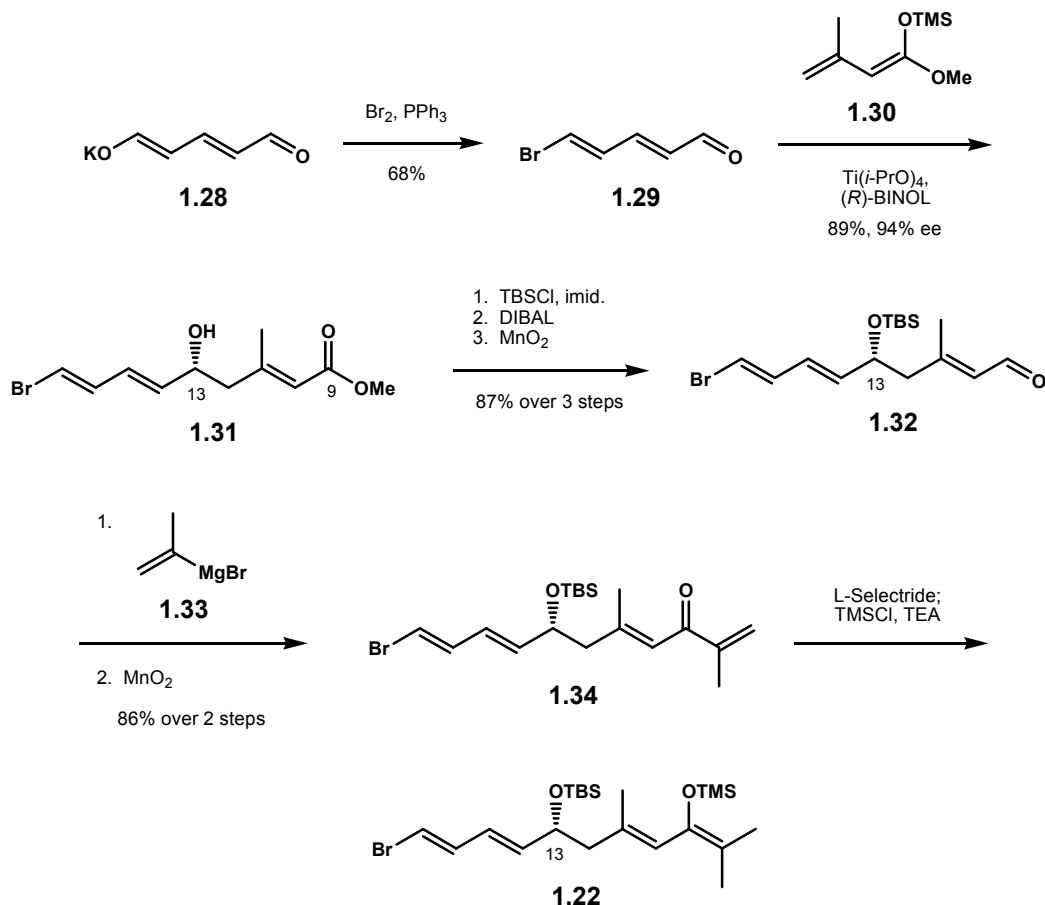
**Scheme 1.2**

#### 1.8.1.1.2. Preparation of Enol Silane **1.22**

Scheme 1.3 lays out an efficient route for the production of enol silane fragment **1.22**. Bromination of potassium glutaconaldehyde<sup>56</sup> **1.28** according to the method of Duhamel provided bromodienal **1.29** in 68% yield.<sup>57, 58</sup> The ensuing asymmetric vinylogous Mukaiyama aldol reaction with ketene acetal **1.30**, promoted by Ti(IV)-(R)-BINOL complex,<sup>59, 60</sup> successfully introduced the C9 – C12 carbon framework and simultaneously installed the requisite C13 stereocenter as shown in adduct **1.31**. Silylation of the C13 hydroxyl group as a TBS ether, ester reduction with DIBAL, and allylic alcohol oxidation sequentially produced enal **1.32**. Following addition of isopropenyl magnesium bromide to this aldehyde, the resulting allylic alcohol was then oxidized with MnO<sub>2</sub> to enone **1.34**. Interestingly, exposure of enone **1.34** to L-selectride led to regioselective 1,4-reduction at the sterically less encumbered site. The *in situ*



trapping of the corresponding lithium enolate with a mixture of TMSCl and TEA provided the target enol silane **1.22**, which was immediately used in the next step without further purification.

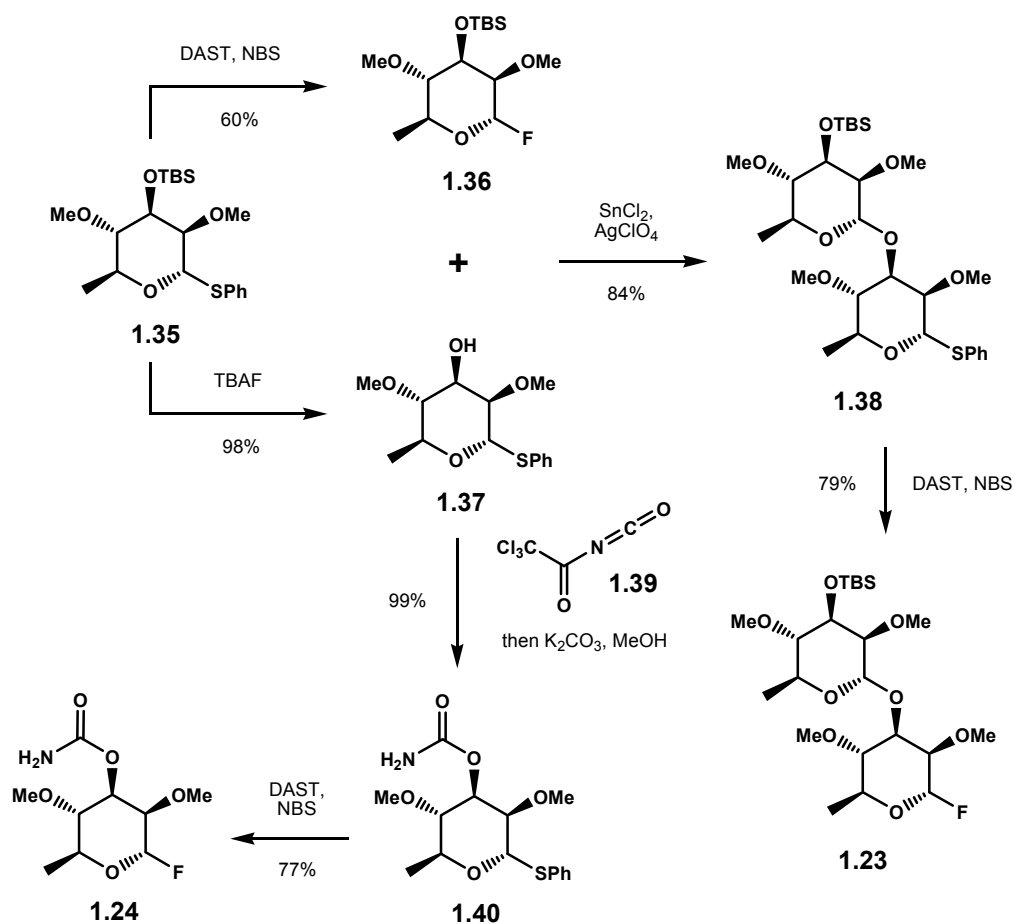


Scheme 1.3

#### 1.8.1.1.3. Preparation of Fluorosugars **1.23** and **1.24**

For the preparation of pendant fluorosugar coupling fragments **1.23** and **1.24** respectively for aurisides A **1.16** and B **1.17**, Paterson envisioned a convergent approach from thiosugar **1.35**, readily accessible in nine steps from *L*-rhamnose.<sup>61</sup> Formation of

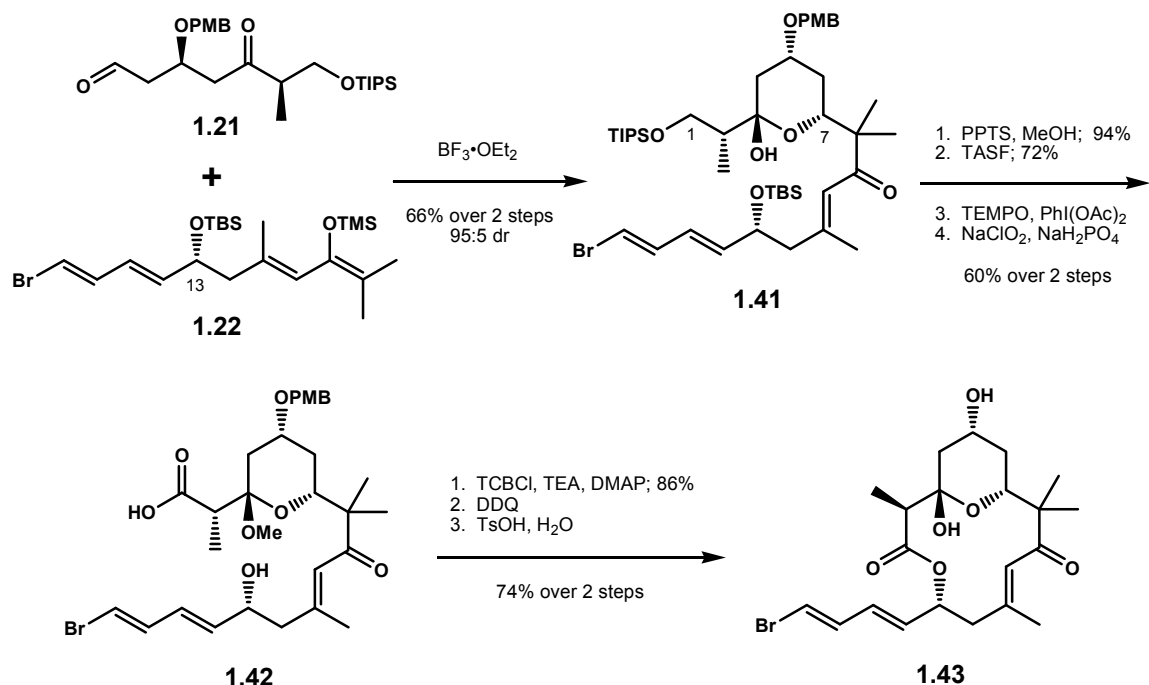
disaccharide **1.23** began with independent exposure of thiosugar **1.35** with DAST in the presence of NBS or TBAF to respectively yield fluorosugar **1.36** and thiosugar **1.37**.<sup>62</sup> Mukaiyama glycosylation of these two sugars, promoted by  $\text{SnCl}_2$  and  $\text{AgClO}_4$ , afforded thiodisaccharide **1.38**,<sup>63</sup> which was fluorinated under the DAST – NBS conditions to the target fluorosugar fragment **1.23**. Treatment of thiosugar **1.37** with isocyanate **1.39** followed by basic methanolysis installed the requisite carbamate moiety **1.40**.<sup>64</sup> Transformation to fluorosugar **1.24** readily took place in a respectable yield once again under the DAST – NBS conditions, Scheme 1.4.



Scheme 1.4

#### 1.8.1.1.4. Construction of Aurisides Aglycon

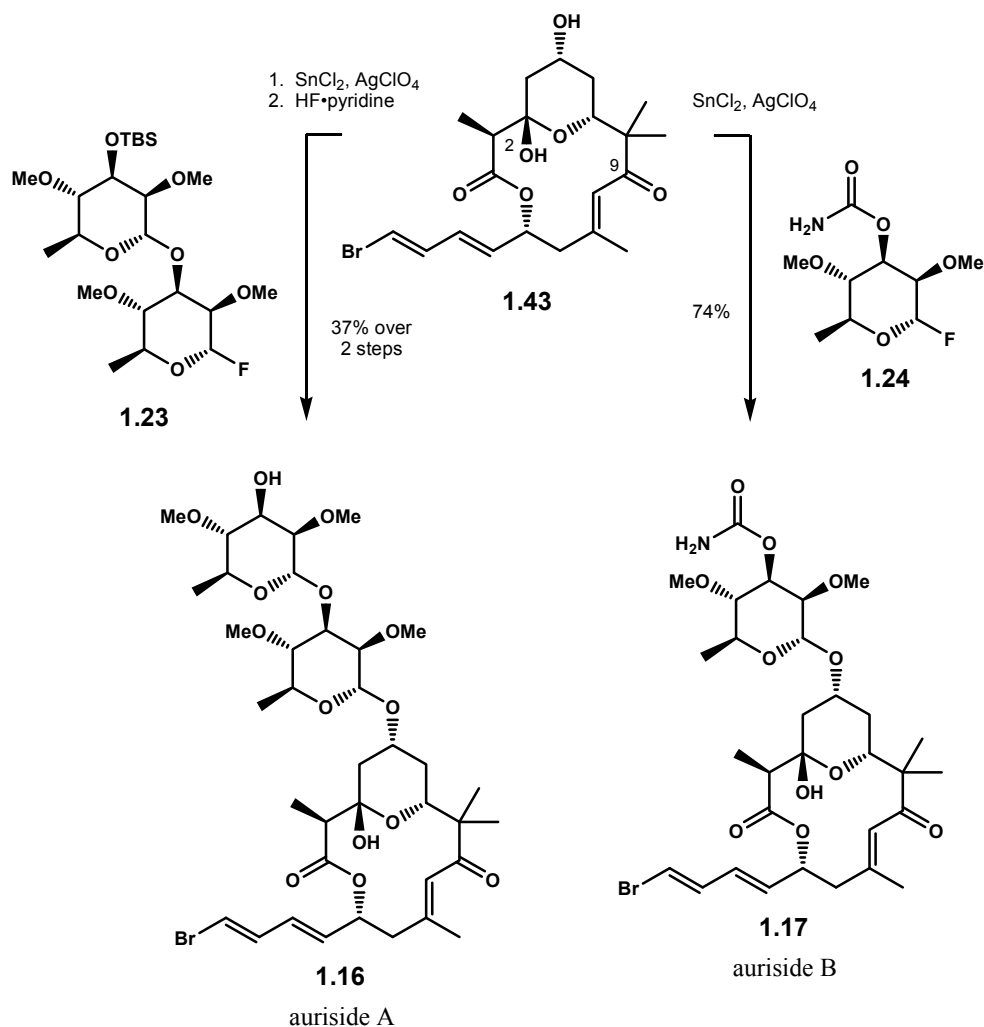
The construction of aurisides aglycon began with a Mukaiyama aldol reaction between aldehyde **1.21** and enol silane **1.22**. Promoted by  $\text{BF}_3 \cdot \text{OEt}_2$ , the aldol product was produced as hemiketalpyran **1.41** in 66% yield with diastereoselectivity of 95:5. The newly generated C7 stereochemistry relied on 1,3-*anti* induction from the C5 PMB ether through an open transition state known as the Evans polar model.<sup>65</sup> Treatment of **1.41** with PPTS and MeOH cleanly introduced the corresponding methyl pyranoside. Sequential removal of the TIPS ether with TASF<sup>66</sup> followed by two-step oxidation<sup>67, 68</sup> of the primary alcohol to the acid furnished macrolactonization precursor **1.42**. Under the Yamaguchi conditions,<sup>69</sup> the corresponding macrolide was affected in 86% yield. Cleavage of the PMB ether with DDQ followed by acidic hydrolysis of the methyl pyranoside to the corresponding hemiketalpyran then completed the synthetic sequence to aurisides macrolide core **1.43**.



Scheme 1.5

#### 1.8.1.1.5. Mukaiyama Glycosylation to Aurisides A and B

To complete the total syntheses of aurisides A **1.16** and B **1.17**, fluorosugars **1.23** and **1.24** were independently introduced to aurisides aglycon **1.43**. Under the established Mukaiyama conditions,<sup>63</sup> glycosylation of **1.43** with **1.23** followed by deprotection of the remaining TBS ether provided auriside A in 37% over 2 steps; whereas with fluorosugar **1.24**, auriside B was successfully produced in 74% yield.

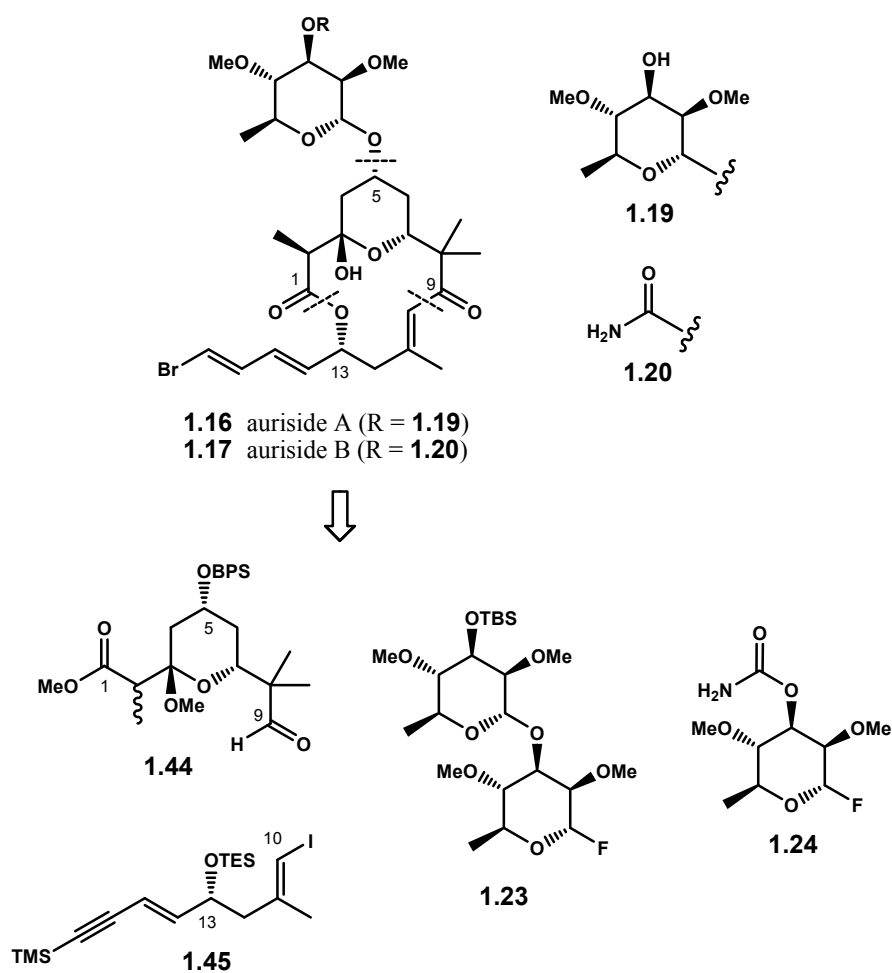


**Scheme 1.6**

### 1.8.1.2. Yamada's Approach

Immediately upon their successful isolation and characterization of aurisides A **1.16** and B **1.17**,<sup>44</sup> Yamada and co-workers undertook a total synthesis venture to these natural products in order to bring more materials for further biological assays. The communication of this project appeared in 1998,<sup>48</sup> and their successful second generation synthesis was published in 2006.<sup>47</sup> As depicted in Scheme 1.7, the retrosynthesis of

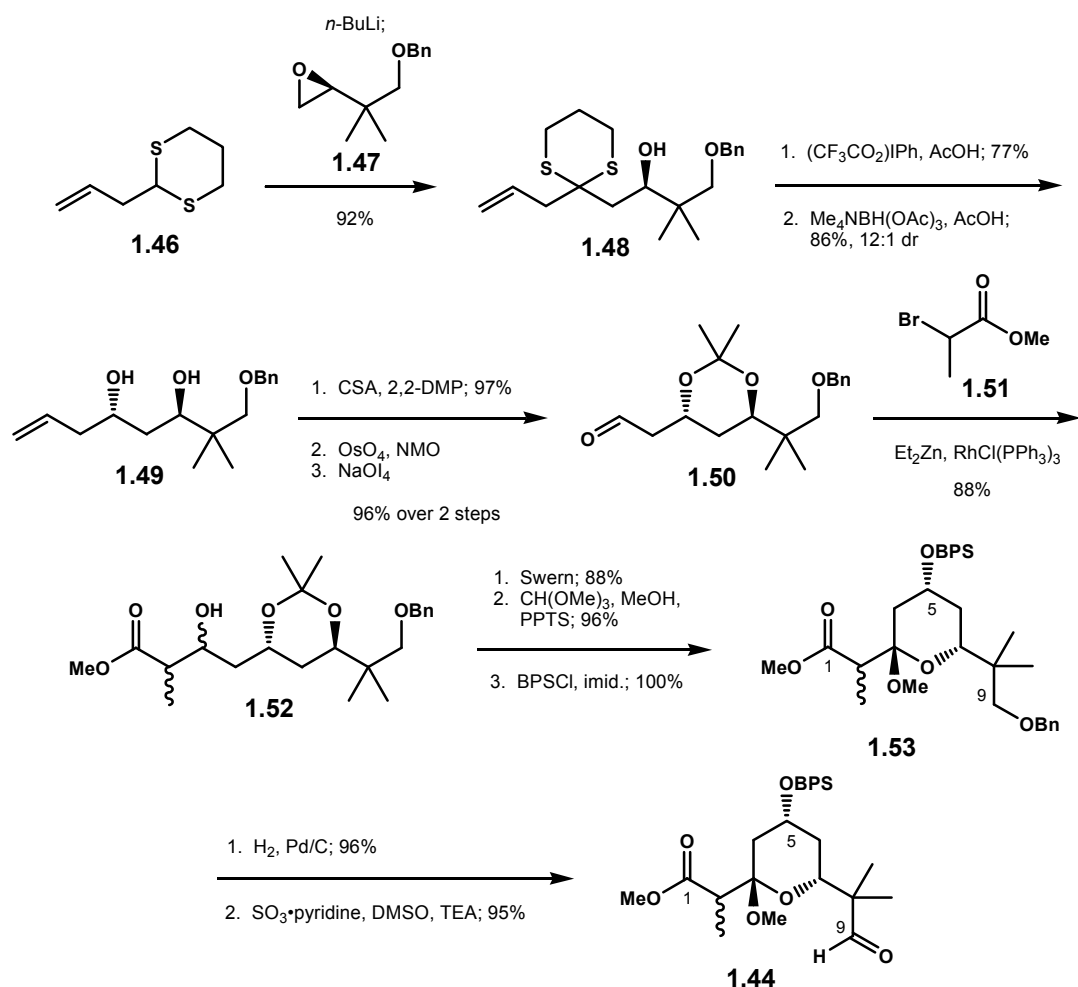
aurisides as described by Yamada involved bond disconnections which resulted in three synthetic components with equal complexity: aldehyde **1.44**, vinyl iodide **1.45**, and fluorosugars **1.23** for auriside A and **1.24** for auriside B. Aldehyde **1.44** and vinyl iodide **1.45** were assembled using the Nozaki-Hiyama-Kishi (NHK) reaction. Following Yamaguchi macrolactonization, fluorosugars **1.23** or **1.24** were incorporated by the method of Mukaiyama.



Scheme 1.7

#### 1.8.1.2.1. Preparation of Aldehyde 1.44

Yamada's route to aldehyde **1.44** began with an alkylation reaction of lithium carbanion generated from allyldithiane **1.46** with readily accessible epoxide **1.47**<sup>70</sup> to produce alcohol **1.48**. Removal of the dithiane moiety<sup>71</sup> followed by reduction of the resulting  $\beta$ -hydroxy ketone under Evans' protocol<sup>72</sup> furnished 1,3-*anti* diol **1.49** in 86% yield with diastereoselectivity of 12:1. Sequential acetonide formation and oxidative cleavage of the terminal olefin with the OsO<sub>4</sub> – NaIO<sub>4</sub> method afforded aldehyde **1.50**, which upon exposure to a rhodium-catalyzed Reformatsky-type reaction with methyl 2-bromopropionate **1.51** yielded aldol product **1.52** as a mixture of diastereomers.<sup>73</sup> Swern oxidation,<sup>74</sup> acid-catalyzed acetonide fragmentation and pyran cyclization, and protection of C5 hydroxyl as a BPS ether provided methyl pyranoside **1.53**. Subsequent transformation to aldehyde **1.44** was achieved via sequential hydrogenolysis of the C9 benzyl ether and Parikh-Doering oxidation of the resulting primary alcohol, Scheme 1.8.



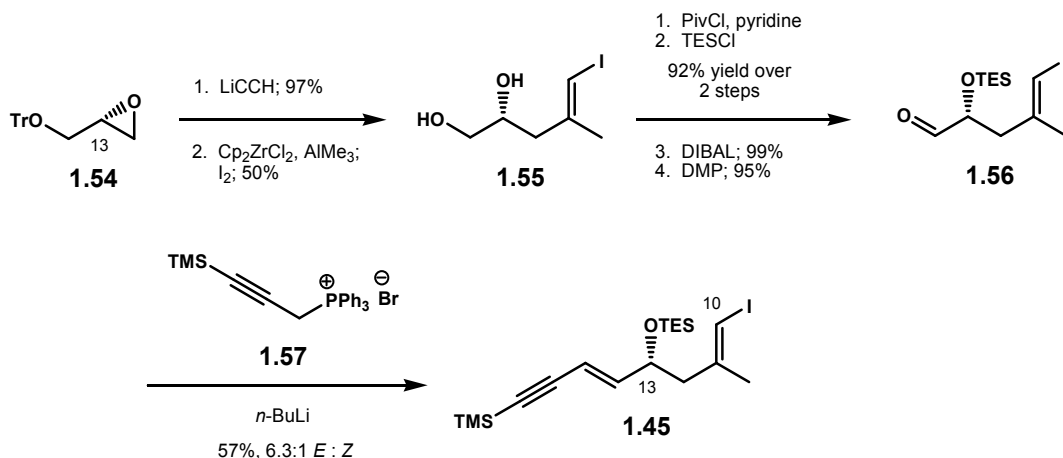
**Scheme 1.8**

#### 1.8.1.2.2. Preparation of Vinyl Iodide **1.45**

As shown in 1.9, the synthesis of vinyl iodide fragment **1.45** began with addition of lithium acetylide to (*R*)-glycidyl trityl ether **1.54**. Carbometallation of the corresponding terminal acetylene with a mixture of  $\text{Cp}_2\text{ZrCl}_2$  and  $\text{AlMe}_3$  followed by iodine quench gave rise to the requisite vinyl iodide functionality.<sup>75</sup> Under these reaction conditions, the trityl protecting group was also readily cleaved, which unmasked diol **1.55**. Selective protecting group manipulation successfully furnished the C13 TES ether,



and the ensuing Dess-Martin oxidation yielded aldehyde **1.56**. Wittig olefination of the resulting aldehyde with phosphorane **1.57** provided the desired fragment **1.45**.



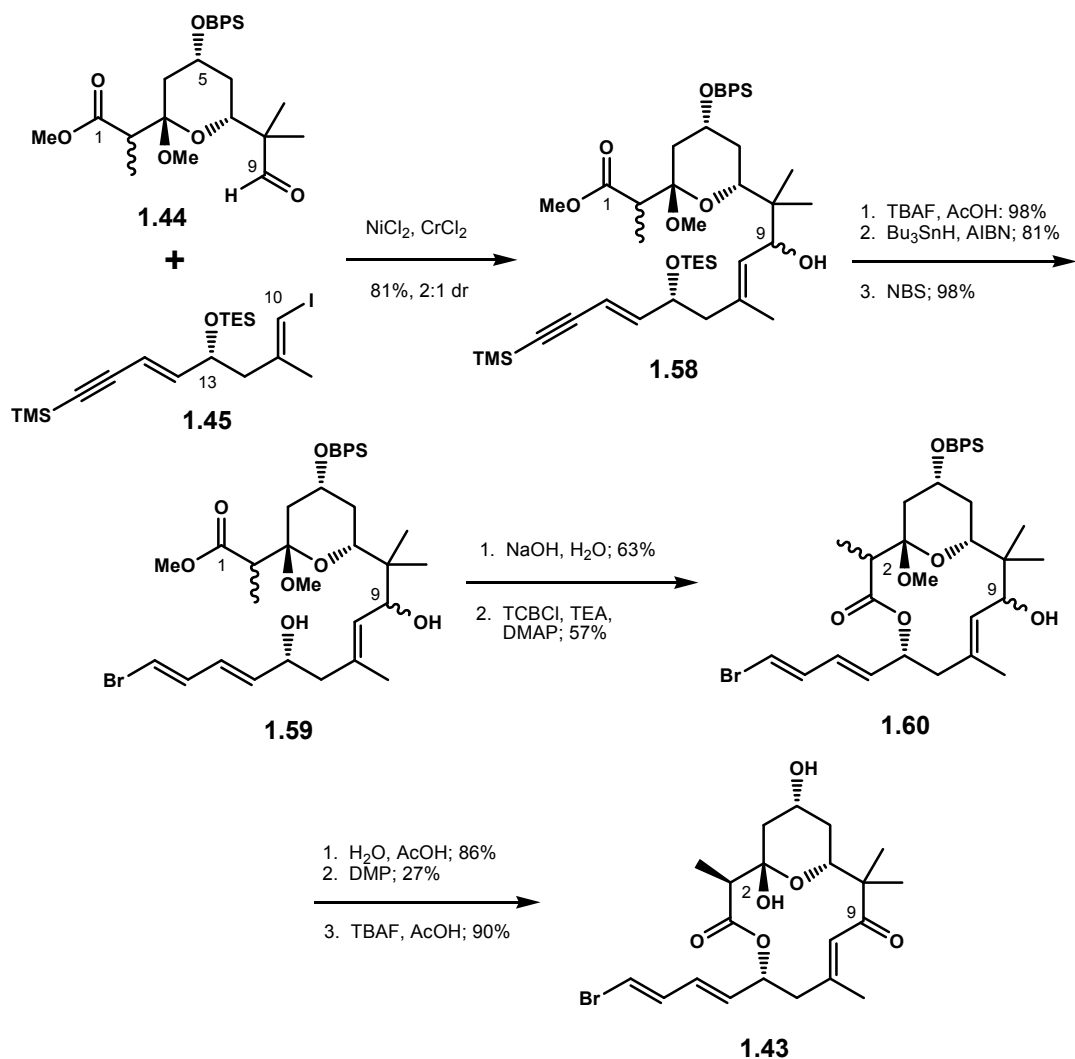
Scheme 1.9

#### 1.8.1.2.3. Construction of Aurisides Aglycon

The endgame strategy to aurisides was realized by the NHK coupling of aldehyde **1.44** to vinyl iodide **1.45** which afforded allylic alcohol **1.58** as inseparable 2:1 mixture of diastereomers at the newly generated C9 stereocenter.<sup>76, 77</sup> Removal of the TES ether and the TMS acetylene under buffered TBAF conditions, followed by chemoselective hydrostannylation<sup>78</sup> and bromination installed the vinyl bromide portion, as shown in structure **1.59**. Upon basic saponification, the macrolactonization was affected by the Yamaguchi method to give macrolide **1.60**,<sup>69</sup> Scheme 1.10.

Acid-promoted hydrolysis of the methyl pyranoside moiety, followed by oxidation of the C9 alcohol generated the corresponding enone. At this point, the C2 diastereomers were separable by chromatography, and the desired 2*S* stereoisomer was

successfully isolated in 27% yield. Finally, removal of the C5 BPS ether upon treatment with a mixture of acetic acid and TBAF liberated the macrolide core of aurisides **1.43**.

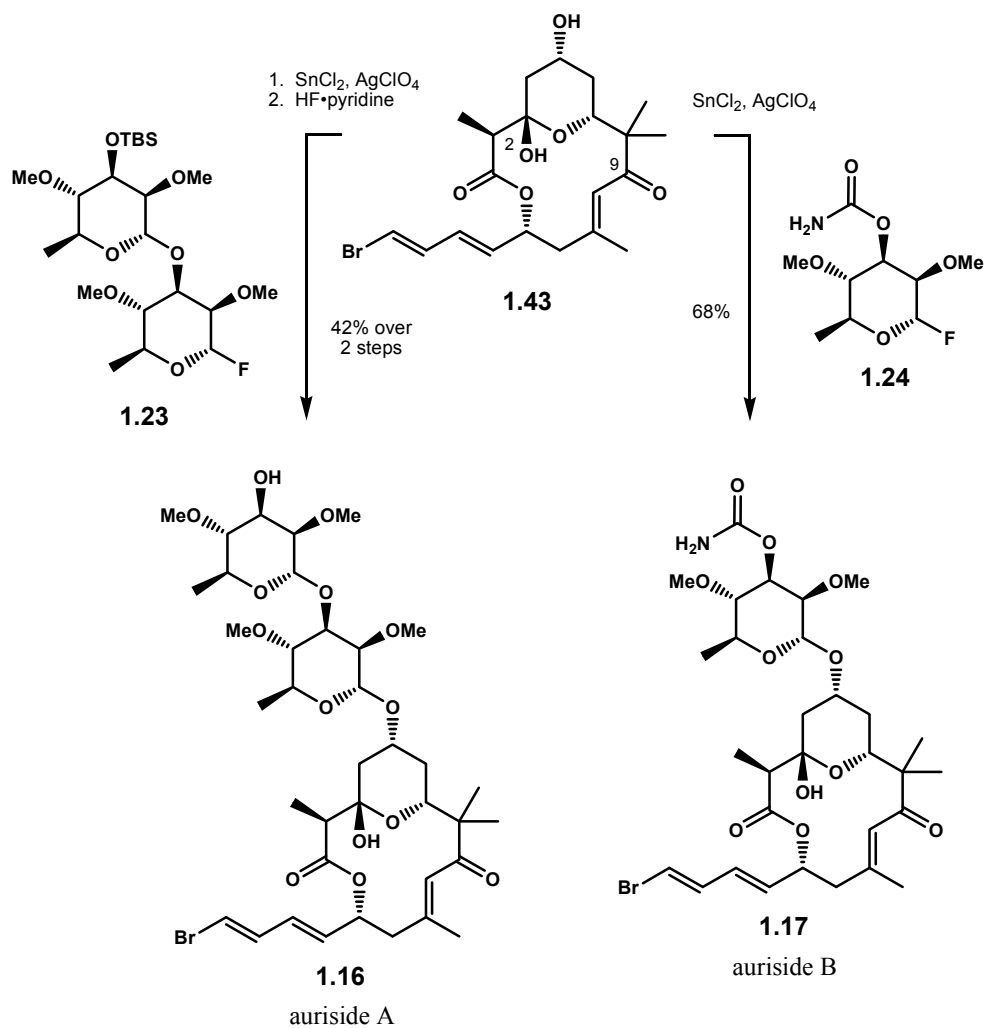


**Scheme 1.10**

#### 1.8.1.2.4. Mukaiyama Glycosylation to Aurisides A and B

As shown in Scheme 1.11, installation of the sugar residues then completed the total syntheses of the aurisides. The glycosylation reaction of aurisides aglycon **1.43**

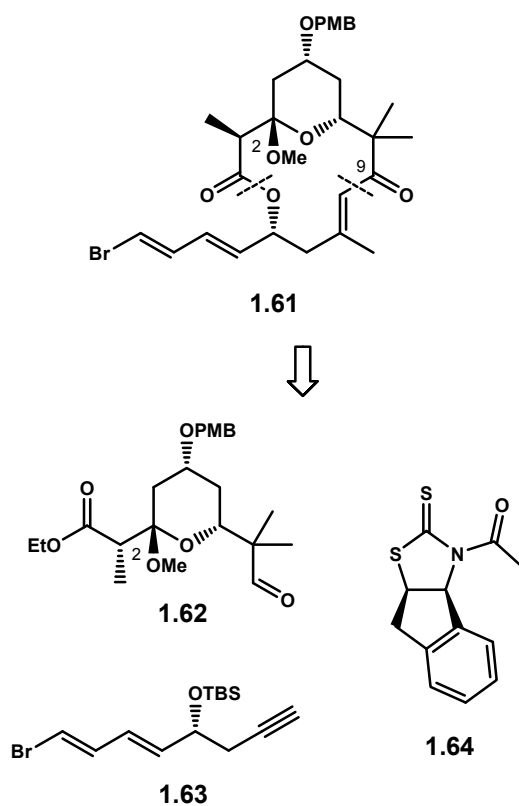
with fluorosugars **1.23** and **1.24** under the established Mukaiyama's protocol<sup>63</sup> followed by relevant TBS deprotection furnished respectively aurisides A **1.16** and B **1.17** in similar yields to those reported by Paterson.<sup>46</sup>



**Scheme 1.11**

### 1.8.1.3. Olivo's Approach

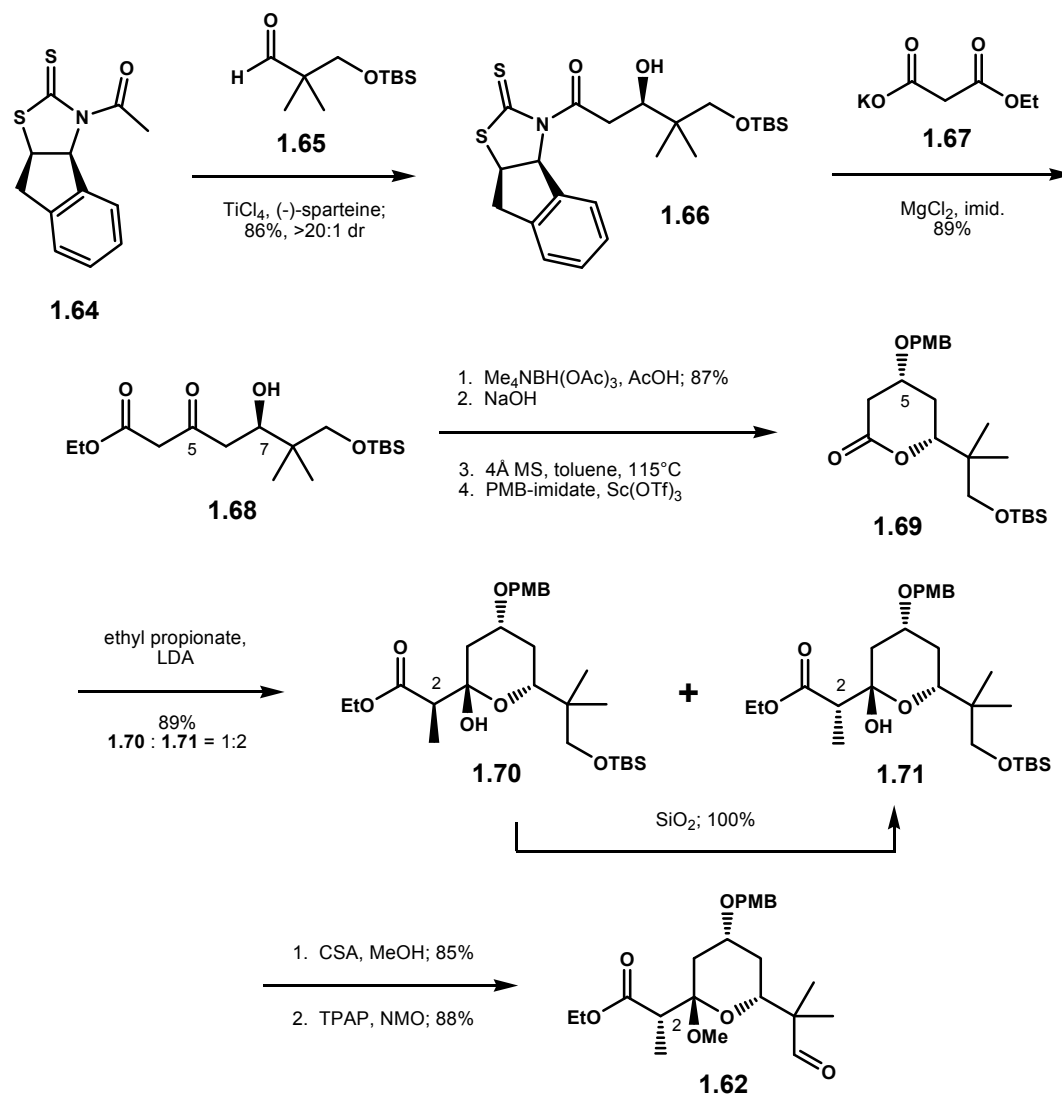
Olivo and co-workers recently published their efforts for the construction of auriside aglycon **1.61** previously utilized in Paterson's synthesis. As shown in Scheme 1.12, auriside aglycon **1.61** was constructed from two major synthetic fragments: aldehyde **1.62** and acetylene **1.63**. Their synthesis was highlighted by the utilization of a new class of highly versatile chiral auxiliary **1.64** particularly in asymmetric acetate aldol reactions.<sup>79</sup>



Scheme 1.12

#### 1.8.1.3.1. Construction of Methyl Pyranoside **1.62**

The synthesis of auriside aglycon **1.61** described by Olivo and Tello-Aburto began with the construction of methyl pyranoside **1.62**. As shown in Scheme 1.13, the reaction between indene-based thiazolidinethione **1.64** and aldehyde **1.65** under Crimmins conditions<sup>80-83</sup> afforded asymmetric aldol adduct **1.66** in 86% yield as a single diastereomer.<sup>79</sup> Displacement of the chiral auxiliary with potassium ethyl malonate gave direct access to  $\beta$ -ketoester **1.68**.<sup>84</sup> Sequential Evans 1,3-*anti* reduction,<sup>72</sup> which introduced the C5 stereochemistry, saponification, cyclization, and protection of C5 hydroxyl as a PMB ether<sup>85</sup> provided lactone **1.69**. Exposure to Meinwald reaction with ethyl propionate provided ethyl ester **1.70** and **1.71** as a separable mixture of diastereomers. The C2 methyl center in **1.70** was then successfully inverted to the desired diastereomer **1.71** in quantitative yield after prolonged exposure to silica gel. The ensuing acidic methanolysis installed the methyl pyranoside functionality and simultaneously cleaved the C9 TBS ether. TPAP-NMO oxidation of the resulting primary alcohol completed the construction of fragment **1.62**.<sup>86</sup>

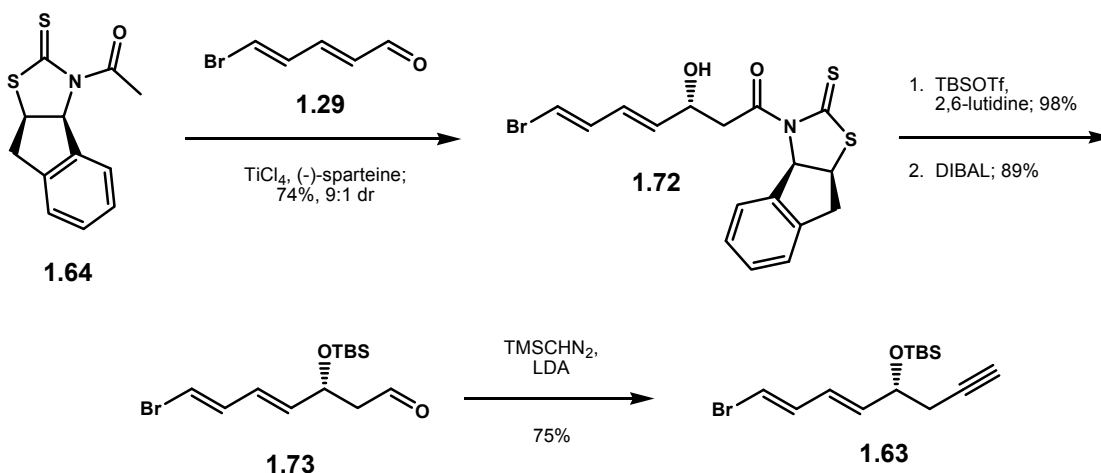


**Scheme 1.13**

#### 1.8.1.3.2. Preparation of Alkyne 1.63

The synthesis of alkyne fragment **1.63** commenced with an asymmetric acetate aldol reaction between aldehyde **1.29** and chiral auxiliary **1.64** which yielded **1.72** in 74% yield with a diastereomeric ratio of 9:1.<sup>79</sup> TBS protection and reductive removal of the

auxiliary afforded aldehyde **1.73**; subsequent alkynylation with TMS-diazomethane provided fragment **1.63**, Scheme 1.14.

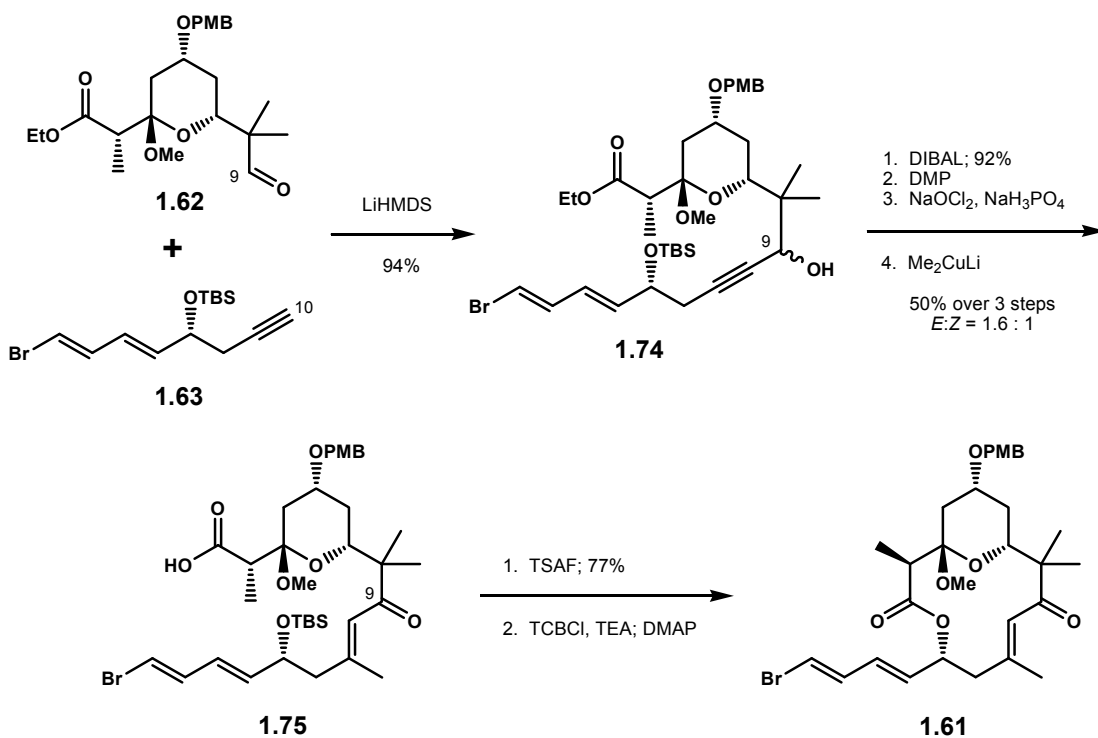


**Scheme 1.14**

#### 1.8.1.3.3. Preparation of Alkyne **1.63**

The successful coupling of fragments **1.62** and **1.63** was achieved upon exposure to LiHMDS. Deprotonation of the acetylene proton provided the corresponding anion which smoothly added to the aldehyde, thereby giving C9 alcohol **1.74** as a mixture of diastereomers. The subsequent ester reduction with DIBAL yielded the corresponding primary alcohol in 92% yield. Exposure to Dess-Martin reagent<sup>87</sup> then readily oxidized the C1 and C9 hydroxy groups to their corresponding carbonyls, and further oxidation of the aldehyde to the carboxylic acid was achieved under using Pinnick conditions.<sup>68</sup> Introduction of the C11 methyl group was affected by a conjugate addition with methylcuprate to yield enone **1.75** as a 1.6 : 1 mixture of olefin isomers. Removal of the

lone TBS ether with TSAF<sup>66</sup> provided the seco acid which was then subjected to the Yamaguchi reaction<sup>69</sup> to give macrolide **1.61**, Scheme 1.15.



Scheme 1.15

### 1.8.2. Dolastatin 19

Dolastatin 19 **1.15** represents another example of cytotoxic macrolide glycoside isolated from a prolific secondary metabolite producer, sea hare *D. auricularia*, this time collected in 1996 from the Gulf of California off the coast of Danzante Island, Mexico. The isolation and the characterization of this natural product was reported by Pettit and co-workers.<sup>45</sup> A mere 0.5 mg of dolastatin 19 was extracted from 600 kg of the harvested marine animal. The *in vitro* biological assays of this marine natural product revealed its



potent activity against two human cancer cell lines with GI<sub>50</sub> values of 0.72 µg/mL for breast MCF-7 and 0.76 µg/mL for colon KM20L2. The extremely low natural abundance necessitated total synthesis of dolastatin 19 for further biological evaluation of this macrolide.

### 1.8.2.1. Structural Revision

Dolastatin 19 was originally assigned as structure **1.76** based on the observed NOE correlations. In addition to the 14-membered ring, dolastatin 19 possesses the requisite C3 – C7 pyran ring and non-oxygenated hydrophobic side chain. These structural features make apparent the similarity between dolastatin 19 and callipeltosides **1.7 – 1.10**,<sup>17, 18</sup> phorbosides **1.11 – 1.15**,<sup>42</sup> and aurisides **1.16 – 1.17**.<sup>44</sup>

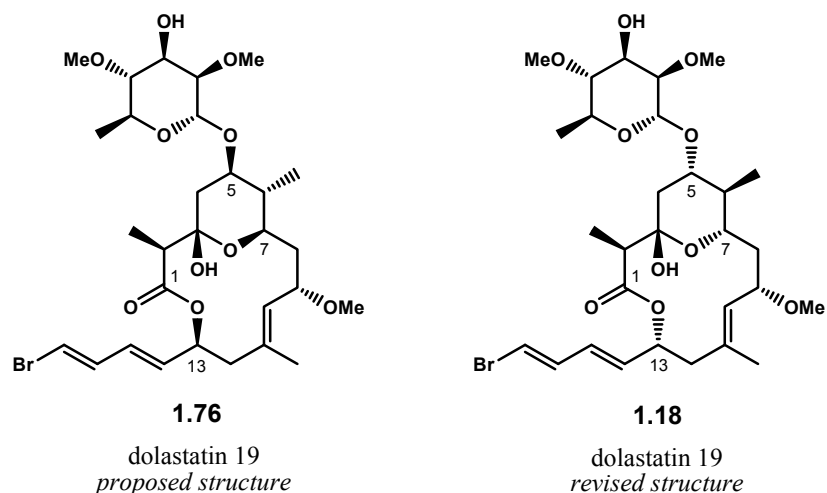


**Figure 1.7**

Further examination of stereochemistry presented in the proposed structure **1.76**, particularly at the C5 – C7 stereotriad and at C13, these four stereogenic centers were assigned opposite to those of callipeltosides, phorbasides, and aurisides. This rather suspicious stereochemical inconsistency is most obvious when these natural products are presented as their corresponding seco acids, Figure 1.8. Paterson argues that the anticipated common cyanobacterial biogenesis of these macrolides suggests that the initial stereochemical assignment proposed by Pettit appears to be incorrect. Based on this assumption and brief conformational analyses,<sup>88</sup> Paterson has proposed a revised structure of dolastatin 19 involving inversion of configuration both at C5 – C7 stereotriad and at the remote C13 hydroxyl leading to seco acid **1.81** and thus a revised structure of dolastatin 19 **1.18**. Total synthesis confirmed revised structure **1.18** and provided justification for Paterson's hypothesis.<sup>88, 89</sup>

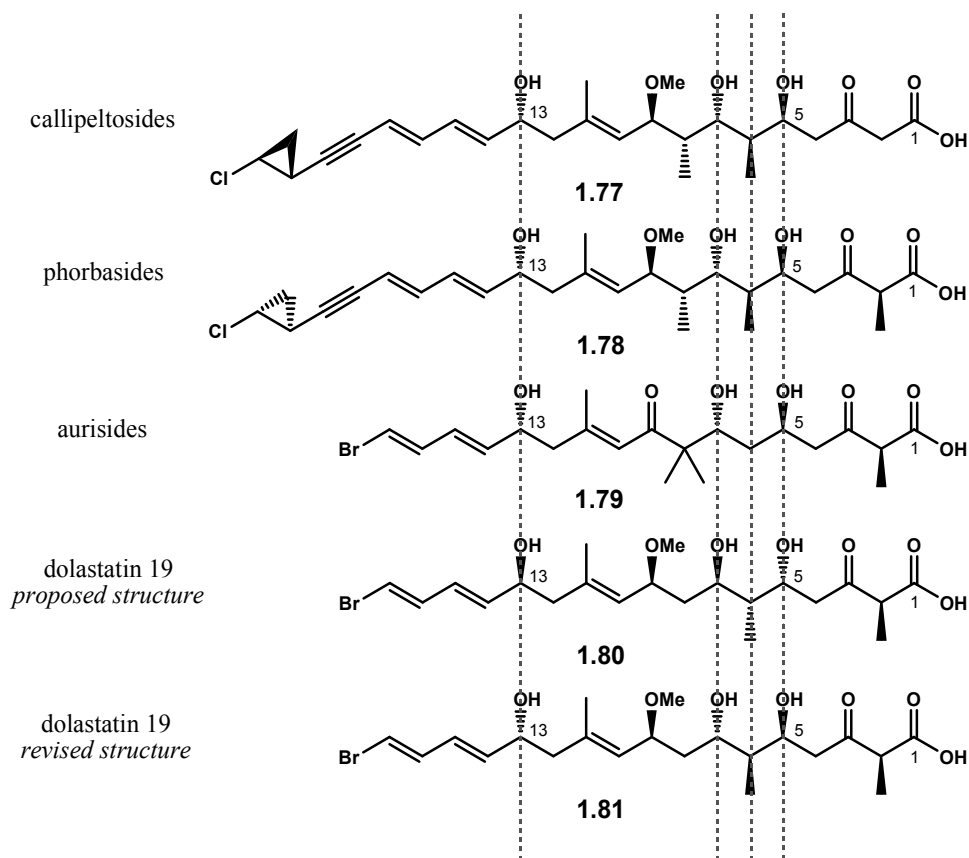
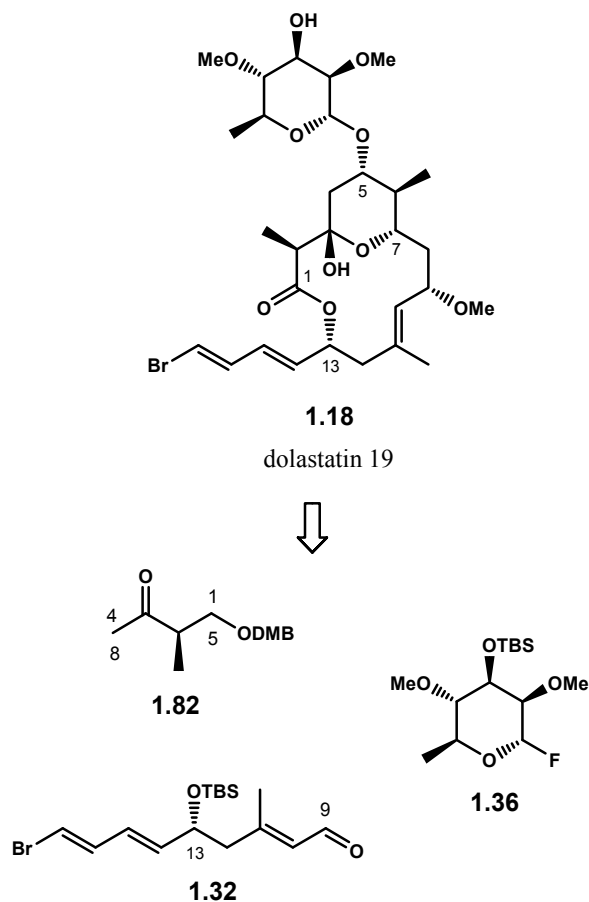


**Figure 1.8**

### 1.8.2.2. Paterson's Approach

Paterson and co-workers reported the first total synthesis of dolastatin 19 **1.18** as a communication in 2006;<sup>89</sup> the full account of their research was published one year later.<sup>88</sup> As shown in Scheme 1.16, Paterson's elegant route to this macrolide was highlighted by bond disconnections into three simple synthetic fragments: aldehyde **1.32**, ketone **1.82**, and fluorosugar **1.36**. The construction of dolastatin 19 aglycon was made accessible through an iterative boron-mediated aldol reactions using ketone **1.82**, which set up the C1 – C14 carbon framework. Following Yamaguchi macrolactonization,

Mukaiyama glycosylation of fluorosugar **1.33** finished the total synthesis of the macrolide glycoside.

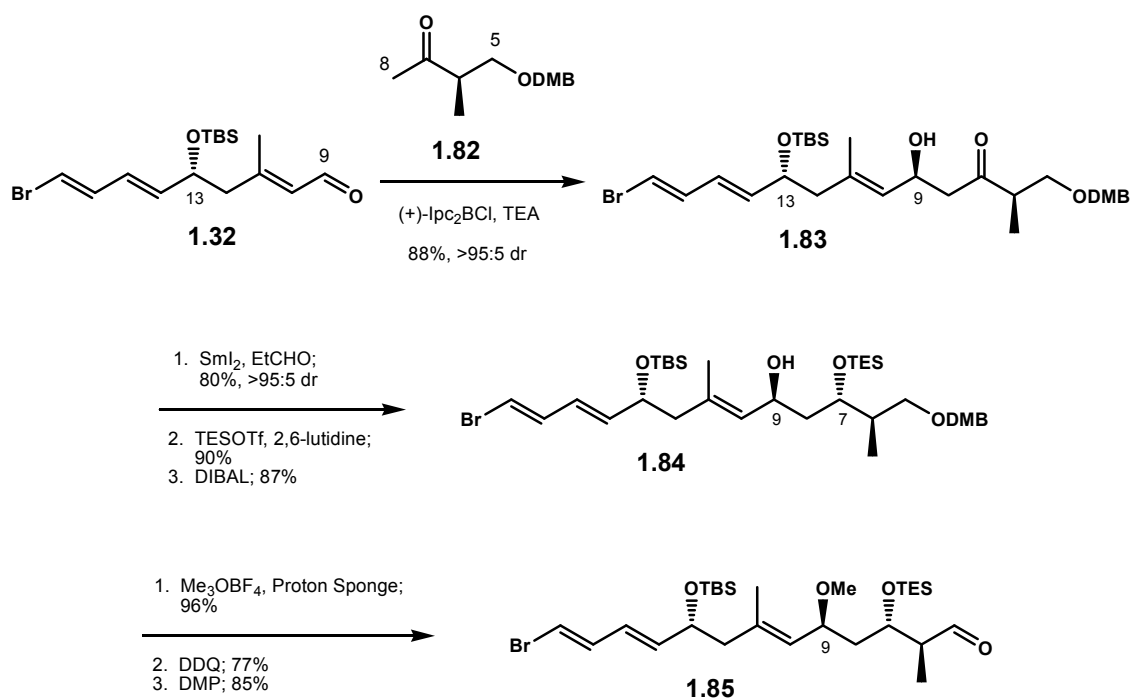


**Scheme 1.16**

#### 1.8.2.2.1. The First Aldol Reaction

The total synthesis of dolastatin 19 began with a chiral boron-mediated aldol reaction<sup>53, 54</sup> between ketone **1.82**<sup>90</sup> and aldehyde **1.32**,<sup>46</sup> the latter of which was previously utilized in the total synthesis of aurisides A **1.16** and B **1.17**. Under the reaction conditions, aldol adduct **1.83** was produced in 88% yield nearly as a single

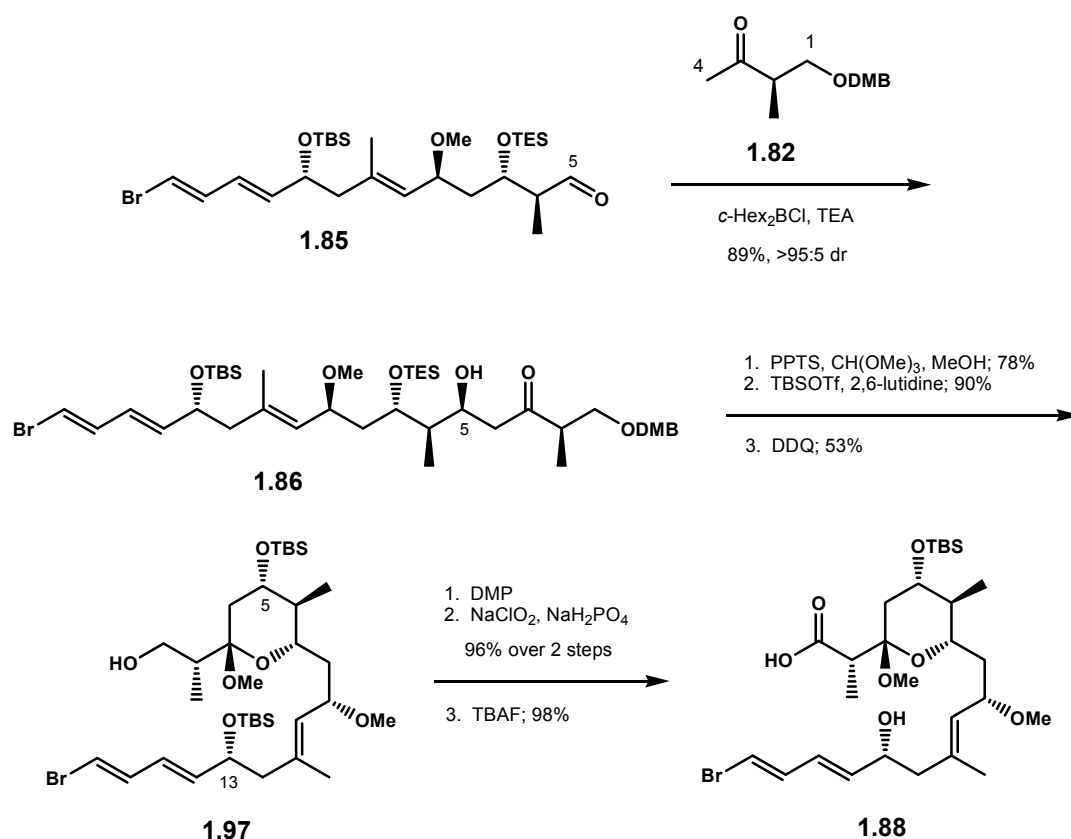
diastereomer. Elaboration of the  $\beta$ -hydroxy ketone moiety to the corresponding C7 – C9 *anti* diol was cleanly affected by the Evans-Tischenko reduction.<sup>91</sup> Protection of the resulting C7 hydroxyl as a TES ether followed by treatment with DIBAL liberated alcohol **1.66**. The C9 methyl ether of dolastatin 19 was then introduced upon exposure to Meerwein's salt and Proton Sponge.<sup>92</sup> Cleavage of the DMB ether with DDQ and subsequent Dess-Martin oxidation furnished aldehyde **1.85**,<sup>87</sup> which was primed for the second aldol reaction, Scheme 1.17.



**Scheme 1.17**

#### 1.8.2.2.2. The Second Aldol Reaction

With aldehyde **1.85** in hand, the focus turned to the second aldol reaction. Enolization of ketone **1.82** with *c*-Hex<sub>2</sub>BCl and TEA followed by addition of aldehyde **1.85** afforded aldol adduct **1.86** in 89% yield with diastereoselectivity of >95:5 based on the predicted Felkin-Anh model. This reaction completed the installation of dolastatin 19 carbon framework. Selective removal of the C7 TES ether under acidic methanolysis formed the corresponding methyl pyranoside. Silylation at C5 hydroxyl as a TBS ether followed by cleavage of DMB ether with DDQ provided complex alcohol **1.87**. Subsequent two-step oxidation<sup>68, 87</sup> of C1 hydroxyl to the carboxylic acid followed by TBAF deprotection of the C13 TBS ether finally furnished macrolactonization precursor **1.88** in good yield, Scheme 1.18.

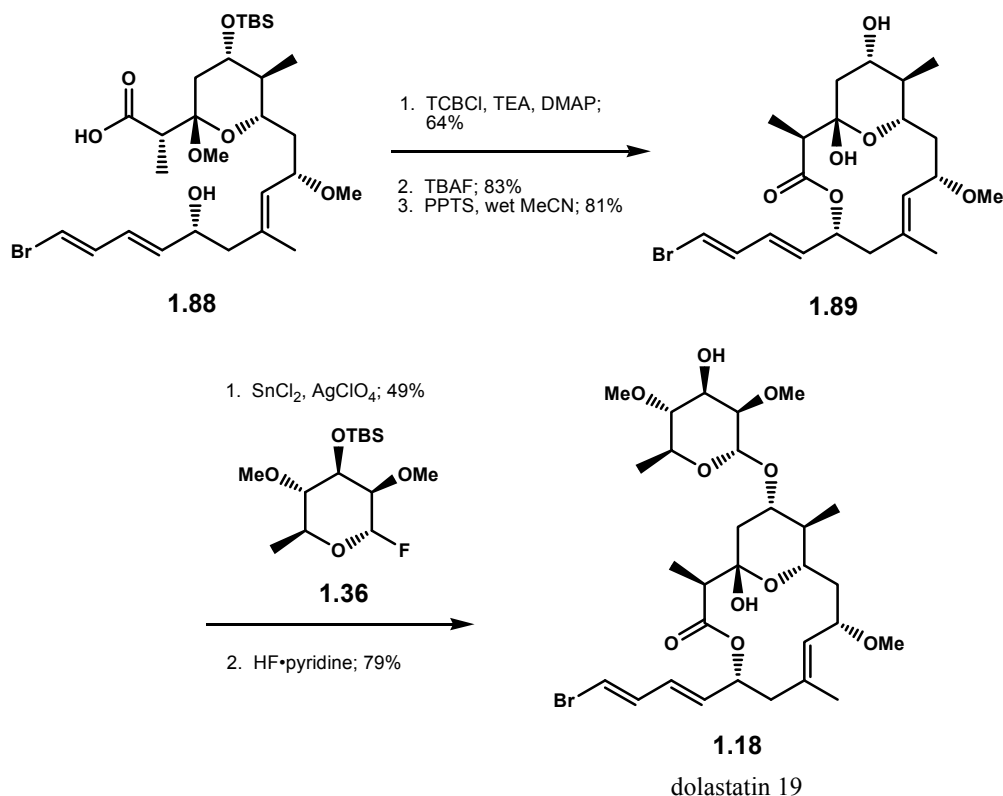


**Scheme 1.18**

### 1.8.2.2.3. Macrolactonization and Glycosylation

As demonstrated in Scheme 1.19, the endgame to dolastatin 19 was fairly straightforward. Exposure of seco acid **1.88** under the Yamaguchi conditions efficiently enclosed the macrolactone ring.<sup>69</sup> Sequential removal of the C5 TBS ether with TBAF and acidic hydrolysis with PPTS in wet acetonitrile then provided dolastatin 19 aglycon **1.89**. Completion of the synthesis of dolastatin 19 required a stereocontrolled glycosylation reaction of fluorosugar **1.36**, which proceeded in 49% yield under the standard Mukaiyama conditions,<sup>63</sup> promoted by  $\text{SnCl}_2$  and  $\text{AgClO}_4$ . Removal of the remaining TBS ether completed the total synthesis of dolastatin 19 **1.18**. Spectroscopic

analyses of the synthetic material were consistent with those of the natural sample, thereby confirming the stereochemically revised structure of dolastatin 19 as the correct structure of the natural product.



Scheme 1.19

### 1.9. Macrolides from Calcareous Sponge *Leucascandra caveolata*

Leucascandrolide B **1.90** represents the last example of macrolides containing 2-hemiketalpyran moiety embedded within the C3 – C7 segment. The natural product is a 16-membered macrolide isolated from calcareous sponge *Leucascandra caveolata* collected from the northeastern coast of New Caledonia. The isolation report was



published in 1999 by Pietra and co-workers;<sup>93</sup> 73 mg natural product, which accounted for 0.0003% of the freeze-dried sponge, was isolated. The biological assays of leucascandrolide B revealed only marginal cytotoxicity on tumor cell lines, with IC<sub>50</sub> values of 5 µg/mL on KB cells and >10 µg/mL on P388 murine leukemia cells. Leucascandrolide B also showed no antibiotic activity against animal-pathogenic yeast *Candida albicans*. As of late, efforts toward the total synthesis of this macrolide have not been disclosed in the literature.

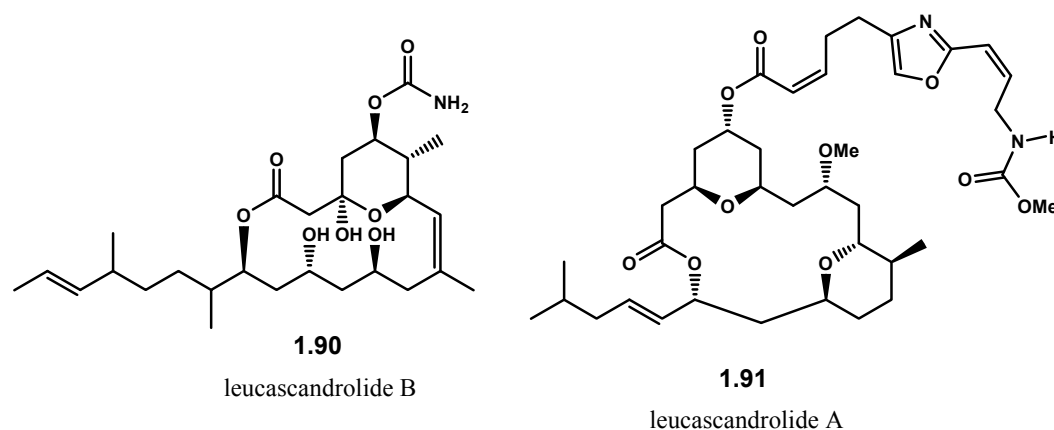
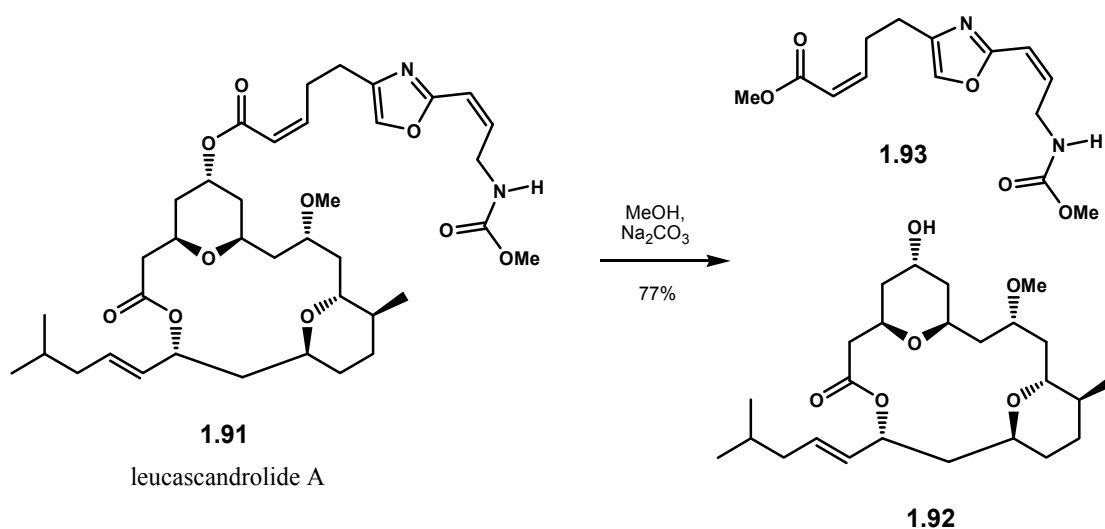


**Figure 1.9**

Three years prior to the discovery of leucascandrolide B **1.90**, Pietra and co-workers reported the isolation and characterization of another secondary metabolite from the same marine sponge, leucascandrolide A **1.91**,<sup>94</sup> in 70 mg quantity from 240 grams of the freeze-dried sponge. Interestingly, the structure of leucascandrolide A is significantly different from that of leucascandrolide B. Leucascandrolide A is an 18-membered macrolide; its structure is highlighted by two tetrahydropyran rings embedded within the macrolactone ring; one of which resides in the C3 – C7 segment, thereby satisfying our

prerequisites for the scope of this chapter. Unlike the previously discussed macrolides, the C3 – C7 pyran ring in leucascandrolide A does not bear 2-hydroxyl substitution, and this motif significantly provides a unique variation among the series of cyanobacterial macrolides that have been discussed within the context of this chapter. In addition to the pendant hydrophobic residue, leucascandrolide A also possesses a rather peculiar oxazole carbamate bearing side chain of uncertain biogenesis.

Leucascandrolide A is the first extremely bioactive macrolide isolated from calcareous sponge.<sup>94</sup> In fact, the biological activity of leucascandrolide A was truly remarkable. For instance, both organic and aqueous extracts from freeze-dried *L. caveolata* exhibit strong inhibitory effects to phytopatogenic fungi *Fusarium oxysporum*, *Helminthosporium sutivum*, *Plytophioru hevea*, *Boiryiis cinerea*, *Pyriculariu ovyzae*, and *Candidu albicans*. Additionally, cytotoxicity assays of leucascandrolide A exhibit IC<sub>50</sub> values of 0.05 µg/mL and 0.25 µg/mL for KB throat epithelial cancer cell lines and P388 murine leukemia cell lines, respectively. Further biological evaluations revealed that leucascandrolide A macrolide moiety **1.92** is essential for the observed cytotoxicity (100% toxicity at 0.5 – 10 µg/mL) and that the oxazole carbamate side chain significantly contributes to the antifungal properties of the natural product.



**Scheme 1.20**

The unique structure of leucascandrolide A has raised questions regarding the biogenesis of the metabolite. Although the exact biogenesis of leucascandrolides has yet to be evaluated, structural similarities with some of the aforementioned macrolides particularly of the macrolactone core, i.e. the oxygenation and substitution patterns, the size of the macrolactone ring, the presence of C3 – C7 pyran functionality, and the hydrophobic side chain, strongly suggest its cyanobacterial origins. Pietra stated that samples of *L. caveolata* collected in 1994 further north with the respect to the 1989 sampling site as well as those collected off the northeastern coast of New Caledonia did not contain any trace of both leucascandrolides. These findings may be indicative the microbial origin of these compounds.<sup>94</sup> The fact that the structures of leucascandrolides A and B are profoundly different implicates a mixed assembly of microbes as the most likely source for the production of these two isolated metabolites.

It is well known that cyanobacterium *Aphanocapsa feldmanni* readily coexists in an endosymbiotic fashion with many calcareous sponges.<sup>95</sup> Importantly however, only *L.*

*caveolata* are known to have produced macrolides. It is also important to note that the 1989 sampling, from which leucascandrolides were isolated, contained extensive dead portions of the sponge. Pietra suggests that the putative microbes seem to be opportunistic rather than symbiotic, thereby explaining the presence or the absence of these microbes among different host sponge samples.<sup>94</sup> Nevertheless, this argument can be disputed by the fact it is also unclear whether the death of the sponge was a result of aggressive colonization of the microbes or simply caused by accidental poisoning. The possibility of the microbes excreting leucascandrolides to defend themselves against predators which may or may not have existed in different parts of the collection site cannot be ruled out.

Due to its unique structural features and potent bioactivities, leucascandrolide A **1.91** has been subjected to numerous total syntheses.<sup>96-118</sup> Review articles detailing selected total syntheses of leucascandrolide A have been recently published independently by Paterson<sup>119</sup> and Kalesse.<sup>120</sup>

#### **1.10. Macrolide from Marine Sponges Related to *Daedalopelta sollas***

In 2007, Wright and co-workers reported the isolation of neopeltolide **1.95** from a deepwater sponge of the family Neopeltidae collected off the north Jamaican coast.<sup>121</sup> Although the exact species of the specimen was not identified, the sponge appeared most closely related to the species *Daedalopelta sollas*. Neopeltolide was isolated as colorless oil in 0.004% from 105 grams of the frozen Neopeltidae sponge. Initially, the structure of neopeltolide was proposed as structure **1.94**, Figure 1.10. However, this structure was

proved incorrect and consequently revised to **1.95** by means of total synthesis (*vide infra*). Neopeltolide is a fully saturated 14-membered macrolide, similar to lyngbyaloside B **1.5** and lyngbouilloside **1.6** with the C3 oxidation state of the pyran ring and the pendant oxazole carbamate side chain being identical to those of leucascandrolide A **1.91**. The structural homology between neopeltolide and unrelated macrolides thus strongly supports the hypothesis which advocates cyanobacterial biosynthetic origin of this natural product.

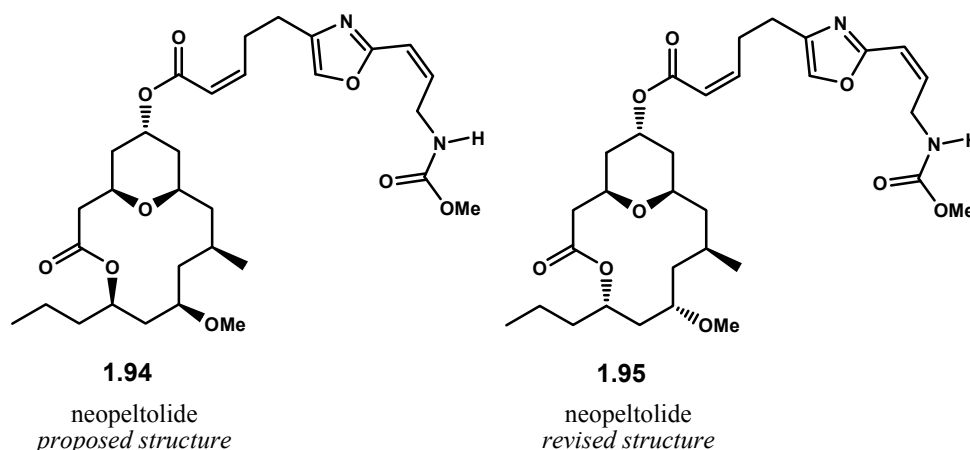


**Figure 1.10**

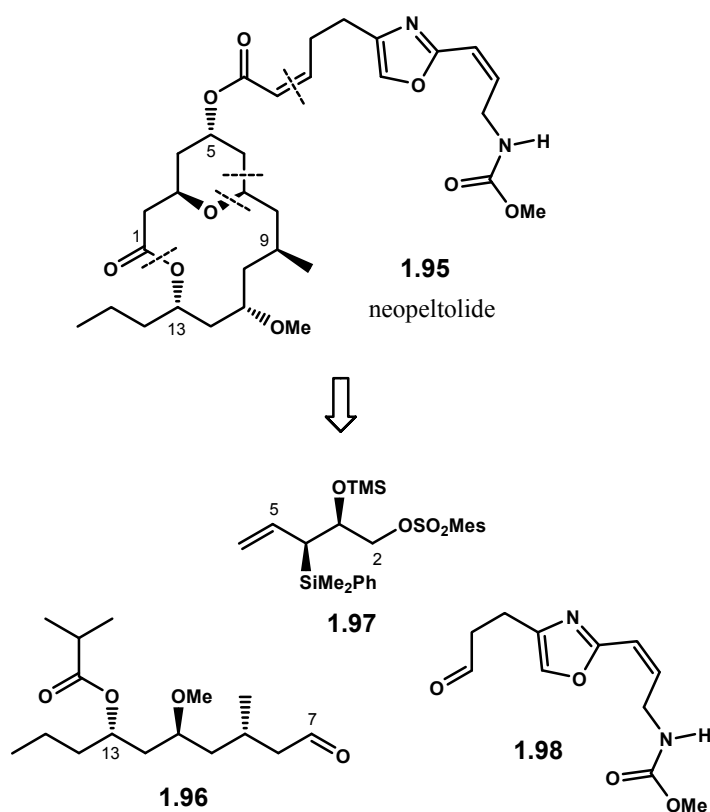
Neopeltolide exhibits interesting biological activities. It is cytotoxic against several cancer lines, including P388 murine leukemia, A-549 human lung adenocarcinoma, and NCI-ADR-RES human ovarian sarcoma, with their respective  $IC_{50}$  values of 0.56, 1.2, and 5.1 nM. Moreover, neopeltolide also shows strong cytostatic inhibitory effects against PANC-1 pancreatic and DLD-1 colorectal cell lines. In addition, growth inhibition of pathogenic yeast *Candida albicans* is also observed in the presence of neopeltolide with an MIC value of 0.62  $\mu\text{g/mL}$ . As recently proposed by

Kozman and co-workers, the mode of action of neopeltolide may involve inhibition of mitochondrial ATP synthesis with cytochrome *bc*<sub>1</sub> complex as the primary cellular target.<sup>122</sup>

The broad-based and exceptional biological activities makes neopeltolide a prime target for total syntheses. Indeed, within months after the isolation report, six accounts in the total synthesis of neopeltolide were reported shortly independently Panek,<sup>123</sup> Scheidt,<sup>124</sup> Lee,<sup>125</sup> Maier,<sup>126</sup> Sasaki,<sup>127</sup> and Kozmin.<sup>122</sup>

#### 1.10.1. Panek's Approach

The first total synthesis of neopeltolide, which led to its stereochemical reassignment, was reported in late 2007 by the Panek group.<sup>123</sup> Panek's retrosynthetic approach to neopeltolide is highlighted by bond disconnections to give three synthetic fragments: aliphatic aldehyde **1.96**, allyl silane **1.97**, and oxazole aldehyde **1.98**, Scheme 1.21. The coupling of aldehyde **1.96** and allyl silane **1.97** to construct the C3 – C7 tetrahydropyran segment exploited the [4+2] annulation strategy. Late-stage introduction of pendant oxazole aldehyde chain **1.98** was accomplished via the Still-Gennari olefination reaction.

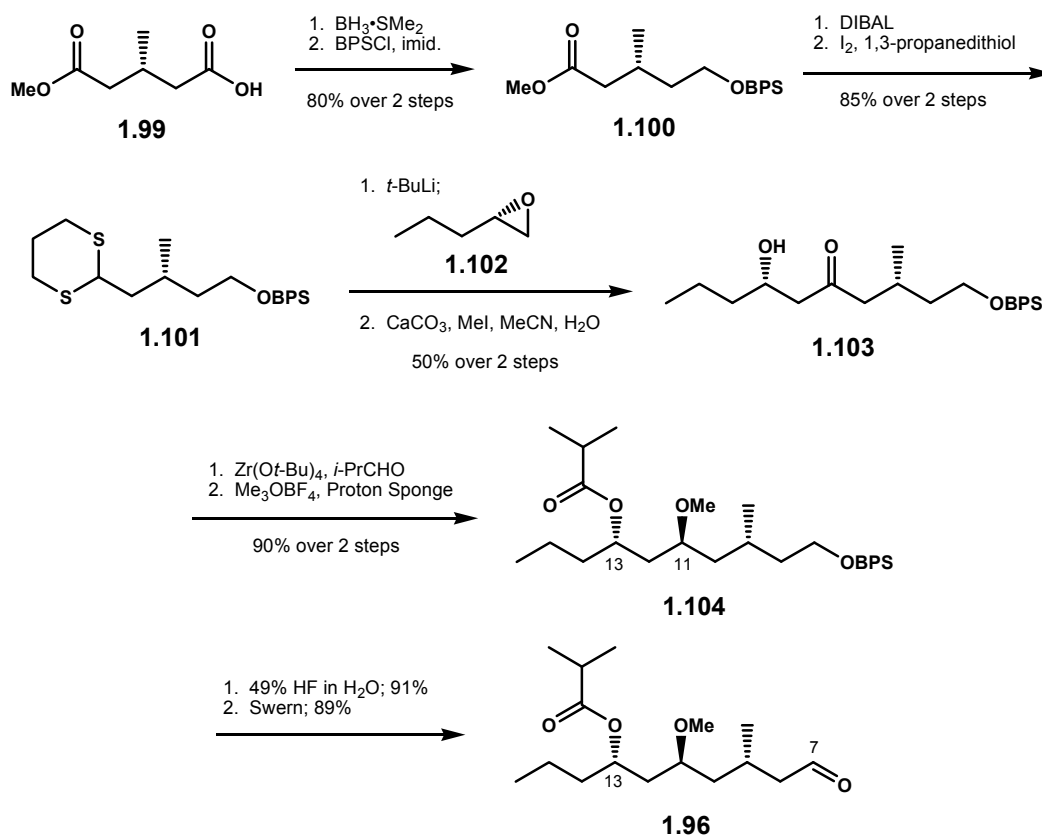


**Scheme 1.21**

#### 1.10.1.1. Preparation of Aldehyde 1.96

The preparation of C7 – C13 aldehyde fragment **1.96** began with commercially available (*R*)-3-methyl-glutarate **1.99**. Chemoselective reduction of the carboxylic acid<sup>128</sup> moiety with  $\text{BH}_3 \cdot \text{SMe}_2$  afforded the corresponding primary alcohol, which after protection provided BPS ether **1.100**. The ensuing DIBAL treatment reduced the ester functionality to the aldehyde which was then readily transformed to dithioacetal **1.101** under an iodine-catalyzed condensation reaction with 1,3-propanedithiol. Deprotonation of dithioacetal **1.101** with *tert*-butyllithium followed by trapping of the resulting anion with epoxide **1.102** completed the C7 – C16 carbon framework of neopeltolide. The

ketone functionality was then unmasked upon exposure of the dithiane to methyl iodide in the presence of calcium carbonate to furnish  $\beta$ -hydroxy ketone **1.103**. A modified Evans-Tishchenko reaction installed the required C11 – C13 *anti* stereochemistry.<sup>129</sup> Under these reaction conditions, a readily differentiated 1,3-*anti* diol was produced with diastereoselectivity of 14:1. Subsequent methylation at C11 then afforded ester **1.104**.<sup>92</sup> Removal of the BPS ether followed by Swern oxidation<sup>74</sup> of the corresponding alcohol completed the synthesis of aldehyde fragment **1.96**.

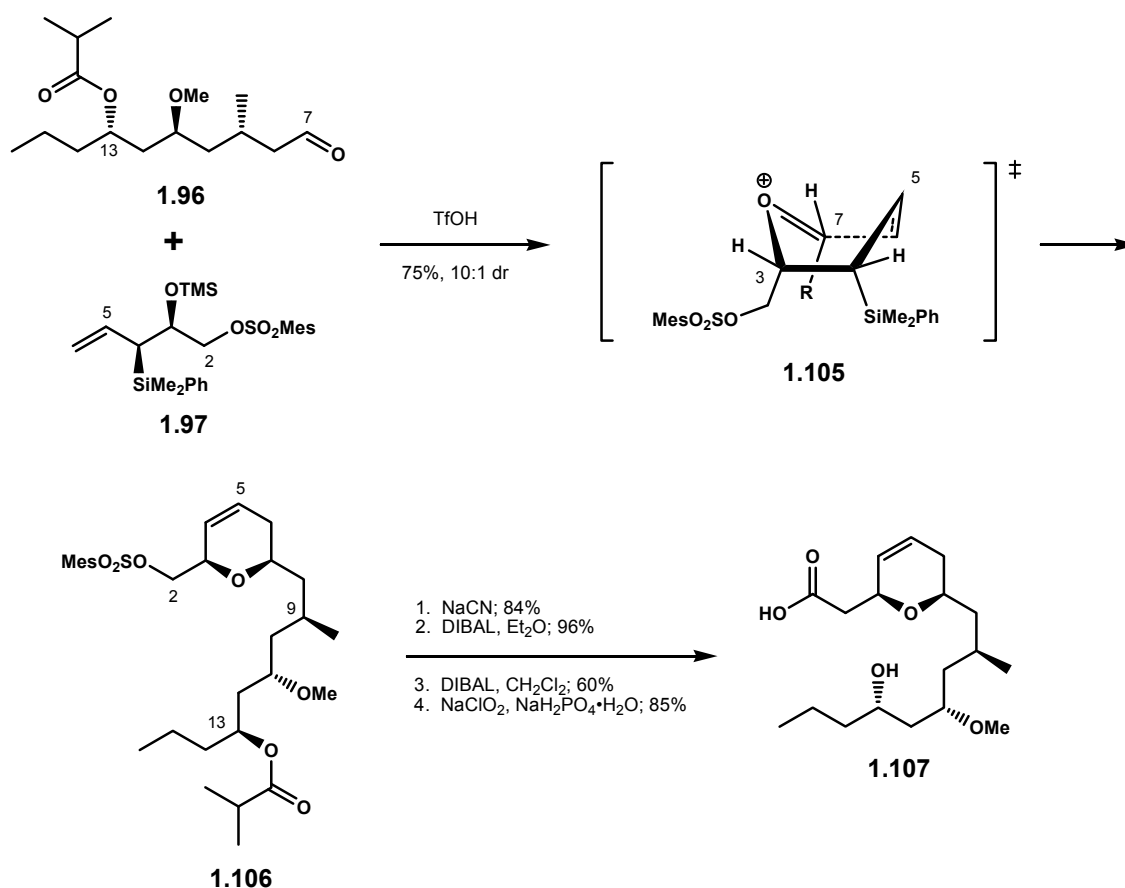


Scheme 1.22



### 1.10.1.2. [4+2] Annulation

The construction of the C3 – C7 tetrahydropyran segment of neopeltolide was realized with a triflic acid promoted coupling reaction of aldehyde **1.96** and chiral allyl silane **1.97**. This [4+2] annulation reaction, a methodology originally developed in Panek's laboratories, successfully produced dihydropyran **1.106** in 75% yield with 10:1 diastereomeric ratio.<sup>130</sup> Boat-like structure **1.105** describes the transition state that accounts for the observed stereoselectivity.

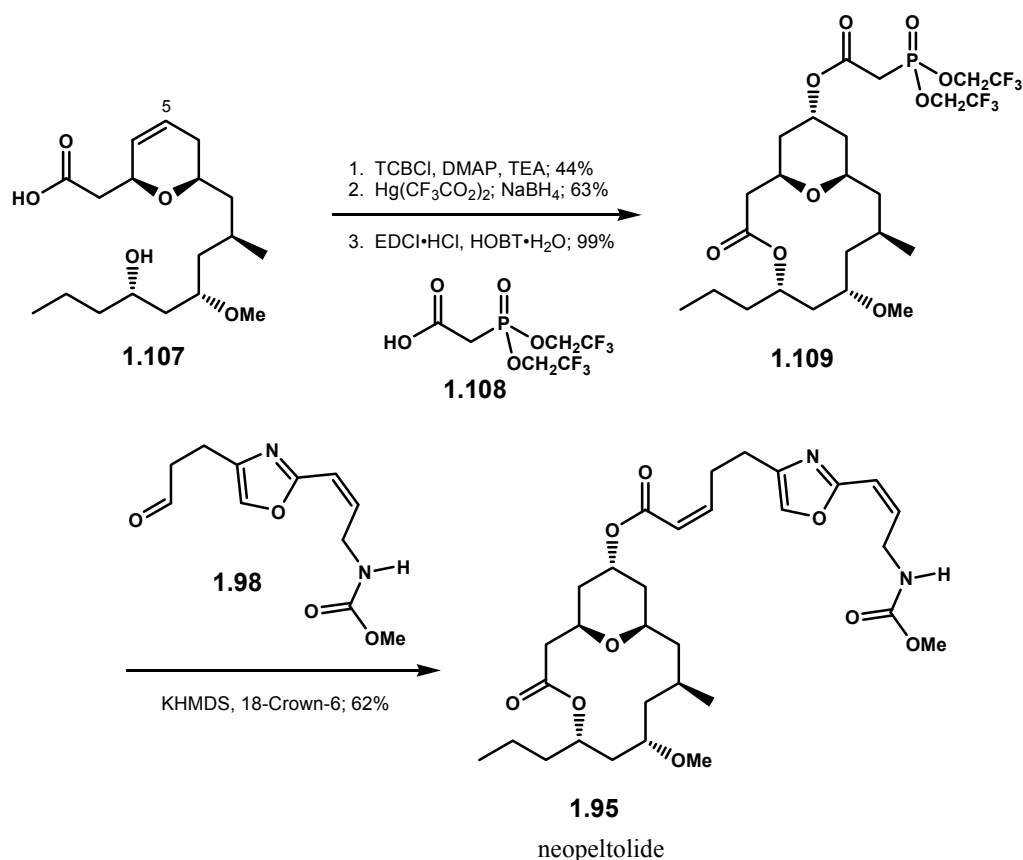


Scheme 1.23

Treatment of **1.106** with sodium cyanide served to displace the C2 sulfonate, and thereby introducing the masked carboxylic acid functionality at C1. Chemoselective reductive removal of the C13 acyl protecting group and reduction of the cyanide sequentially provided the corresponding aldehyde. Pinnick oxidation<sup>68</sup> to the carboxylic acid then furnished macrolactonization precursor **1.107**, Scheme 1.23.

#### 1.10.1.3. Endgame Strategy

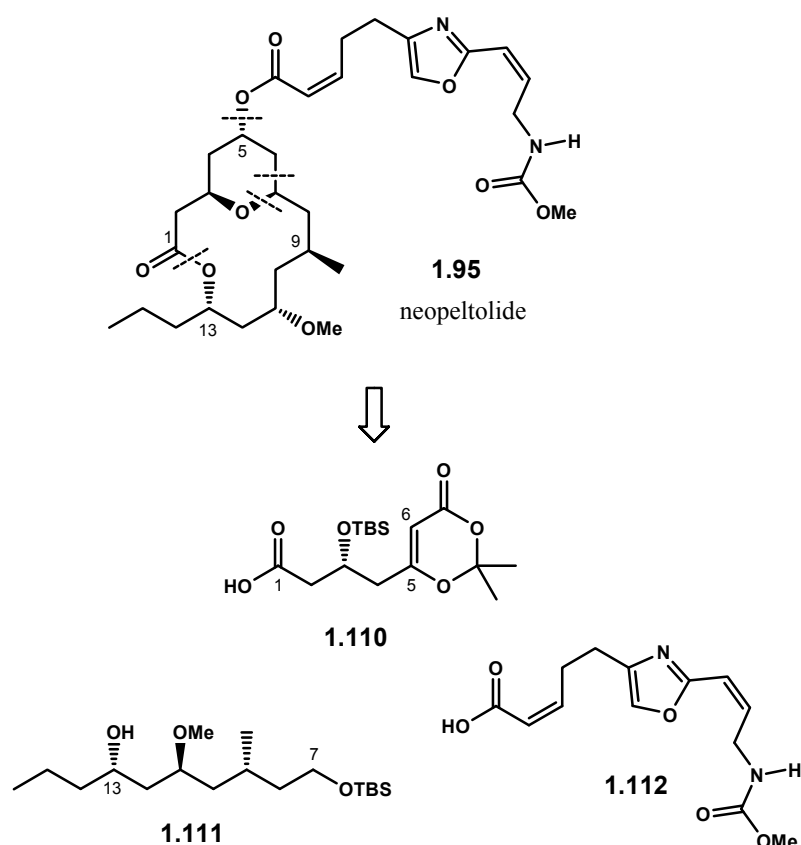
As demonstrated in Scheme 1.24, the macrolactonization of precursor **1.107** to the corresponding macrolide was affected under the Yamaguchi protocols.<sup>69</sup> The ensuing regioselective oxymercuration<sup>131</sup> installed C5 hydroxyl in the axial orientation, which was then readily acylated with phosphonate **1.108**<sup>132</sup> in near quantitative yield. Coupling of macrolide **1.109** and aldehyde **1.98**<sup>98</sup> under the Still-Gennari olefination conditions<sup>133</sup> successfully produced neopeltolide in 62% yield.



**Scheme 1.24**

### 1.10.2. Scheidt's Approach

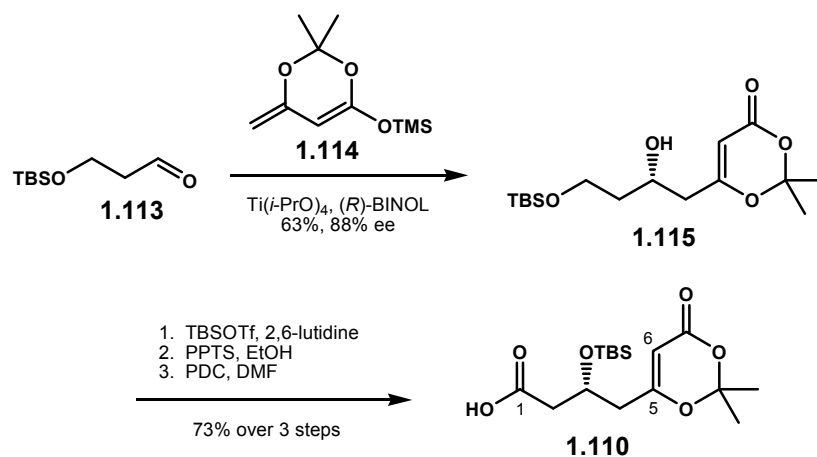
Concurrently and independent of Panek, Scheidt and co-workers reported their total synthesis and stereochemical revision to neopeltolide.<sup>124</sup> As shown in Scheme 1.25, retrosynthesis of neopeltolide as described by Scheidt and co-workers included bond disconnections to give three synthetic fragments: dioxinone **1.110**, alcohol **1.111**, and oxazole carbamate **1.112**. The construction of neopeltolide macrolide core involved a novel macrolactonization which took place upon the installation of the tetrahydropyran ring.



**Scheme 1.25**

#### 1.10.2.1. Preparation of Dioxinone 1.110

The synthesis of C1 – C6 fragment of neopeltolide commenced with an asymmetric vinylogous aldol reaction of aldehyde **1.113** and dienoxysilane **1.114** catalyzed by Ti(IV)-(*R*)-BINOL complex.<sup>134</sup> These reaction conditions installed the requisite stereochemistry of C3 hydroxyl with enantiomeric excess of 88%. Subsequent silylation of the C3 secondary alcohol followed by selective removal of C1 TBS ether under acidic conditions unmasked the primary alcohol which upon treatment with PDC was oxidized to the corresponding carboxylic acid **1.110**.

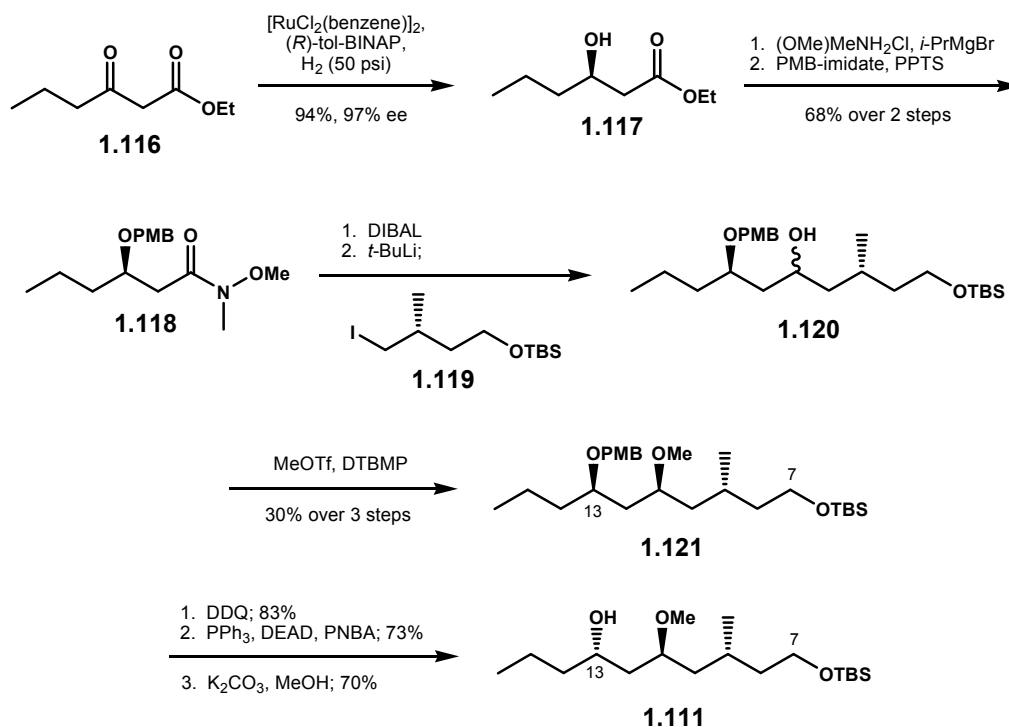


**Scheme 1.26**

#### 1.10.2.2. Preparation of Alcohol 1.111

Construction of fragment **1.111** began with enantioselective Noyori reduction of methyl 3-oxohexanoate **1.116** to  $\beta$ -hydroxy ester **1.117**.<sup>135</sup> Subsequent conversion of the methyl ester conversion to the Weinreb amide<sup>136</sup> and protection of the secondary alcohol as a PMB ether afforded **1.118** in 68% yield over 2 steps. Following DIBAL reduction of the Weinreb amide which introduced the aldehyde functionality, addition of alkyllithium species generated *in situ* by lithium-halogen exchange of **1.119** provided alcohol **1.120** as a mixture of diastereomers. Alkyl iodide **1.119** was prepared in two steps: reduction of a known Myer's ephedrine-based methylation adduct **1.122**<sup>137</sup> and subsequent iodination of the resulting primary alcohol **1.123**, Scheme 1.28. Exposure of alcohol **1.120** to MeOTf in the presence of DTBMP<sup>138</sup> installed the requisite C11 methyl ether, and at this point, the *syn* diastereomer **1.121** was separable by chromatography and isolated in 30% yield overall from amide **1.118**. The Mitsunobu reaction<sup>139</sup> was applied to invert the C13

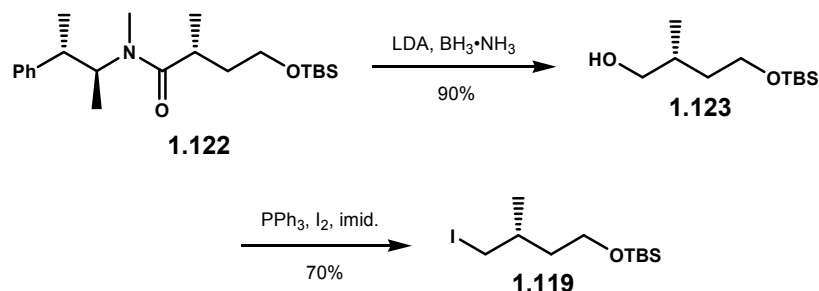
stereochemistry after removal of the PMB ether with DDQ, and thus, finish the sequence to fragment **1.111**.



**Scheme 1.27**

The above progression to fragment **1.111** appear cumbersome and rather laborious given the fact that late stage stereochemical inversion at C13 hydroxyl group could have been prevented had the (*S*)-tol-BINAP enantiomer been exploited as the chiral ligand in the early Noyori reduction step. However, Scheidt and co-workers noted that they previously had carried out a 100-gram-scale Noyori reduction to **1.117** for the synthesis of originally proposed structure of neopeltolide **1.94** without realizing that the C11 and C13 stereochemistry of neopeltolide had been incorrectly assigned. Resultantly, a new synthetic sequence for stereochemically-revised neopeltolide **1.95** was

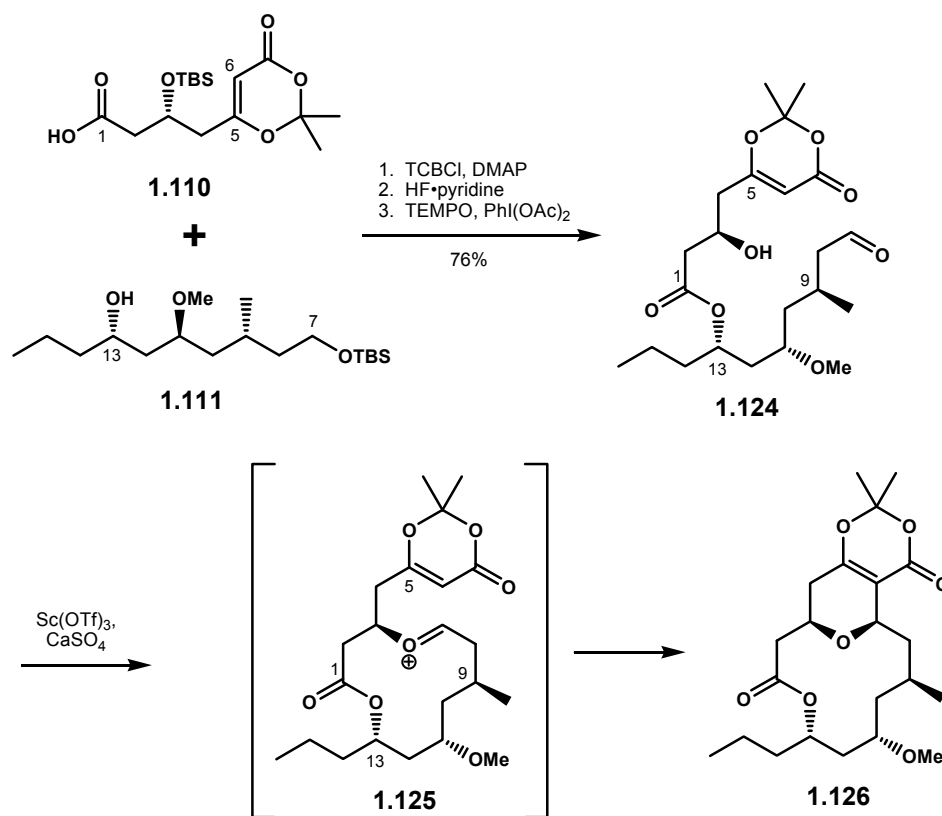
generated using the original material despite the inevitable protecting group manipulations and stereochemical inversion at C13.



### Scheme 1.28

### 1.10.2.3. Novel Prins Macrolactonization

With availability of the required fragments, the macrolide core of neopeltolide was brought together initially by the Yamaguchi esterification of carboxylic acid **1.110** and alcohol **1.111**.<sup>69</sup> Subsequent removal of C3 and C7 TBS ethers followed by chemoselective TEMPO oxidation<sup>67</sup> furnished the macrolactonization aldehyde precursor **1.124**. The novelty of Scheidt's route to neopeltolide is highlighted by unprecedented macrolactonization utilizing Prins type cyclization of dioxinone functionality which gave complex tricyclic compound **1.126**, although in low yield. This unique transformation was promoted by Sc(OTf)<sub>3</sub>, which induced condensation of the C3 hydroxyl to the C7 aldehyde presumably to provide oxocarbenium ion intermediate **1.125**.

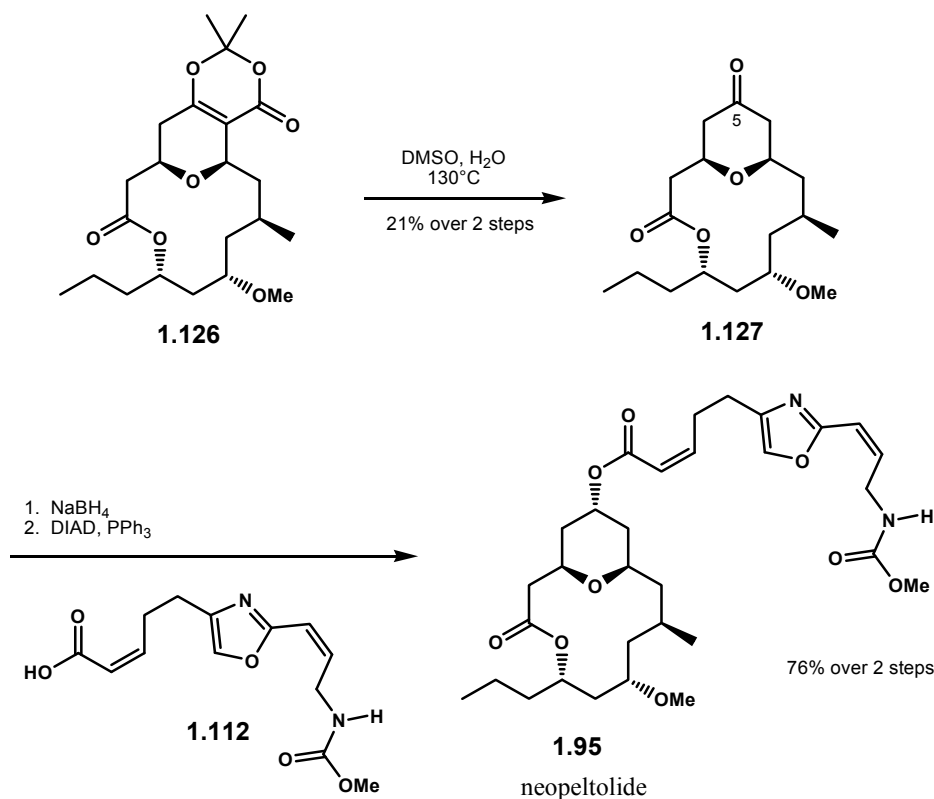


Scheme 1.29

#### 1.10.2.4. Endgame Strategy

The endgame strategy to neopeltolide proceeded via removal of the dioxinone moiety under decarboxylative conditions to give pyranone **1.127** in 21% yield from precursor **1.124**. The ensuing NaBH<sub>4</sub> reduction stereoselectively installed C5 hydroxy group in the equatorial position. Stereochemical inversion upon the introduction of a known oxazole carbamate fragment **1.112** under the Mitsunobu conditions<sup>111, 117</sup> completed the total synthesis of neopeltolide, Scheme 1.30.

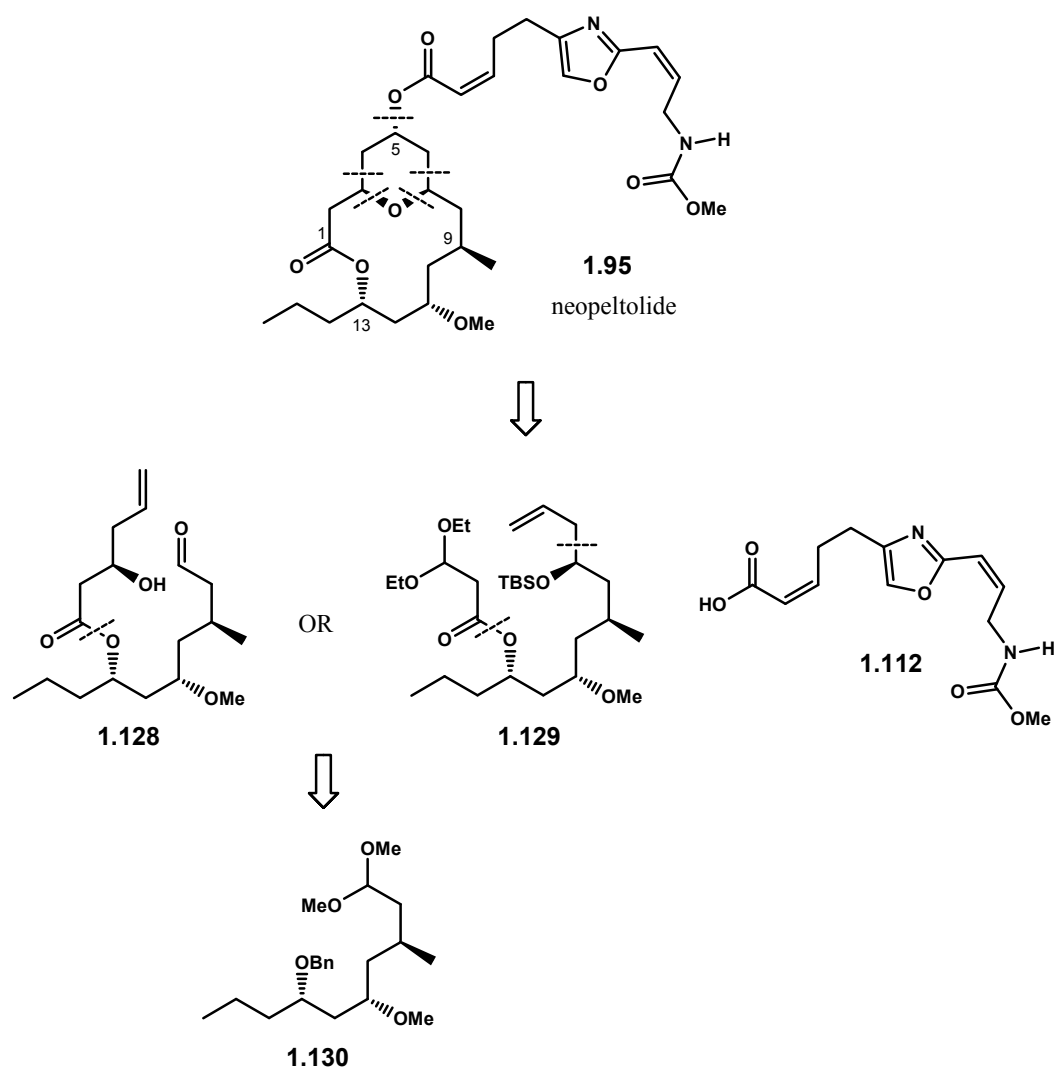




**Scheme 1.30**

### 1.10.3. Lee's Approach

Recognizing the potential of Prins cyclization in a one-step construction of neopeltolide bicyclic core demonstrated by the work of Scheidt, Eun Lee and co-workers<sup>125</sup> revised and implemented this strategy to solve the low yielding problem plagued in the Scheidt's route. Lee proposed a Prins-cyclization method using two alternative precursors, **1.128** and **1.129**; both were readily available from common intermediate **1.130**, Scheme 1.31.

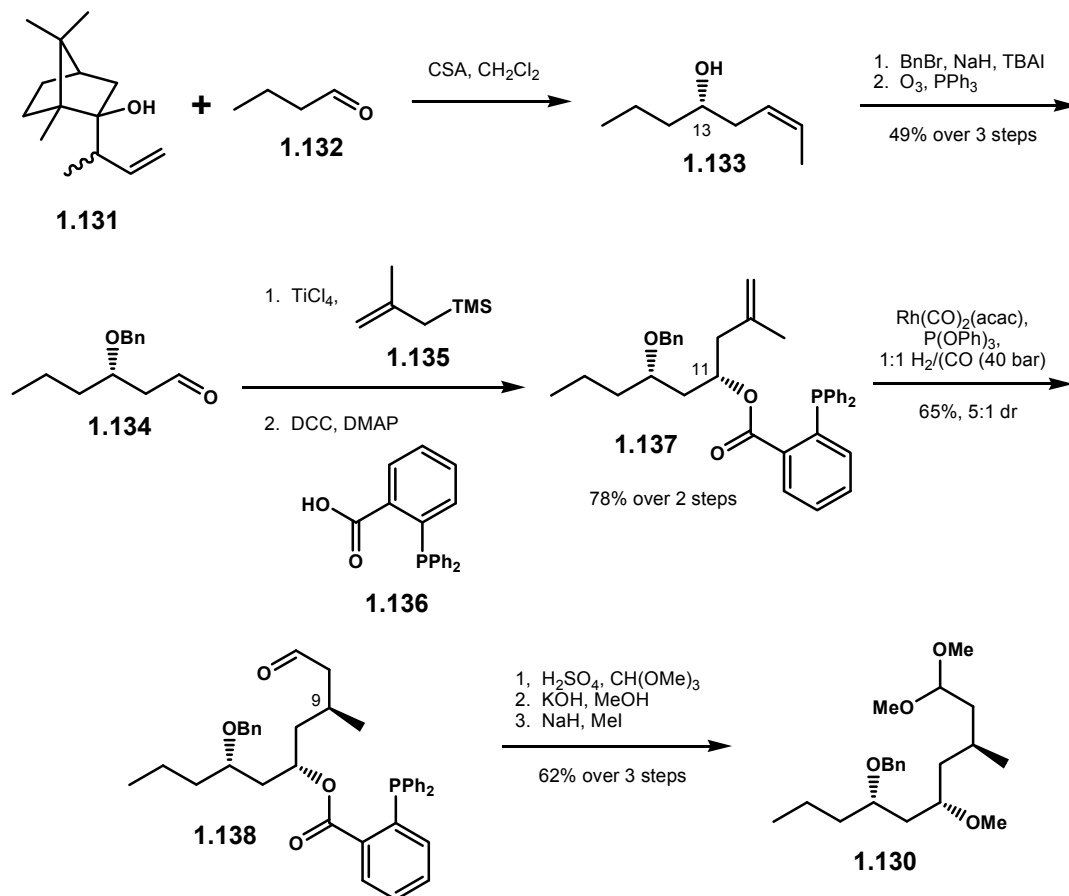


**Scheme 1.31**

#### 1.10.3.1. Preparation of Common Intermediate 1.130

The preparation of common intermediate **1.130** began with camphor-based asymmetric crotylation of butanaldehyde **1.132** to give alcohol **1.133** in the presence of CSA.<sup>140</sup> Subsequent benzylation of the secondary alcohol and oxidative cleavage then afforded acetate aldol adduct **1.134** in 49% yield over three steps. Chelation controlled methylation and protection of the resulting secondary alcohol with

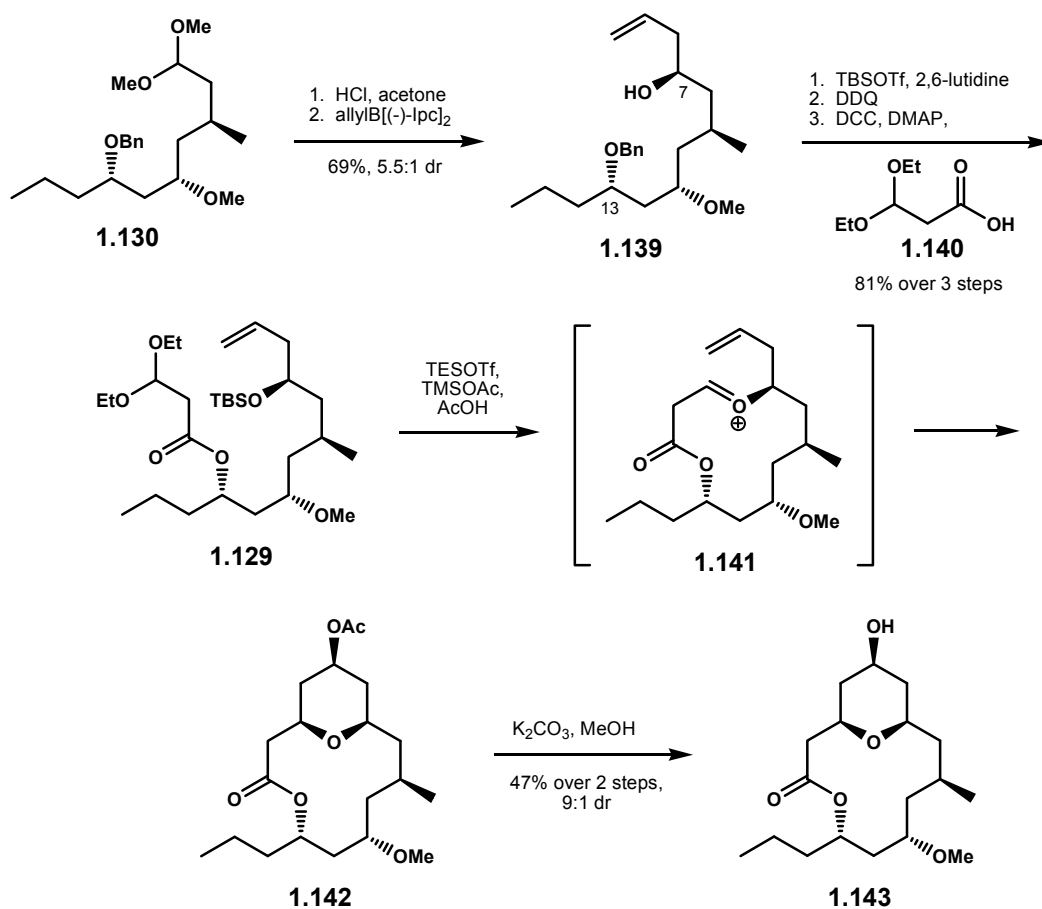
diphenylphosphinobenzoic acid **1.136** produced homoallylic ester **1.137**. The ensuing substrate directed hydroformulation then resulted in  $\beta$ -methyl aldehyde **1.138** in 65% yield with diastereomeric ratio of 5:1.<sup>141</sup> Dimethylacetal formation, followed by C11 deacylation and methylation furnished common intermediate **1.130**, Scheme 1.32.



Scheme 1.32

#### 1.10.3.2. Much Improved Prins Macrolactonization

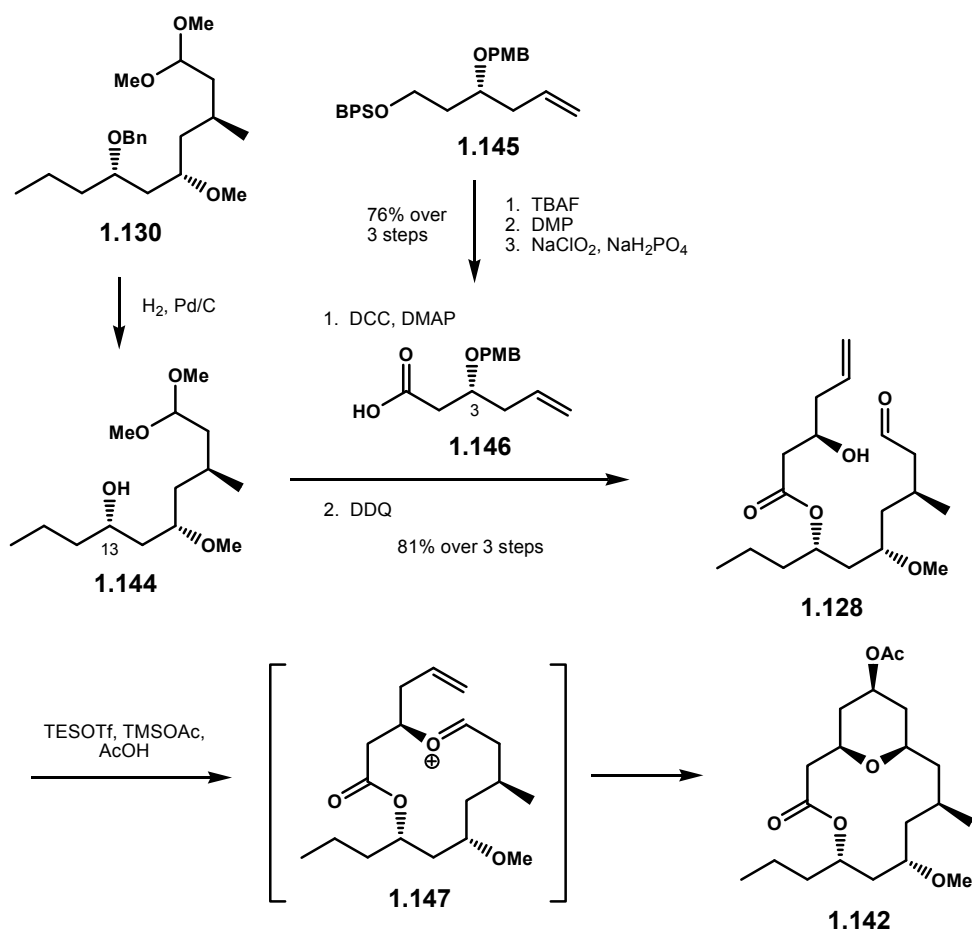
Hydrolysis of the dimethyl acetal moiety and subsequent asymmetric allylation of the resulting aldehyde by the method of Brown produced homoallylic alcohol **1.139** in 69% with a diastereomeric ratio of 5.5:1.<sup>142</sup> After protection of the C7 hydroxyl as a TBS ether, the C13 hydroxyl group was unmasked with DDQ and esterified with 3,3-diethylpropanoic acid **1.140**. This sequence provided the first macrolactonization precursor **1.129**. Exposure of this material to TESOTf and TMSOAc in AcOH produced Prins cyclization product **1.142** with diastereoselectivity of 9:1.<sup>143</sup> The minor diastereomer was assumed to have been generated via a loss of stereochemical information at C7 due to a potentially competitive oxonia-Cope rearrangement pathway of oxocarbenium intermediate **1.141**.<sup>144</sup> The ensuing basic methanolysis removed the C5 acetate group and successfully completed the bicyclic macrolide core of neopeltolide **1.143** in 47% yield over two steps.



**Scheme 1.33**

### 1.10.3.3. Alternative Prins Macrolactonization

Preparation of precursor **1.128** was necessary for the alternative Prins cyclization. Hydrogenolysis of common intermediate **1.130** unmasked the C13 hydroxyl group which was then readily esterified with carboxylic acid **1.146**, readily available in three steps<sup>68, 87</sup> from a known homoallylic PMB ether **1.145**.<sup>145</sup>

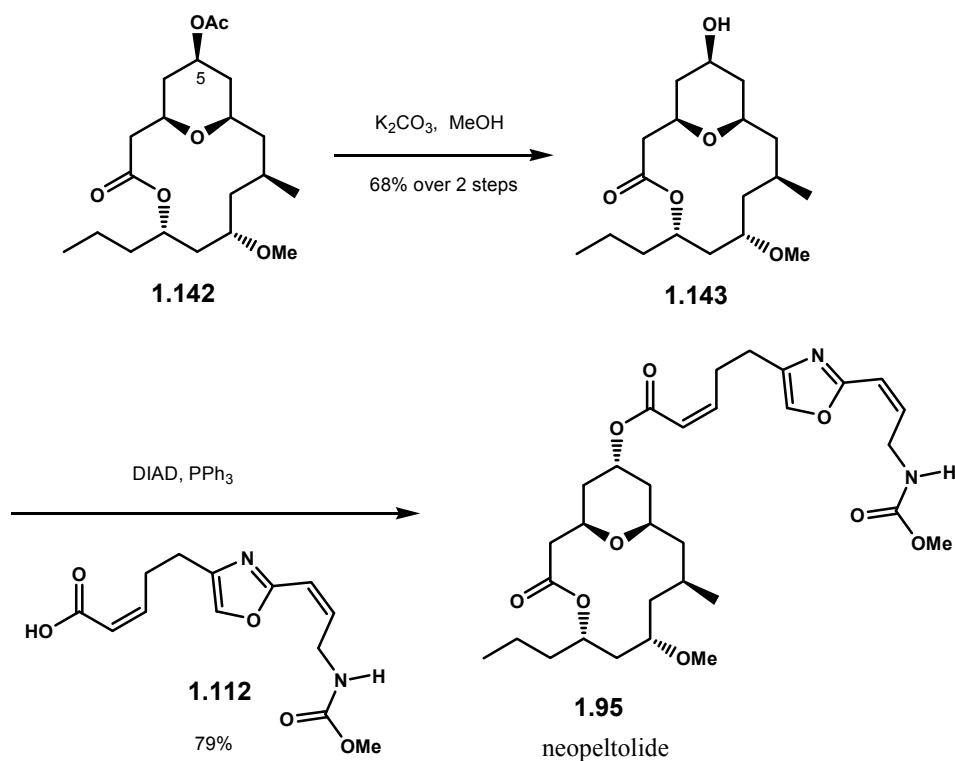


**Scheme 1.34**

Subsequent removal of the PMB ether furnished macrolactonization precursor **1.128**. Under the typical Prins conditions, neopeltolide macrolactone core **1.142** was produced as a single diastereomer, this time presumably via oxocarbenium ion intermediate **1.147**, Scheme 1.34.

#### 1.10.3.4. Endgame Strategy

As shown in Scheme 1.35, removal of the C5 acetate under basic methanolysis conditions unmasked the equatorial C5 hydroxyl. Finally, the Mitsunobu reaction with oxazole carbamate **1.112** completed the total synthesis to neopeltolide **1.95**.

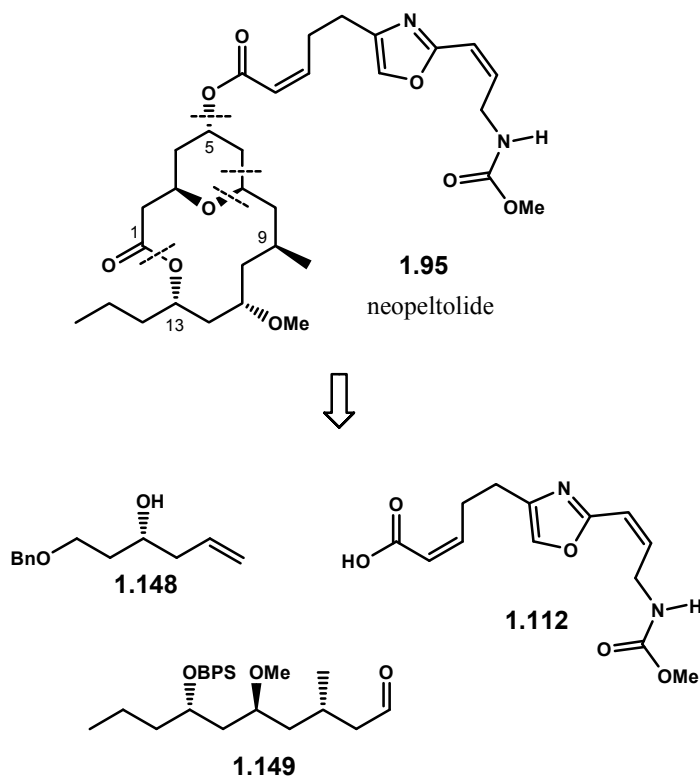


Scheme 1.35

#### 1.10.4. Maier's Approach

Recently, Maier and Vintonyak published the fourth total synthesis to neopeltolide. The macrolide was divided into three fragments: homoallylic alcohol **1.148**, aldehyde **1.149**, and oxazole carbamate **1.112**, Scheme 1.36. The tetrahydropyran

ring was once again constructed via Prins cyclization, and macrolactone ring was installed via the Yamaguchi method.



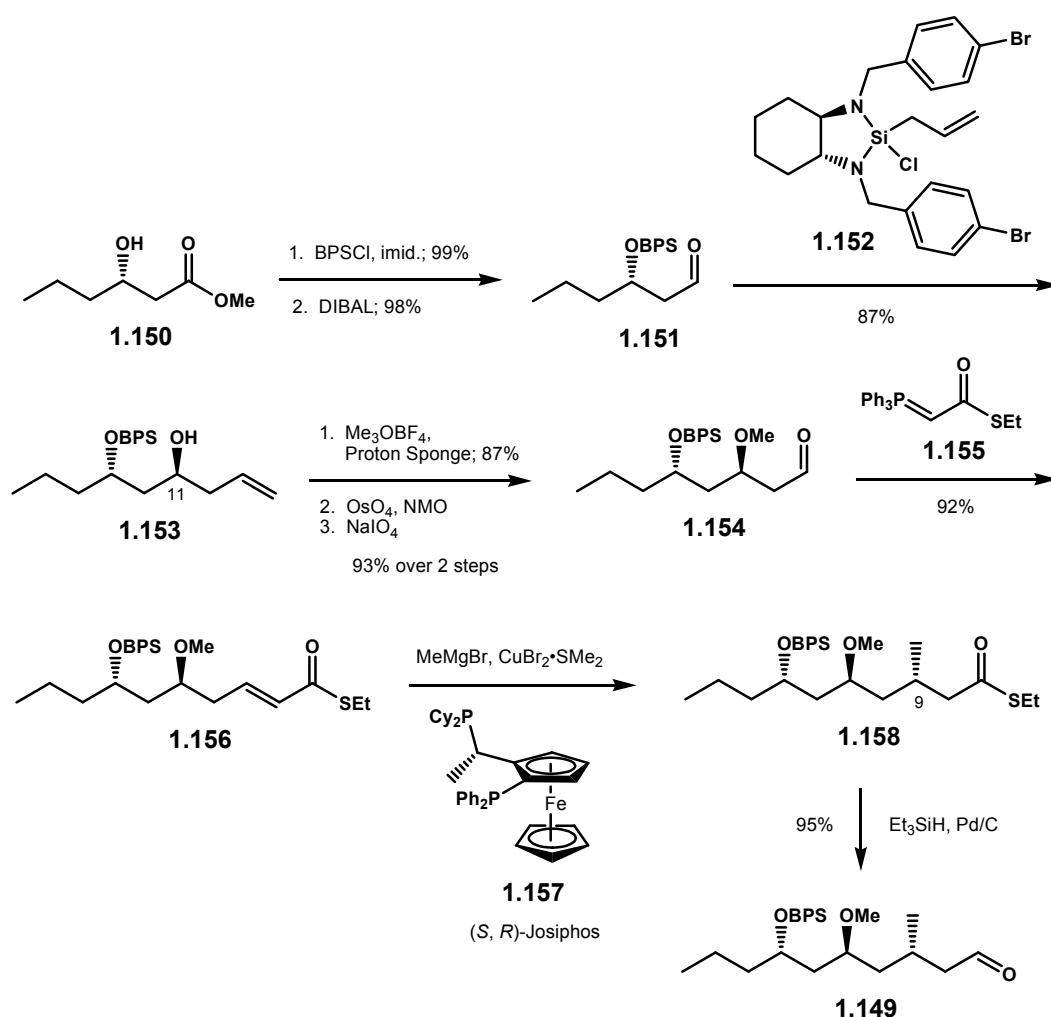
**Scheme 1.36**

#### 1.10.4.1. Preparation of Aldehyde 1.149

As shown in Scheme 1.37, Maier began his synthetic quest to neopeltolide with enantiomerically enriched  $\beta$ -hydroxy ester **1.150**, which was obtained via Noyori reduction<sup>135</sup> of methyl 3-oxohexanoate **1.116** similar to that presented in Scheme 1.27. Sequential BPS protection of the secondary alcohol and ester reduction under DIBAL conditions afforded aldehyde **1.151**, which was then subjected to Leighton's chiral



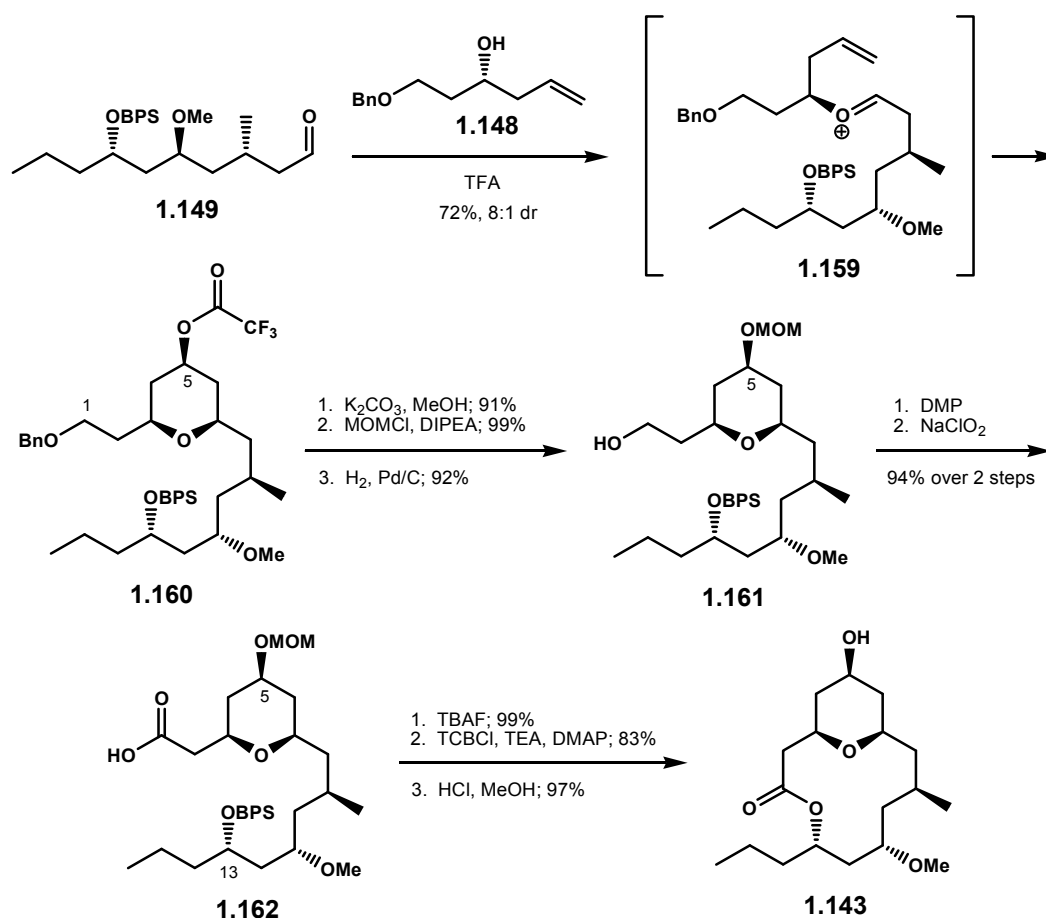
allylation reagent **1.152** to give homoallylic alcohol **1.153**.<sup>146</sup> The C11 hydroxyl was methylated with Meerwein's salt in the presence of Proton Sponge,<sup>147</sup> and subsequent oxidative cleavage of the terminal olefin provided aldehyde **1.154**. The vinylogation of aldehyde **1.154** with phosphorane **1.155**<sup>148</sup> yielded  $\alpha,\beta$ -unsaturated thioester **1.156**. The ensuing Feringa-Minnaard reaction was employed to install the requisite C9 methyl stereocenter.<sup>149</sup> Hydrogenolysis of thioester **1.158** then finally furnished aldehyde **1.149**.



Scheme 1.37

#### 1.10.4.2. Completion to Neopeltolide Macrolide Core

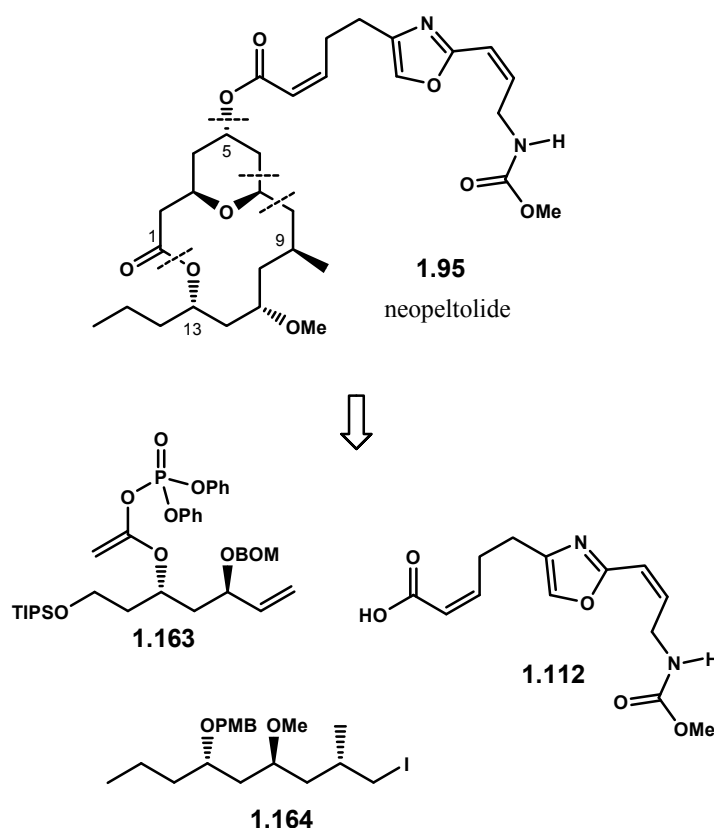
Aldehyde **1.149** was coupled with homoallylic alcohol **1.148** in the presence of TFA to produce Prins-cyclization product **1.160** in 72% yield with a diastereomeric ratio of 8:1. The proposed intermediacy of the reaction is depicted as oxocarbenium ion **1.159**. Removal of the C5 trifluoroacetate group, reprotection of the resulting secondary alcohol as MOM ether, and hydrogenolysis of C1 benzyl ether afforded primary alcohol **1.161**. Two-step oxidation<sup>68, 87</sup> to the carboxylic acid followed by removal of the C13 BPS ether under TBAF conditions set up the corresponding macrolactonization precursor **1.162**. The macrolactone bond was constructed under the Yamaguchi conditions,<sup>69</sup> and the neopeltolide macrolide core **1.143** was liberated upon acidic methanolysis of the C5 MOM ether, Scheme 1.38.



**Scheme 1.38**

### 1.10.5. Sasaki's Approach

Sasaki and co-workers recently reported their work on the total synthesis of neopeltolide.<sup>127</sup> As shown in Scheme 1.39, their approach was highlighted by bond disconnections that gave three fragments: enol phosphate **1.163**, alkyl iodide **1.164**, and oxazole carbamate **1.112**. The assembly of fragments **1.163** and **1.164** was envisioned via the Suzuki-Miyaura reaction<sup>150, 151</sup> followed by coupling with carboxylic acid **1.112** by the method of Mitsunobu.

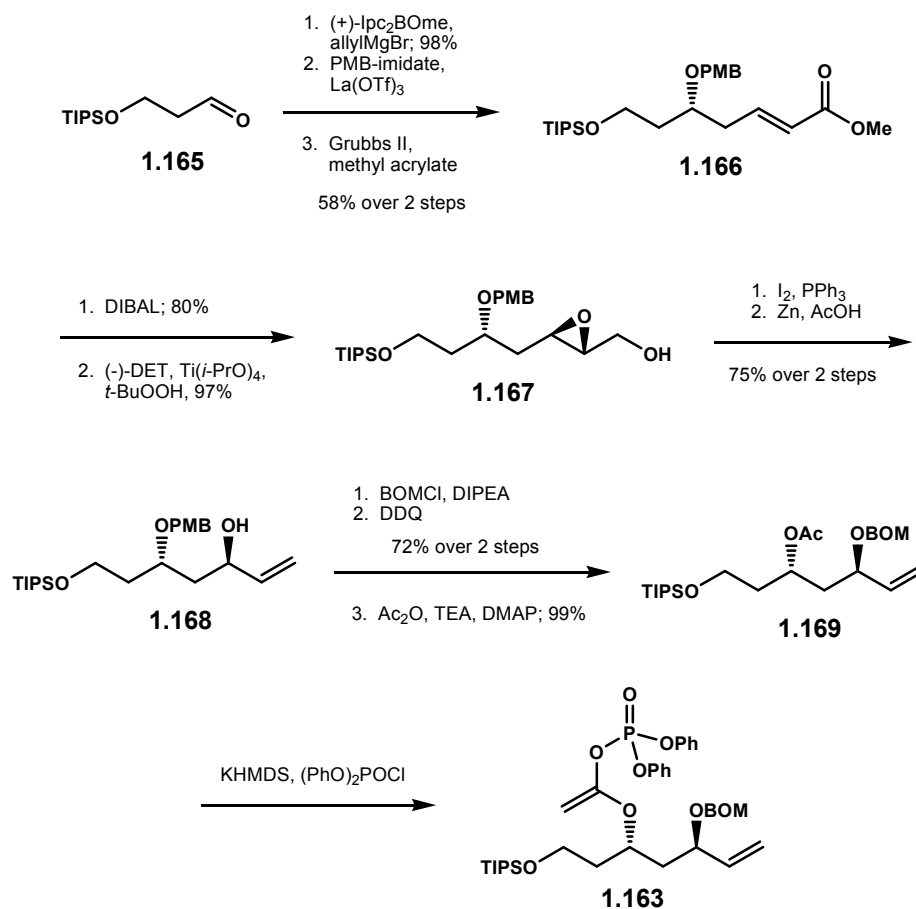


**Scheme 1.39**

#### 1.10.5.1. Preparation of Enol Phosphate **1.163**

The preparation of enol phosphate **1.163** commenced with Brown asymmetric allylation of aldehyde **1.165**.<sup>142</sup> Protection of the resulting homoallylic alcohol as a PMB ether followed by olefin cross metathesis with methyl acrylate promoted by the Grubbs 2<sup>nd</sup> generation catalyst provided  $\alpha,\beta$ -unsaturated ester **1.166**.<sup>152</sup> Reduction of the methyl ester to the corresponding allylic alcohol set up a substrate for the ensuing Sharpless epoxidation.<sup>153, 154</sup> Elaboration of the alcohol to the primary olefin **1.168** was delivered by a sequence of halogenation – reduction. Sequential protection of the newly generated alcohol as a BOM ether, removal of the PMB ether and acetylation of the free alcohol

then provided **1.169**. Deprotonation of the acetyl group followed by trapping of the resulting potassium enolate with  $(\text{OPh})_2\text{POCl}$  furnished enol phosphate **1.163**.

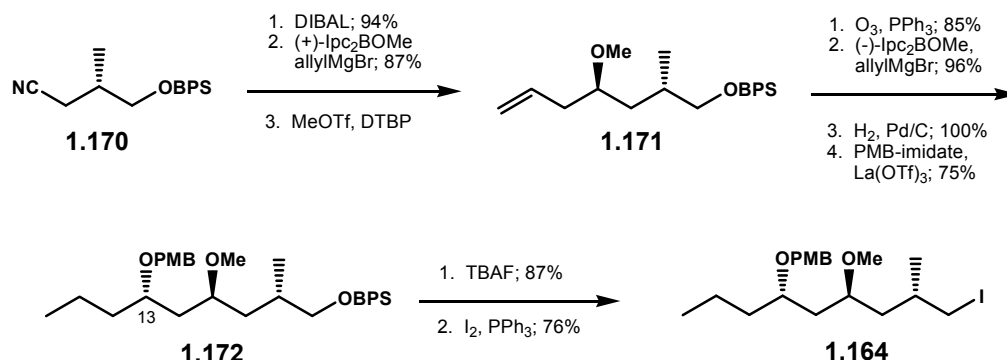


**Scheme 1.40**

#### 1.10.5.2. Preparation of Alkyl Iodide 1.164

The synthesis of alkyl iodide **1.164** began with a known nitrile **1.170**.<sup>155</sup> DIBAL reduction to the aldehyde followed by Brown allylation<sup>142</sup> and methylation produced methyl ether **1.171**. Oxidative cleavage of the terminal olefin to the aldehyde followed by a second Brown allylation<sup>142</sup> set the stereochemistry of the C13 hydroxyl. The

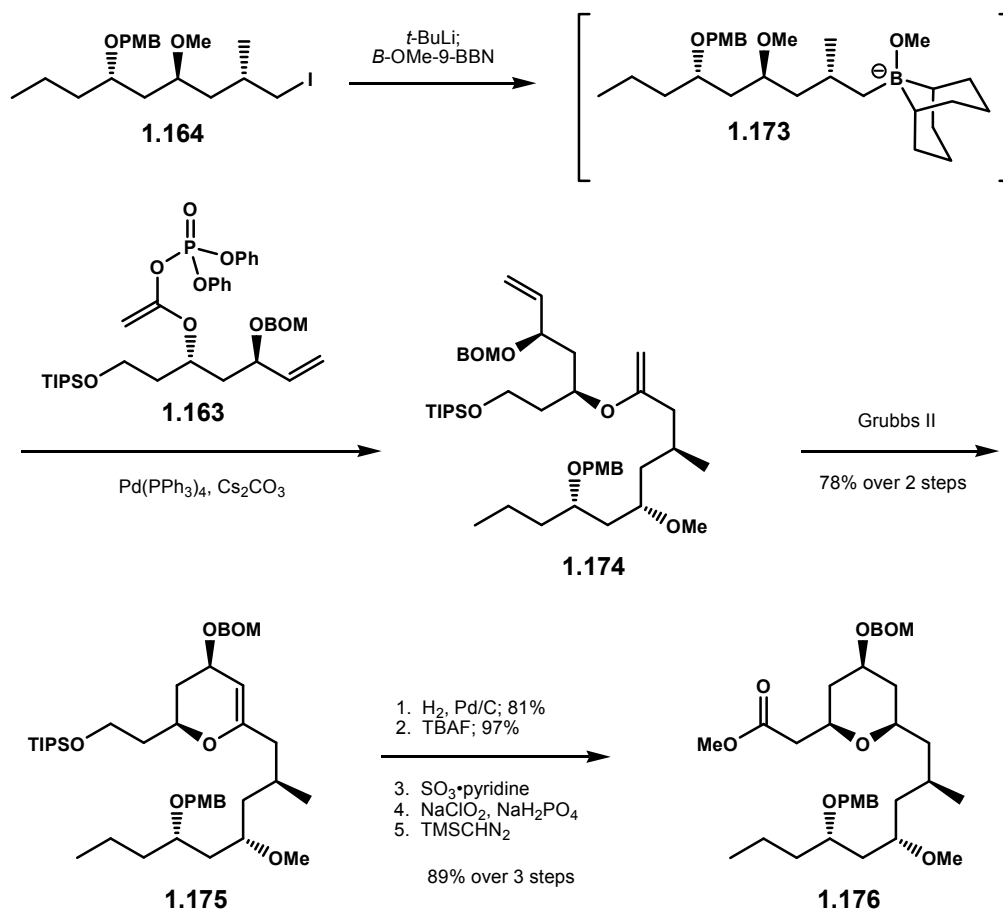
ensuing hydrogenation of the terminal olefin followed by protection of the remaining alcohol as a PMB ether gave mixed ether **1.172**. Removal of the BPS ether and iodination then afforded **1.164**.



**Scheme 1.41**

### 1.10.5.3. Construction of 2,4,6-Trisubstituted Tetrahydropyran

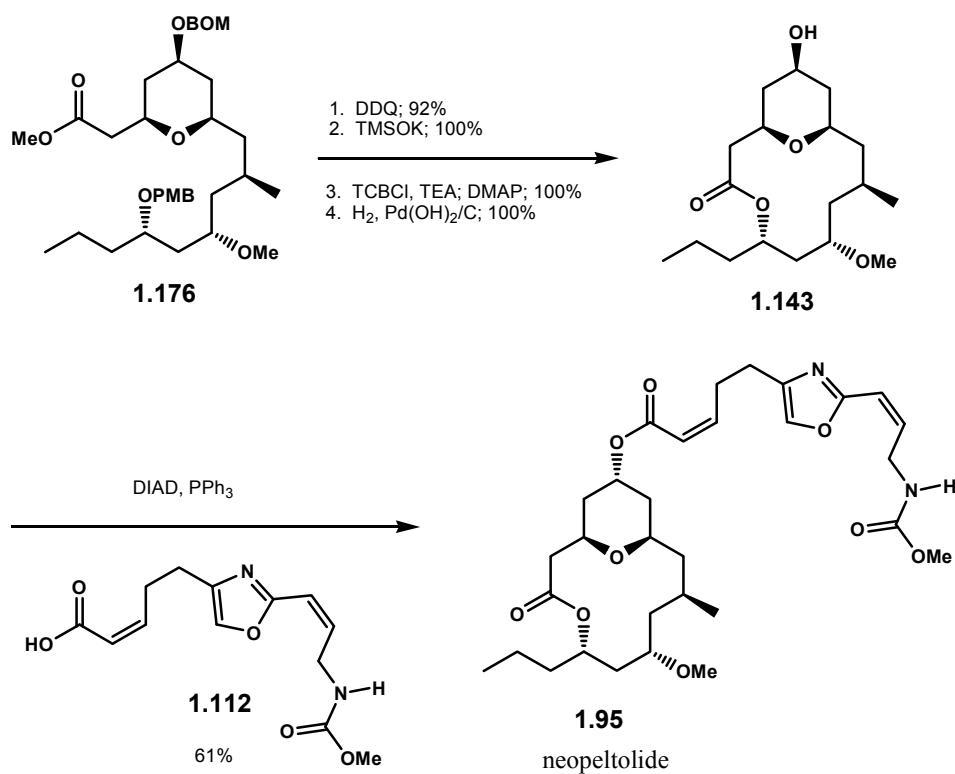
The assembly of advanced fragments **1.163** and **1.164** was realized under the Suzuki-Miyaura reaction.<sup>150, 151</sup> Lithiation of alkyl iodide **1.164** followed by trapping with *B*-OMe-9-BBN provided intermediate **1.173**, which was reacted *in situ* with enol phosphonate **1.163** in aqueous Cs<sub>2</sub>CO<sub>3</sub> and Pd(PPh<sub>3</sub>)<sub>4</sub> to give acyclic enol ether **1.174**. Ring closing metathesis catalyzed by Grubbs 2<sup>nd</sup> generation provided glycal **1.175**.<sup>152</sup> Selective hydrogenation of the glycal successfully installed the requisite stereochemistry of the tetrahydropyran ring. Removal of the TIPS ether followed by a two-step oxidation and esterification then furnished methyl ester **1.176**.



**Scheme 1.42**

#### 1.10.5.4. Endgame Strategy

The endgame to neopeltolide was straightforward. Sequential removal of the PMB ether followed saponification provided the corresponding seco acid, which upon exposure to the Yamaguchi macrolactonization gave the macrolide.<sup>69</sup> Removal of the BOM ether under hydrogenolysis unmasked the C5 hydroxyl, and coupling of fragment **1.112** via the method of Mitsunobu completed the total synthesis of neopeltolide.

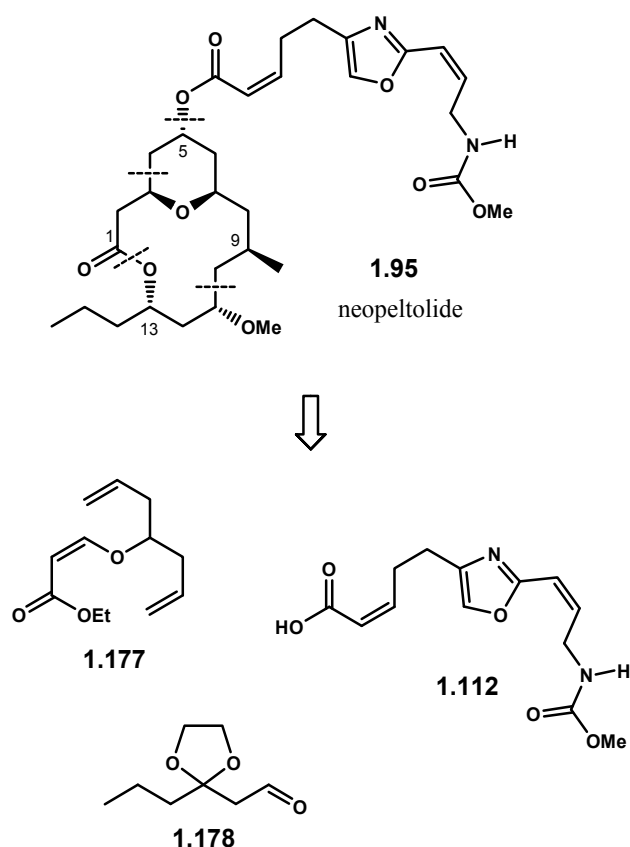


**Scheme 1.43**

#### 1.10.6. Kozmin's Approach

Kozmin and co-workers recently published the latest total synthesis of neopeltolide.<sup>122</sup> Bond disconnections of the macrolide, as shown in Scheme 1.44, resulted in three synthetic fragments: diene **1.177**, aldehyde **1.178**, and oxazole acid **1.112**. The assembly of neopeltolide's tetrahydropyran core was accomplished via Prins desymmetrization<sup>115</sup> of diene **1.177**, which eventually led to the production of racemic neopeltolide.



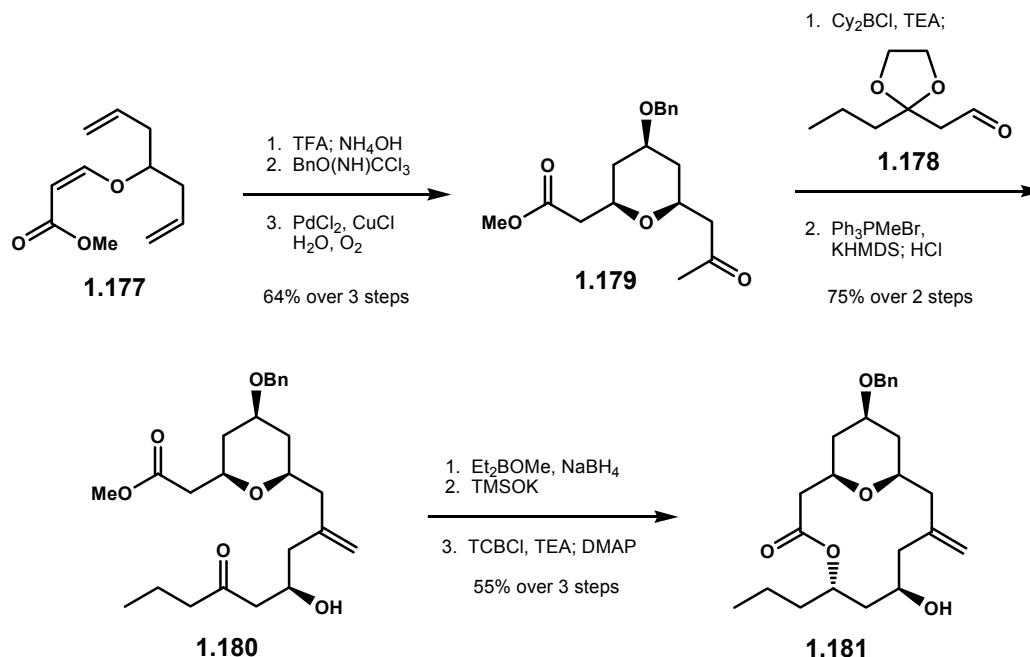


**Scheme 1.44**

#### 1.10.6.1. Macrolactone Construction

Kozmin's total synthesis of neopeltolide began with readily accessible diene **1.177**. Exposure to TFA and subsequent saponification served to desymmetrize **1.177** to the Prins cyclization product, the tetrahydropyran core of neopeltolide.<sup>115</sup> Protection of C5 hydroxyl as a benzyl ether followed by Wacker-Tsuji oxidation afforded ketone **1.179**.<sup>156</sup> The ensuing soft enolization of the ketone provided the corresponding boron enolate, which readily reacted with aldehyde **1.178** to set up the C10 – C11 connectivity.<sup>157, 158</sup> The ensuing Wittig methylenation of C9 carbonyl and acidic

hydrolysis unmasked ketone **1.180**. The introduction of C13 hydroxyl was realized in a chelation-controlled, stereoselective 1,3-*syn* reduction of  $\beta$ -hydroxy ketone.<sup>159</sup> The ensuing saponification of the ethyl ester and Yamaguchi macrolactonization<sup>69</sup> of the corresponding seco acid provided macrolide **1.181**.

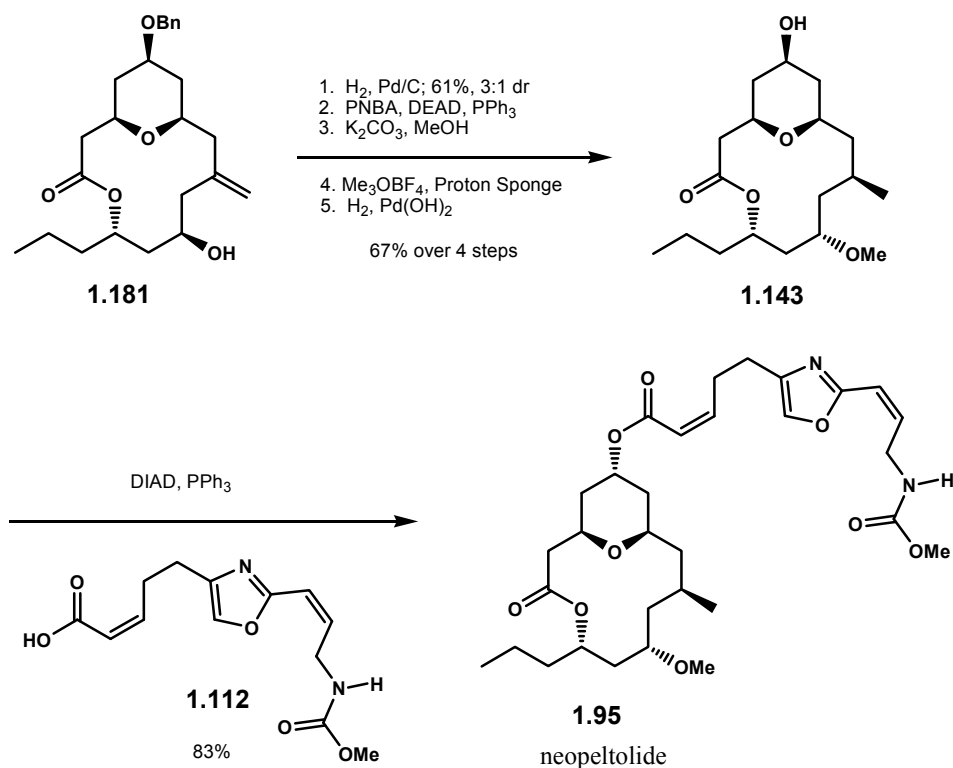


**Scheme 1.45**

#### 1.10.6.2. Stereochemical Elaboration and Endgame Strategy

Kozmin's total synthesis of neopeltolide continued with extensive elaboration of the stereochemistry for the macrolactone. This process began with hydrogenation of **1.163** under  $\text{Pd/C}$  catalysis which installed the requisite C9 methyl stereochemistry in 61% yield as a 3:1 mixture of diastereomers. The ensuing Martin-modified Mitsunobu inversion<sup>139</sup> corrected the C11 hydroxy group, which was readily subjected to *O*-

methylation under Meerwein's salt and Proton Sponge.<sup>92</sup> Reductive removal of C5 benzyl ether and subsequent installation of oxazole carbamate side chain with the method of Mitsunobu completed the sixth total synthesis of neopeltolide.



Scheme 1.46

### 1.11. Macrolides from Red Alga *Polycavernosa tsudai* and *Acanthophora specifera*

In 1991, a severe case of human food poisoning from ingestion of edible red alga *Polycavernosa tsudai* (*Gracilaria edulis*) was reported in Guam.<sup>6</sup> Of thirteen people affected, three fatalities occurred from cardiac arrests. As a result, research was immediately launched to identify the cause. A polyketide natural product, polycavernoside A **1.1**, proved the causative toxin. This conclusion was based on the

similarity of observed symptoms in experimental animals and human patients. It was noticed that the toxicity in the collected samples rapidly decreased over several isolation periods and eventually disappeared, suggesting that the toxin production by the alga was just a mere transient phenomenon. However, ten years later, another dreadful food poisoning from red alga consumption, this time *Acanthophora specifera*, was reported in the Philippines.<sup>7</sup> Thirty six people were victimized; eight of whom did not survive. Once again, research was initiated, and interestingly, the same toxin, polycavernoside A proved responsible for the outbreak.

From 2.6 kilograms of *P. tsudai*, 0.4 mg of polycavernoside A was successfully isolated.<sup>160</sup> Polycavernoside A **1.1** is a 16-membered macrolide with several interesting structural features. Similar to other macrolides presented in this chapter, polycavernoside A contains the requisite C3 – C7 tetrahydropyran segment. In addition to the interesting disaccharide residue, which was identified as *O*-2,3-di-*O*-methylfucopyranosyl-(1''-3'')-*O*-2,4-di-*O*-methylxylopyranosyl-(1'-5), the pendant hydrophobic chain of the natural product is highlighted by unique triene functionality; all of which possess *E* olefin geometry.<sup>161</sup>

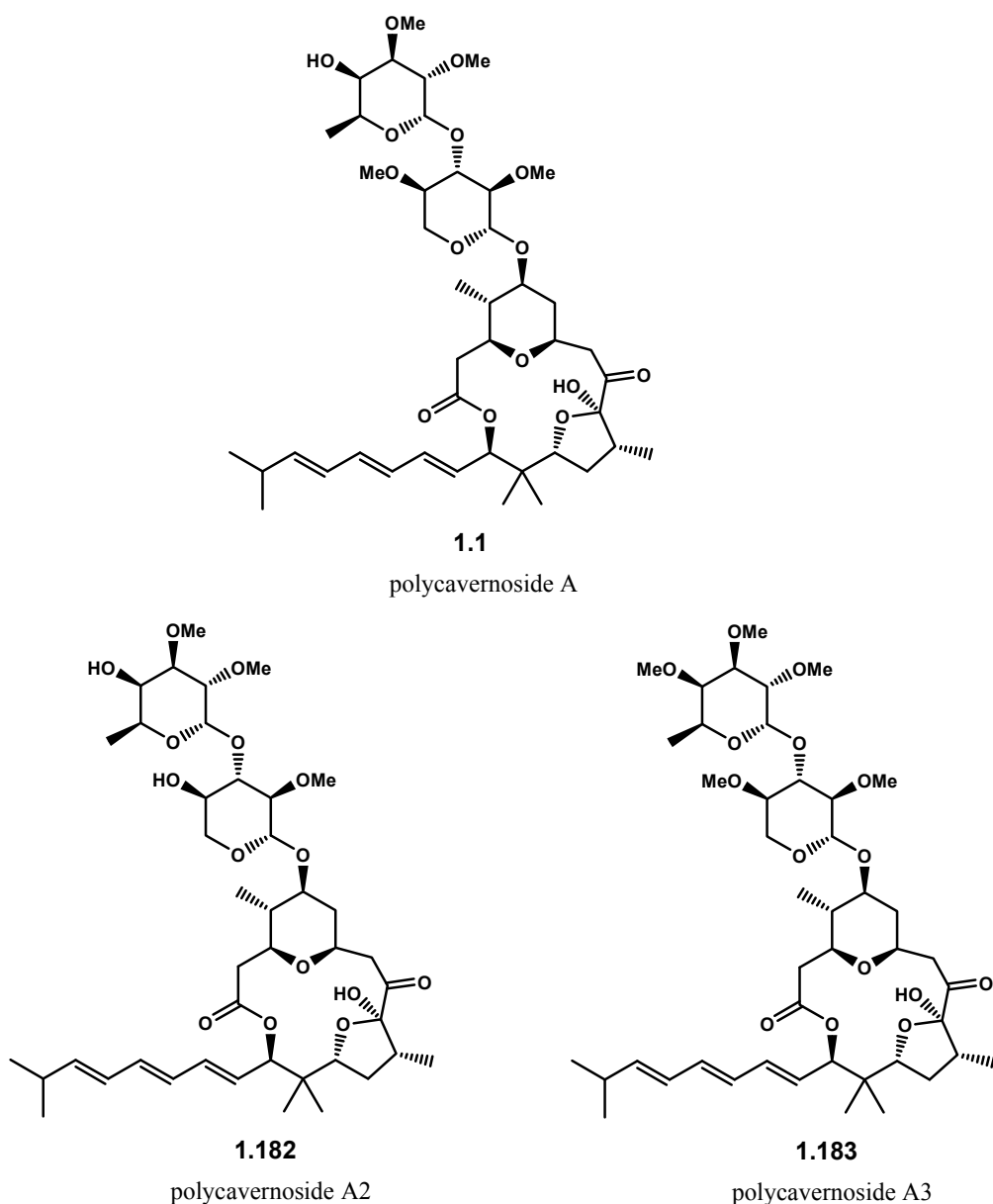
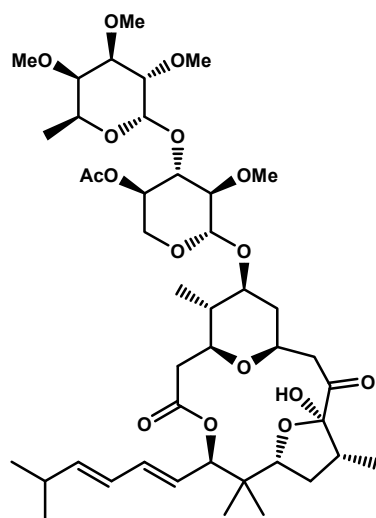


**Figure 1.11**

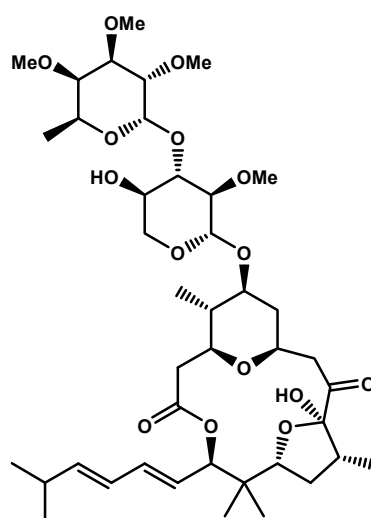
Since its initial isolation, numerous structural analogues of polycavernoside A have been isolated. These include polycavernosides A2 **1.182** and A3 **1.183**,<sup>162</sup> Figure 1.11, B **1.184** and B2 **1.185**,<sup>162</sup> as well as C **1.186** and C2 **1.187**,<sup>163</sup> Figure 1.12. Interestingly, the aglycon structure of polycavernosides C and C2 are different from those of polycavernosides A, A2, A3, B, and B2 in a sense that they exist as the “open-form”

structural analog of C10 – C13 hemiketal-furan. In contrast to polycavernoside A, the *in vivo* biological examinations of polycavernoside C against mice indicated no toxicity at LD<sub>99</sub> being greater than 0.2 mg/kg, a lethal dosage for polycavernoside A. Despite the fact that all of these macrolides were isolated from red alga *P. tsudai*, their structural similarity to those produced directly by cyanobacteria, such as acutiphycins, lyngbyalosides, and lyngboillose, strongly suggests polycavernoside cyanobacterial biosynthetic origin.



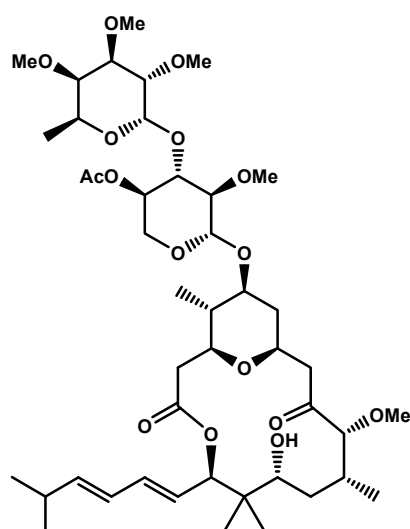
**1.184**

polycavernoside B



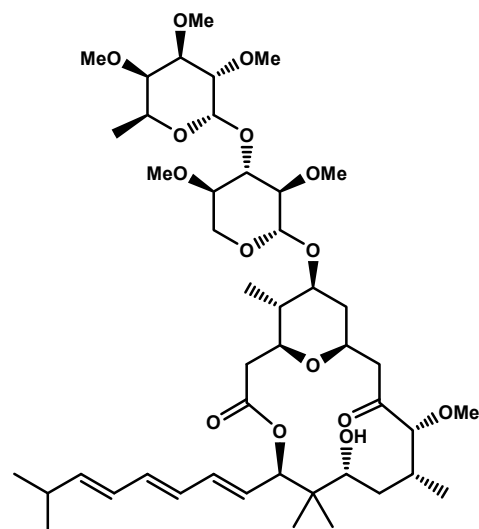
**1.185**

polycavernoside B2



**1.186**

polycavernoside C



**1.187**

polycavernoside C2

**Figure 1.12**

Due to the exceptionally potent toxicity against humans combined with the fact that natural samples of polycavernoside A are extremely limited or even no longer available, total synthesis is the only viable means to acquire enough materials for comprehensive investigation and understanding the bioactivity of this natural product.

There are three elegant total syntheses of polycavernoside A reported up to date, independently by Murai,<sup>164</sup> Paquette,<sup>165, 166</sup> and White.<sup>167, 168</sup> These total syntheses have been recently reviewed by Paquette and Yotsu-Yamashita.<sup>169</sup> Additionally, extensive biological evaluations and structure-activity-relationship studies of this toxin have also been published.<sup>170, 171</sup> Recent studies suggested that the mode of action of polycavernoside A analog **1.188** have involved membrane depolarization due to an increase in cytosolic calcium levels.<sup>170</sup>

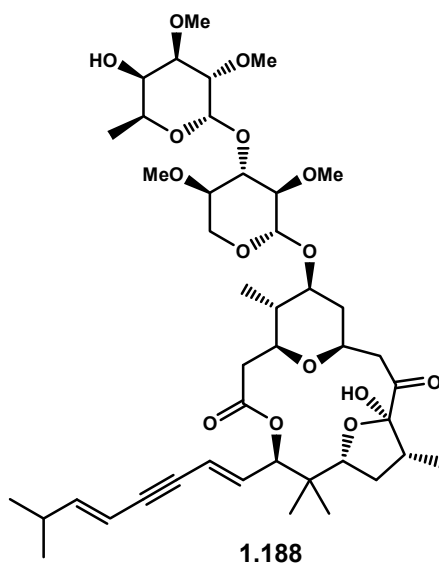


**Figure 1.13**

## 1.12. Conclusion

Cyanobacteria are an extremely prolific source of biologically important natural products, particularly those classified as macrolides. By restricting our literature search parameters for cyanobacterial macrolides that contain a tetrahydropyran moiety in the C3



– C7 segment, we were able to identify several macrolides, including acutiphyccins **1.2 – 1.3**, lyngbyalosides **1.4 – 1.5**, lyngbouilloside **1.6**, callipeltosides **1.7 – 1.10**, phorbasides **1.11 – 1.15**, aurisides **1.16 – 1.17**, dolastatin **1.18**, leucascandrolides **1.90 – 1.91**, neopeltolide **1.95**, polycarvernolides **1.1, 1.182 – 1.187**.

Albeit many of these macrolides were produced and isolated from non-cyanobacterial microorganisms, the strong structural resemblance of these compounds to those directly produced by cyanobacteria provides enough support for a hypothesis suggesting their cyanobacterial biogenesis, either from a symbiotic relationship of the producing microorganisms with cyanobacteria or via ingestion of cyanobacteria by the producing microorganisms.

Many of the macrolides presented in this chapter display significant biological activities, which include anticancer, antibacterial, or even antifungal properties. Thus, it is clear that this class of natural products denotes a promising hit in drug discovery. Furthermore, the structural complexity contained within these macrolides may lead to the discovery of new biological targets. Unfortunately, natural products often exist in an extremely low natural abundance. Consequently, comprehensive biological study of most of these compounds will require total synthesis, a daunting and labor-intensive task typically pursued by academic groups. It is to our hope that the continuation of these strong efforts coupled with industrial partnerships lead to new, more effective better drugs which will inevitably benefit mankind.

## CHAPTER TWO

### (+)-ACUTIPHYCIN: ISOLATION AND TOTAL SYNTHESSES

#### 2.1. Purpose

The purpose of this chapter is to detail literature reviews pertinent to cytotoxic macrolide (+)-acutiphycin. Several aspects within this topic will be covered, including brief descriptions on the isolation, characterization, and solution conformation of the macrolide, as well as detailed discussions on three accounts on its total synthesis independently reported by the Smith, Kiyooka, and Jamison groups.

#### 2.2. Isolation and Biological Activity

In light of searching for new antineoplastic natural products, the late Richard E. Moore and co-workers from the University of Hawaii have been exploring the blue-green algae, in particular the Oscillatoriaceae, as the source of such agents. In 1984, Moore and co-workers reported the isolation of acutiphycins, Figure 2.1, from a crude extract of *Oscillatoria acutissima*.<sup>12</sup> This algae was found in a freshwater pond in Manoa Valley, Oahu, collected, and then grown in mass culture in their laboratories. From 275 grams of

freeze-dried algae, 9.2 grams of crude extract were isolated, which ultimately yielded 300 mg of (+)-acutiphycin, **2.1**, and 320 mg of (+)-20,21-didehydroacutiphycin, **2.2**; both as white solids. Initial biological evaluations of these natural products revealed that they were cytotoxic against KB and NIH/3T3 cells with  $ED_{50} < 1 \mu\text{g/mL}$ . Furthermore, the acutiphycins were active against Lewis lung carcinoma with  $T/C \geq 150$  at 50 mg/kg.

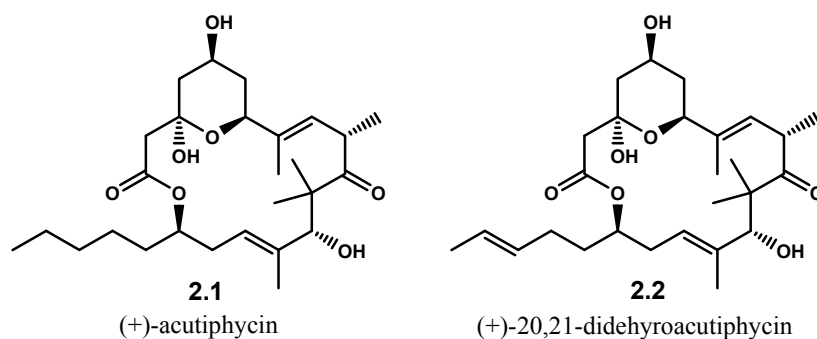


**Figure 2.1**

## 2.3. Structural Elucidation

The overall structure of acutiphycins, including their absolute stereochemistry, was unambiguously determined by using chemical degradation studies as well as detailed NMR experiments.

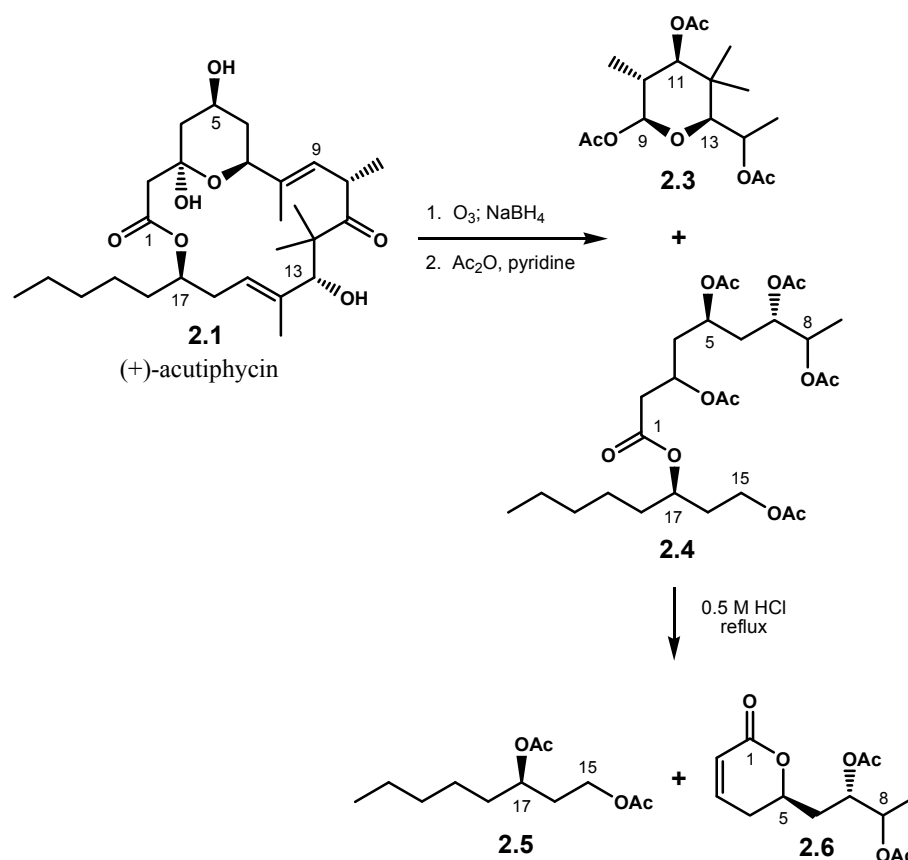
### 2.3.1. NMR Experiments

The  $^1\text{H}$  and  $^{13}\text{C}$  NMR spectroscopy data of acutiphycin **2.1** indicated that acutiphycin possessed six methyl groups, eight methylene carbons, seven methine

carbons, six quaternary carbons, and three exchangeable protons. The molecular mass of acutiphycin was found to be 480 daltons, which corresponded to molecular composition of  $C_{27}H_{44}O_7$ . From the  $^{13}C$  signals at 214.4 and 170.9 ppm, three of these oxygens were of ketone and ester functionalities. The next two oxygens were assigned as secondary alcohols. This was confirmed by the fact that peracetylation of acutiphycin incorporated only two acetate groups. The remaining two oxygens appeared to be hemiketal based on the  $^{13}C$  signal at 96.2 ppm, a typical chemical shift for such functionality. Three of the six quaternary carbons were assigned for the hemiketal, ketone, and ester groups. The remainders were accounted for two trisubstituted ethenyl and one saturated carbon containing *gem*-dimethyl groups. From further coupling constant determinations and NOE observations, acutiphycin appeared to possess a trisubstituted tetrahydropyran ring and a pendant *n*-pentyl side chain. Finally, the overall structure of acutiphycin was assembled through decoupling experiments.

### 2.3.2. Chemical Degradation Studies

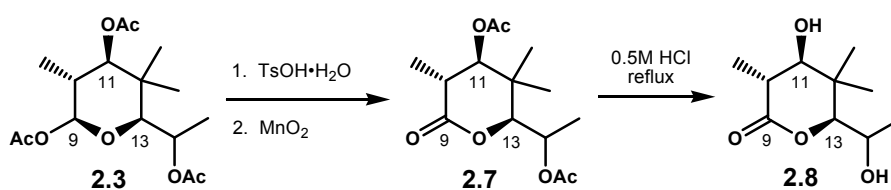
The gross structure of acutiphycin was also deduced via carefully planned chemical degradation methods. Exposure of acutiphycin to ozonolysis followed by reductive workup produced a mixture of alcohols. Upon peracetylation of these alcohols, two major products were isolated: tetrahydropyran **2.3** and ester **2.4**. Ester **2.4** was further treated with acidic hydrolysis which produced diacetate **2.5** and lactone **2.6**, Scheme 2.1. Analyses of these three small fragments provided useful information regarding the connectivity and stereochemistry of acutiphycin.



**Scheme 2.1**

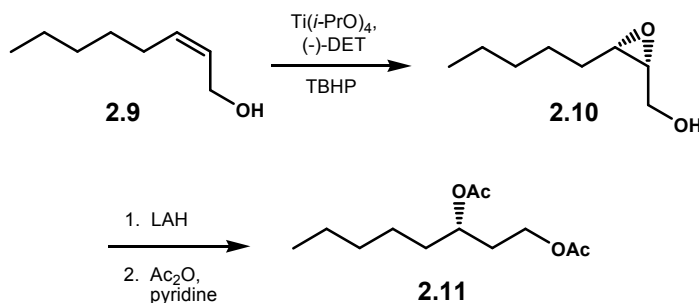
The structure of **2.3** was deduced from detailed  $^1\text{H}$  NMR analyses. From the large vicinal coupling constant, the protons at C9, C11, and C13 all appeared to be in axial positions. The stereochemistry at C11 of **2.3** was generated from the reduction of its respective C11 ketone of acutiphycin. Interestingly, C9 remained as a masked aldehyde which indicated that the borohydride workup did not fully reduce its ozonide precursor. The ketone functionality at C14 generated in the ozonolysis was also reduced to a secondary alcohol with a high degree of stereocontrol; however, its relative stereochemistry was not established. The absolute stereochemistry of fragment **2.3** was determined by a CD study of **2.7** and **2.8**. As shown in Scheme 2.2, conversion of **2.3** to

lactone **2.7** was achieved via sequential acidic hydrolysis and oxidation. Further acidic hydrolysis of **2.7** finally afforded diol **2.8**. The CD curve of **2.7** and **2.8** showed a negative Cotton effect at  $[\theta]_{227}$  -2860 and  $[\theta]_{224}$  -2860 respectively.<sup>172-174</sup> This observation suggested the absolute configurations at C10 and C13 being *R* and *S* respectively, which consequentially corresponded to the stereochemistry of C10 and C13 in acutiphycin being *S* and *R*.



**Scheme 2.2**

In the meantime, the absolute stereochemistry of fragment **2.5** was deduced via synthesis and comparison of optical rotation. The short synthesis to enantiomerically enriched diacetate **2.11** was accomplished with asymmetric epoxidation of allylic alcohol **2.9** to epoxy alcohol **2.10** under Sharpless protocol,<sup>153, 154</sup> followed by regioselective reductive ring opening and peracetylation, Scheme 2.3. The optical rotation of natural and synthetic fragments **2.5** and **2.11** was found  $[\alpha]_D^{25} = -18^\circ$  and  $[\alpha]_D^{25} = +15.2^\circ$  respectively. Thus, the configuration at C17 of acutiphycin was assigned as *R*.



**Scheme 2.3**

The absolute stereochemistry of the tetrahydropyran ring was determined by CD spectrum of fragment **2.6**, which showed a positive Cotton effect at  $[\theta]_{257} +1150$ . This indicated that the stereochemistry at C5 in **2.6** was *R*, which corresponded C5 in acutiphycin being *S*. From the coupling constant measurement, the proton at C7 appeared to be in axial position. Therefore, the stereochemistry at C7 in acutiphycin had to be *S*.

### 2.3.3. NOE-Based Conformational Analysis

The virtual solution conformation of acutiphycin in a non-polar medium (1:1  $\text{CDCl}_3/\text{C}_6\text{D}_6$ ) was proposed as conformer **2.12** shown in Figure 2.2. NOE experiments revealed that irradiation of the methyl group on C8 produced a strong NOE on the C6-axial and the C10 protons. This suggested that the C6-axial, C8, and C10 protons were positioned such that they were nearly eclipsing one another. A strong NOE was also observed on the C9 proton when the C7 proton was irradiated. This implied that these protons also had to be eclipsing. Additionally, irradiation of the C8 methyl group also produced a strong NOE with the C13 proton indicating that the C13 proton was oriented

toward the C8 methyl group and the C10 proton. Irradiation of C10 produced a significant NOE on one of the two C12 methyl groups, which suggested an inward orientation of this methyl group into the macrolide plane.

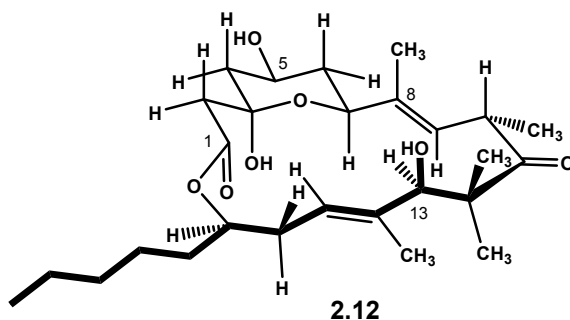


**Figure 2.2**

## **2.4. Previous Total Syntheses**

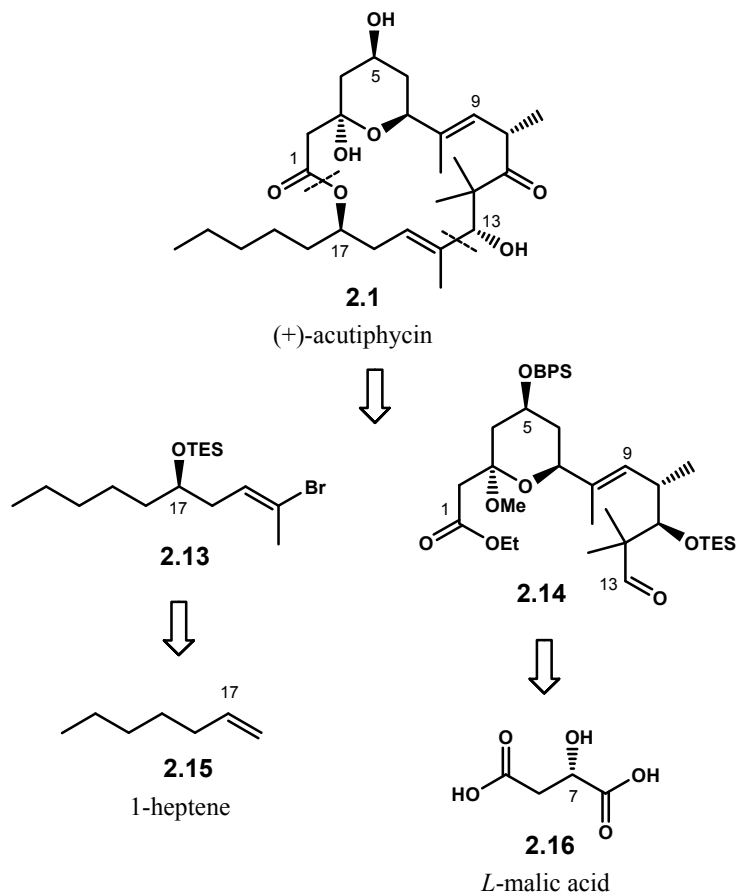
(+)-Acutiphycin is an attractive target for total synthesis due to its potent biological activity. Since its isolation, there are two completed total syntheses and one effort towards its seco acid. The first total synthesis of acutiphycin was reported by Smith and co-workers.<sup>175, 176</sup> Soon after, Kiyooka and Hena reported their efforts in the construction of acutiphycin seco acid.<sup>177, 178</sup> More recently, Jamison and Moslin successfully produced the second total synthesis.<sup>179, 180</sup>

### **2.4.1. Smith's Approach**

In 1995, Smith and co-workers reported a short communication detailing their successful approach to the first total synthesis of acutiphycin and 20,21-



didehydroacutiphyacin.<sup>175</sup> The corresponding full article appeared in 1997.<sup>176</sup> Scheme 2.4 described Smith's retrosynthesis which disconnected the C13-C14 and the macrolactone bonds, thus providing two fragments **2.13** and **2.14**. These fragments would be prepared individually from 1-heptene **2.15** and L-malic acid **2.16**.

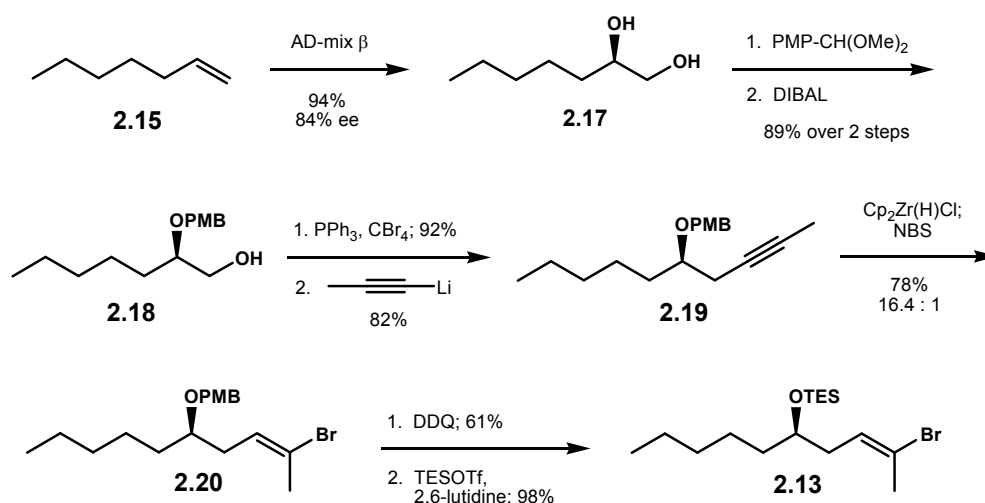


**Scheme 2.4**

#### 2.4.1.1. Preparation of Fragment 2.13

As shown in Scheme 2.5, the synthesis of fragment **2.13** commenced with Sharpless asymmetric dihydroxylation of 1-heptene **2.15**.<sup>181</sup> Protection of the resulting

diol as a PMB acetal followed by DIBAL reduction<sup>182</sup> provided primary alcohol **2.18**. Subsequent bromination<sup>183</sup> followed by coupling with 1-lithio-1-propyne afforded alkyne **2.19**. Alkyne **2.19** was then subjected to hydrozirconation with NBS quench to provide highly regio- and stereoselective vinyl bromide **2.20**.<sup>184, 185</sup> The synthesis of fragment **2.13** was completed upon removal of the PMB group with DDQ and re-protection of the resulting secondary alcohol as a TES ether.

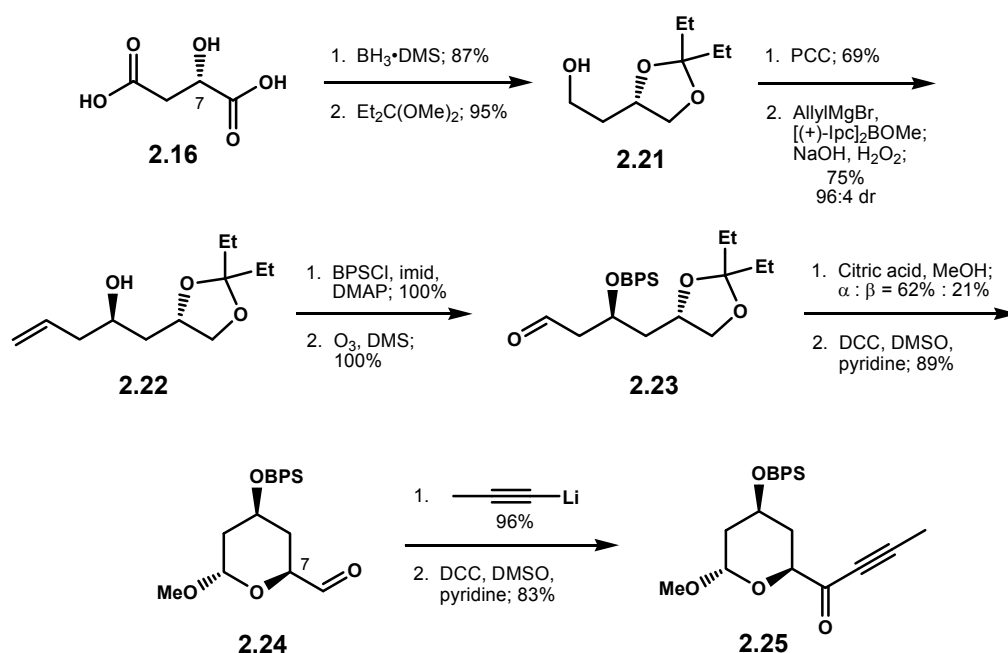


Scheme 2.5

#### 2.4.1.2. Preparation of Fragment 2.14

The preparation of fragment **2.14** began with commercially available L-malic acid. The stereochemistry of the hydroxyl group contained within this molecule corresponded to that of C7 in acutiphycin. Reduction of L-malic acid<sup>186</sup> to its corresponding triol followed by ketal formation provided thermodynamically favored dioxolane **2.21** in good yields.<sup>187, 188</sup> The remaining primary alcohol was oxidized with

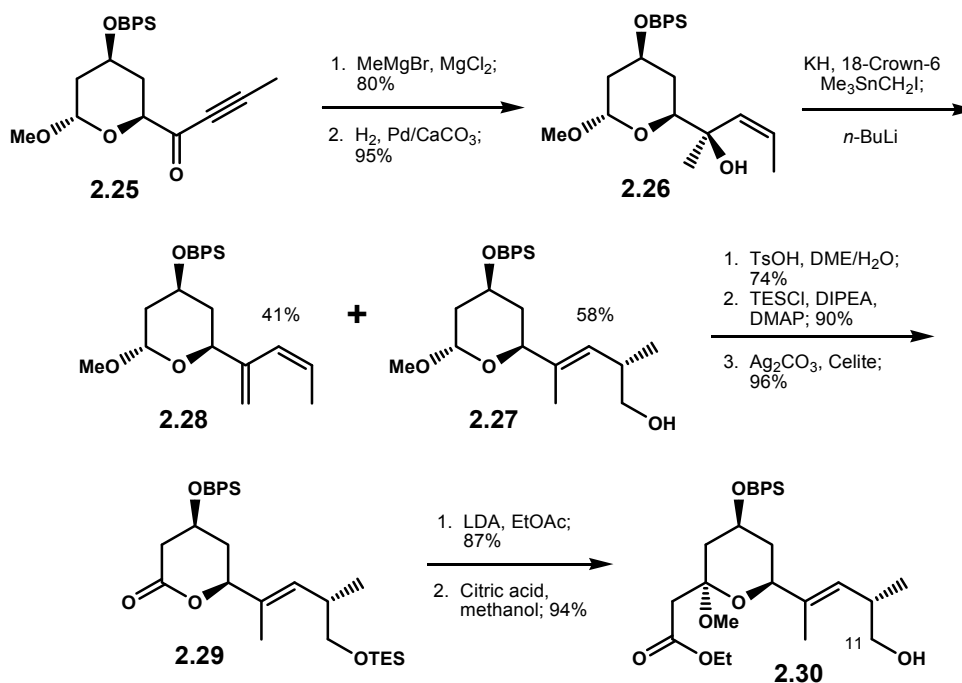
PCC to the aldehyde<sup>189</sup> which was then subjected to the Brown asymmetric allylation, thus yielding homoallylic alcohol **2.22** almost as a single diastereomer.<sup>142</sup> Sequential protection of the newly generated alcohol as a BPS ether and oxidative cleavage of the terminal olefin provided aldehyde **2.23**. Treatment of aldehyde **2.23** with acidic methanol solution induced ketal fragmentation and subsequent cyclization to furnish thermodynamically favored  $\alpha$ -methyl pyranoside as dictated by the anomeric effect. Moffatt oxidation<sup>190</sup> of the resulting primary alcohol to aldehyde **2.24**, addition of 1-lithio-1-propyne, and another Moffatt oxidation produced ketone **2.25** in good yields, Scheme 2.6.



Scheme 2.6

Exposure of ketone **2.25** to chelation-controlled<sup>191</sup> addition of MeMgBr and hydrogenation with Lindlar catalyst afforded tertiary allylic alcohol **2.26**, Scheme 2.7.

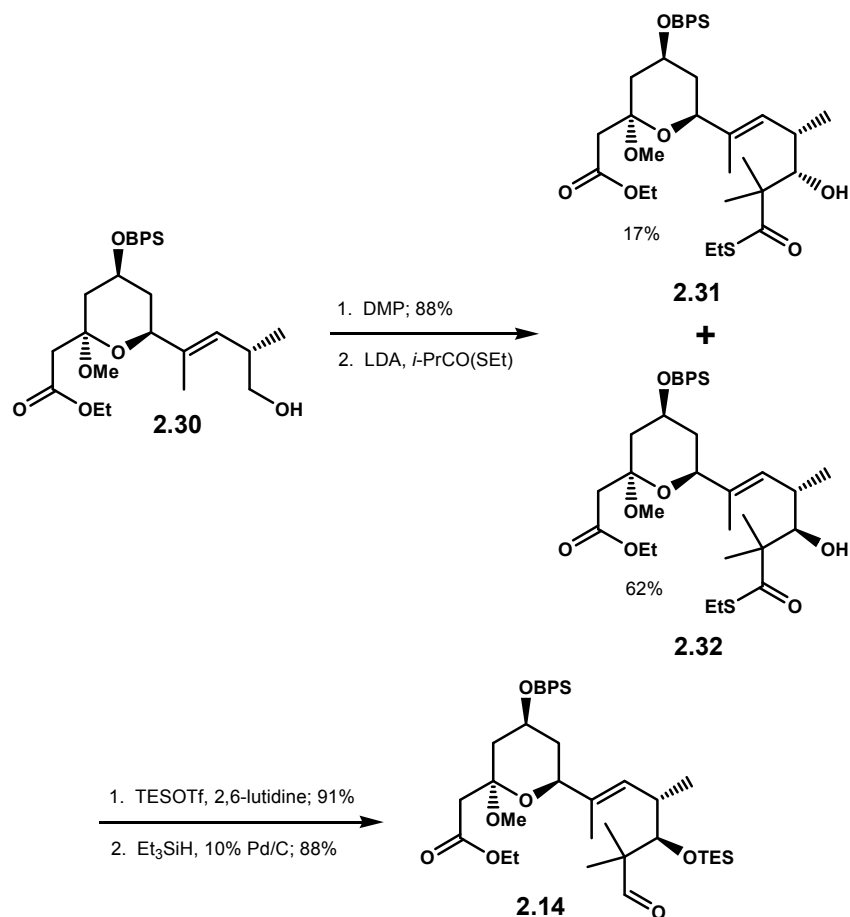
Subsequent rearrangement of tertiary alcohol to homoallylic alcohol **2.27** was realized via [2,3]-sigmatropic rearrangement.<sup>192, 193</sup> Unfortunately, the desired alcohol **2.27** was only obtained in 58%. A significant byproduct diene **2.28**, presumably generated from E2 elimination of the hindered stannyl ether, was also produced in 41%. Sequential acidic hydrolysis, chemoselective protection of C11 hydroxyl as a TES ether, and oxidation of the resulting lactol provided lactone **2.29** in excellent yields.<sup>194</sup> Addition of the lithium enolate of ethyl acetate followed by acidic methanolysis installed the tetrahydropyran moiety. These conditions also removed the C11 TES ether providing alcohol **2.30**.



**Scheme 2.7**

The ensuing oxidation under Dess-Martin protocol<sup>87</sup> and addition of the lithium enolate of ethyl isobutanethioate to the corresponding aldehyde then furnished epimeric alcohol **2.31** and **2.32** in 17% and 62% yield, respectively. The stereochemical outcome

of alcohol **2.32** was predicted by the Cram model<sup>195</sup> and verified by the Mosher ester analysis.<sup>196</sup> The secondary alcohol was protected as a TES ether, and subsequent reduction of the thioester to aldehyde according to the method of Fukuyama<sup>197</sup> completed the synthesis of fragment **2.14**, Scheme 2.8.

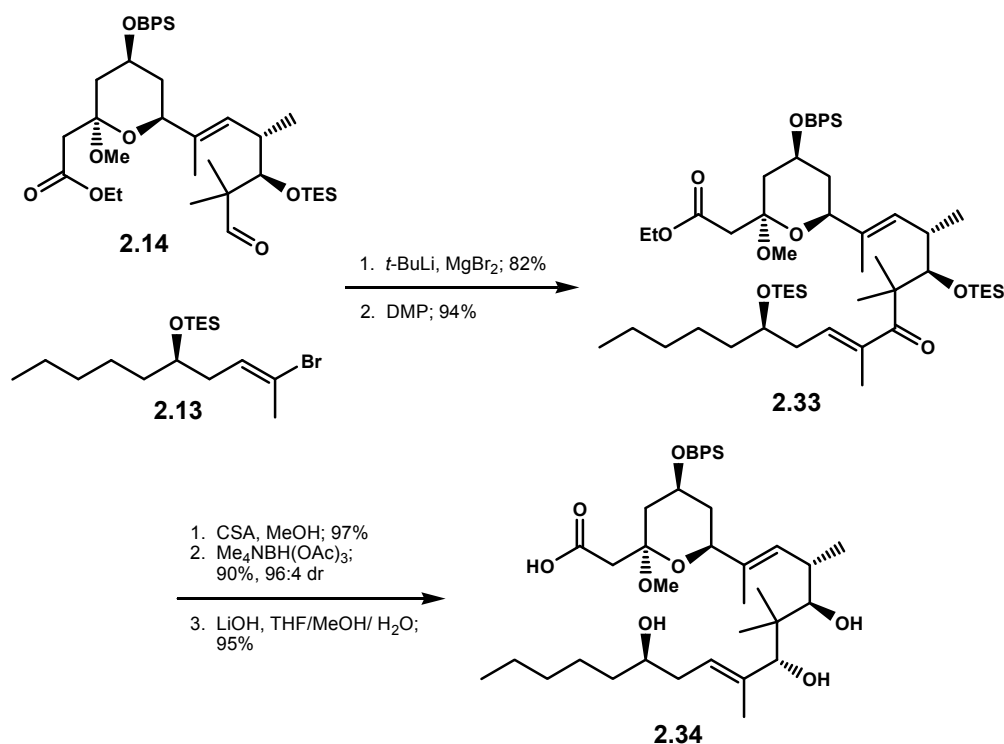


Scheme 2.8

#### 2.4.1.3. Fragments Coupling and Endgame Strategy

With fragments **2.13** and **2.14** in hand, Smith and co-workers then turned their attention to the coupling of these building blocks. Lithiation of vinyl bromide **2.13**

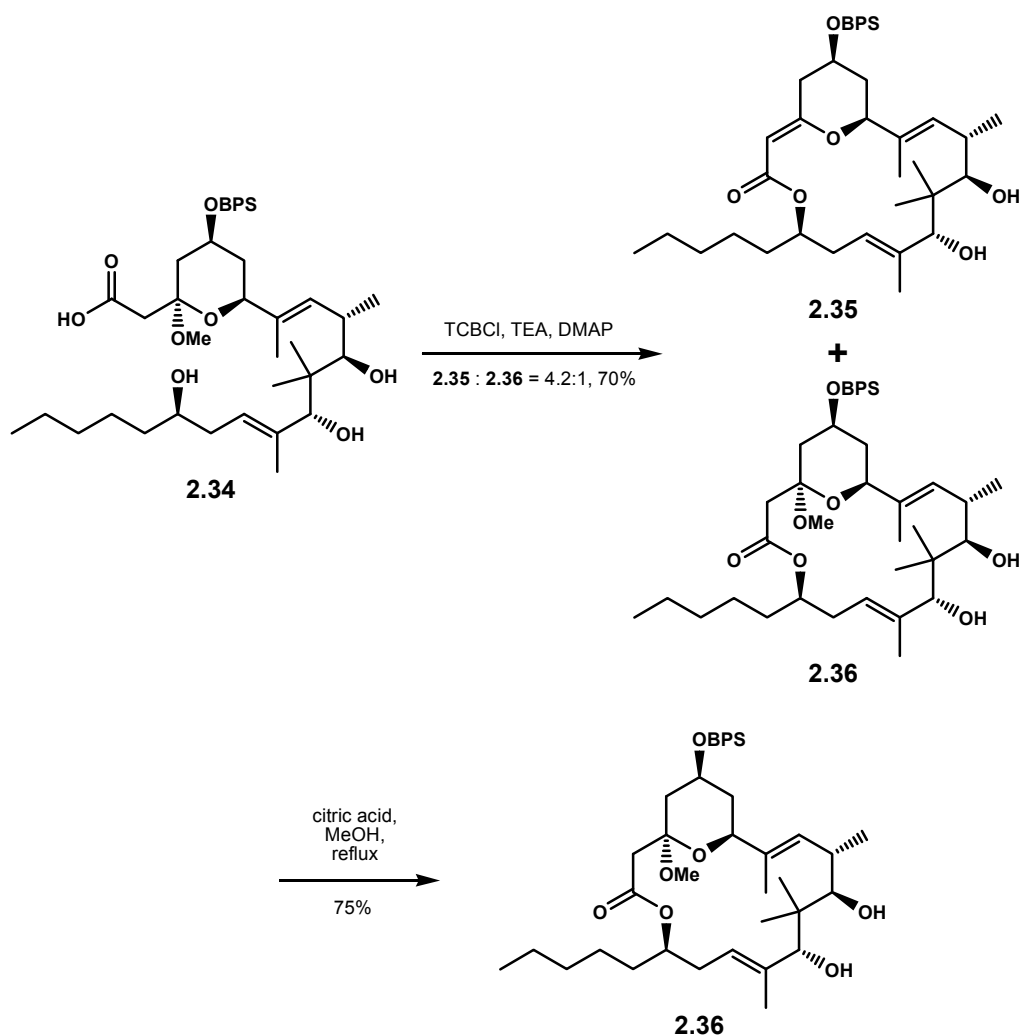
followed by transmetallation with magnesium bromide provided the vinyl Grignard reagent which added smoothly to aldehyde **2.14**. This reaction provided the expected alcohol adducts as a 1:1 mixture of diastereomers which was then oxidized under Dess-Martin conditions<sup>87</sup> to enone **2.33**. Exposure of this enone to acidic methanolysis removed the two TES ethers. The ensuing Evans' *anti* reduction<sup>72</sup> converted the  $\beta$ -hydroxy ketone moiety to the corresponding 1,3-*anti* diol in high yield and diastereoselectivity. Saponification finally yielded seco acid **2.34**, Scheme 2.9.



Scheme 2.9

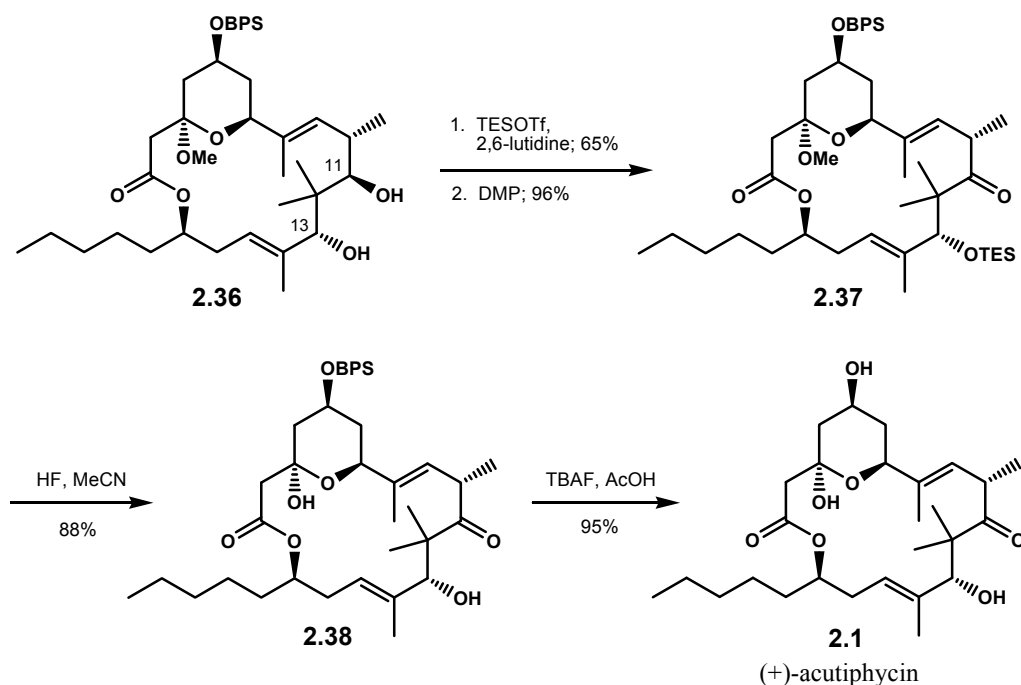
#### 2.4.1.4. Endgame Strategy

The macrolactonization of seco acid **2.34** was realized by exploiting the protocol developed by Yamaguchi.<sup>69</sup> This method, however, provided a mixture of predominantly macrolide triene **2.35** and macrolactone **2.36** in a combined yield of 70%. This problem was readily corrected by treating the macrolide mixture in refluxing acidic methanol. These conditions successfully reinstall the methyl pyranoside functionality in 75% yield.



Scheme 2.10

The endgame sequence to acutiphycin commenced with regioselective protection of the less hindered C13 hydroxyl as a TES ether. The ensuing Dess-Martin oxidation<sup>87</sup> of the remaining C11 hydroxy group gave ketone **2.37**. Removal of the C13 TES ether under HF/MeCN conditions unmasked the hydroxyl group and at the same time hydrolyzed the methyl pyranoside, thus providing hemiketalpyran **2.38**. Removal of the C5 BPS ether under AcOH buffered TBAF solution<sup>198</sup> completed the total synthesis of acutiphycin **2.1**, Scheme 2.11.



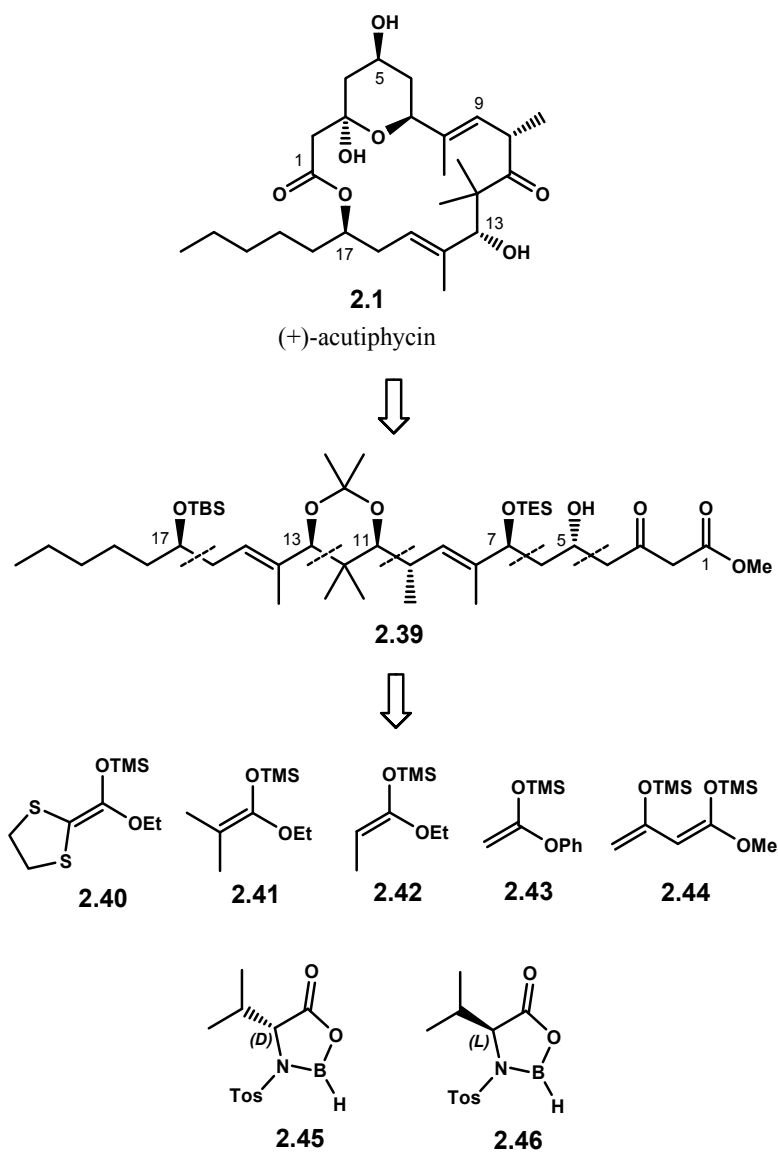
Scheme 2.11

#### 2.4.2. Kiyooka's Approach

In 1999, Kiyooka and Hena published their efforts in the construction of the seco acid of acutiphycin. This work was highlighted by the extensive use of their



oxazaborolidinone-promoted asymmetric aldol methodology.<sup>177, 178</sup> As described in Scheme 2.12, the construction of acutiphycin's seco acid **2.39** was approached from a linear strategy involving five consecutive aldol reactions which beautifully set up the required five stereogenic hydroxyl centers. The versatility of these so called "Kiyooka aldol" reactions was demonstrated by the use of promoters **2.45** and **2.46** with five different silyl nucleophiles **2.40** – **2.44**. These promoters, which is a pair of enantiomers readily prepared *in situ* from a reaction between commercially available amino acids *N*-Tos-*L*- or *D*-valine and borane-THF complex, determines the stereochemical configuration of the aldol adduct.



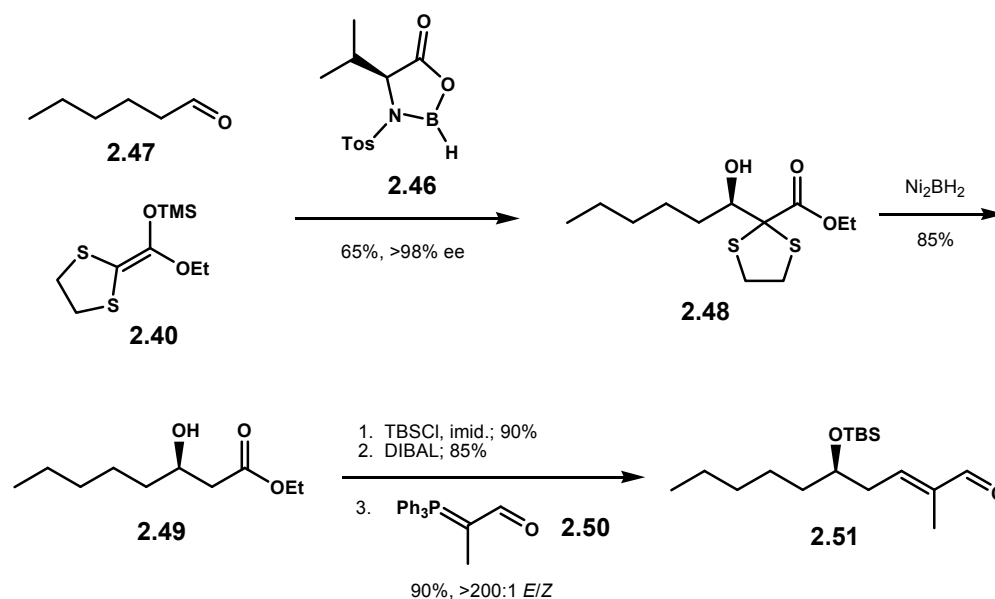
Scheme 2.12

#### 2.4.2.1. The First Aldol Reaction

Kiyooka's synthesis to acutiphycin commenced with the first aldol reaction which successfully coupled hexanaldehyde **2.47** with dithiolane silyl nucleophile **2.40**. Promoted by oxazaborolidinone **2.46**, this reaction produced aldol adduct **2.48** in 65%

yield with enantiomeric purity of greater than 98%.<sup>199</sup> Desulfuration of **2.48** with nickel boride then provided acetate aldol **2.49**.<sup>200</sup> Subsequent protection, ester reduction to the aldehyde, and vinylogation with phosphorane **2.50** afforded enaldehyde **2.51** in good yields, Scheme 2.13. This overall sequence in fact represents acetate aldol equivalence. Kiyooka stated that based on their previous studies, the necessity of using a dithiolane aldol reaction arose from the fact that without this steric influence at the  $\alpha$  position, the acetate aldol product would be obtained with significantly lowered enantioselectivity.<sup>201,</sup>

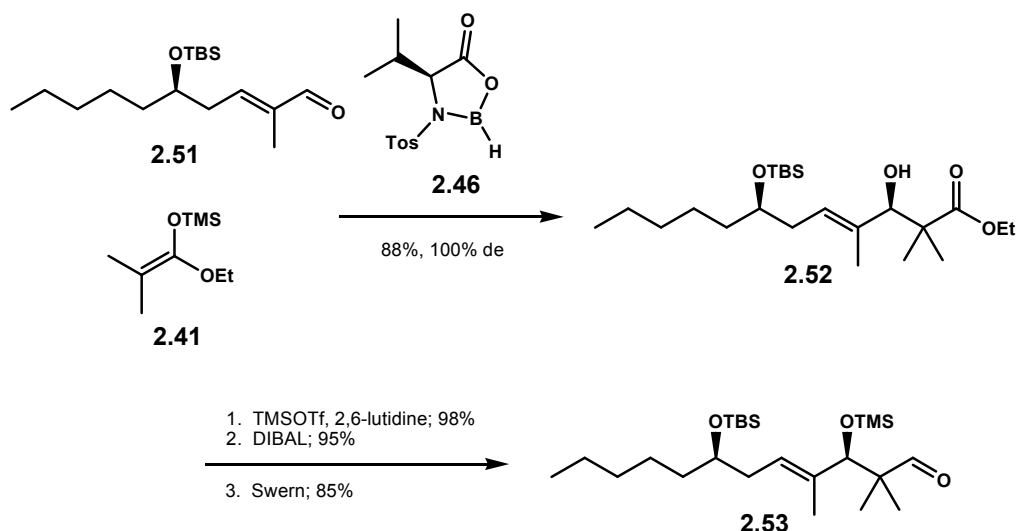
202



#### 2.4.2.2. The Second Aldol Reaction

Aldehyde **2.51** was then exposed to the second aldol reaction, this time using ketene acetal **2.41** and promoter **2.46**. This reaction gave adduct **2.52** in high yield as a

single diastereomer. Protection of the resulting hydroxyl group as a TMS ether proceeded smoothly, and the following reduction – oxidation sequence yielded the desired aldehyde **2.53**.

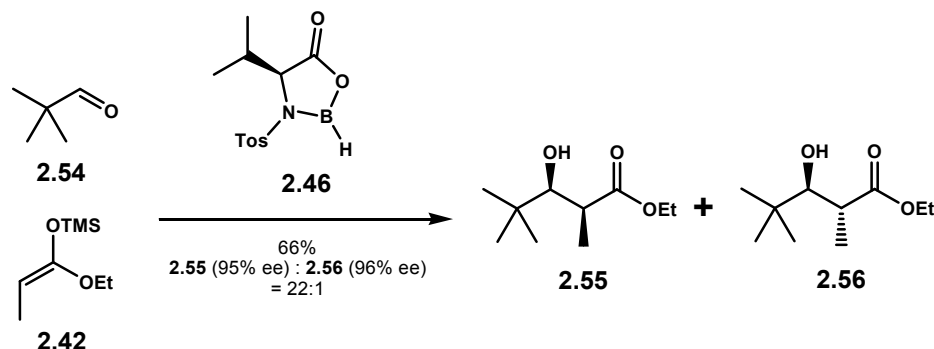


**Scheme 2.14**

#### 2.4.2.3. The Third Aldol Reaction

With aldehyde **2.53** in hand, their next effort was then focused in the installation of the two stereogenic centers at C11 and C12 of seco acid **2.39**. In order to establish this 1,2-*anti* relative stereochemistry requirement, Kiyooka and Hena employed *E*-silyl ketene acetal **2.42** as the nucleophilic partner. Much to their surprise, when ketene acetal **2.42** was reacted with sterically congested pivalaldehyde **2.54** as a test substrate in the presence of oxazaborolidinone **2.46**, the 1,2-*syn* aldol adduct **2.55** was predominantly produced over the desired 1,2-*anti* aldol adduct **2.56** in the ratio of 22:1. Nevertheless,

the individual aldol adducts themselves contained an extremely high level of enantiomeric purity.



**Scheme 2.15**

The observed stereochemical outcome of the hydroxy group in aldol adducts **2.55** and **2.56** can be explained from the conformational stability of intermediate **2.57** generated upon complexation of the chiral oxazaborolidinone **2.46** and pivalaldehyde **2.54**. As shown in Figure 2.3, the upward orientation of the isopropyl group subsequently directs the aldehyde at the bottom of the oxazaborolidinone plane. As previously demonstrated by Corey and co-workers,<sup>203, 204</sup> the hydrogen bonding interaction between the aldehyde and the Lewis acid appears to further rigidify this conformation. Thus, an attack of nucleophile to the aldehyde at the sterically less encumbered face thus sets up the observed stereochemistry of the hydroxyl group.

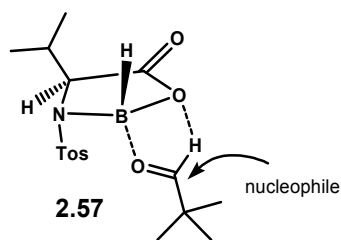


**Figure 2.3**

However, in order to explain the observed and unexpected 1,2-*syn* stereochemistry in Scheme 2.15, for an asymmetric nucleophile, such as  $\alpha$ -methyl silyl ketene acetal **2.42**, the orientation of the nucleophile upon approach to the Lewis acid-aldehyde complex **2.57** must be taken into an account. Figure 2.4 depicts six possible transition states for such an approach. By comparison, it is clear that transition state **2.58**, which leads to 1,2-*syn*, appears most favorable due to optimal minimization of destabilizing gauche interactions between the methyl and *tert*-butyl groups as well as between the *tert*-butyl and ketene acetal groups.

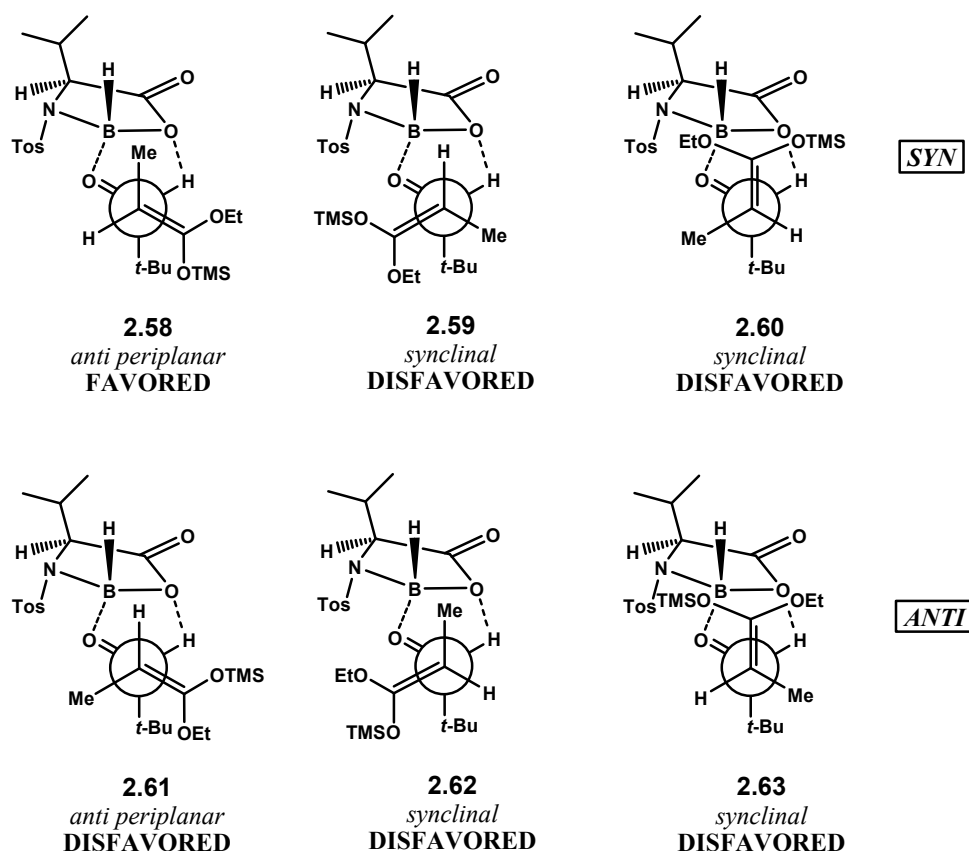
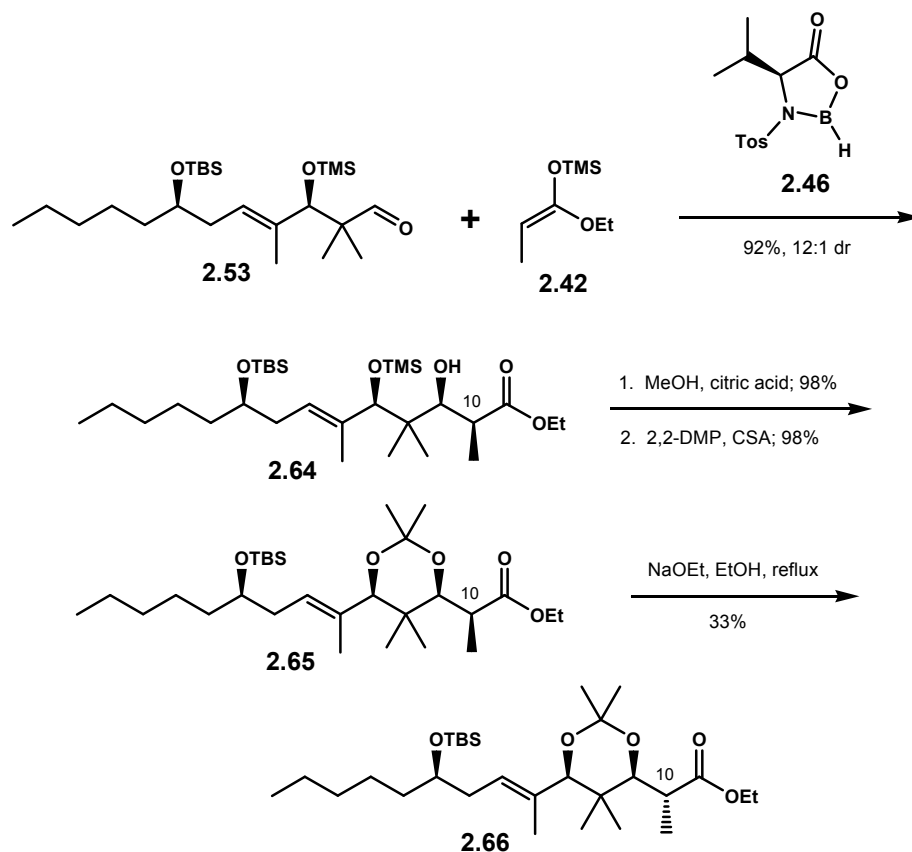


**Figure 2.4**

As shown in Scheme 2.16, when identical reaction conditions were applied to aldehyde **2.53**, the 1,2-*syn* aldol product **2.64** was also obtained predominantly over the desired 1,2-*anti* stereochemistry in 12:1 selectivity with the combined yield of 92%. Again, excellent facial selectivity was maintained within each diastereomer. However, adduct **2.64** now contained the C10 stereochemistry opposite to that of acutiphycin, and a stereochemical correction was obviously required.



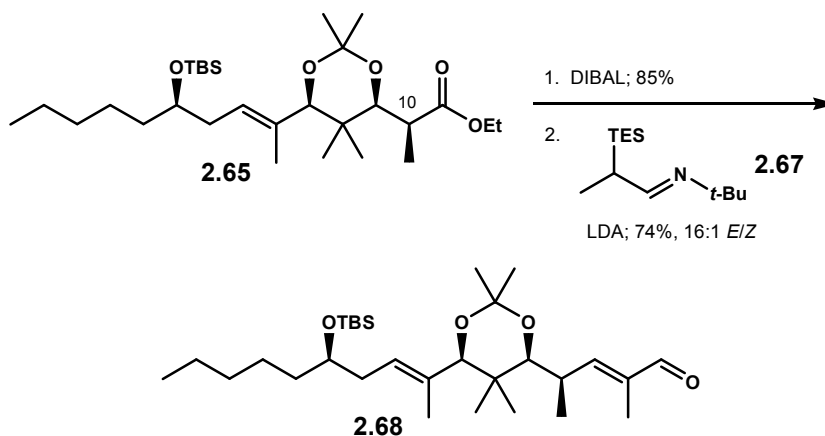
**Scheme 2.16**

The C10 stereochemical correction was proposed via epimerization. Removal of the TMS ether under acidic methanolysis followed by protection of the resulting 1,3-*syn* diol as acetonide **2.65**. Exposure to a refluxing solution of sodium ethoxide in ethanol successfully epimerized the C10 stereocenter; however, the 1,2-*anti* adduct **2.66** was isolated only in 33% yield.

Since the epimerization process was unfortunately ineffective, Kiyooka decided to continue on with their project using the incorrect C10 epimer **2.65**. In order to prepare the substrate for the upcoming forth aldol reaction, ester **2.65** was reduced to the



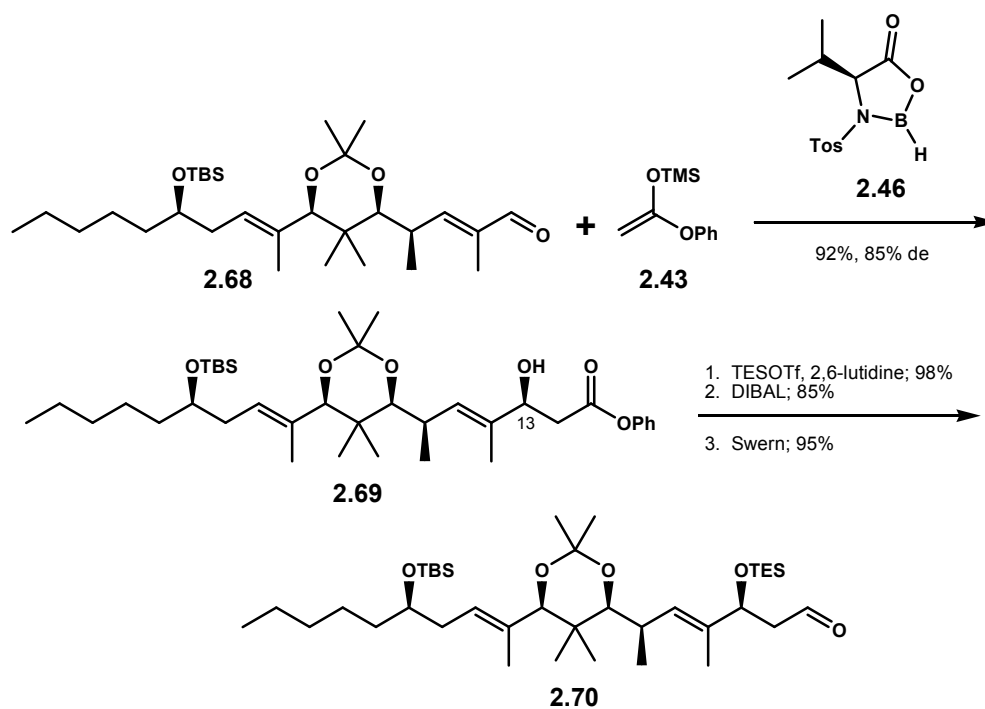
corresponding aldehyde. Immediate vinylogation of this aldehyde with  $\alpha$ -silyl imine **2.67** under LDA conditions,<sup>205</sup> provided  $\alpha,\beta$ -unsaturated aldehyde **2.68** in 74% yield.



**Scheme 2.17**

#### 2.4.2.4. The Fourth Aldol Reaction

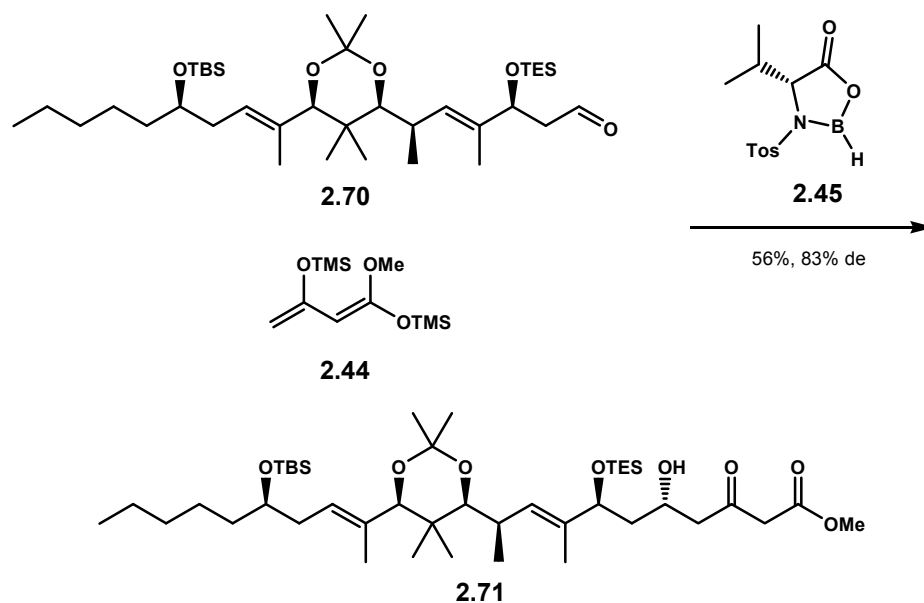
The next step in Kiyooka's route to acutiphycin required an installation of an acetate aldol unit. Although the conditions to achieve the highest enantioselectivity have been described in Scheme 2.13, the use of dithiolane silyl nucleophile **2.38** was not feasible in this case as the subsequent desulfurization under reductive conditions might also reduce the internal olefins. For this reason, the use of unsubstituted ketene acetal **2.43** was then considered. Indeed, a reaction of ketene acetal **2.43** and aldehyde **2.68**, once again promoted by oxazaborolidinone **2.46**, directly produced acetate aldol **2.69** in 84% yield, however, with slightly lowered diastereoselectivity. Subsequent protection of the C13 hydroxyl as a TES ether followed by a reduction – oxidation sequence afforded aldehyde **2.70**.



**Scheme 2.18**

#### 2.4.2.5. The Fifth Aldol Reaction

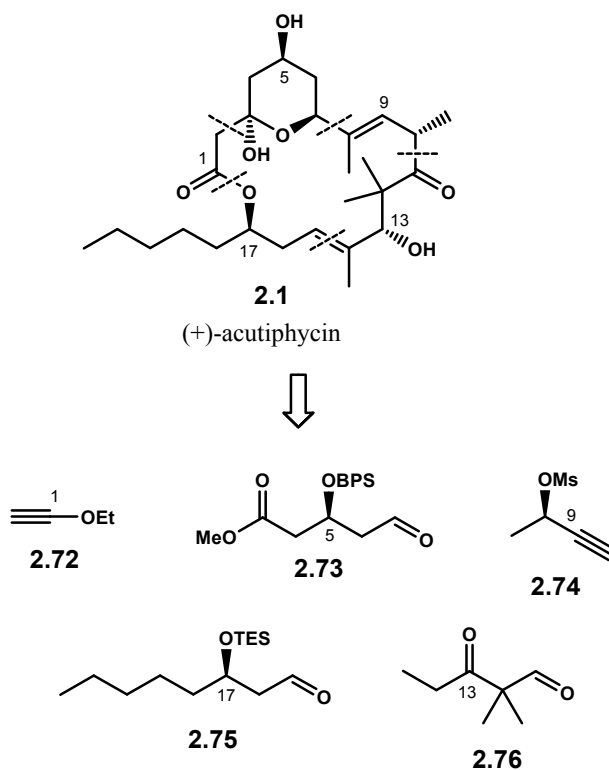
As described in Scheme 2.19, the final installation of Kiyooka aldol reaction was realized by the utilization of Chan's diene **2.44**,<sup>206</sup> which set up the  $\gamma$ -hydroxy- $\beta$ -ketoester C1 – C5 moiety of acutiphycin. This reaction required promoter oxazaborolidinone **2.45** in order to acquire the necessary C5 stereochemistry. These conditions afforded the seco acid of C10 epimer **2.71** in 56% yield with diastereomeric purity of 83%, thus concluding Kiyooka's quest to acutiphycin.



**Scheme 2.19**

### 2.4.3. Jamison's Approach

In 2006, Jamison and Moslin at Massachusetts Institute of Technology published a communication describing their elegant synthetic approach to acutiphyacin **2.1**.<sup>179</sup> The full article detailing their work was published a year later.<sup>180</sup> Jamison envisioned the construction of acutiphyacin via the assembly of five simple fragments **2.72** – **2.76** with ethoxyethyne **2.72** served as a lynchpin to close the macrolactone ring.

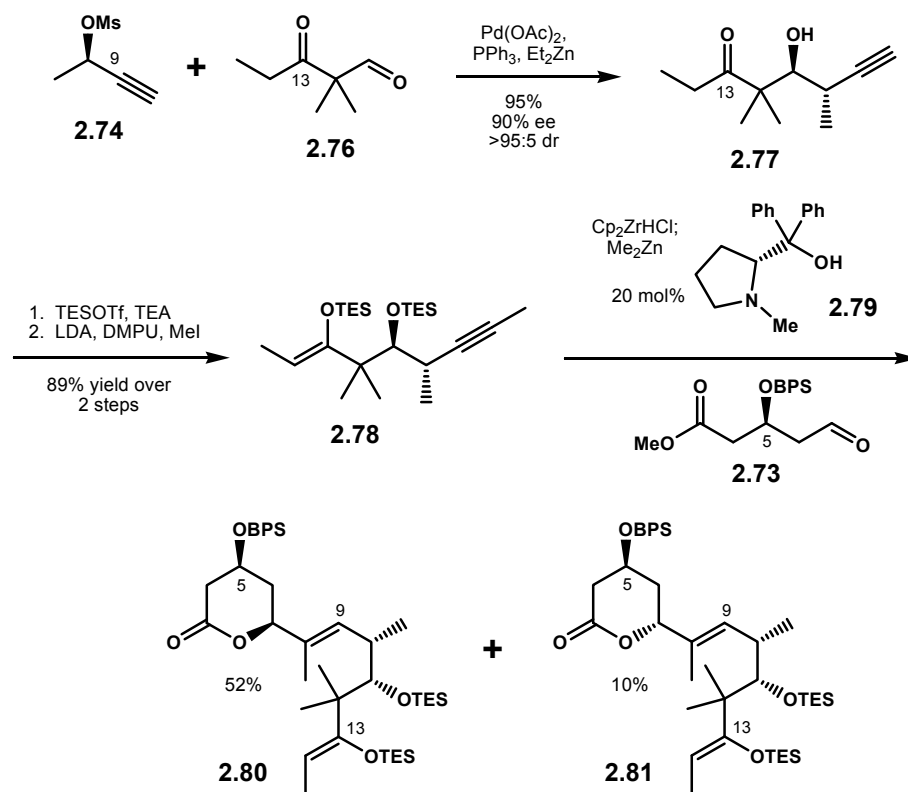


**Scheme 2.20**

#### 2.4.3.1. Concise Five-Fragment Coupling

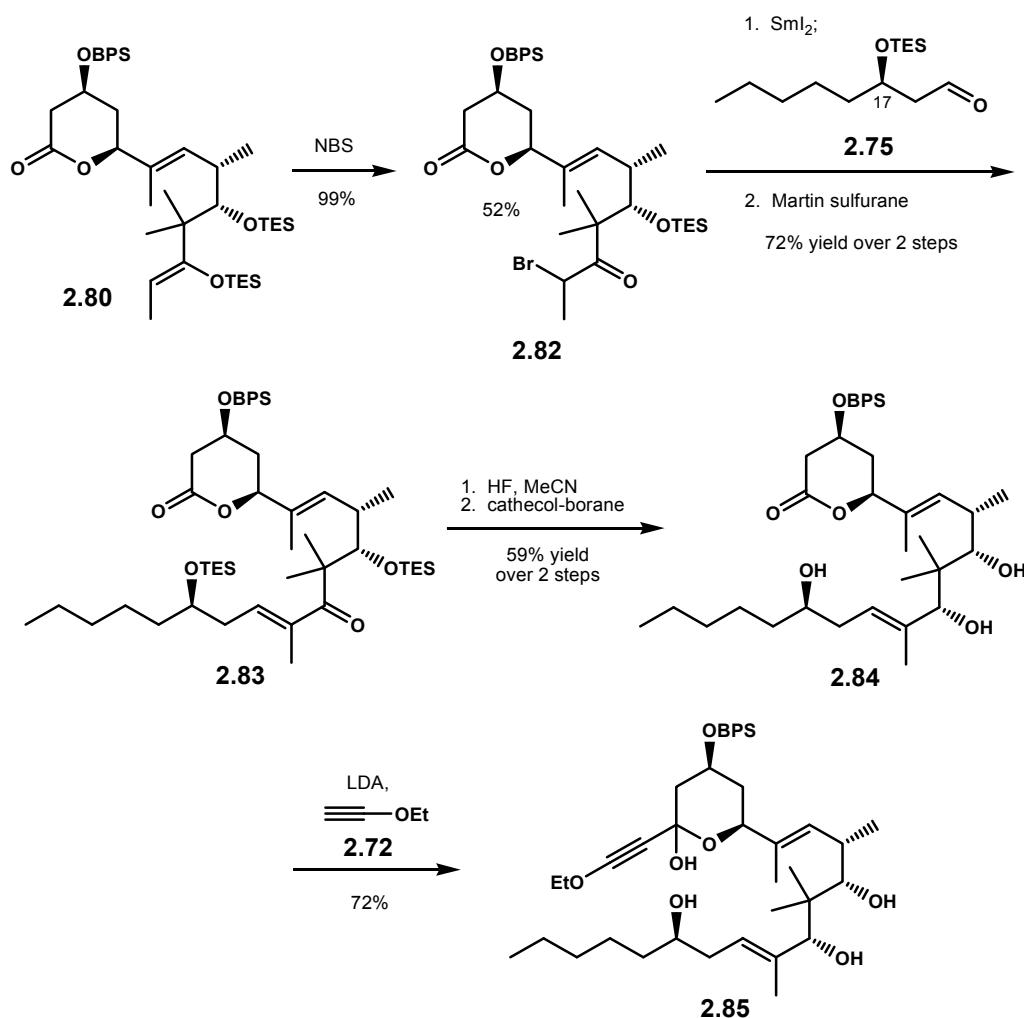
Jamison and Moslin began their synthesis to acutiphycin with a coupling reaction of fragments **2.74**<sup>207</sup> and **2.76**.<sup>208</sup> The palladium-catalyzed reaction of these two fragments following the protocol established by Marshall provided  $\beta$ -hydroxy ketone **2.77** in 95% yield with excellent both enantio- and diastereoselectivity.<sup>209</sup> Treatment of this adduct with TESOTf – TEA mixture then protected the C11 hydroxyl as a TES ether and at the same time enolized the C13 carbonyl to the corresponding Z-silyl enol ether. Subsequent methylation afforded enyne **2.78** in 89% yield over two steps. Enyne **2.78** was then coupled with fragment **2.73** using a method developed by Wipf which involved

hydrozirconation, transmetalation, and asymmetric carbonyl addition.<sup>210, 211</sup> This sequence provided chromatographically separable lactone **2.80** and its C7 epimer **2.81** in respectively 52% and 10% yields, Scheme 2.21.



Scheme 2.21

The coupling of lactone **2.80** and fragment **2.75** was envisioned through an intermolecular Reformatsky reaction. Lactone **2.80** was first exposed to an electrophilic bromination reaction which provided the requisite  $\alpha$ -bromo ketone **2.82** in near quantitative yield. Enolization of **2.82** was then achieved using  $\text{SmI}_2$ , and the subsequent addition to aldehyde **2.75** afforded the corresponding  $\beta$ -hydroxy ketone.<sup>212</sup>

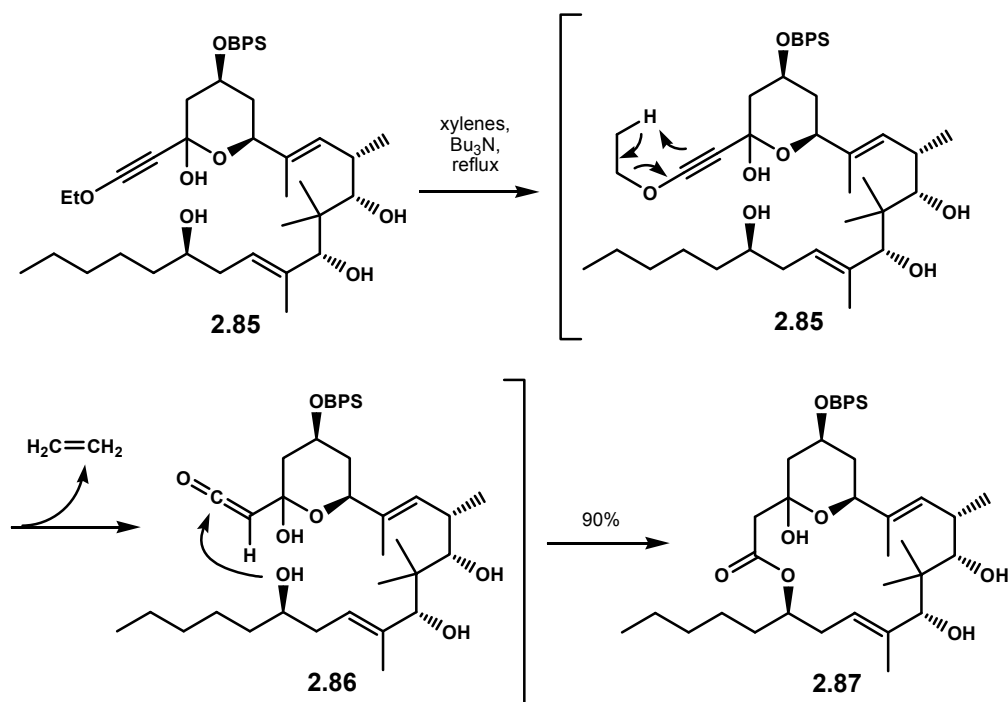


**Scheme 2.22**

Dehydration of this aldol product with Martin sulfurane reagent<sup>213</sup> provided enone **2.83** in 72% yield over two steps. Selective removal of the TES ether followed by substrate directed reduction<sup>214</sup> yielded the 1,3-*syn* diol **2.84**. Ethoxyethyne **2.72** was finally introduced upon deprotonation, and addition to C3 carbonyl produced the macrolactonization substrate tetraol **2.85**.

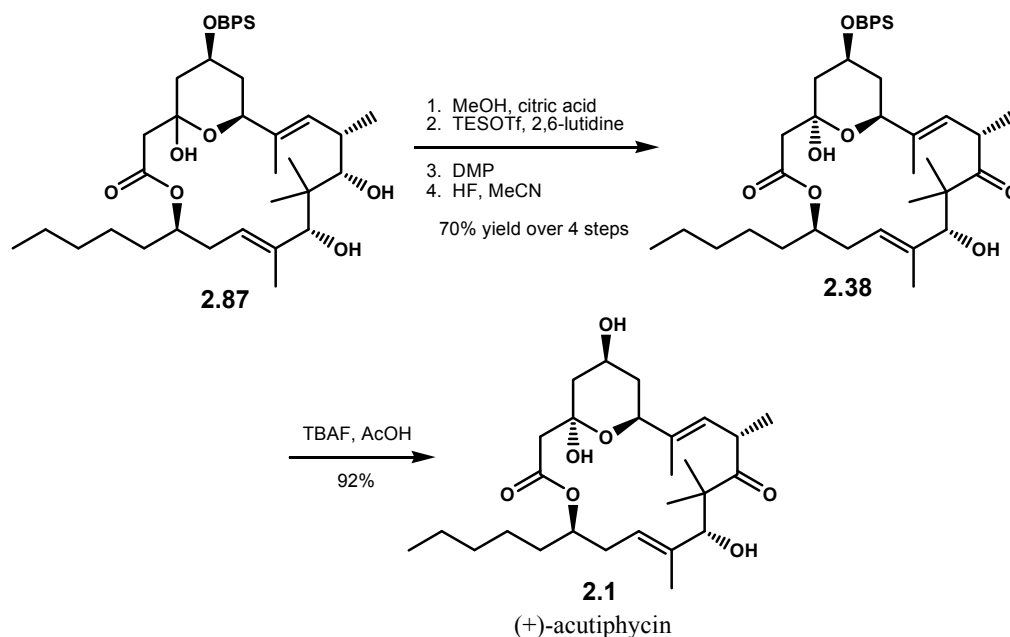
### 2.4.3.2. A Novel Macrolactonization Strategy

The highlight of Jamison's route to acutiphycin was presented in their macrolactonization strategy. The macrolactonization of **2.85** was realized using a thermal-induced retro-ene reaction.<sup>215, 216</sup> Jamison demonstrated that a slow addition of tetraol **2.85** to refluxing xylenes and tributylamine liberated ethylene gas to provide ketene **2.86** which was readily trapped intramolecularly with the least hindered and yet remote C17 hydroxyl, thus affording macrolide **2.87** in excellent yield. Although this type of macrolactonization has been previously explored for much simpler substrates,<sup>217, 218</sup> the first utilization of such a strategy in the total synthesis of complex natural products was demonstrated by this work.



Scheme 2.23

With macrolide **2.87** in hand, protection of the C3 hemiketal as a methyl pyranoside was achieved under acidic methanolysis. Utilizing the last four-step sequence previously reported by Smith which included selective protection and oxidation of C11 and C13 hydroxy groups respectively, and global deprotection, Jamison successfully completed the second total synthesis of acutiphycin, Scheme 2.24.



**Scheme 2.24**

## 2.5. Conclusion

This chapter details literature reviews pertinent to the acutiphycins. (+)-acutiphycin **2.1** and (+)-20,21-didehydroacutiphycin, **2.2** were isolated from *Oscillatoria acutissima*, and their initial biological testing revealed potent cytotoxicity. The overall



structure of acutiphycin was deduced through detailed 1D and 2D NMR experiments as well as systematic chemical degradation studies.

Since its isolation, three major articles describing the efforts towards the total synthesis of acutiphycin have been published. The first total synthesis was reported by the Smith group in 1995. In his article, Smith provided a synthetic scheme that would allow the production for both acutiphycin and 20,21-didehydroacutiphycin. Despite the lengthy route plagued with multiple reduction – oxidation sequences, Smith laid out an important foundation for future total syntheses of this natural product. Not so long after Smith's account, Kiyooka and co-workers reported their own approach to acutiphycin in which Kiyooka extensively utilized his oxazaborolidinone promoted aldol methodology to construct all the stereogenic centers required for the polyketide. More recently, Jamison also produced an article concerning a unique synthetic approach to this natural product. Jamison's route so far proved the shortest, and the work was highlighted by an unprecedented retro-ene reaction utilized in the key macrolactonization step.

## CHAPTER THREE

### SYNTHETIC STUDIES TOWARDS (+)-ACUTIPHYCIN

#### **3.1. Purpose**

The purpose of this chapter is to detail our studies towards the total synthesis of cytotoxic polyketide (+)-acutiphycin. In addition to the development of new acetate aldol methodology, these studies will present a convergent approach to the natural product via the production of two key synthetic fragments. The synthesis of these fragments will be highlighted by via the utilization of asymmetric vinylogous aldol technologies, and their coupling study will also be discussed.

#### **3.2. The Role of Natural Products as Anticancer Drugs**

Cancer is the second leading cause of death in the United States in recent years.<sup>219</sup> Significant efforts to find better methods of prevention, detection, and treatment of patients are ongoing both in academia and industry. Multiple chemotherapeutic drugs have been developed and marketed by major pharmaceuticals. Yet, due to a recent rapid development of the high-throughput screening methods coupled with the rise of

combinatorial chemistry, a disturbing trend reveals that pharmaceuticals are becoming less interested in natural products as a potential source for the next generation of chemotherapeutic drugs. Natural products are often viewed incompatible to the high-throughput screening environment due their highly complex structural architectures and low natural abundance. As a result, such projects have been significantly downsized and have become increasingly a burden solely to small biotech companies or academic research groups.

Kevin Davies has highlighted that although the high-throughput methods and combinatorial chemistry allow the production and biological evaluation of thousands of chemical structures in just a fraction of time, the current pharmacopoeia only lists 272 discrete biological targets. This practice accordingly resulted in the development of 22 drugs for new biological targets in the past decade.<sup>220</sup> These numbers may seem significant, but in reality it is inconsequential compared to the proposed 8,000 potential druggable proteins in the human genome. Newman and Cragg have recently published an article that clearly answers the question regarding the relevancy of natural products in modern drug discoveries.<sup>221</sup> Between the years of 1981 and 2006, as high as 75% of all approved new, small-molecule chemical entities for antimicrobials, anticancer, antihypertensive, and anti inflammatory drugs were derived from natural products.

Many natural products are produced by their respective organisms as secondary metabolites, presumably for the main weaponry in their defense mechanisms. The structural complexity contained within natural products are often considered privileged as these structures have been assembled and modified through evolutions; therefore, natural products will most likely exhibit specific biological properties.<sup>222</sup> Natural products also

encompass extremely vast structural diversity compared to those of synthetic materials generated by combinatorial chemistry, thus presenting immense opportunities for the discovery of new biological targets.

An outstanding example of a natural product that has been administered as a potent cancer chemotherapeutic drug is paclitaxel **3.1**. Paclitaxel, which is isolated from the bark of Pacific Yew trees, belongs to the diterpene class of natural products.<sup>223</sup> The blockbuster drug was approved by the FDA in 1992 and has been marketed by Bristol-Myers Squibb under the trade name Taxol. Its annual sale peaked in 2000 reaching \$1.6 billion.<sup>224</sup> A more recent advancement in anticancer drug discovery is highlighted by the approval of azaepothilone B analog **3.2** by the FDA in late 2007.<sup>225</sup> Bristol-Myers Squibb will be marketing this drug under the trade name Ixempra for the treatment of aggressive metastatic or locally advanced breast cancer that is no longer responding to currently available chemotherapeutic drugs. The epothilones are in the class of polyketide natural products.

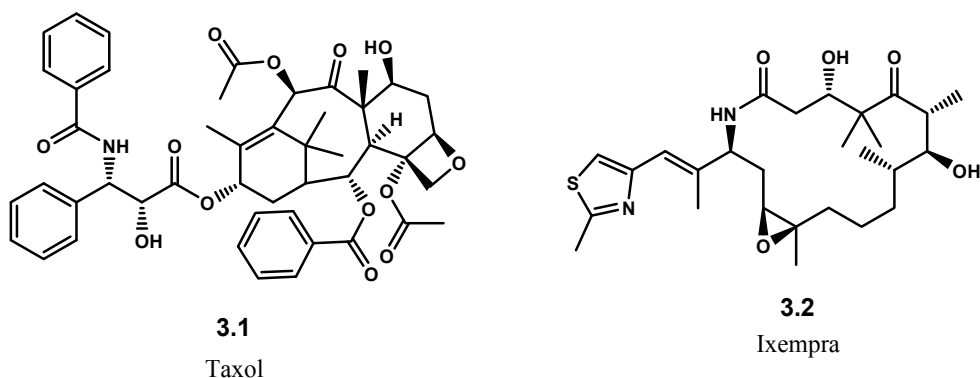


**Figure 3.1**

### 3.3. Taylor Group Interests in Polyketide Natural Products

Our group has immense interests in cytotoxic polyketide natural products for our contributions in the fight against cancer. Our interests in polyketides, as supposed to other class of natural products, are founded on several factors. First, polyketides encompass an enormous structural diversity that potentially allows for the discovery of new biological targets and modes of action. Second, many polyketides are readily accessible via total synthesis using currently available synthetic methodologies. This warrants suppliability of the material for further biological evaluations, structural modifications, and conformational analyses. Third, the unique structural architectures of polyketides often present challenges that warrant the development of novel synthetic methods. Finally, a recent advancement in biochemistry, particularly in the field of PKS-mediated biosynthesis through engineered microorganisms, supports an efficient production of polyketides through fermentation. This technology places polyketides in the leading edge of process research.

Our group has built successful programs surrounding this research area. For example, as shown in Figure 3.2, we have prepared several biologically important polyketides through total syntheses. For instance, in 2001, a former graduate student, Yue Chen, completed and reported the total synthesis of epothilones B **3.3** and D **3.4**.<sup>226</sup> In 2004, another former graduate student, Kristen Flemming, published the first total synthesis to myriaporones 1, 3, and 4, structures **3.5**, **3.6a**, and **3.6b** respectively.<sup>227</sup> Additionally, her successful total synthesis allowed for a complete structural assignment to the natural products previously not determined upon isolation and characterization.

More recently, a former postdoctoral fellow, Meizhong Jin, completed the total synthesis of peloruside A **3.7**, and the account was reported in 2005.<sup>228</sup>

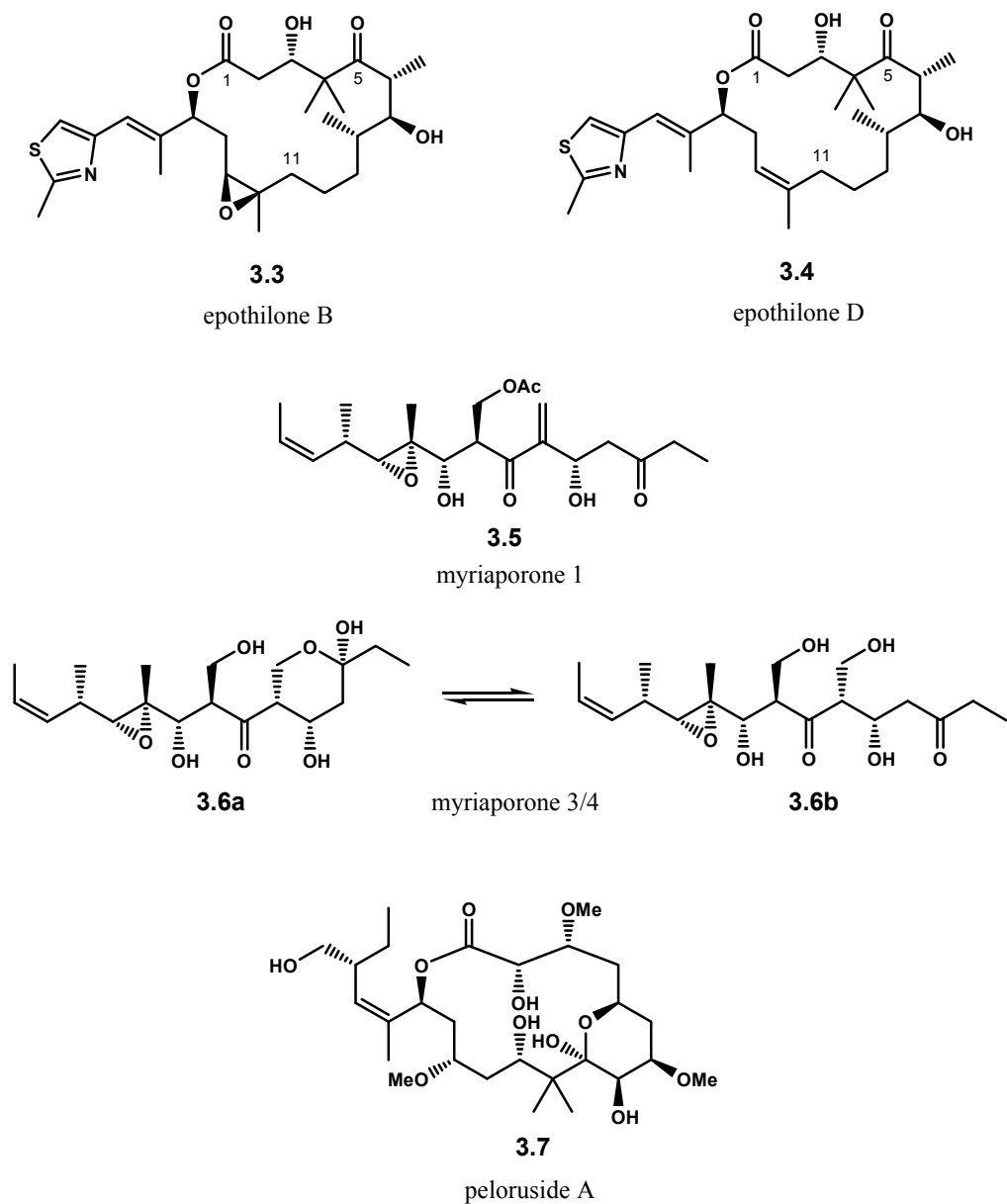


**Figure 3.2**

In addition to several synthetic methodology projects, structure- and conformation-activity-relationship studies, as well as precursor directed PKS-biosynthesis, our group is also currently expanding our library to several other polyketide targets. These include 20-desoxyapoptolidine aglycone **3.8**,<sup>229</sup> ambruticin **3.9**,<sup>230</sup> gephyronic acid **3.10**,<sup>231</sup> tedalonide **3.11**,<sup>232</sup> and acutiphyacin **3.12**.<sup>12</sup>

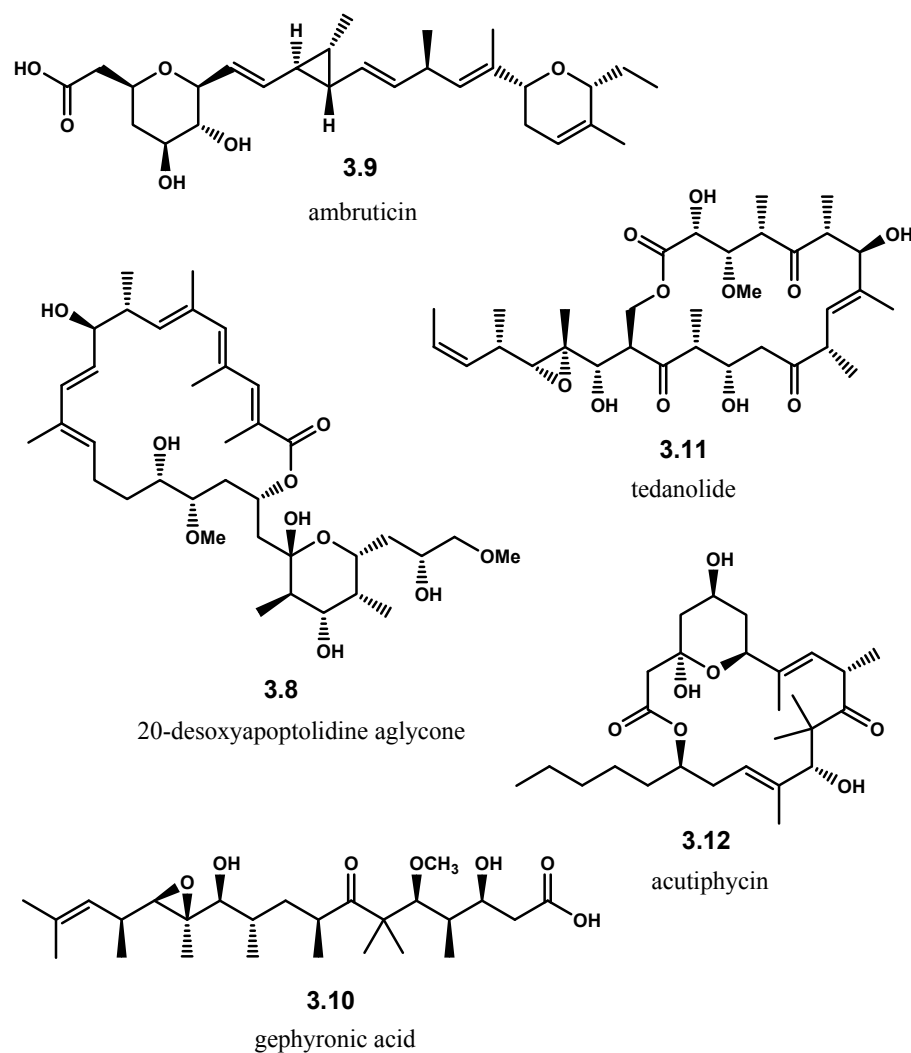


**Figure 3.3**

### 3.4. (+)-Acutiphycin as an Attractive Target

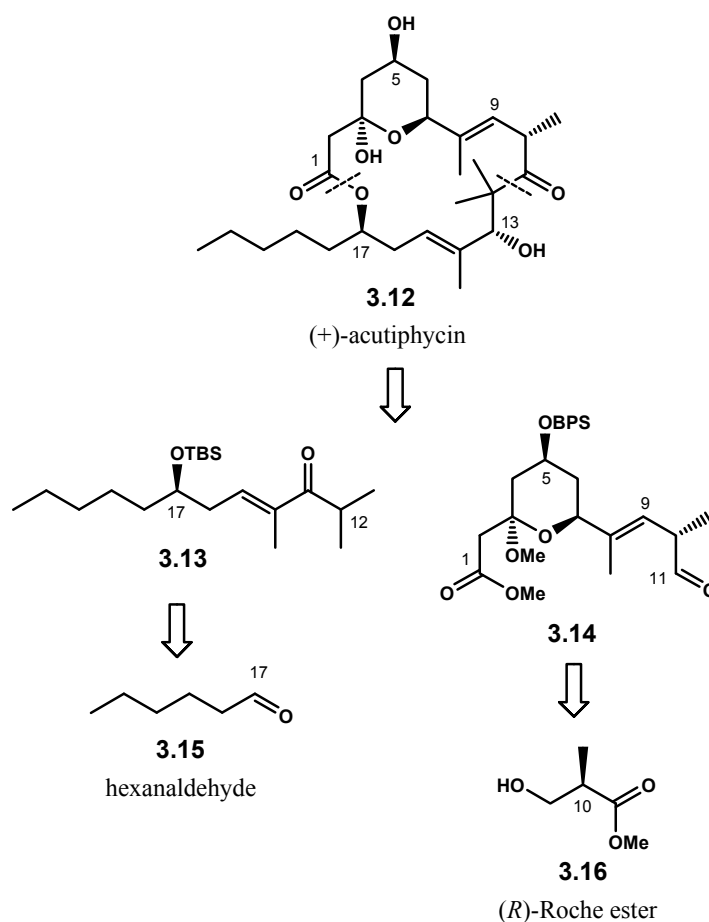
To expand our efforts in the research of polyketide natural products as potential anticancer drug candidates, we became interested in acutiphycin **3.12** and initiated the project in 2003. There are several reasons why acutiphycin is an extremely attractive target. First, as described in Chapter Two, Section 2.2, the initial biological evaluations of acutiphycin upon isolation revealed its potent cytotoxicity against cancer cells. However, despite the two total syntheses that have been reported, these biological evaluations have not yet been repeated and confirmed. More importantly, the mode of action of acutiphycin is still undetermined. Second, through private communications, we learned that the blue-green alga, *Oscillatoria acutissima*, from the original isolation pond and from laboratory cultures no longer produced acutiphycin. Thus, total synthesis would be the only viable method to acquire this natural product for its further biological study. Third, acutiphycin contains an 18-membered macrocyclic ring system that possesses interesting conformational properties. This will allow us to model and execute our novel conformation-activity-relationship study to probe acutiphycin's true biologically active conformer when bound to the target proteins. Fourth, acutiphycin represents a class of polyketide natural product with minimal post-PKS modifications. This would help with identifying the true pharmacophore of the polyketide through a systematic structure-activity-relationship study. Lastly, provided by the fact that acutiphycin is no longer produced by the microorganism, the identification and isolation of the PKS-gene clusters responsible for the natural product become extremely important.



We envision that the expression and cloning of the PKS-gene cluster in another microbial host, such as *E. coli*, should enable the production of acutiphycin via fermentation.

### 3.5. Retrosynthetic Analysis

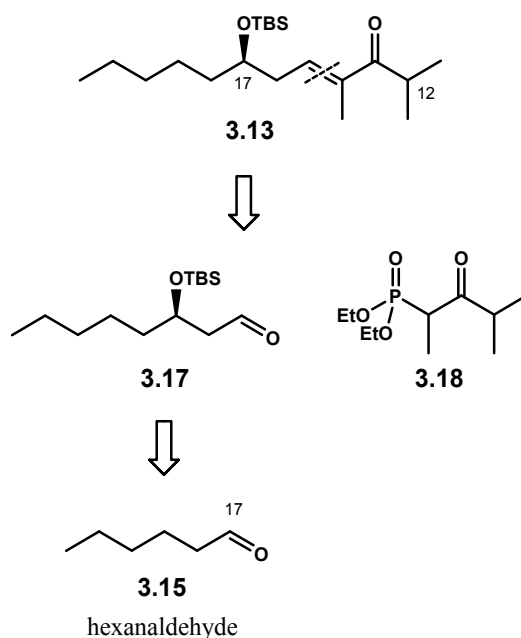
Since our interests in acutiphycin extend beyond total synthesis, our retrosynthetic analysis to this natural product must be designed such that a rapid generation of analogues is readily facilitated through the preparation of simple synthetic fragments. As shown in Scheme 3.1, we proposed two major disconnections at C11 – C12 and the macrolactone bonds; this would provide fragments **3.13** and **3.14**. These two fragments would be coupled via a late-stage aldol reaction followed by macrolactonization. Fragment **3.13** should be readily accessible in several simple steps from hexanaldehyde **3.15**. Fragment **3.14** would require more extensive synthetic operations from commercially available chiral pool (*R*)-Roche ester **3.16**, which readily contained stereochemistry of the C10 methyl in acutiphycin.



**Scheme 3.1**

### 3.6. Preparation of Fragment 3.13

Scheme 3.2 shows further retrosynthesis to synthetic fragment **3.13**. Fragment **3.13** possesses two key functionalities that comprise the C17 TBS ether group with *R* stereochemistry and C13 – C15 enone with *E* olefin geometry. The enone would be stereoselectively installed using the Horner-Wadsworth-Emmons (HWE) olefination reaction with acetate aldol **3.17** and ketophosphonate **3.18**. In the meantime, the construction of acetate aldol **3.17** from hexanaldehyde would entail asymmetric reactions to set up the requisite C17 stereochemistry.



**Scheme 3.2**

### 3.6.1. Acetate Aldol via Homoaldol Methodology

In conjunction with our total synthesis program, our group is actively involved in the development of synthetic methodology that aims for key functionalities in our target polyketide natural products. For example, our group has successfully developed an enantioselective cyclopropanation reaction<sup>233, 234</sup> and applied this methodology to construct the cyclopropane moiety of ambruticin **3.9**. Another outcome of our synthetic methodology program is exemplified by our stereoselective olefination strategy via thionyl chloride rearrangement.<sup>235</sup> This method has been used to efficiently prepare the C1 – C11 triene portion of apoptolidin **3.8**.

Peloruside A **3.7** has more recently inspired our newly developed electrophile-induced ether transfer reaction. This technology allows the production of 1,3-*syn* diol

monoether, a key structural feature in the C3 – C5 and C15 – C17 regions of the natural product.<sup>236</sup> Furthermore, the ether transfer methodology has been successfully expanded to the generation of stereochemically rich 2,4,6-trisubstituted tetrahydropyran<sup>237, 238</sup> and 2,6-disubstituted 3,4-dihydropyran rings.<sup>239</sup> An application of these methods to complex molecule synthesis is highlighted by a stereoselective construction of the oxacycle core of polyketides phorboxazole A **3.19** and swinholide A **3.20**. The electrophile-induced ether transfer methodology and its expansion will be discussed in detail in the later chapters of this dissertation.

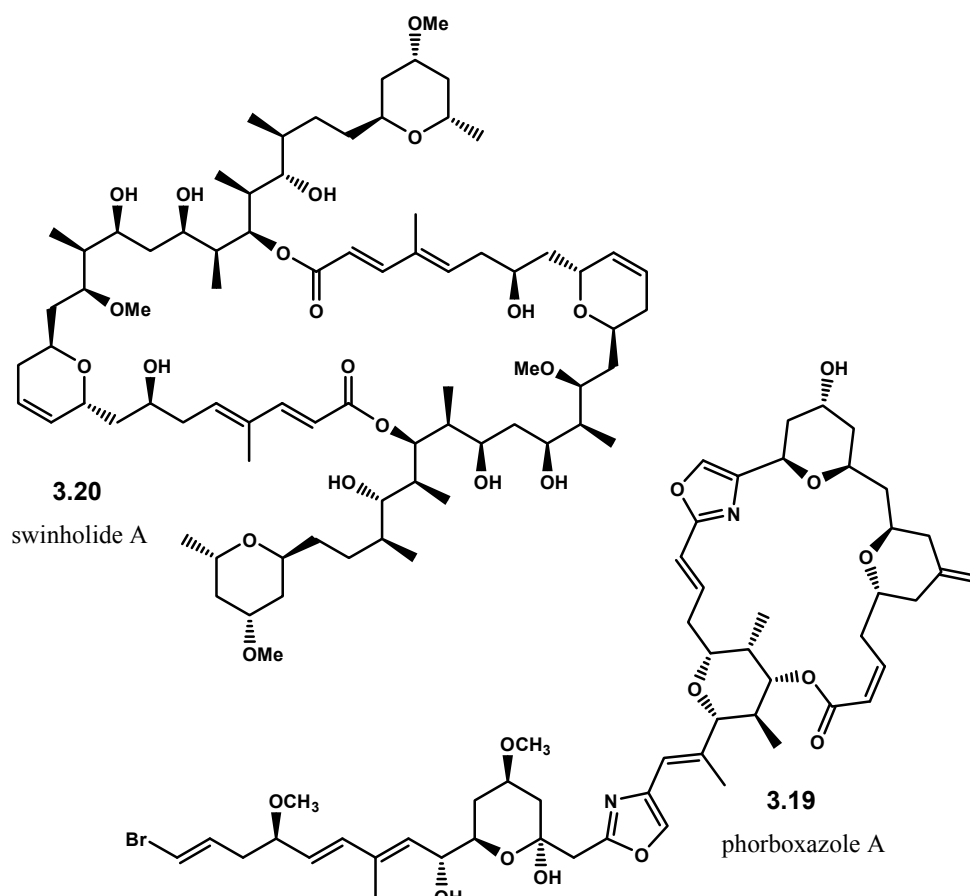
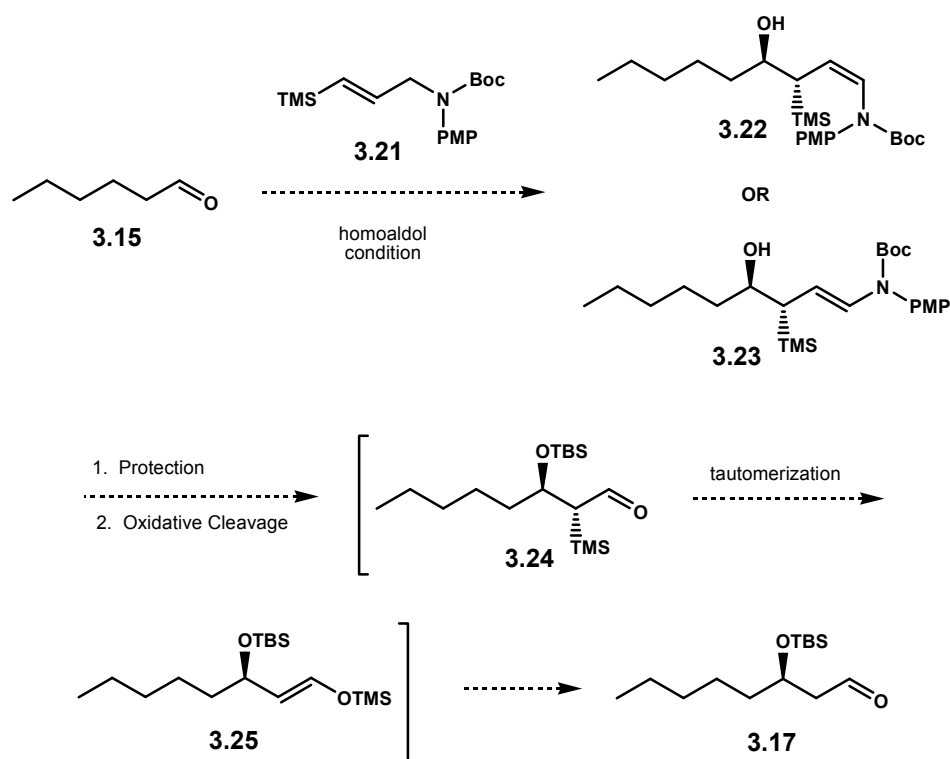


**Figure 3.4**

The enantioselective preparation of an acetate aldol adduct, such as **3.17**, has been known to be a rather problematic synthetic protocol. A classic method for this functionality typically begins with asymmetric allylation of an aldehyde, followed by subsequent protection of the corresponding homoallylic alcohol and oxidative cleavage of the terminal olefin. Despite numerous enantioselective allylation methods have been developed,<sup>240</sup> many of these reactions are unattractive particularly in a large scale. The limitation typically encompasses the scope of reaction, unacceptable level of enantioselectivity, the cost of reagents, and a challenging operation as well as purification. Alternatively, acetate aldol functionality can be approached from a chiral auxiliary based reaction;<sup>79</sup> however, once again, substrate compatibility often plagues the efficiency of the method.

For these reasons, our group became interested in developing a unique method to the acetate aldol. As shown in Scheme 3.3, we should be able to efficiently construct acetate aldol **3.17** in a three-step sequence. The first step involves a homoaldol reaction between hexanaldehyde **3.15** with *N*-enecarbamate **3.21**.<sup>241</sup> As described shortly, depending upon the choice of transmetallating agent, the homoaldol reaction will produce either olefin isomeric adduct **3.22** or **3.23**. After TBS protection, the homoaldol products will be exposed to oxidative cleavage conditions, which should yield  $\alpha$ -TMS aldehyde **3.24**.  $\alpha$ -TMS aldehyde **3.24** is expected to readily undergo rapid desilylation via tautomerization to **3.25**,<sup>242</sup> thus affording acetate aldol **3.17**.

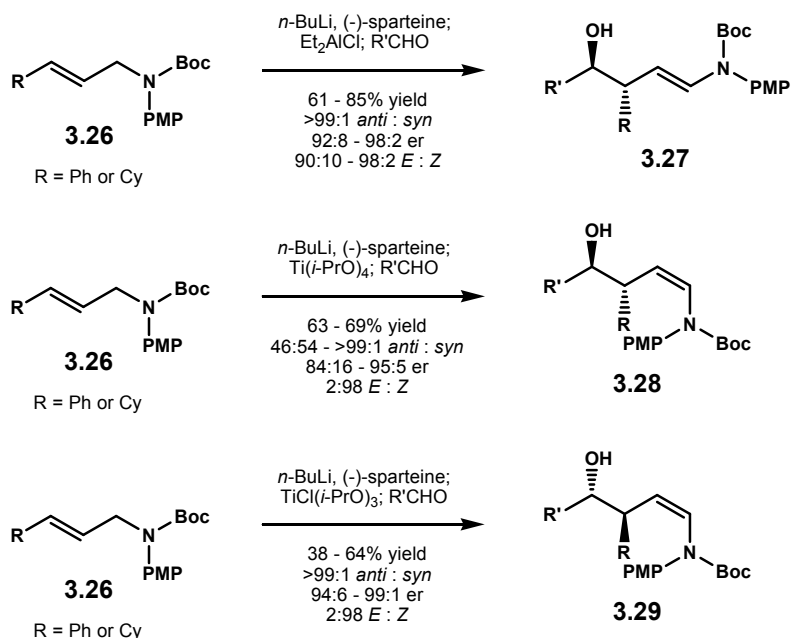


Scheme 3.3

### 3.6.1.1. Peter Beak's Homoaldol Reactions

In 2004, Peter Beak and co-workers reported the use of *N*-enecarbamate **3.26** in the homoaldol reaction.<sup>241</sup> They demonstrated that asymmetric deprotonation of **3.26** with *n*-butyllithium in the presence of (-)-sparteine,<sup>243</sup> followed by transmetallation with Et<sub>2</sub>AlCl and an addition of aldehyde produced *anti* homoaldol adduct **3.27** in good yield and stereoselectivity. Interestingly, when Ti(*i*-PrO)<sub>4</sub> was employed as the transmetallating agent, the absolute stereogenic centers of homoaldol adduct **3.28** was retained as those in **3.27**, but the olefin geometry was inverted to the *Z* isomer. In contrast with TiCl(*i*-PrO)<sub>3</sub>, homoaldol adduct **3.29** was produced with *Z* olefin geometry, but the two stereogenic centers within the molecule were found opposite of those of **3.27**.

and **3.28**. The enantioselectivity in this homoaldol reaction arises from chiral additive (-)-sparteine. Since its enantiomer (+)-sparteine is not commercially available, this useful methodology demonstrates that both enantiomers of the homoaldol products are accessible by simply switching the transmetallating agent.



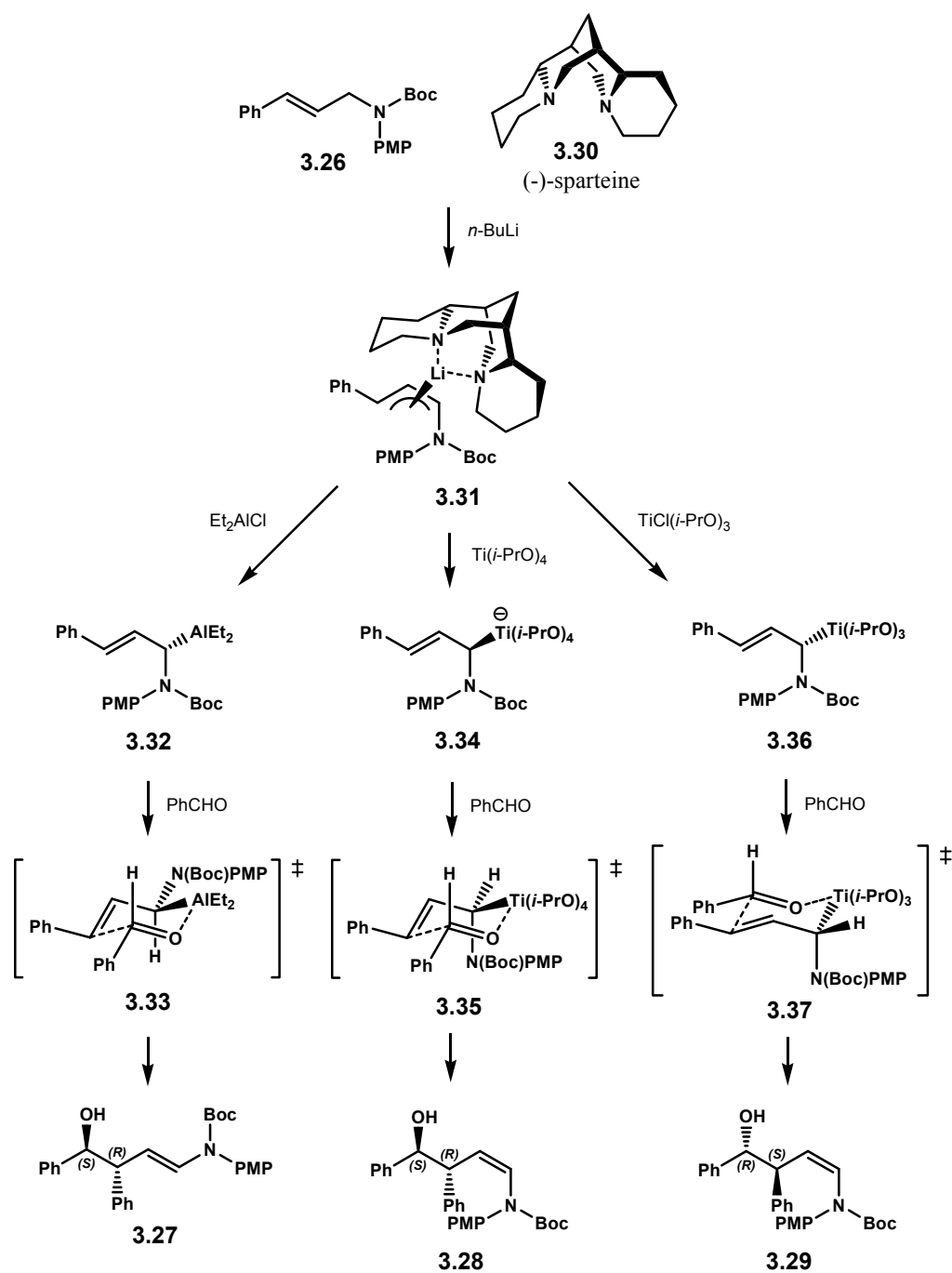
**Scheme 3.4**

The mechanism for the Beak's reaction is proposed as follows. As shown in Scheme 3.5, asymmetric deprotonation of *N*-enecarbamate **3.26** with *n*-butyllithium in the presence of (-)-sparteine **3.30** leads to  $\eta^3$  allyllithium complex **3.31**. Transmetalation with Et<sub>2</sub>AlCl proceeds with inversion of configuration to give allylaluminum intermediate **3.32**, which then reacts with benzaldehyde in a Zimmerman-Traxler six-membered transition state **3.33** to provide homoaldol product **3.27** with (3*R*,4*S*) absolute stereoconfiguration. Likewise, when allyllithium **3.31** is treated with TiCl(*i*-PrO)<sub>3</sub>, the

transmetallating process also occurs with inversion of configuration. Subsequent addition of benzaldehyde to the resulting allyltitanium species **3.36** is proposed to proceed via a six-membered transition state **3.37** that leads to product **3.29** with (3*S*,4*R*) absolute stereochemistry. In contrast, with Ti(*i*-PrO)<sub>4</sub>, the transmetallation proceeds with retention of configuration to give **3.34**. Upon addition of benzaldehyde, homoaldol adduct **3.28** is produced presumably via transition state **3.35**.

When comparing transition states **3.33**, **3.35**, and **3.37**, it appears that size of the Lewis acid plays an important role in controlling the stereochemical outcome of the homoaldol reaction. As depicted in transition states **3.35** and **3.37**, in order to minimize unfavorable steric repulsion with the bulky Ti(*i*-PrO)<sub>4</sub> and Ti(*i*-PrO)<sub>3</sub>, the N(Boc)PMP group must be oriented pseudoaxially. As a result, while maintaining the integrity of the Zimmerman-Traxler model, the aldehyde will be approached appropriately to set up respectively the 4*S* and 4*R* stereochemistry in **3.45** and **3.48**. In addition, the pseudoaxial orientation of N(Boc)PMP group will also result in the observed *Z* olefin geometry. In the case of allylaluminum **3.32**, such steric repulsion seems very minimal. As a result, as shown in transition state **3.33**, the N(Boc)PMP group is oriented pseudoequatorially which allows addition of benzaldehyde from the *si* face, thus providing 4*S* absolute configuration in homoaldol adduct **3.27**.

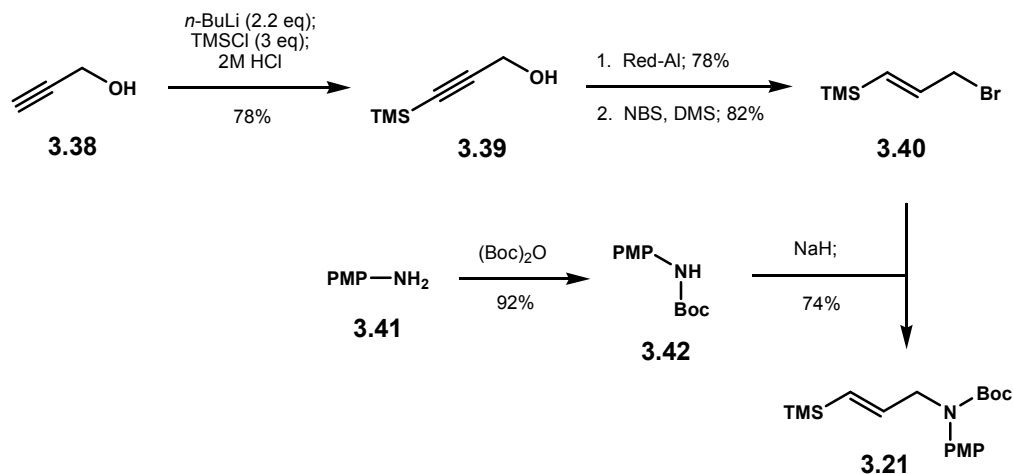




Scheme 3.5

### 3.6.1.2. Homoaldol Reactions with Beak's Auxiliary 3.21

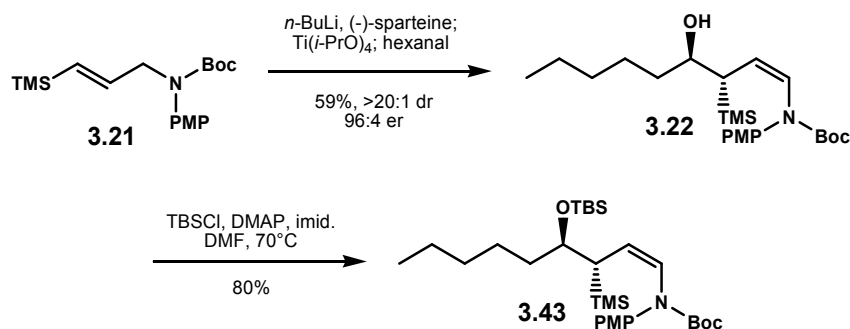
The acetate aldol methodology began with the synthesis of a designed auxiliary **3.21** that contained a vinylic TMS group. The presence of this vinylic substitution has been found crucial to maintain a high level of enantioselectivity in the asymmetric deprotonation step.<sup>244, 245</sup> Starting with propargyl alcohol **3.38**, silylation at the acetylene carbon gave alcohol **3.39**. Reduction of the propargyl group followed by NBS-promoted bromination of the resulting allylic alcohol afforded allyl bromide **3.40**. Protection of commercially available *p*-anisidine **3.41** as carbamate **3.42** followed by subsequent deprotonation with NaH provided the sodium salt that reacted with allyl bromide **3.40** to provide Beak's auxiliary **3.21**.



Scheme 3.6

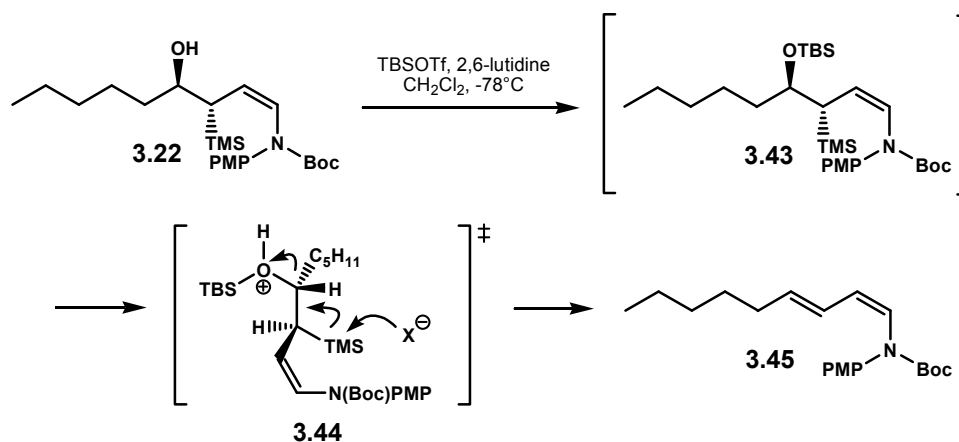
When *N*-enecarbamate **3.21** was exposed to the homoaldol aldol conditions with  $\text{Ti}(i\text{-PrO})_4$  as the transmetallating agent, homoaldol adduct **3.22** was produced in 59% yield. A chiral HPLC analysis of this product determined its enantiomeric ratio to be

96:4. Protection of the sterically hindered hydroxyl group as a TBS ether was best achieved with a mixture of TBSCl, DMAP, and imidazole in DMF at 70°C over 48 hours, Scheme 3.7.



Scheme 3.7

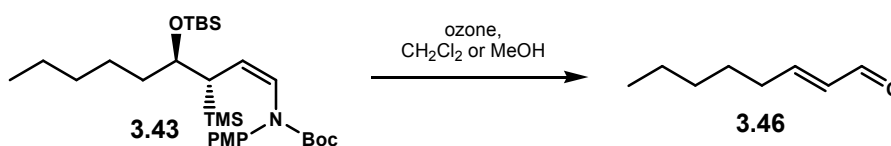
When TBS protection of **3.22** was carried out in the presence of TBSOTf and 2,6-lutidine in CH<sub>2</sub>Cl<sub>2</sub> at -78°C, Peterson elimination readily took place and gave diene **3.45**.<sup>246</sup> The geometry of the newly generated olefin was assigned *E* based on the observed <sup>1</sup>H NMR coupling constant of the relevant protons. Although the Peterson elimination pathway was unexpected, this result serendipitously confirmed the *anti* relative configuration of the two stereogenic centers contained in the homoaldol product. As shown in Scheme 3.8, the mechanism which accounts for product **3.45** is proposed through a generation of TBS ether **3.43** followed by E2 elimination as depicted in transition state **3.44**, that requires *anti* periplanar orientation between the –OTBS and –TMS groups.



Scheme 3.8

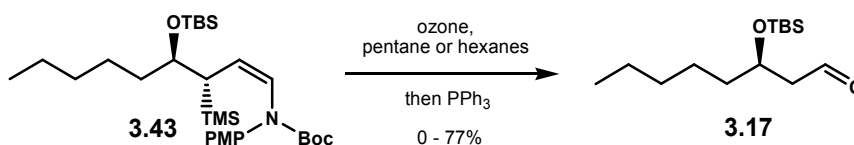
### 3.6.1.3. Ozonolysis Study

Installation of the aldehyde functionality was proposed via oxidative cleavage of the terminal olefin in the TBS protected homoaldol adduct **3.43** followed by *in situ* tautomerization. Unfortunately, this process was found challenging. Our initial study revealed that exposure of **3.43** to strong oxidants such as  $\text{KMnO}_4$  or  $\text{OsO}_4$  failed to oxidize the double bond. When **3.43** was subjected to a much stronger oxidant, such as ozone, as a solution in  $\text{CH}_2\text{Cl}_2$ , oxidative cleavage did occur, however, to yield  $\alpha,\beta$ -unsaturated aldehyde **3.46** instead of providing the desired acetate aldol **3.17**. A similar result was observed when ozonolysis was carried out in methanol.



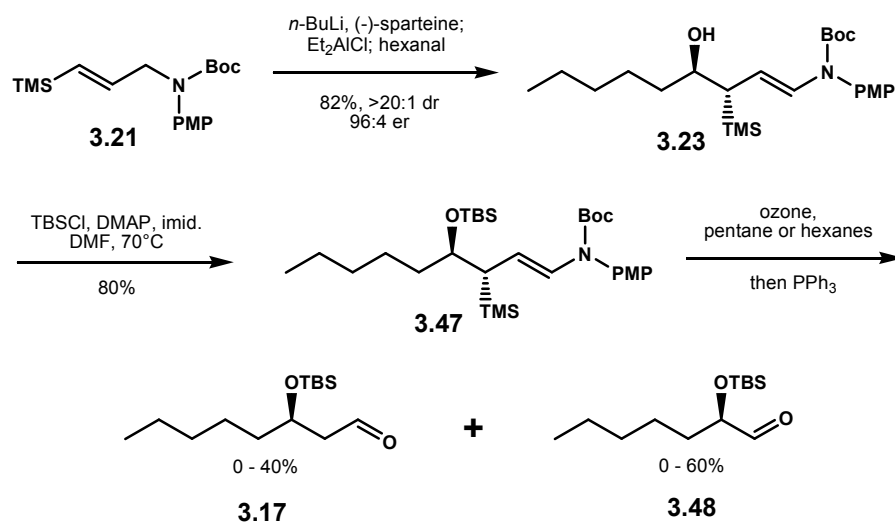
Scheme 3.9

Interestingly, ozonolysis of **3.43** followed by reductive workup in non-polar mediums, such as pentane or hexanes, successfully produced the target acetate aldol **3.17**. However, to our disappointment, this result proved irreproducible. Multiple ozonolysis attempts were carried out, and each attempt afforded **3.17** in significantly varying isolated yield ranging from decomposition materials to as high as 77% yield.



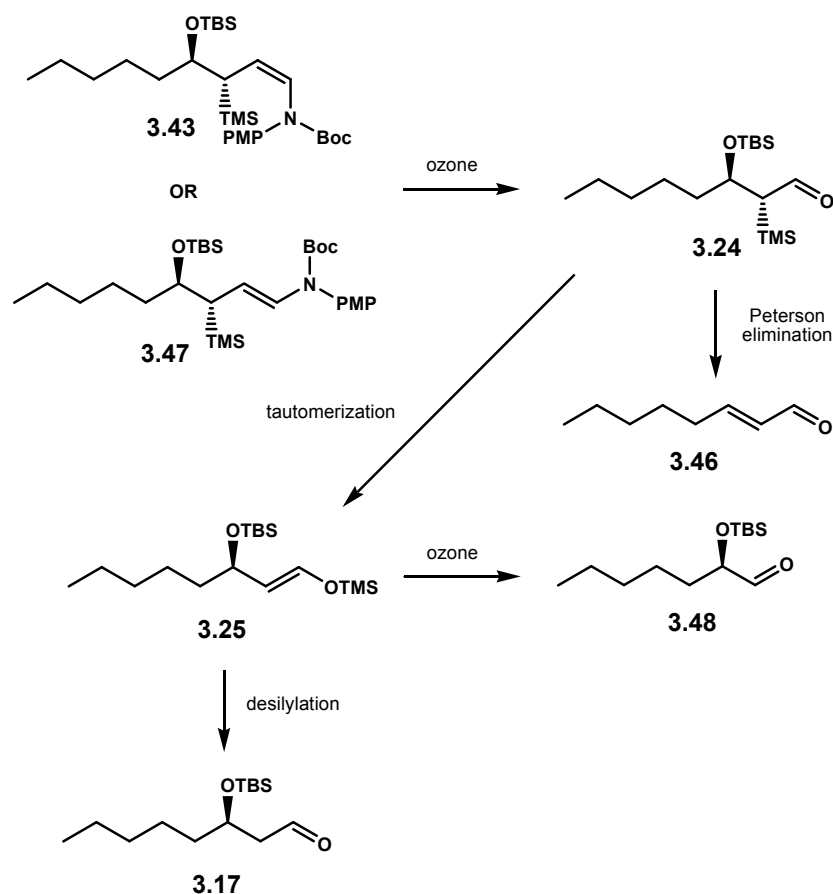
**Scheme 3.10**

At this point, we suspected that the olefin geometry perhaps would affect the outcome of the ozonolysis process. The homoaldol reaction of *N*-enecarbamate **3.21** with Et<sub>2</sub>AlCl as the transmetallating agent produced product **3.23** in 82% yield almost as a single stereoisomer. The enantiomeric ratio of this product was found 96:4 based on a chiral HPLC analysis. Protection of the hydroxyl group as a TBS ether was carried out under the previously described conditions. Interestingly, ozonolysis of homoaldol adduct **3.47** in either pentane or hexanes produced not only the desired acetate aldol **3.17** but also α-OTBS aldehyde **3.48**, which was not previously observed with **3.43**. Similar to that of **3.43**, ozonolysis of **3.47** was also found irreproducible. The best isolated yield for the desired target **3.17** was only 40%; whereas, undesired aldehyde **3.48** was once obtained in as high as 60% yield.



**Scheme 3.11**

To summarize the results presented in Schemes 3.9 – 3.11, the overall ozonolysis processes are proposed as follows. Upon rapid oxidative cleavage of homoaldol adducts **3.43** and **3.47** under ozonolysis conditions,  $\alpha$ -TMS aldehyde **3.24** appears to have been readily formed prior to the reductive workup. Under the reaction conditions,  $\alpha$ -TMS aldehyde **3.24** undergoes competitive tautomerization to silyl enol ether **3.25** or Peterson elimination in polar solvents to **3.46**, presumably promoted by the presence of excess ozone. Silyl enol ether **3.25** then either proceeded to desilylation, which furnished the desired acetate aldol **3.17**, or a competitive second oxidative cleavage that eventually yielded  $\alpha$ -OTBS aldehyde **3.48**. A similar chain-shortening process has been observed in the ozonolysis study of allylstannane systems by Dussault and co-workers.<sup>247</sup>

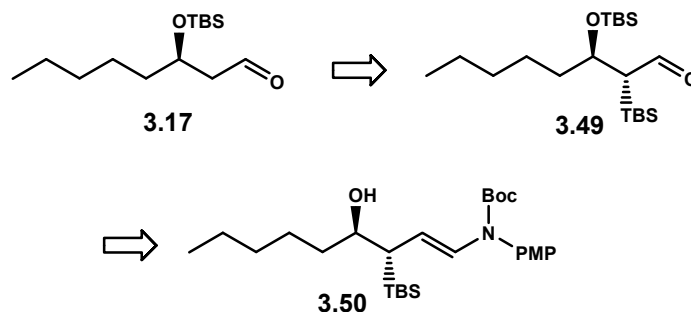


**Scheme 3.12**

#### 3.6.1.4. Study with Redesigned TBS Auxiliary

The major problem to the above schematic would arguably lie in the premature tautomerization process of  $\alpha$ -silyl aldehyde **3.24** that ultimately led to the unexpected second oxidative cleavage. We propose that the  $\alpha$ -silyl aldehyde should be isolable if the spontaneous tautomerization process is shut down. The ensuing independent removal of the  $\alpha$ -silyl group, for example under acidic conditions, should then provide the desired acetate aldol. As demonstrated in Scheme 3.13, the prevention of tautomerization would be explored with the use of  $\alpha$ -TBS aldehyde **3.49**, which should be accessible from

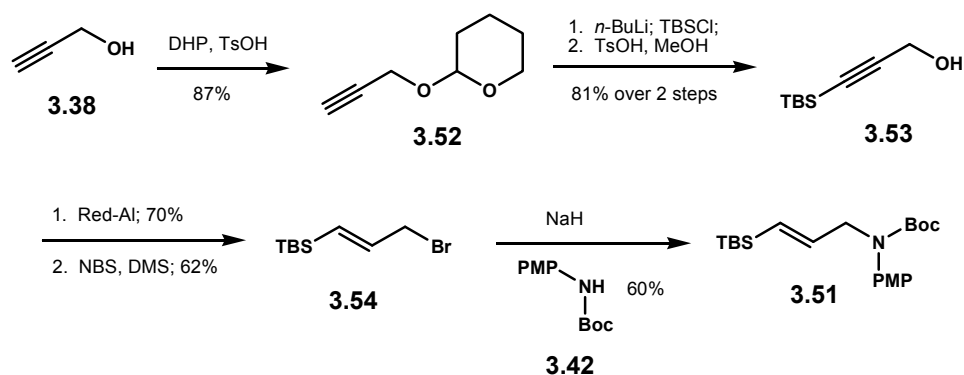
homoaldol adduct **3.50**. The TBS group is known to have much greater stability compared to that of TMS group under a variety of reaction conditions. Such functionality should survive under strong oxidative conditions.



**Scheme 3.13**

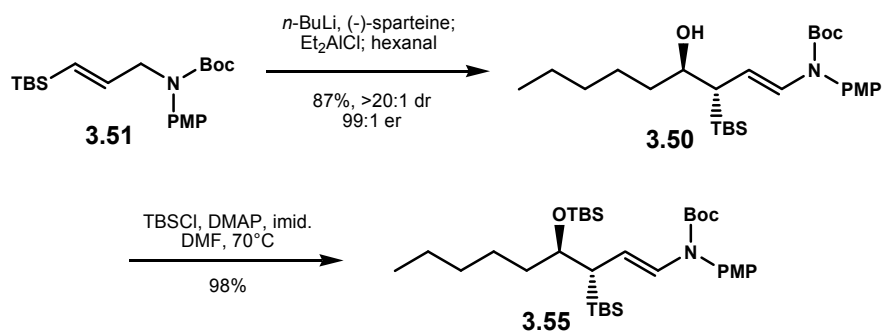
The synthesis of homoaldol adduct **3.50** would require a redesigned *N*-enecarbamate auxiliary **3.51**. As shown in Scheme 3.12, upon protection of propargyl alcohol as a THP ether **3.52**, silylation at acetylene carbon followed by acidic methanolysis provided propargylic alcohol **3.53**. Alkyne reduction followed by bromination of the corresponding allylic alcohol then afforded allylic bromide **3.54**. A coupling reaction of this allylic bromide with the sodium salt of carbamate anion **3.42** completed the synthesis of auxiliary **3.51**.





Scheme 3.14

As shown in Scheme 3.15, homoaldol adduct **3.50** was readily produced in high yield with excellent stereoselectivity upon exposure of *N*-enecarbamate **3.51** to the homoaldol conditions. Protection of the homoaldol adduct as a TBS ether under previously optimized conditions afforded **3.55**.



Scheme 3.15

For the oxidative cleavage step, exposure of **3.55** to ozone in hexanes produced a mixture of the expected  $\alpha$ -TBS aldehyde **3.49** and the undesired chain-shortened  $\alpha$ -OTBS aldehyde **3.48** in a 3:1 ratio with a combined yield of 85%. While the use of  $\text{CH}_2\text{Cl}_2$  as a reaction medium only yielded decomposition, ozonolysis of **3.55** in a polar, protic

solvent, such as methanol, successfully produced  $\alpha$ -TBS aldehyde **3.49** in 90% yield. These conditions effectively suppressed the generation of  $\alpha$ -OTBS aldehyde **3.48** to 19:1 ratio, Table 3.1.

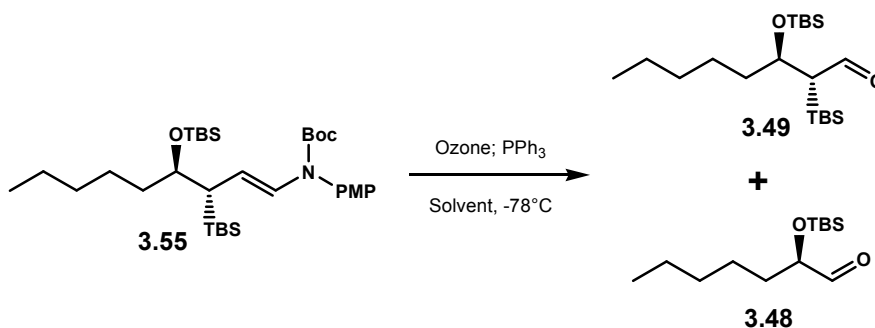


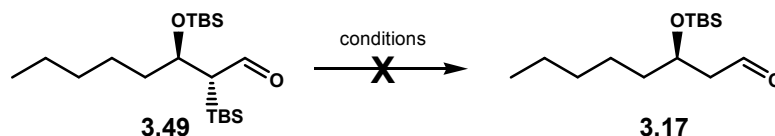
**TABLE 3.1**

Entry	Solvent	Yield <sup>[a]</sup>	3.49 : 3.48 <sup>[b]</sup>
1	hexanes	85%	3:1
2	methanol	90%	19:1
3	$\text{CH}_2\text{Cl}_2$	decomposition	---

[a] Yield isolated as a mixture of **3.49** and **3.48**. [b] Ratio was measured based on  $^1\text{H}$  NMR integration.

Efforts were subsequently focused towards desilylation of **3.49** to access acetate aldol **3.17**. Unfortunately, this was unfruitful. For example, starting material **3.49** was unaffected when treated with a mixture of acidic acid or PPTS in methanol. However, with a stronger acid, such TFA or HCl, rapid decomposition was immediately observed. Numerous attempts to convert **3.49** to **3.17** were also executed in basic methanolysis conditions, which were also found ineffective. Treatment of **3.49** to either  $\text{K}_2\text{CO}_3$  or

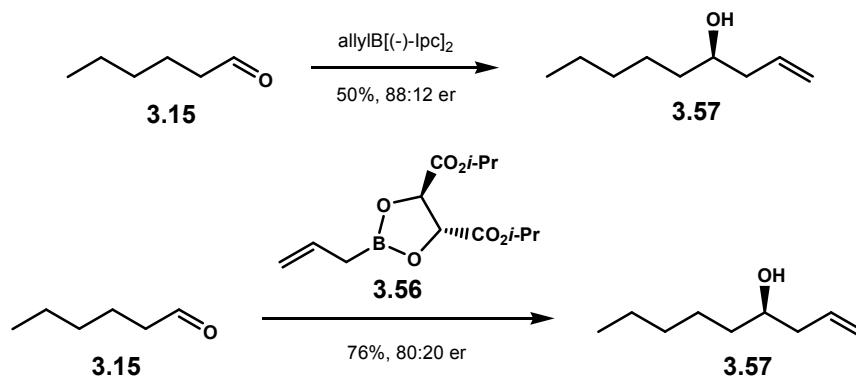
Cs<sub>2</sub>CO<sub>3</sub> in methanol only provided a mixture of compounds; none of which was the target acetate aldol **3.17**.



**Scheme 3.16**

### 3.6.2. Acetate Aldol via Asymmetric Allylation

Realizing that the methodology quest had not produced the anticipated results, we had to consider a classical route for the production of acetate aldol **3.17**. This route would entail an asymmetric allylation reaction, followed by protection of the resulting homoallylic alcohol and oxidative cleavage of the terminal olefin. As shown in Scheme 3.17, allylation of hexanaldehyde under Brown's method produced homoallylic alcohol **3.57** in 50% yield with enantiomeric ratio of 88:12.<sup>142</sup> Although the Brown's method is known to be high yielding, the poor yield observed in our case might have been contributed in the removal of the IpcOH byproducts. Alternatively, we also employed another allylation method, such as that of the Roush.<sup>248</sup> The utilization of allylborane **3.56** enabled the production of homoallylic alcohol **3.57** in 76% yield, however, with lowered enantioselectivity, 80:20.



**Scheme 3.17**

The transition states that account for stereoselectivity in these allylation reactions are depicted in Figure 3.5. Although both transformations have been proposed to undergo via the Zimmerman-Traxler like transition states, the factors that govern the facial selectivity are subtly different. In the Brown's allylation, the facial selectivity is thought to have been solely induced by the profound steric influence of large, chiral isopinocampheyl (Ipc) ligands as shown in transition state **3.58**. However, this is not the case for the tartrate-based allylation. Diisopropyltartrate, compared to Ipc, is a much smaller chiral molecule that may not provide significant steric influence with directing facial addition. In fact, Roush proposes that the stereoselectivity may originate from the minimization of electrostatic repulsion between non-bonded electrons as depicted in transition state **3.59**.

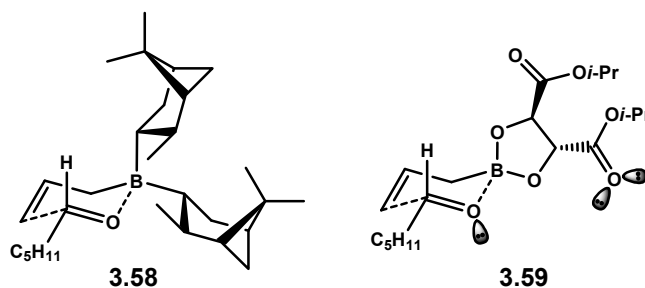
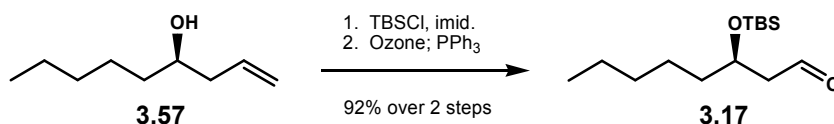


**Figure 3.5**

Completion to target acetate aldol **3.17** was simply achieved by protecting homoallylic alcohol **3.57** under established conditions as its corresponding TBS ether. Subsequent ozonolysis and reductive workup thus afforded **3.17** in 92% yield over two steps, Scheme 3.18.

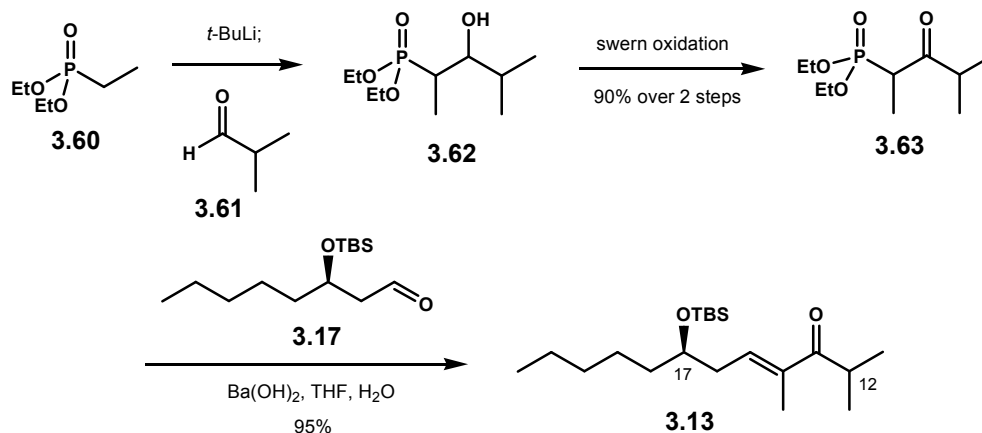


**Scheme 3.18**

### 3.6.3. The Horner-Wadsworth-Emmons Reaction

The production of synthetic fragment **3.13** which represents the southern portion of acutiphycin was furnished by the Horner-Wadsworth-Emmons (HWE) reaction between acetate aldol **3.17** and  $\beta$ -ketophosphonate **3.63**.  $\beta$ -Ketophosphonate **3.63** was readily produced in a two-step acylation sequence from commercially available phosphonate **3.60**.<sup>249</sup> By employing a protocol developed by Paterson,<sup>250</sup> the HWE

coupling reaction promoted by Ba(OH)<sub>2</sub> cleanly afforded the target fragment **3.13** in 95% yield with a single olefin geometry.



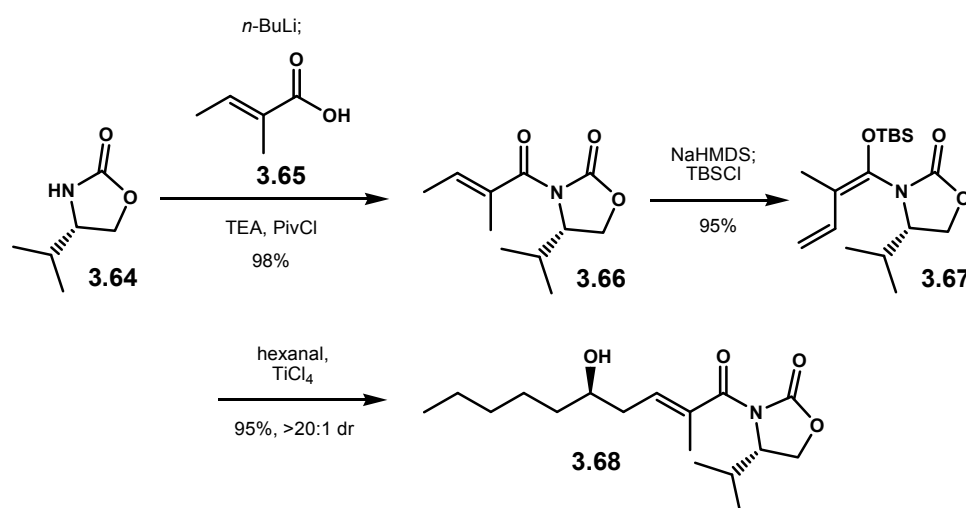
**Scheme 3.19**

#### 3.6.4. The Vinylogous Mukaiyama Aldol Reaction with *N,O*-Ketene Acetal

Around the time when we completed the synthesis of fragment **3.13**, Kobayashi and co-workers published a communication detailing their methodology development in asymmetric vinylogous Mukaiyama aldol reactions using chiral *N,O*-ketene acetal **3.67**.<sup>251</sup> This report caught our interest as this methodology would enable significant shortening of the synthetic sequence to fragment **3.13**. More importantly, this method would also solve the low enantioselectivity problem plagued in the previously discussed asymmetric allylation reactions.

As demonstrated in Scheme 3.20, the preparation of *N,O*-ketene acetal **3.67** was straightforward. Acylation of oxazolidinone **3.64** with tiglic acid **3.65** provided imide **3.66** in 98% yield. Deprotonation of imide **3.66** with NaHMDS followed by trapping of

the resulting sodium enolate with TBSCl provided *N,O*-ketene acetal **3.67** in 95% yield as a single olefin isomer. Remarkably, this ketene acetal was stable in silica gel, thus allowing simple column chromatography purification. Exposure of *N,O*-ketene acetal **3.67** to a premixed solution of hexanaldehyde and TiCl<sub>4</sub> at -78°C cleanly produced  $\delta$ -hydroxy- $\alpha$ -methyl- $\alpha,\beta$ -unsaturated imide **3.68** in 95% yield as a single diastereomer.



**Scheme 3.20**

The above vinylogous Mukaiyama aldol reaction represents a rare example of completely remote 1,7-asymmetric induction. The mechanism for this extraordinary reaction is proposed through transition state models depicted in Figure 3.6. Based on his computational analyses, Kobayashi proposes that the conformation of *N,O*-ketene acetal **3.67** can be illustrated as conformer **3.69** in which the isopropyl group is oriented nearly perpendicular to the diene plane. This overhanging isopropyl group will enable facial differentiation toward the approaching aldehyde. In addition, as illustrated in transition

state model **3.70**, orientation of the aldehyde in respect to the nucleophile must be in such a manner that minimization of the overall gauche interactions was attained.

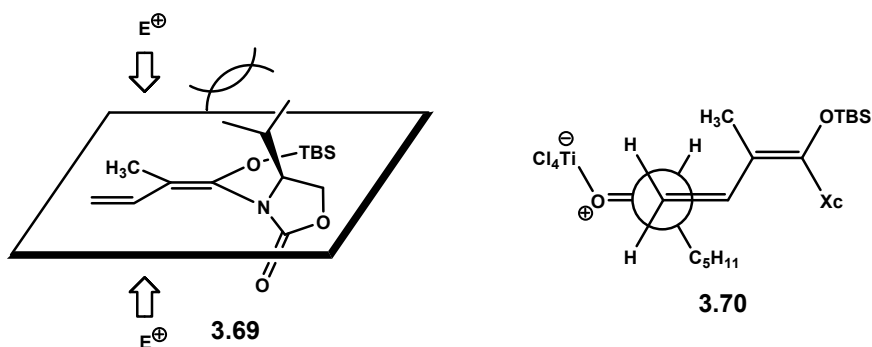
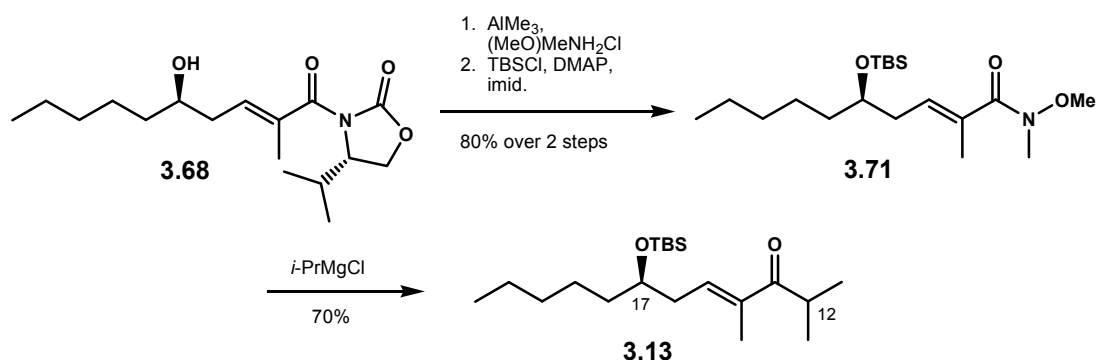


**Figure 3.6**

Imide **3.68** was then transformed to the corresponding Weinreb amide **3.71** upon treatment with  $\text{AlMe}_3$  and *N,O*-dimethylhydroxyl amine HCl salt.<sup>136</sup> Subsequent TBS protection of the secondary alcohol provided amide **3.71** in 80% yield over two steps. The ensuing slow addition of isopropylmagnesium chloride to amide **3.71** in ether at 0°C afforded fragment **3.13** in 70% yield. With this new, much improved synthetic route, fragment **3.13** was prepared in just four steps from hexanal with an overall yield of 53%.

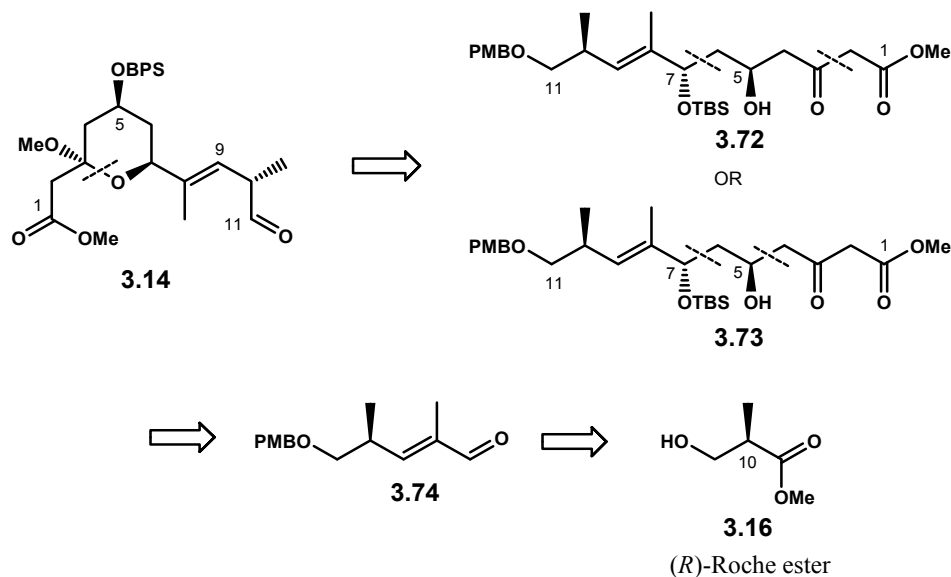


**Scheme 3.21**



### 3.7. Preparation of Fragment 3.14

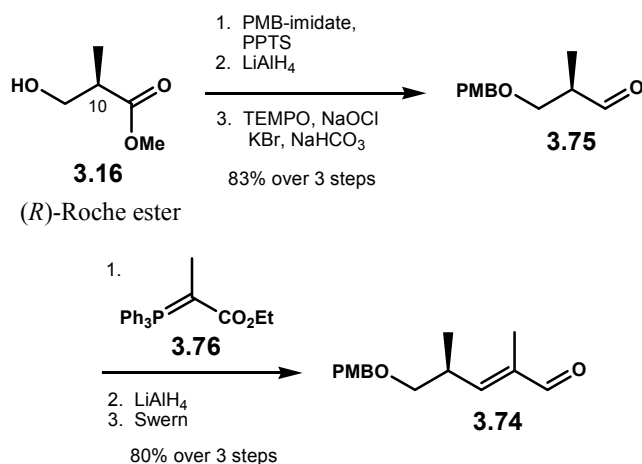
Synthetic fragment **3.14** represents the northern portion of acutiphycin. There are several key structural features within this fragment that must be carefully taken into consideration when designing the retrosynthesis. In addition to the C5 and C7 hydroxyl stereogenic centers, this fragment also contains a methyl stereocenter at C10, which would be carried through from commercially available chiral pool (*R*)-Roche ester. We propose two different strategies to install the requisite hydroxyl centers. These approaches would be realized via either *four plus two* or *two plus four* carbon atom additions based on bond disconnections as depicted in **3.72** and **3.73** respectively. The methyl pyranoside moiety would be readily constructed by simple acidic methanolysis, Scheme 3.22.



Scheme 3.22

### 3.7.1. Preparation of Aldehyde 3.74

Our synthetic work to fragment **3.14** commenced with a large-scale preparation of  $\alpha,\beta$ -unsaturated aldehyde **3.74**. As shown in Scheme 3.23, treatment of (*R*)-Roche ester with PPTS and PMB-imide,<sup>55</sup> followed by LAH reduction and TEMPO – bleach oxidation afforded chiral aldehyde **3.75** in 83% yield over three steps. This mild oxidation method was chosen because it was inexpensive and scalable for large-scale reactions.<sup>252</sup> We also noted that the quality of the commercial bleach significantly affected the outcome of the TEMPO oxidation. From our experience, the regular Clorox brand appeared to give the best results. Aldehyde **3.75** was typically produced in quantitative yield with Clorox, and there was no evidence for racemization. Meanwhile, other generic brands, such as the Meijer or Wal-Mart brands often resulted in low yield and significant racemization.

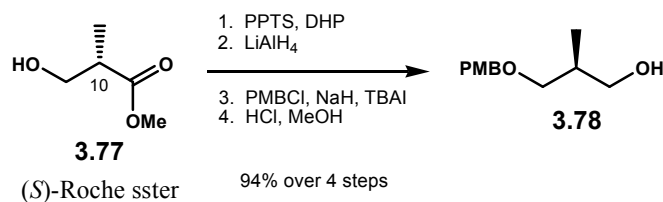


Scheme 3.23

Aldehyde **3.75** was then immediately vinylogated through the Wittig reaction with phosphorane **3.76**, which installed the required *E* olefin. The ensuing reduction and Swern oxidation then yielded aldehyde **3.74** in 80% yield over three steps. This sequence was highly robust and allowed us to easily prepare more than 50 grams of material in just a single batch.

Our group has utilized the abovementioned large-scale preparation of  $\alpha,\beta$ -unsaturated aldehyde to several other target polyketides, such as the myriaporones, tedanolides, gephyronic acid, and ambruticin. However, these targets would require (*S*)-Roche ester **3.77** as the starting chiral pool. The production of aldehyde **3.75** for acutiphyacin may also originate from this enantiomer of Roche ester, and this would require an inversion of the methyl stereochemistry. As demonstrated in Scheme 3.24, the methyl stereochemical inversion was relatively straightforward and accomplished in just four simple steps.

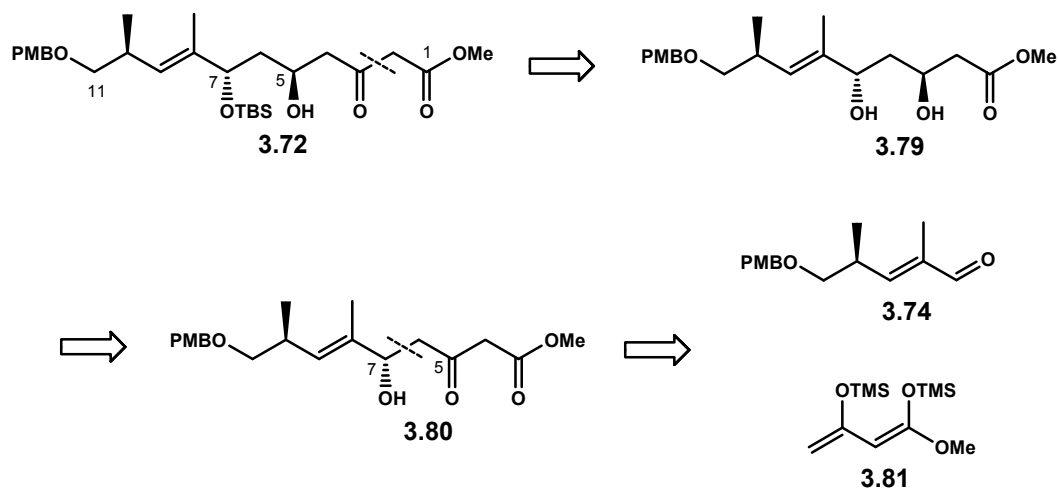
Protection of (*S*)-Roche ester **3.77** as a THP ether followed reduction, protection of the resulting primary alcohol as a PMB ether, and removal of the THP group under acidic methanolysis successfully produced alcohol **3.78** in 94% yield over four steps. These sequence was successfully applied up to 30 grams of (*S*)-Roche ester **3.77**. Alcohol **3.78** was produced with >95% enantiomeric purity under these conditions, and only one column chromatography purification was necessary after the four-step sequence.



**Scheme 3.24**

### 3.7.2. Four Plus Two Carbon Atoms Addition

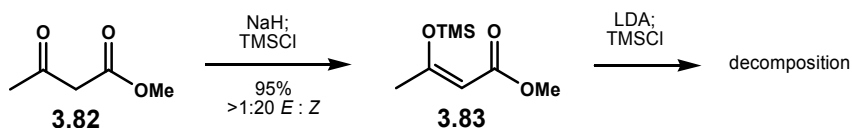
With the successful preparation of aldehyde **3.74**, we then focused on the installation of C5 and C7 hydroxyl stereogenic centers. As shown in Scheme 3.25, we envision that fragment **3.72** should be accessible from *anti* diol **3.79**, that would be prepared via directed reduction of  $\beta$ -hydroxy ketone **3.80**. The C7 hydroxyl stereochemistry would be established via an asymmetric vinylogous aldol reaction between aldehyde **3.74** and Chan's diene **3.81** as the nucleophilic partner.



**Scheme 3.25**

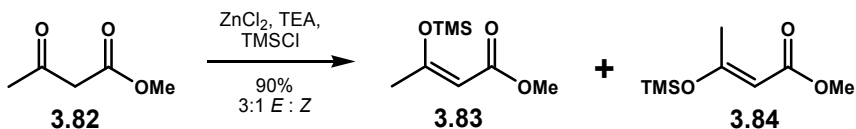
### 3.7.2.1. Preparation of Chan's Diene 3.81

Numerous literature precedents describing the preparation of Chan's diene **3.81** are available; however, we could not reproduce any of these established procedures.<sup>206</sup> For example, a typical preparation of Chan's diene **3.81** included exposure of methyl acetoacetate **3.82** to hard enolization conditions which produced enol silane **3.83** as a single olefin isomer. Unfortunately, the second enolization with LDA only yielded decomposition material.



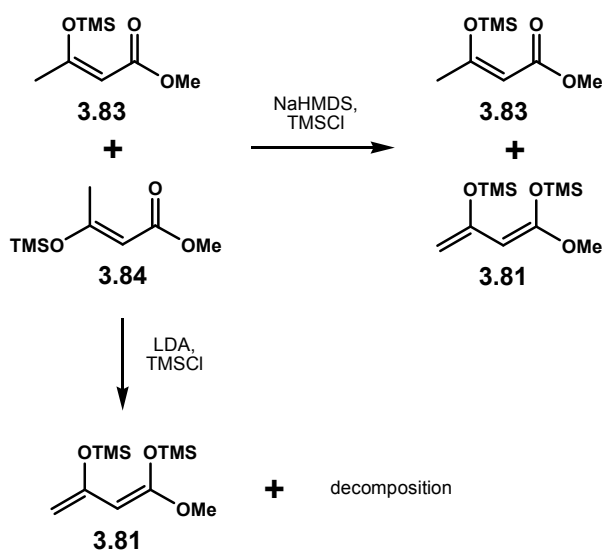
Scheme 3.26

We speculated that the olefin geometry of enol silane **3.83** played an important role in the second enolization process. In order to access the opposite olefin isomer, methyl acetoacetate was treated with a mixture of catalytic amount of ZnCl<sub>2</sub>, TEA, and TMSCl.<sup>253</sup> These soft enolization conditions indeed produced an inseparable mixture of *Z* and *E* enol silane **3.83** and **3.84** respectively in a ratio of 1:3.



Scheme 3.27

When the above mixture of enol silanes **3.83** and **3.84** was reacted to LDA and TMSCl, the crude  $^1\text{H}$  NMR indicated the presence of Chan's diene **3.81**, however contaminated with a significant amount of decomposition materials, Scheme 3.28. The  $^1\text{H}$  NMR patterns of the decomposition material was found identical to those obtained from enolization of *Z* enol silane **3.83**. The use of another base for the second enolization reaction, such as NaHMDS, led to a crude mixture containing the desired Chan's diene **3.81** and unreacted *Z* enol silane **3.83**. Separation of Chan's diene **3.81** from unreacted **3.83** by a low temperature vacuum distillation method was fairly straightforward due to the volatility of enol silane **3.83**. To confirm that enol silane **3.83** was unreactive toward enolization with NaHMDS, an authentic sample obtained from Scheme 3.26 was exposed to identical enolization conditions. Indeed, crude  $^1\text{H}$  NMR only showed the presence of starting material **3.83**.



**Scheme 3.28**

A possible explanation to the above chemical behavior may be proposed as follows. Deprotonation of *E* enol silane **3.84** with NaHMDS may potentially undergo a cyclic eight-membered transition state as depicted in structure **3.85**. Such a cyclic transition state is not permissible with *Z* enol silane **3.83** due to the torsional constraint embedded within the olefin geometry. Cyclic transition states larger than the Zimmerman-Traxler six-membered model, particularly in deprotonation reactions, have been previously proposed. An example would be the seven- or nine-membered transition state proposed by Fuji and Kawabata in their study of memory of chirality.<sup>254, 255</sup>

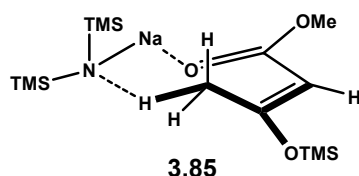
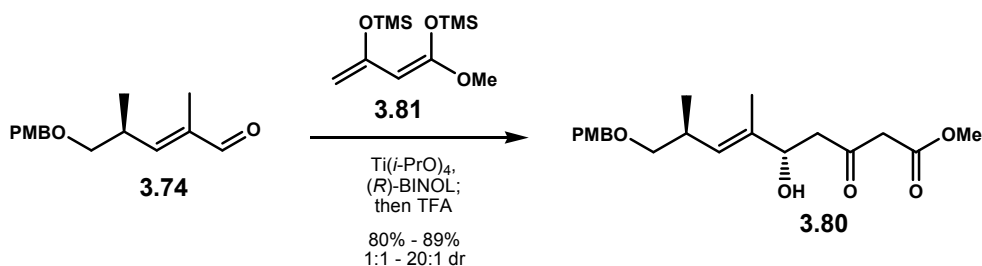


**Figure 3.7**

### 3.7.2.2. Titanium(IV)-BINOL Promoted Asymmetric Aldol Reaction

Soriente and co-workers have demonstrated that asymmetric addition of Chan's diene **3.81** to a variety of aldehyde can be smoothly promoted by a catalytic amount of Ti(IV)-BINOL complex.<sup>60, 134, 256-258</sup> This complex is readily formed *in situ* by premixing Ti(*i*-PrO)<sub>4</sub> and BINOL in the presence of 4Å molecular sieves. The stereochemistry of the resulting vinylogous aldol product is determined by chirality of the BINOL ligand. For our system, (*R*)-BINOL is required to install the *S* stereochemistry at C7 hydroxyl. When Soriente's conditions were applied to aldehyde **3.74**, to our surprise, the diastereoselectivity of the reaction was inconsistent. From multiple attempts, the aldol

product was isolated ranging from once as a single diastereomer to a complete mixture of diastereomers at another instance.

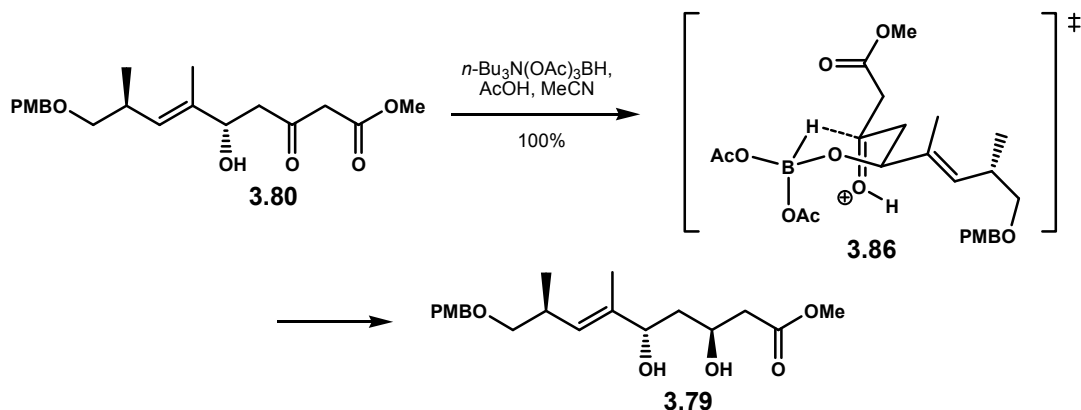


**Scheme 3.29**

### 3.7.2.3. Directed Reduction, Enolate Addition, and Cyclization

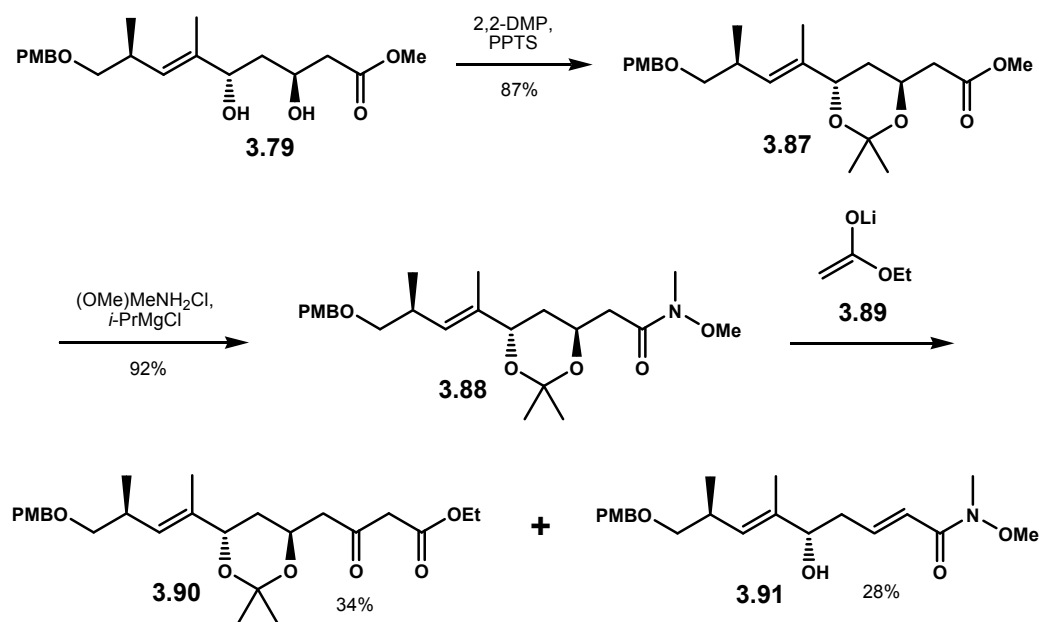
Despite the inconsistent diastereoselectivity, we decided to investigate the legitimacy of the present route by subjecting aldol product **3.80** to the planned synthetic sequence. Reduction of **3.80** with tetraethylammonium triacetoxyborohydride in the presence of acetic acid afforded 1,3-*anti* diol **3.79** in quantitative yield as a single diastereomer.<sup>72</sup> The proposed transition state that accounted for the observed selectivity is depicted in structure **3.86**.





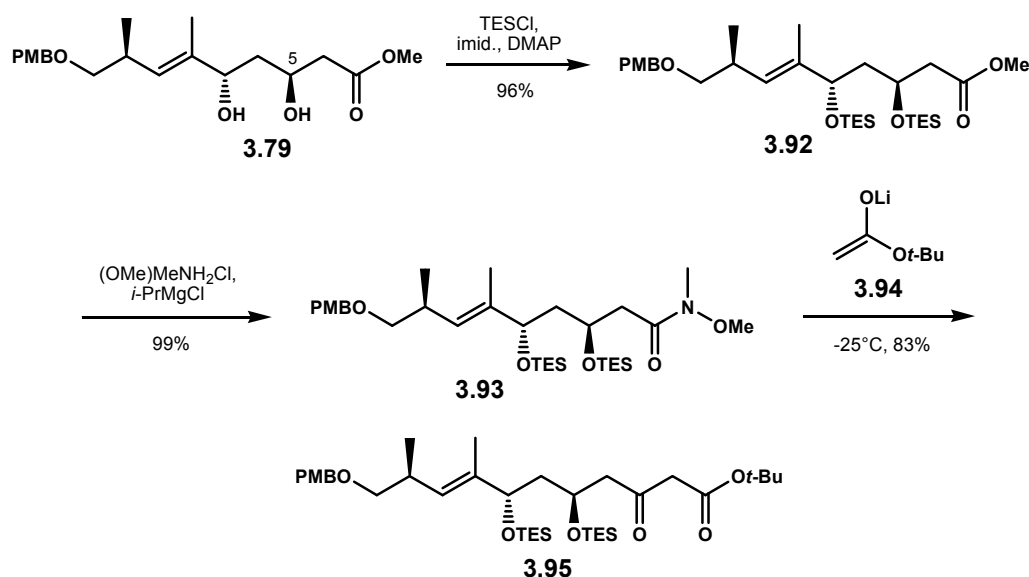
**Scheme 3.30**

Diol **3.79** was then protected as acetonide **3.87**.  $^{13}\text{C}$  NMR assignment of the acetonide carbon centers confirmed the 1,3-*anti* stereochemistry based on the correlations reported by Rychnovsky and co-workers.<sup>259</sup> To complete the carbon backbone of the southern portion of acutiphycin, sequential conversion of the methyl ester **3.87** to Weinreb amide **3.88** and addition of the lithium enolate of ethyl acetate is required. Weinreb amide **3.88** was produced in 92% yield via a known amidation protocol with (OMe)MeNH<sub>2</sub>Cl salt and *i*-PrMgCl.<sup>260</sup> The ensuing addition of lithium enolate of ethyl acetate **3.89** was rather problematic. Likewise with the production of  $\beta$ -ketoester **3.90** in 34% yield, these reaction conditions unfortunately also induced elimination to **3.91** in 28% yield, Scheme 3.31.



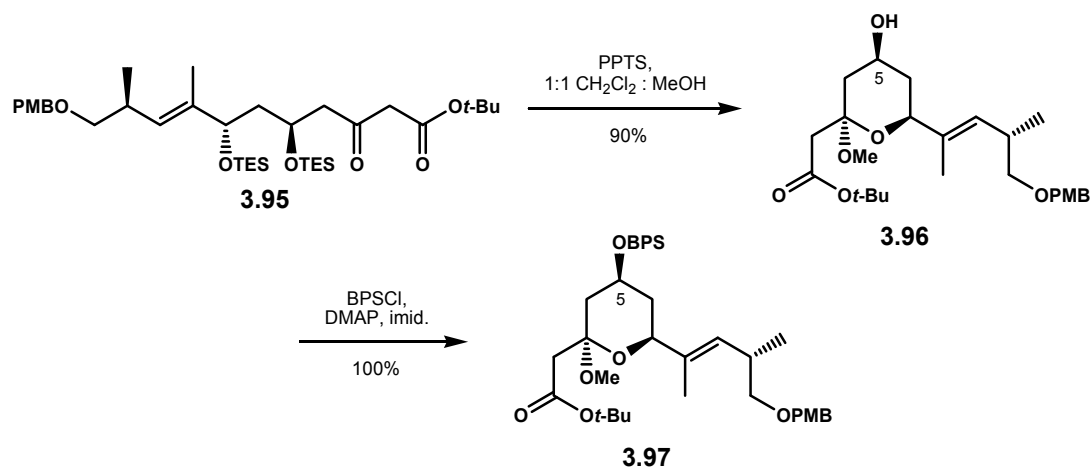
**Scheme 3.31**

To minimize lability of the C5 hydroxyl as a potential nucleofuge, the suitability of silicon-based protecting groups was exploited. Treatment of 1,3-*anti* diol **3.79** to TESCl, imidazole, and DMAP provided *bis*-TES ether **3.92** in 96% yield. A subsequent installation of the Weinreb amide under previously described conditions proceeded in near quantitative yield. To our disappointment, the TES protecting groups appeared to prevent addition of the lithium enolate of ethyl acetate **3.89** to amide **3.93** even at room temperature. Similarly, the lithium enolate of methyl or phenyl acetate also did not yield the expected addition products. However, with lithium enolate of *tert*-butyl acetate **3.94**, the addition reaction readily proceeded at -25°C to afford adduct **3.95** in 83% yield, thus completing the carbon backbone precursor for impending installation of the methyl pyranoside moiety.



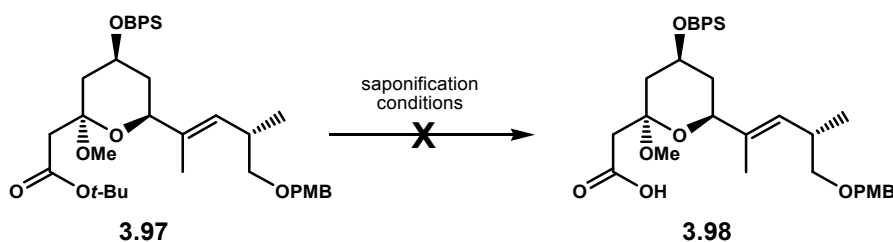
**Scheme 3.32**

The construction of acutiphycin's methyl pyranoside moiety commenced with exposure of  $\beta$ -ketoester **3.95** to acidic methanolysis conditions, Scheme 3.33. The use of a catalytic amount of PPTS in 1:1 mixture of  $\text{CH}_2\text{Cl}_2$  and methanol led to deprotection of the *bis*-TES ether followed by cyclization produced methyl pyranoside **3.96** in 90% yield. The newly incorporated methoxy group was presumably oriented in the axial direction, driven by the anomeric effect stabilization. Exposure of **3.96** to BPSCl, DMAP, and imidazole transformed the C5 hydroxyl group as BPS ether **3.97** in quantitative yield.



**Scheme 3.33**

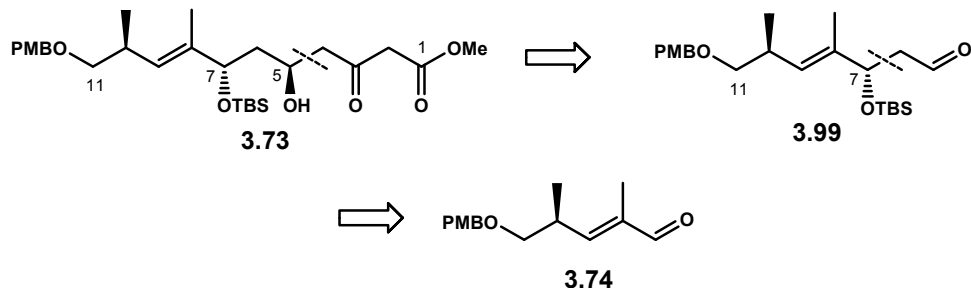
Since the addition of a two-carbon unit to Weinreb amide **3.93** only proved successful with the lithium enolate of *tert*-butyl acetate **3.94**, the utilization of *tert*-butyl ester functionality might impose a major concern as a precursor to late-stage conversion to the acid. Removal of *tert*-butyl group to the corresponding carboxylic acid typically requires strongly acidic conditions, which may possibly destroy the advanced materials. As expected, saponification of **3.97** to carboxylic acid **3.98** was unsuccessful. Under established strongly acidic conditions, such as TFA or HCl, fragment **3.97** readily underwent decomposition. When the reaction was carried out either in mildly acidic (TsOH or AcOH) or basic (KOH) conditions, the *tert*-butyl ester was unaffected.



**Scheme 3.34**

### 3.7.3. Two Plus Four Carbon Atom Addition

With the unsuccessful key saponification step, the overall sequence to the construction of fragment **3.14** must be rerouted. As shown in Scheme 3.35, we plan to install the stereochemistry at C7 hydroxyl group via an acetate aldol sequence. The C5 stereogenic center and the remaining four carbon atoms would be then introduced in an asymmetric Mukaiyama aldol reaction with Chan's diene **3.81** as the nucleophilic partner. Such an aldol reaction should establish the requisite 1,3-*anti* stereochemistry based on the polar induction transition state model developed by Evans and co-workers.<sup>65</sup>

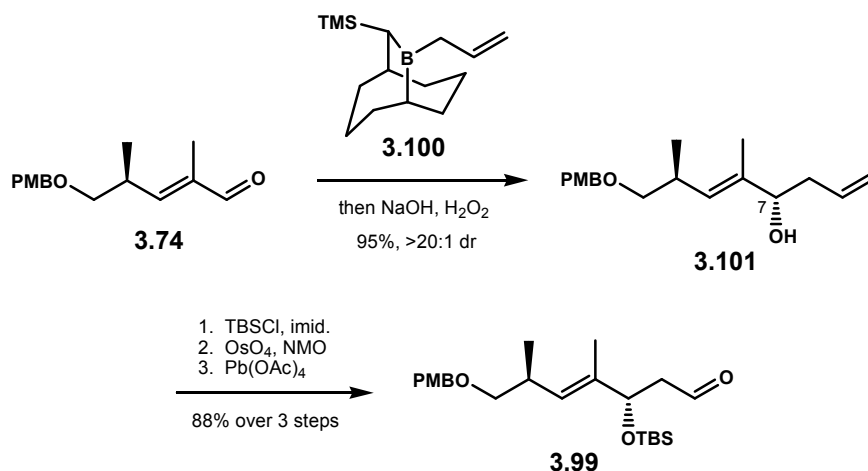


Scheme 3.35

#### 3.7.3.1. Soderquist Allylation and Acetate Aldol

The construction of acetate aldol **3.99** was fairly straightforward. Asymmetric allylation of aldehyde **3.74** promoted by Soderquist's chiral borabicyclodecanes reagent **3.100** afforded homoallylic alcohol **3.101** in 95% yield as a single diastereomer.<sup>261</sup> Upon protection of the C7 hydroxyl group as a TBS ether, the ensuing oxidative cleavage of the

terminal olefin via a dihydroxylation – oxidation sequence then unmasked aldehyde **3.99** in 88% yield over three steps.



**Scheme 3.36**

Soderquist's new borabicyclodecanes reagent has emerged as one of the most powerful and reliable methods in asymmetric allylation, crotylation, allenylation, and propargylation reactions.<sup>261-264</sup> The superiority of this method is highlighted by several factors that were not feasible in other established conditions. For instance, excellent chemical yields and stereoselectivity have been found universal in various aldehydes, and these results were unmatched by other methods. More importantly, the chiral borabicyclodecanes reagents are recoverable and potentially reusable depending upon workup conditions. Handling of these borane reagents and experimental procedure proved relatively easy due to the unusual stability of these reagents.

The transition state that predicts the stereochemical outcome in the Soderquist reaction is presented in Figure 3.8. As shown in structure **3.102**, the Zimmerman-Traxler six-membered model, similar to that of Brown's and Roush's, has been proposed;

however, the mode of stereochemical induction is counterintuitive when judged by the principle of steric repulsion effect. From his low-level computational data, Soderquist proposes that orientation of the approaching aldehyde *cis* to the 10-TMS group is favored over any other conformations. His research also suggests that any attempts for other transition states via B – O or B – allyl bonds rotation is prohibited by the TMS group.

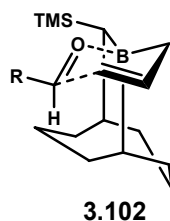
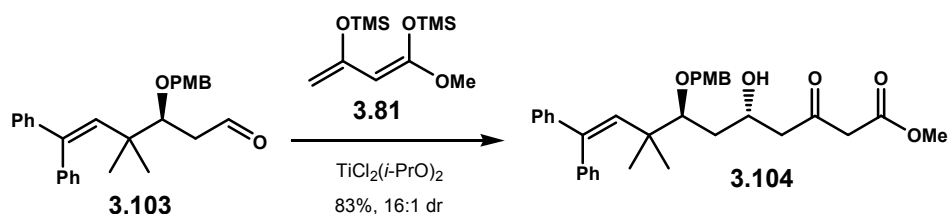


**Figure 3.8**

### 3.7.3.2. Evans Polar Induction Model

With aldehyde **3.99** synthesized, we exploited chemistry previously reported by David Evans and co-workers to stereoselectively install the remaining four carbon atoms. In his synthetic quest to bryostatin A, Evans reported a Mukaiyama aldol reaction between aldehyde **3.103** and Chan's diene **3.81** promoted by  $\text{TiCl}_2(i\text{-PrO})_2$ .<sup>265</sup> The resulting vinylogous aldol product **3.104** was isolated in 83% yield as a 16:1 mixture of diastereomer favoring the 1,3-*anti* stereochemistry, Scheme 3.37.



**Scheme 3.37**

The transition state that accounts for the observed 1,3-*anti* stereochemistry has been proposed through a system known as the Evans' polar induction model. In this transition state model, the conformation of the aldehyde must be aligned in the orientation represented in Newman projection **3.105**. This conformation will achieve minimization dipoles between the activated carbonyl oxide and  $\beta$ -OPMB. The nucleophile will approach the aldehyde from the sterically less demanding face, thus furnishing the *anti* stereochemistry.

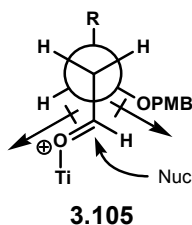
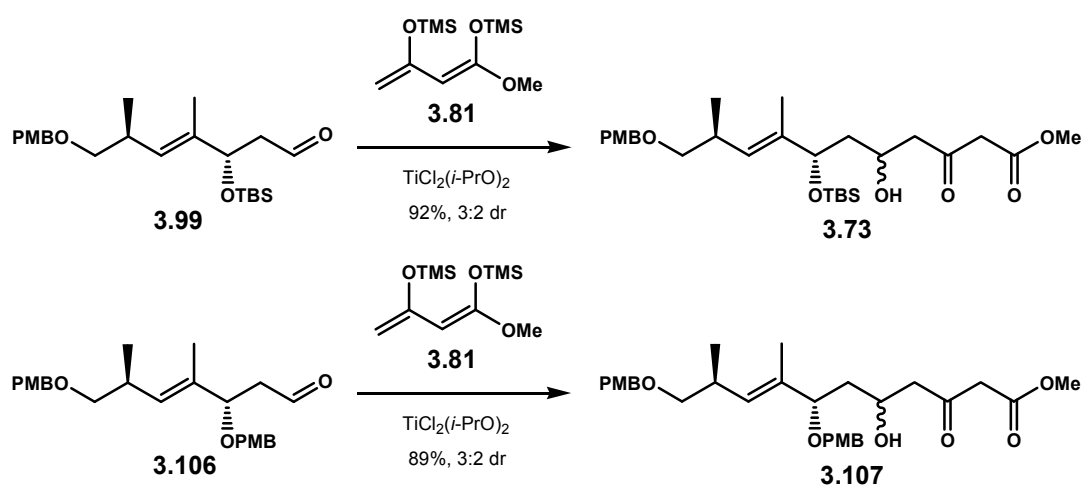


**Figure 3.9**

When the Evans' protocol was applied to our aldehyde **3.99**, the desired aldol product **3.73** was obtained in 92% yield unexpectedly as a 3:2 mixture of diastereomers. We initially believed that the poor stereoselectivity must have originated from the improper choice of protecting group at the C7 hydroxyl. Evans states that the choice of



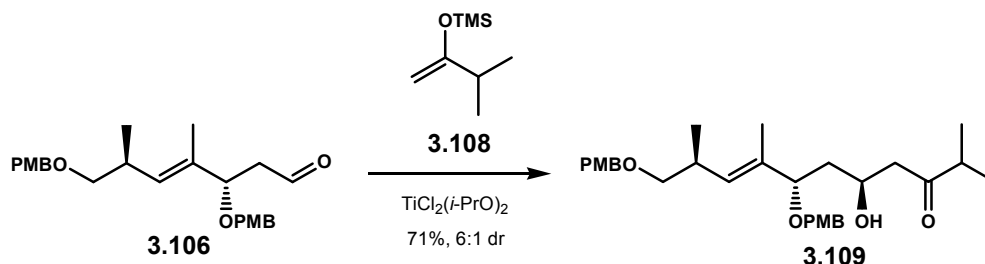
protecting group significantly affects stereoselectivity in his polar induction model.<sup>65</sup> For example, his finding demonstrates that a PMB group creates a significantly stronger polarization effect compared to that of TBS, hence it promotes better stereoselectivity. Based on this report,  $\beta$ -OPMB aldehyde **3.106** was subsequently prepared. Surprisingly, exposure of this aldehyde to the identical Mukaiyama aldol conditions produced aldol adduct **3.107** as a 3:2 mixture of diastereomers.



**Scheme 3.38**

Thorough reaction optimizations in attempt to solve this unforeseen stereoselectivity problem were executed. Numerous reaction conditions, including the choice of solvents, temperatures, and Lewis acids have been screened,<sup>266, 267</sup> and none of these parameters indicated any improvement in diastereoselectivity. We became suspicious if the reactivity of Chan's diene **3.81** may have been responsible for the complete loss in stereoselectivity. In order to test this hypothesis, the Mukaiyama aldol reaction was run this time with enol silane **3.108** as the nucleophilic partner to aldehyde

**3.106.** Unexpectedly, this reaction produced aldol product **3.109** in 71% yield with a diastereomeric ratio of 6:1, Scheme 3.39.



**Scheme 3.39**

It is now clear that Chan's diene **3.81** is most likely too reactive of a nucleophile for a stereoselective aldol reaction with our aldehyde **3.106**. However, one important question remained unclear. Why was excellent diastereoselectivity observed with Evans's aldehyde **3.103**, but completely lost with our aldehyde **3.106**? In order to gain some insights on these crucial issues, all possible transition states that might be accountable for the observed stereoselectivity and the rigidity of each transition state needed to be examined.

We began with analyzing the approach of Chan's diene **3.81** to aldehydes **3.103** and **3.106** upon Lewis acid activation. As shown in Figure 3.10, while maintaining the optimized Evan's polar induction model, Chan's diene **3.81** may potentially approach the aldehyde in six possible modes: four *synclinal* **3.110**, **3.111**, **3.113**, and **3.114**, and two *anti periplanar* **3.112** and **3.115**. Although all of these transition states result in the production of 1,3-*anti* stereochemistry, *anti periplanar* transition states **3.112** and **3.113** as well as *synclinal* **3.115** appeared unfavorable due to obvious steric reasons. While

Chan's diene approaches as depicted in **3.111** and **3.114** may be the apparent favorable transition states, we cannot exclude transition state **3.110** without further, more sophisticated analyses aided by computational methods. For the time being, **3.110** will be regarded as one of the key transition states that may explain the observed stereoselectivity patterns.

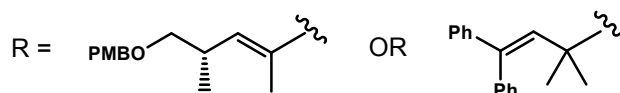
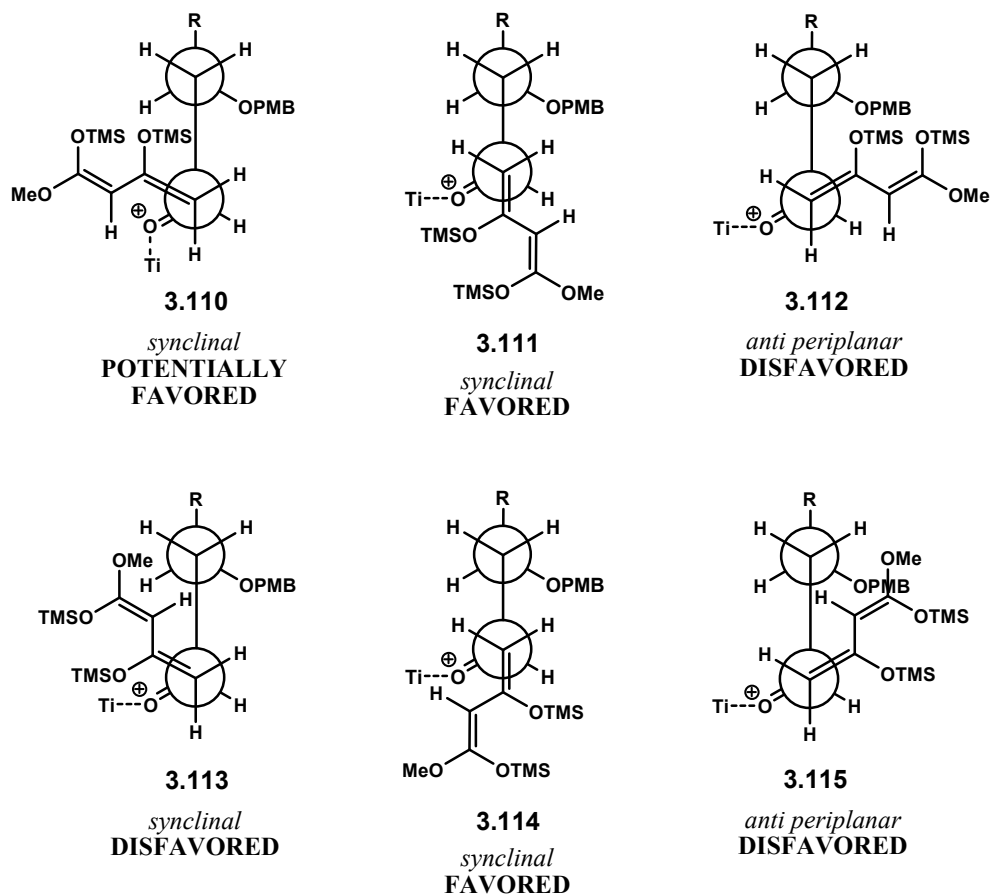
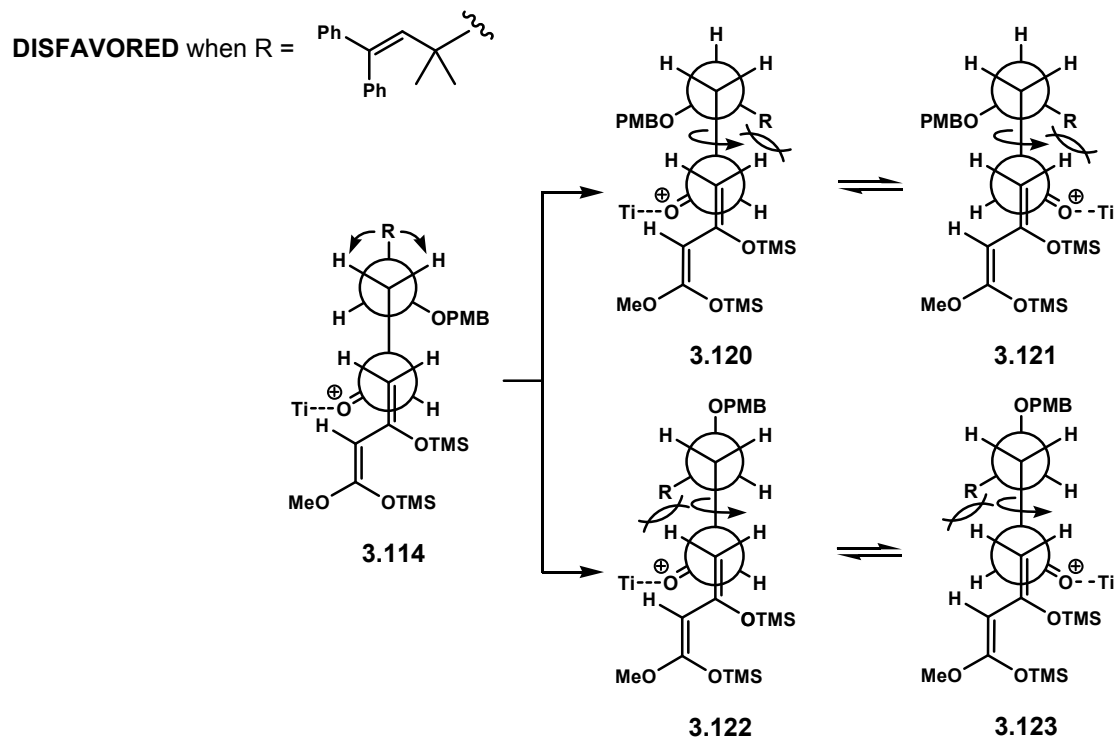
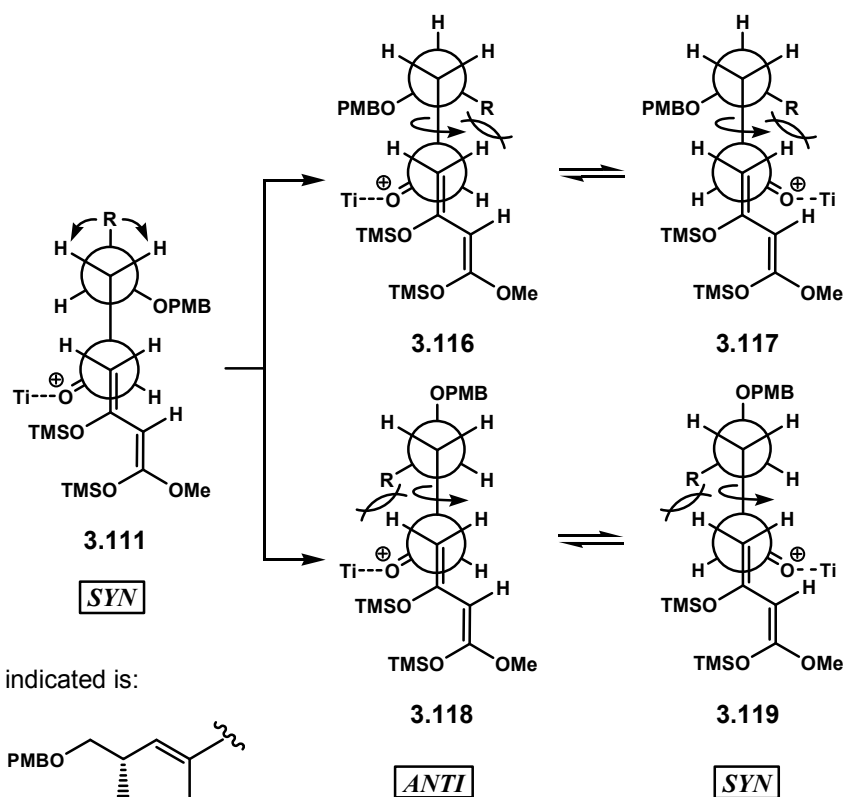


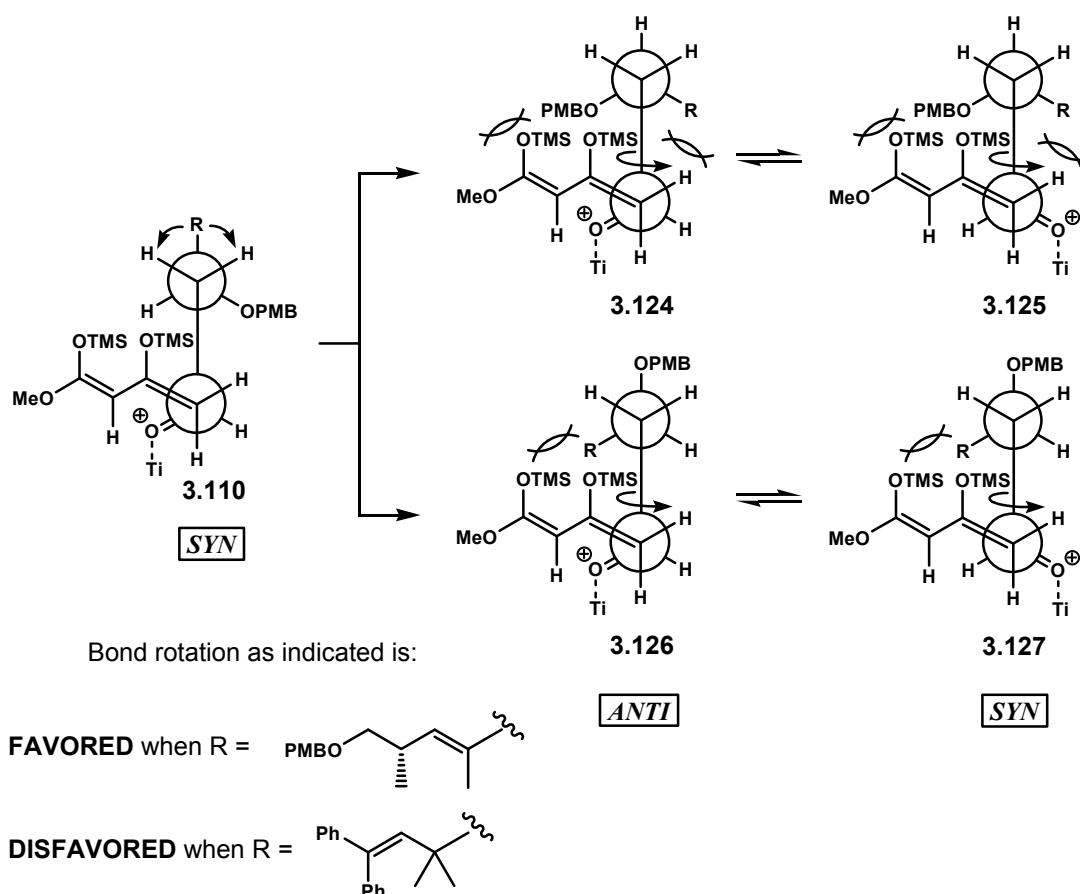
**Figure 3.10**

When comparing **3.103** and **3.106**, the key structural difference between these two aldehydes lies in the substituents at the  $\gamma$  carbon. Evans' aldehyde **3.103** contains a bulky *gem*-dimethyl group, whereas the  $\gamma$  carbon in aldehyde **3.106** is  $sp^2$  hybridized and poses significantly less steric demands. As shown in Scheme 3.40, when we account for this steric effect in transition states **3.111** and **3.114** in addition to the minimization of dipole effects, the presence of a *gem*-dimethyl group in aldehyde **3.103** will reinforce the rigidity of these polarized transition states. The *gem*-dimethyl functionality in fact will prevent a rotation about the  $\alpha,\beta$ -bond since such a rotation will introduce unfavorable steric interactions respectively as shown in **3.116** and **3.118** or **3.120** and **3.122**. However, with a geometrically flat,  $sp^2$  hybridized  $\gamma$ -carbon, this beneficial stereoelectronic effect is no longer present. In aldehyde **3.106**, it appears that the  $\alpha,\beta$ -bond rotation readily compete to give the alternative transition states. This bond rotation will ultimately alternate the aldehyde facial selectivity as shown in transition states **3.117** and **3.121**, which maintain the minimization of dipoles, or transition states **3.119** and **3.123**, in which the polar induction model is completely overlooked. Consequently, addition of Chan's diene does not proceed in a stereoselective fashion.



Scheme 3.40

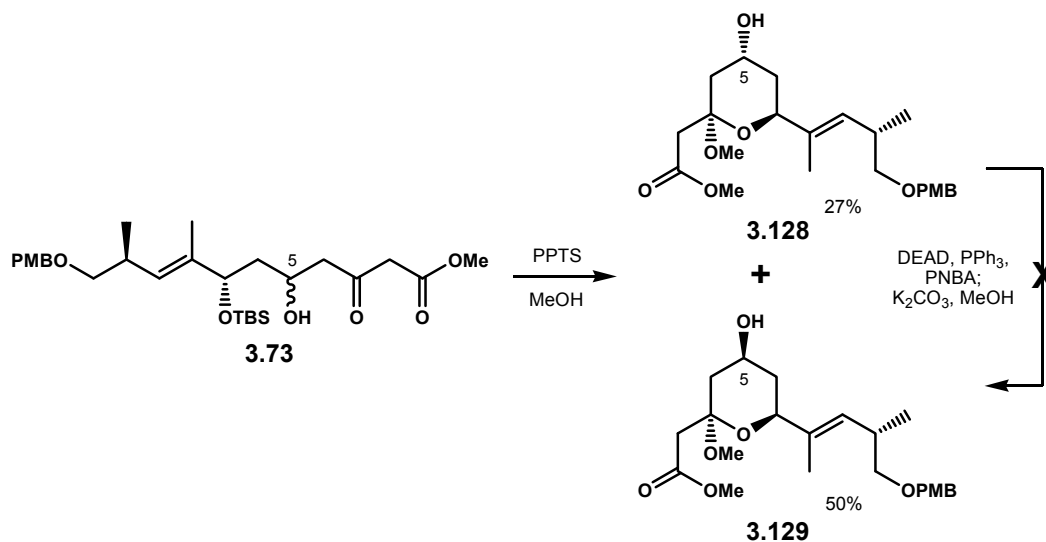
Similar arguments are also applicable when analyzing transition state **3.110**, Scheme 3.41. It is obvious that a rotation about the  $\alpha,\beta$ -bond is prohibited in aldehyde **3.103** as not only will the *gem*-dimethyl group create profound unfavorable steric interactions, but also the PMB ether group as depicted in transition states **3.124** – **3.127**. Once again, with the less sterically demanding  $sp^2$  hybridized  $\gamma$ -carbon, it appears aldehyde **3.106** does not enjoy such a conformational stabilizing effect; hence, the abovementioned competitive bond rotations will result in the production of both *anti* and *syn* stereochemistry.



Scheme 3.41

### 3.7.3.3. Cyclization and Mitsunobu Inversion

To solve the stereoselectivity issue in the key Mukaiyama aldol reaction, we planned to isolate the individual diastereomers and then correct the undesired C5 stereochemistry by the means of Mitsunobu inversion. Since  $\beta$ -hydroxy carbonyl functionality is prone to elimination under Mitsunobu conditions and the fact that the diastereomers of aldol adduct **3.73** were inseparable by column chromatography, construction of the methyl pyranoside prior to the stereochemical inversion became necessary. Exposure to acidic methanolysis cleanly removed the C7 TBS ether, and the subsequent cyclization provided chromatographically separable methyl pyranosides **3.128** and **3.129** in 27% and 50% yields, respectively.



Scheme 3.42

Methyl pyranoside **3.128** was found to contain the undesired C5 stereochemistry based on <sup>1</sup>H NMR coupling constant analyses. Unfortunately, an attempt to invert this

hydroxyl stereocenter under Mitsunobu conditions was unsuccessful,<sup>139</sup> as these conditions led to a competitive elimination pathway that readily gave triene **3.130**.

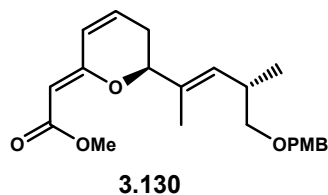
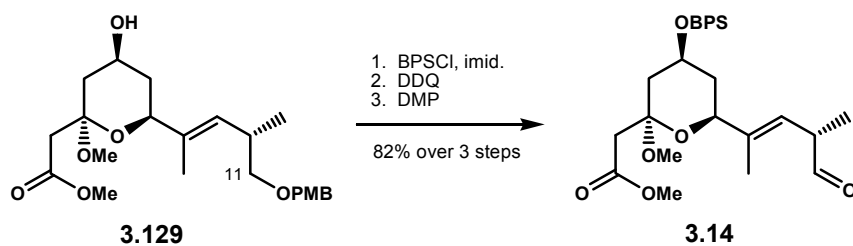


**Figure 3.11**

As demonstrated in Scheme 3.43, the completion to synthetic fragment **3.14** was accomplished in three steps from methyl pyranoside **3.129**. Protection of C5 hydroxyl as a BPS ether followed by removal the PMB ether with DDQ in wet CH<sub>2</sub>Cl<sub>2</sub> exposed the C11 primary alcohol. The ensuing Dess-Martin periodinane oxidation smoothly provided target fragment **3.14** in 82% yield over three steps.

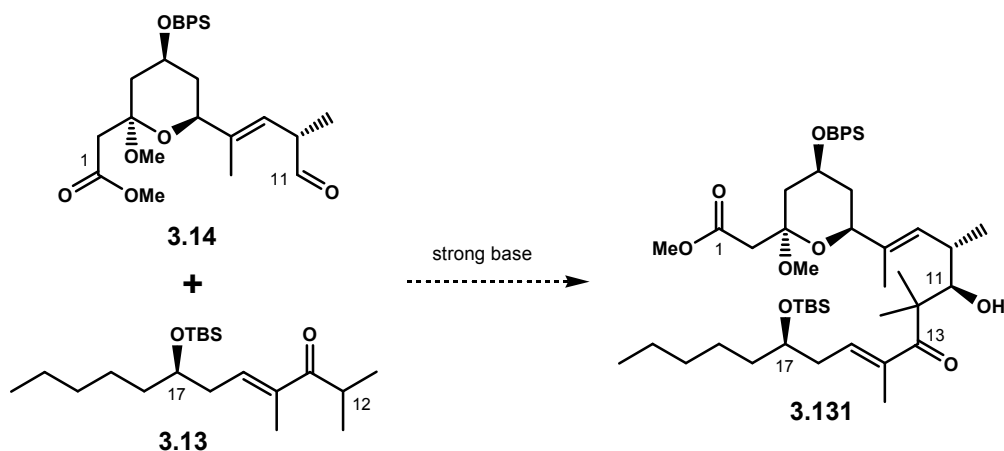


**Scheme 3.43**



### 3.8. Fragments 3.13 and 3.14 Coupling Studies

With fragments **3.13** and **3.14** in hand, we then focused on the coupling strategy and proposed an aldol reaction to yield advanced  $\beta$ -hydroxy ketone **3.131**. We assumed that kinetic enolization of fragment **3.13** with a strong base would provide a lithium enolate species that should add to aldehyde **3.14** in a stereoselective fashion based on the predicted Felkin-Anh transition state.<sup>268</sup> This process would install the requisite C11 stereocenter, Scheme 3.44.

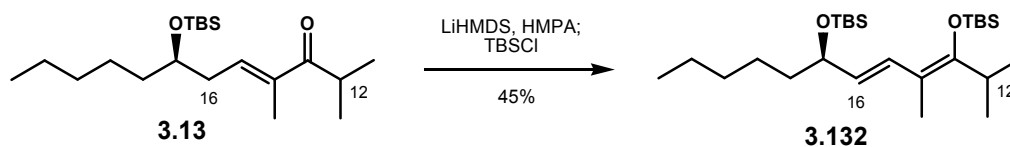


Scheme 3.44

#### 3.8.1. Enolization Study

When the structural features of fragment **3.13** were examined in details, there were two potential sites, C12 and C16, where deprotonation might occur upon exposure to strong base. Deprotonation at C16 might be competitive, but we believed that the adjacent OTBS group should provide enough steric hindrance to slow down such

deprotonation. In order to investigate the site of kinetic deprotonation, we first explored the conversion of fragment **3.13** to its corresponding enol silane. Upon treatment of **3.13** with several strong bases, LDA, with or without HMPA as an additive, was found only to destroy the starting material. The utilization of NaHMDS, KHMDS, and NaH did not provide any enolization product, and starting material **3.13** was quantitatively recovered. The use of LiHMDS readily led to enolization, however at C16, and these conditions provided enol silane **3.132** in 45% yield, Scheme 3.45.



**Scheme 3.45**

Since C16 appeared as the site for kinetic deprotonation, the enolization at C12 may require a thermodynamically controlled, soft enolization method. After screening various conditions, we found that soft enolization of ketone **3.13** to its corresponding enol silane **3.133** was readily affected in the presence of TMSOTf and TEA. However, we also learned that selectivity of this enolization was significantly dependent on the choice solvent and temperature. For example, as shown in Table 3.2, when the enolization was carried out in CH<sub>2</sub>Cl<sub>2</sub> both at room temperature and reflux for 12 hours, enol silanes **3.132** and **3.133** were produced in a 1:1 mixture. No enolization took place in THF, and starting material was quantitatively recovered. When the reaction was carried out in toluene at room temperature, the crude material indicated a mixture of starting material **3.13**, **3.132**, and **3.133** in 3:3:1 ratio. Interestingly, with diethyl ether at room

temperature, the ratio was found 7:1:2, and at reflux, this ratio significantly improved to 10:1:20 favoring the correct isomer of enol silane **3.133**. When CH<sub>2</sub>Cl<sub>2</sub> was used as a co-solvent with ether at room temperature, the ratio reverted back to 10:8:1 favoring the undesired isomer **3.132**. Our optimized conditions were established by exposing enone **3.13** to a mixture of TMSOTf – TEA in diethyl ether, and the reaction was warmed in a sealed tube at 100°C bath for 60 hours. These conditions enabled dramatic improvement of selectivity to 1:1:50.

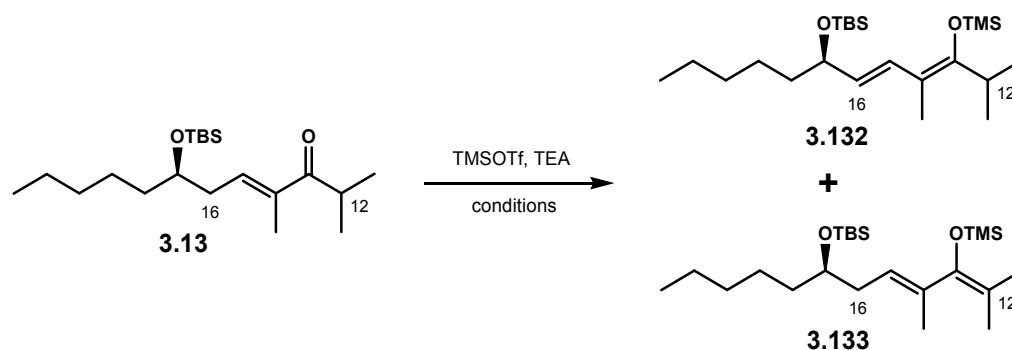


**TABLE 3.2**

Entry	Solvent	Temperature	Time (hrs)	3.13 : 3.132 : 3.133 <sup>[a]</sup>
1	CH <sub>2</sub> Cl <sub>2</sub>	rt	12	0:1:1
2	CH <sub>2</sub> Cl <sub>2</sub>	reflux	12	0:1:1
3	THF	rt	12	1:0:0
4	toluene	rt	12	3:1:3
5	Et <sub>2</sub> O	rt	12	7:1:2
6	1:1 Et <sub>2</sub> O / CH <sub>2</sub> Cl <sub>2</sub>	rt	12	10:8:1
7	Et <sub>2</sub> O	reflux	12	10:1:20
8	Et <sub>2</sub> O	100°C <sup>[b]</sup>	60	1:1:50

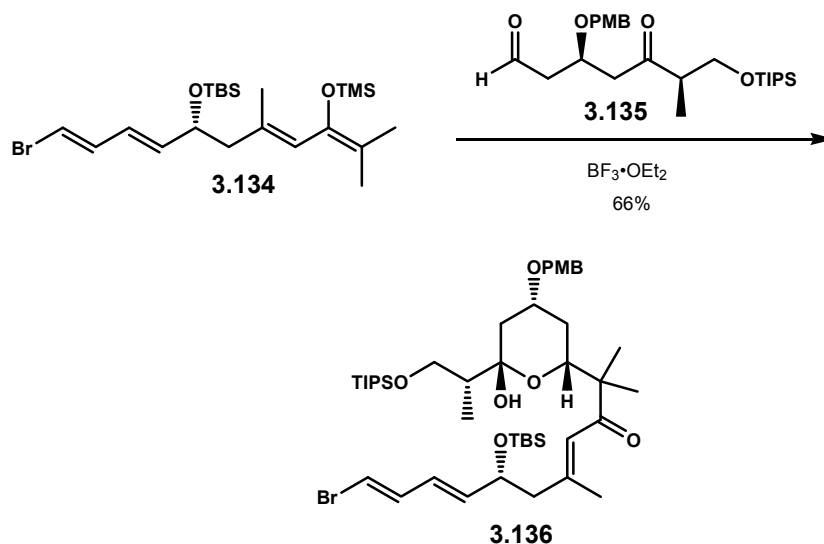
[a] Ratio was measured based <sup>1</sup>H NMR integration. [b] Reaction was carried out in a thick-walled vessel submerged in a 100°C sand bath.

The applicability to a large-scale reaction was demonstrated by exposure of one gram of enone **3.13** to the optimized conditions. Gratifyingly, enol silane **3.133** was consistently isolated in 99% yield in multiple attempts. It is interesting to note that enol silane **3.133** was chromatographically stable under untreated silica gel, and this permitted an easy purification.

### 3.8.2. Mukaiyama Aldol Approach

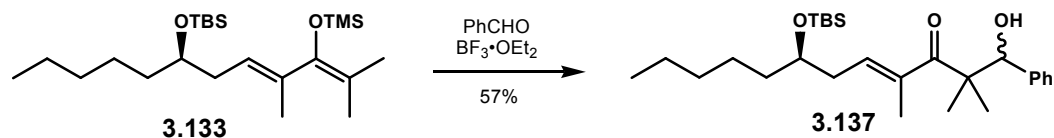
One of the concerns with our aldol coupling strategy surrounds the rather unexplored reactivity of sterically demanding systems. For instance, the southern portion of acutiphycin, represented by enol silane **3.133**, possesses a *gem*-dimethyl group which may significantly reduce its nucleophilicity. This assumption was strongly supported by unusual stability of this enol silane in silica gel. Furthermore, the northern portion acutiphycin, represented by aldehyde **3.14**, contains an  $\alpha$ -methyl center that may provide further steric hindrance.

A rare example for the coupling of highly substituted enol silane to a complex aldehyde has been preceded in the total synthesis of auriside A.<sup>46</sup> Paterson and co-workers have demonstrated a successful Mukaiyama aldol reaction between enol silane **3.134** and aldehyde **3.135** promoted by  $\text{BF}_3 \cdot \text{OEt}_2$  to give a cyclized aldol product **3.316** in 66% as a single diastereomer.



**Scheme 3.46**

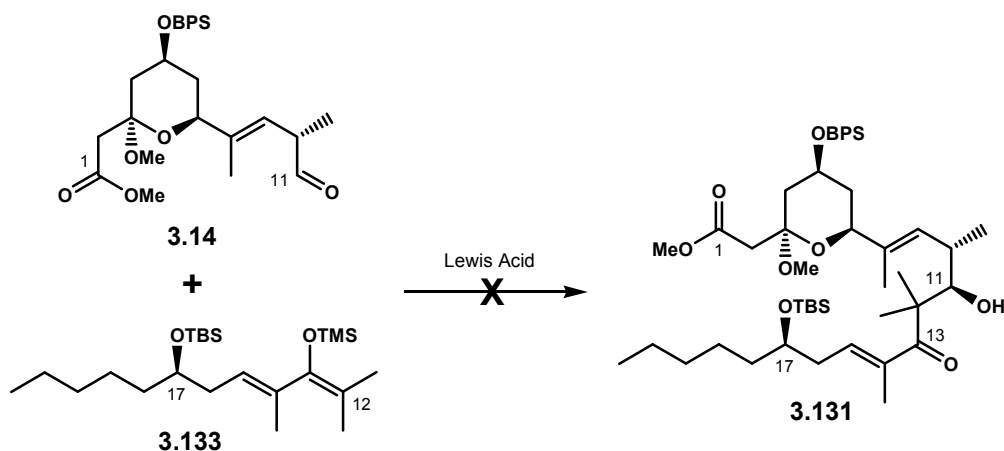
The structural complexity and steric demands of our enol silane **3.133** is reminiscent of that of **3.134**. Therefore, based on Paterson's precedent, we believed that enol silanes **3.133** and **3.134** should have comparable nucleophilicity. This hypothesis was further supported by evidence from our model study. As shown in Scheme 3.47, we observed that enol silane **3.133** smoothly added to benzaldehyde as promoted by  $\text{BF}_3 \cdot \text{OEt}_2$  to produce aldol product **3.137** in 57% yield.



**Scheme 3.47**

When these reaction conditions were applied to aldehyde **3.14**, the intended Mukaiyama reaction did not proceed. In fact, enol silane **3.133** was unaffected and

recovered in quantitative yield upon workup. The crude reaction NMR analyses, furthermore, revealed that the C10 methyl stereocenter of aldehyde **3.14** had been epimerized. We subsequently screened various Lewis acids. However, aluminum-based Lewis acids, such as  $\text{AlMeCl}_2$  or  $\text{AlMe}_2\text{Cl}$ , was found too harsh for the coupling reaction as these conditions only provided decomposition materials. In addition, the use of  $\text{TiCl}_4$  or  $\text{SnCl}_4$  also rapidly decomposed aldehyde **3.14**. Desilylation of enol silane **3.133** to the corresponding ketone **3.13** also occurred with these conditions. With much weaker Lewis acids, such as  $\text{TiCl}(\text{i-PrO})_3$  or  $\text{TiCl}_2(\text{i-PrO})_2$ , the Mukaiyama aldol reaction was unaffected. Once again, these reaction conditions only yielded unreacted enol silane **3.133** and epimerization at C10 methyl center of aldehyde **3.14**.

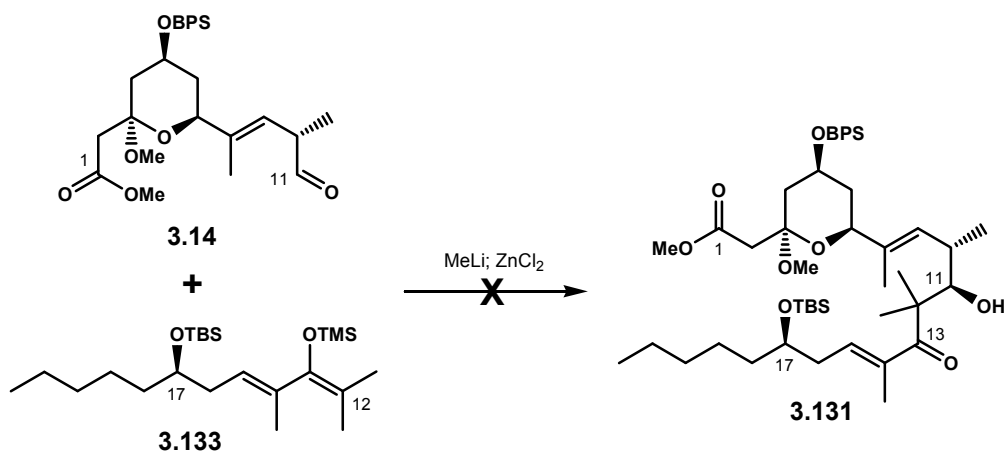


Scheme 3.48

### 3.8.3. House Aldol Approach

Since the Mukaiyama aldol strategy had disappointingly failed to couple fragments **3.133** and **3.14**, we subsequently decided to exploit an aldol strategy

When aldehyde **3.14** was introduced to a solution containing the zinc enolate of enone **3.13**, no coupling product was initially observed at -78°C. However, as the reaction was allowed to slowly warm up to -20°C, a complex mixture immediately began to form. We attempted to increase the nucleophilicity of the enolate by omitting the transmetallation step. However, addition of the resulting lithium enolate to aldehyde **3.14** only produced decomposition materials.

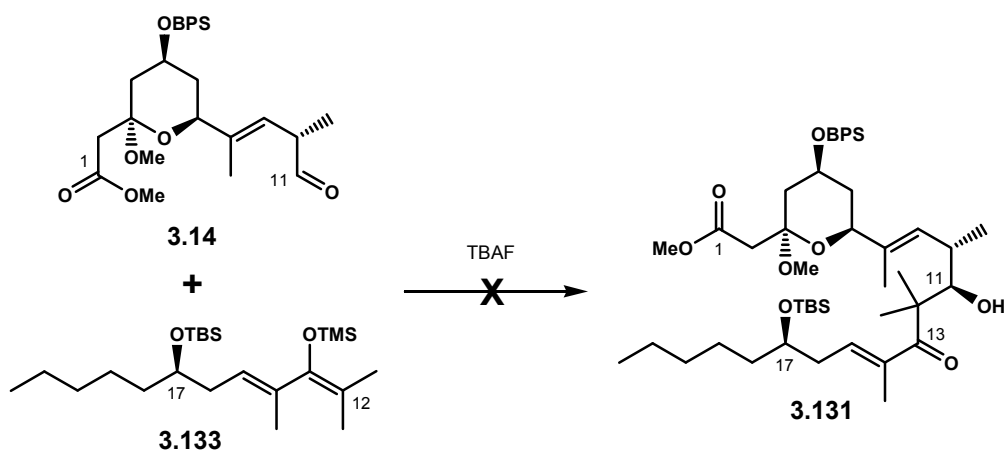


**Scheme 3.50**

#### 3.8.4. TBAF-Mediated Aldol Approach

Kuwajima and co-workers demonstrated that treatment of a highly substituted enol silane with anhydrous TBAF at low temperatures readily removes the silyl group.<sup>271</sup> The resulting highly reactive “naked” enolate species smoothly adds to an aldehyde and generates an aldol product.<sup>272</sup> Unfortunately, when this aldol methodology was applied to enol silane **3.133** and aldehyde **3.14**, decomposition materials were immediately produced.

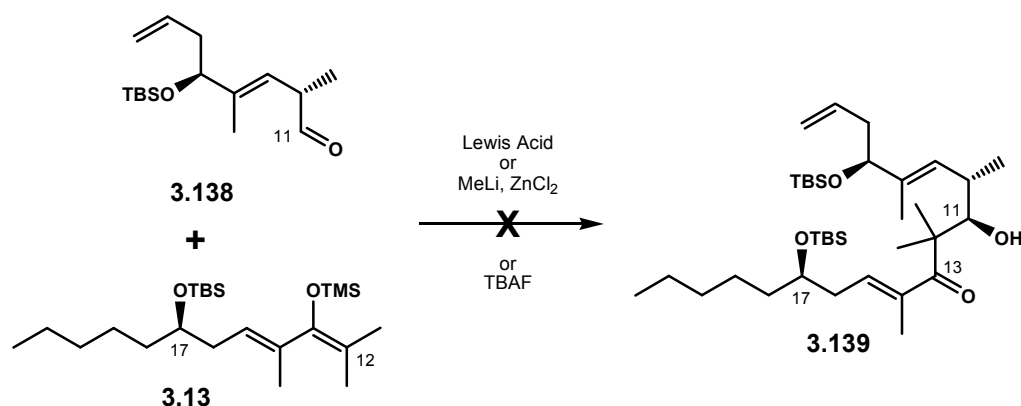




**Scheme 3.51**

### 3.8.5. Coupling With Truncated Aldehyde 3.138

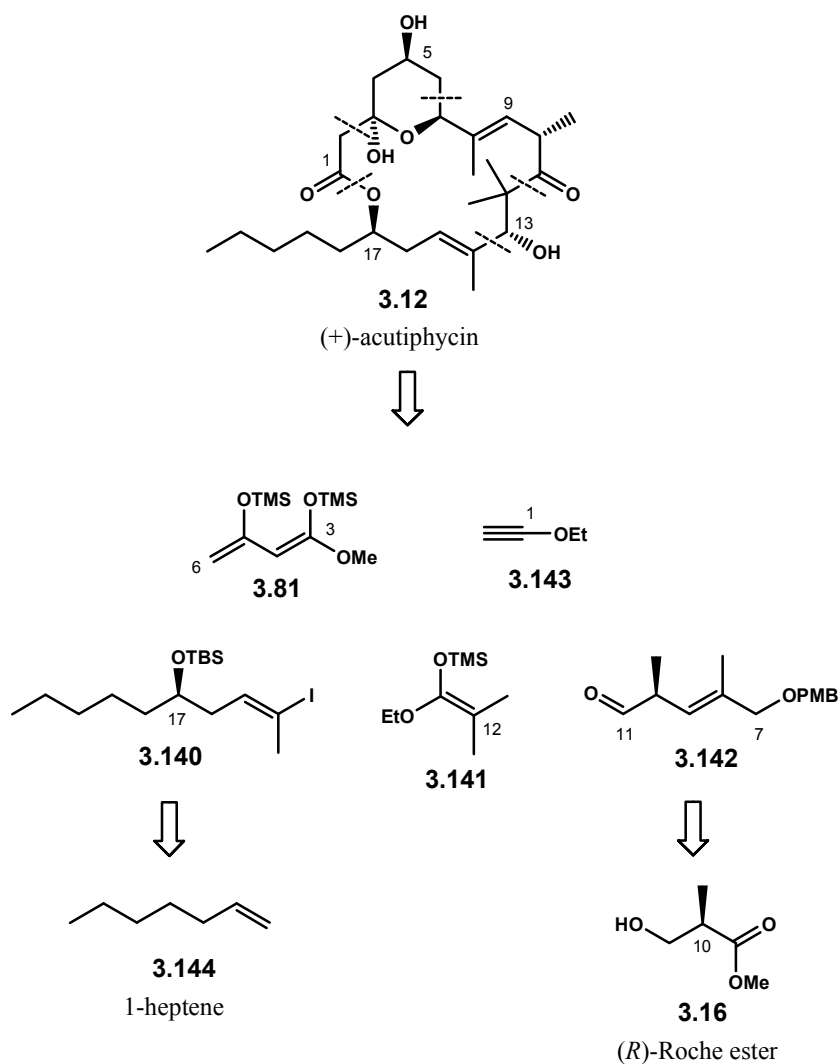
Based on our successful test reactions with benzaldehyde, we concluded that enol silane **3.133** appeared to be reactive enough of a nucleophile for the intended aldol reaction. However, at this point, failures of the above coupling reactions might have been suspiciously caused the poor reactivity between the two fragments presumably due to their steric effect. In order to rule out the unfavorable steric effect that might have been imposed by the methyl pyranoside moiety of the aldehyde, we prepared a truncated aldehyde **3.138** and repeated all of the previously attempted coupling reactions. The results were clear. The coupling of fragments **3.133** and **3.138** also failed under these conditions. From these experiments, we concluded that the source of the problematic steric congestion appeared to be the C10 methyl center, which seemed to have prevented the key nucleophilic addition. Therefore, due to these unforeseeable problems in the coupling strategy, at this point of our study, we had to revise our route to acutiphycin.



**Scheme 3.52**

### 3.9. Revised Strategy

It is clear that the sterically congested C9 – C14 region of acutiphycin presented a significant synthetic predicament; hence, our revised strategy to this macrolide must address this issue early in the synthetic sequence. With our newly redesigned retrosynthesis, we plan to approach acutiphycin in a linear but modular fashion. As shown in Scheme 3.53, acutiphycin would be assembled from five readily accessible synthetic fragments. Vinyl iodide **3.140** and aldehyde **3.142** would be prepared respectively from commercially available 1-heptene **3.144** and (*R*)-Roche ester **3.16**. The problematic connectivity between C11 – C12 would be installed very early by the method of Kiyooka,<sup>199, 201</sup> and finally the late stage macrolactonization would be then affected by a strategy previously demonstrated by Jamison.<sup>179, 180</sup>

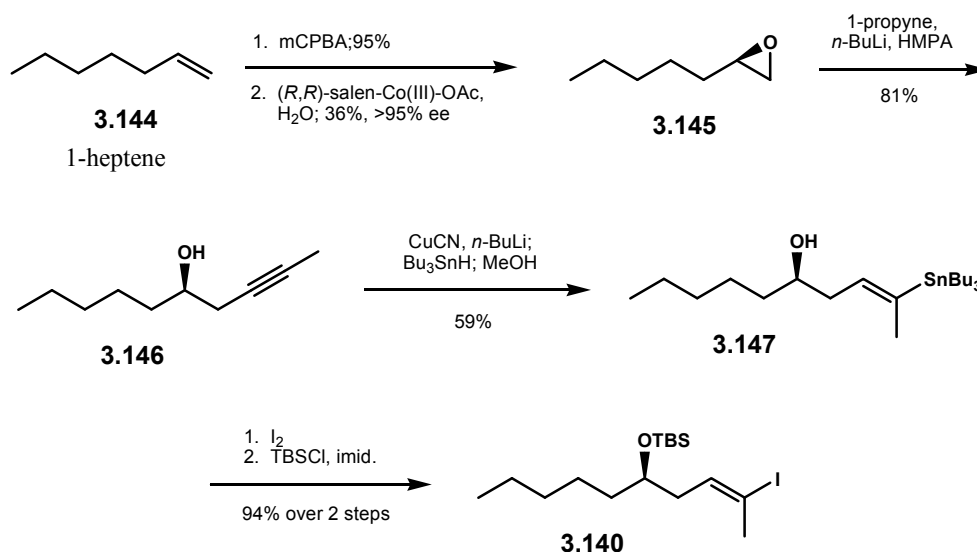


**Scheme 3.53**

### 3.10. Preparation of Vinyl Iodide 3.140

We began our redesigned synthesis to acutiphycin with the preparation of vinyl iodide **3.140** from commercially available 1-heptene **3.144**. Epoxidation followed by Jacobson's hydrolytic kinetic resolution<sup>273</sup> provided enantiomerically enriched epoxide **3.145**. Regioselective addition of 1-lithiopropyne at the sterically less encumbered site then provided alcohol **3.146**. Exposure of the asymmetric internal alkyne to Lipshutz's

hydrostannaylation<sup>274</sup> conditions provided vinylstannane **3.147** in respectable yield with good regioselectivity. Protection of the hydroxy group as a TBSCl ether followed by subsequent treatment with iodine<sup>275</sup> then completed the short synthesis to vinyl iodide **3.140**. We also attempted a direct conversion of the protected terminal alkyne **3.146** to the corresponding vinyl iodide via hydrozirconation – iodine quench;<sup>184, 185</sup> however, this method proved ineffective as the resulting vinyl iodide was obtained as a 1:1 mixture of regioisomers.

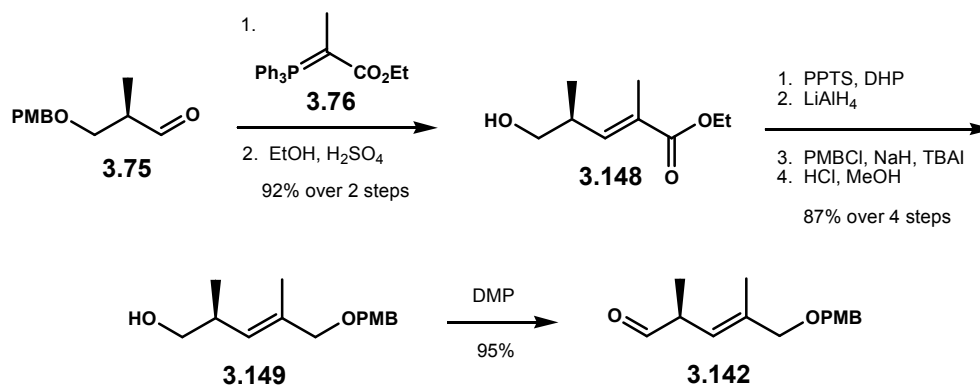


Scheme 3.54

### 3.11. Preparation of Aldehyde **3.142**

For the preparation of aldehyde **3.142**, we began with aldehyde **3.75**, which was readily accessible from (*R*)-Roche ester, in a few steps as demonstrated in Scheme 3.23. Vinylogation of this aldehyde with phosphorane **3.76** followed by removal of the PMB

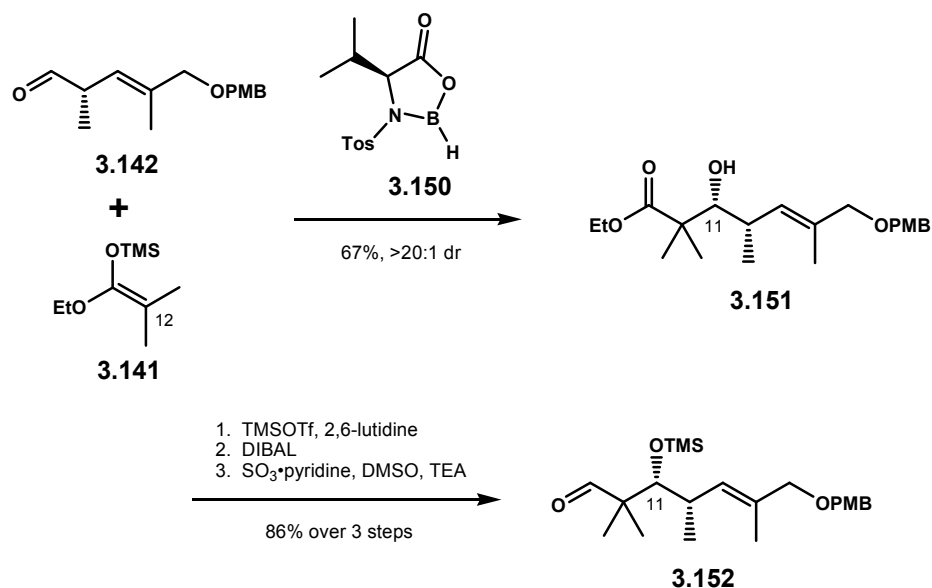
ether under refluxing 1% H<sub>2</sub>SO<sub>4</sub> in ethanol provided hydroxyester **3.148**. Sequential protection of the hydroxy group as a THP ether, ester reduction, conversion of the corresponding primary alcohol to the allylic PMB ether, and removal of the THP group under acidic methanolysis provided alcohol **3.149**. The ensuing oxidation with the Dess-Martin reagent<sup>87</sup> provided the target aldehyde **3.142**, Scheme 3.55.



Scheme 3.55

### 3.12. Construction of C9 – C13 Region

The modular coupling sequence commenced with an aldol reaction using ketene acetal **3.141** as the nucleophilic partner. Under Kiyooka's protocol, which utilized oxazaborolidinone **3.150** as a promoter,<sup>199, 201</sup> the aldol reaction proceeded very smoothly to produce  $\beta$ -hydroxy ester **3.151** in 67% yield as a single diastereomer. This reaction solved the problematic installation of the sterically congested C9 – C13 region of acutiphycin. Subsequent protection of the C11 hydroxyl as a TMS ether, followed by reduction of the ester and reoxidation of the resulting alcohol provided aldehyde **3.152**.



**Scheme 3.56**

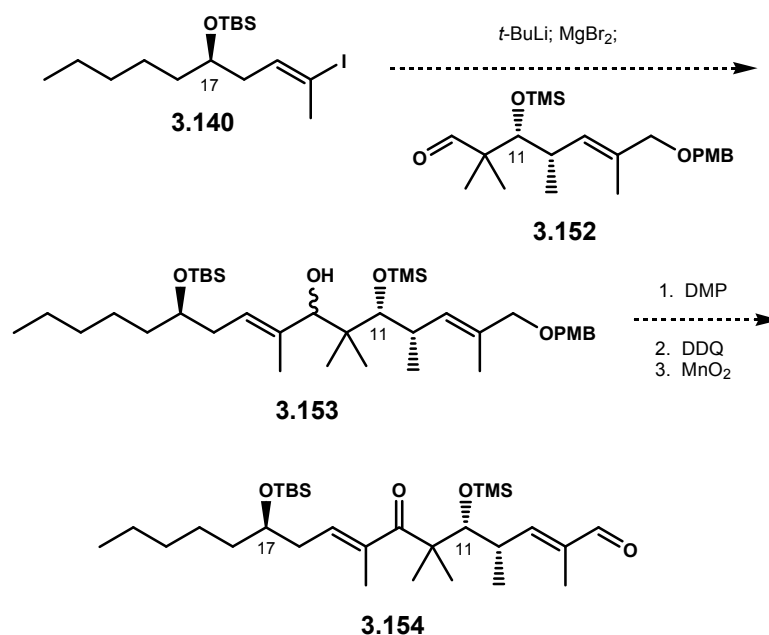
### 3.13. Future Directions

Aldehyde **3.152** represents the current stage of this project, and it is very disappointing that we were not able to complete the total synthesis of acutiphycin at the time when this dissertation was submitted. However, we are confident for its future successful synthesis based on the following proposed two alternative synthetic routes to this macrolide.

#### 3.13.1. Construction of Acutiphycin Carbon Framework

The construction of acutiphycin's carbon framework will continue with an installation of vinyl iodide **3.140** to aldehyde fragment **3.152**. This strategy will involve the formation of a Grignard reagent by exploiting a lithium-iodine exchange followed by

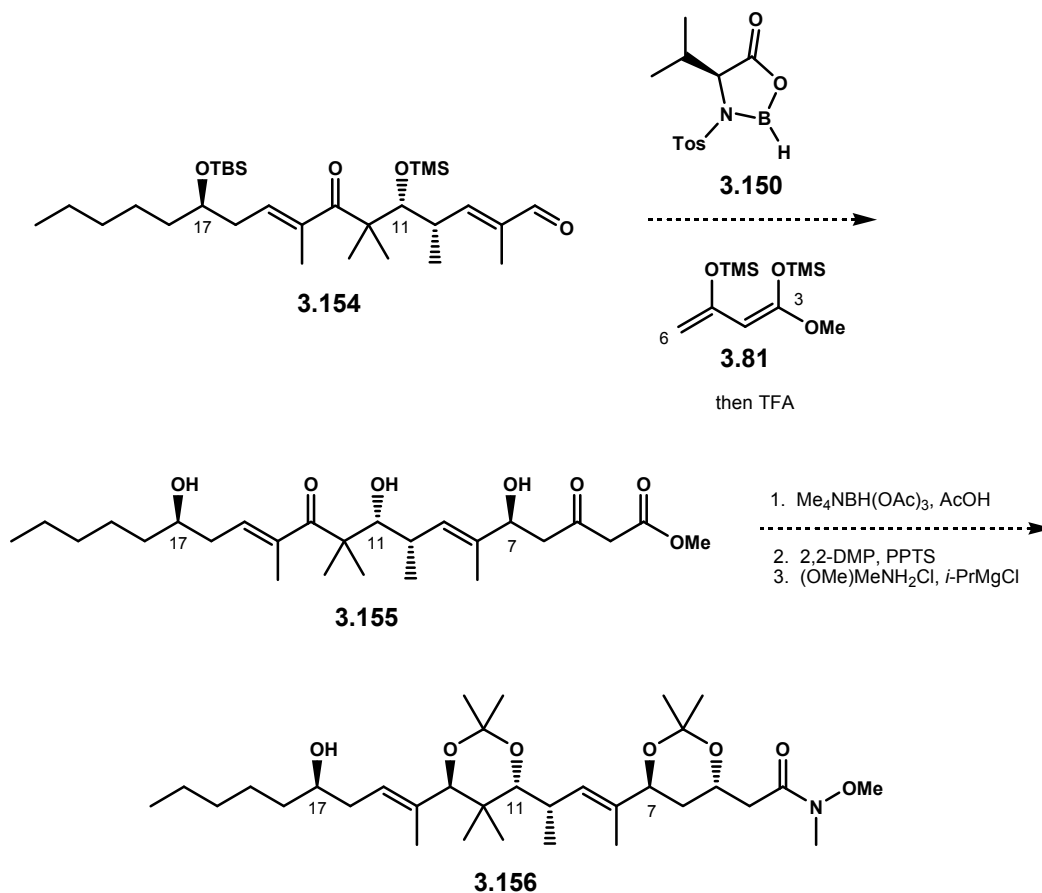
transmetallation. As preceded by the work of Smith,<sup>175, 176</sup> this reaction should give alcohol **3.153**. We do not expect stereoselectivity in this reaction, and the resulting alcohol will subsequently be oxidized to the corresponding ketone. Removal of the PMB ether with DDQ followed by allylic oxidation with MnO<sub>2</sub> should afford  $\alpha,\beta$ -unsaturated aldehyde **3.154**.



**Scheme 3.57**

Aldehyde **3.154** will be subjected to asymmetric aldol reaction with Chan's diene **3.81** to yield  $\delta$ -hydroxy- $\beta$ -ketoester **3.155** upon TFA workup. Although we had previously described the problematic stereoselectivity with this reaction under the method of Soriente in Section 3.7.2.2, the use of oxazaborolidinone promoter **3.150** for such a reaction is preceded and needed to be explored with our substrate.<sup>177, 178</sup> Triol **3.155** will be then exposed to the Evan's 1,3-*anti* reduction, and this should afford the

corresponding pentaol.<sup>72</sup> Protection of the C5 – C7 and C11 – C13 *anti* diols as acetonides followed by conversion of the methyl ester to the Weinreb amide<sup>260</sup> will complete the sequence for C3 – C22 segment of acutiphycin **3.156**, Scheme 3.58.



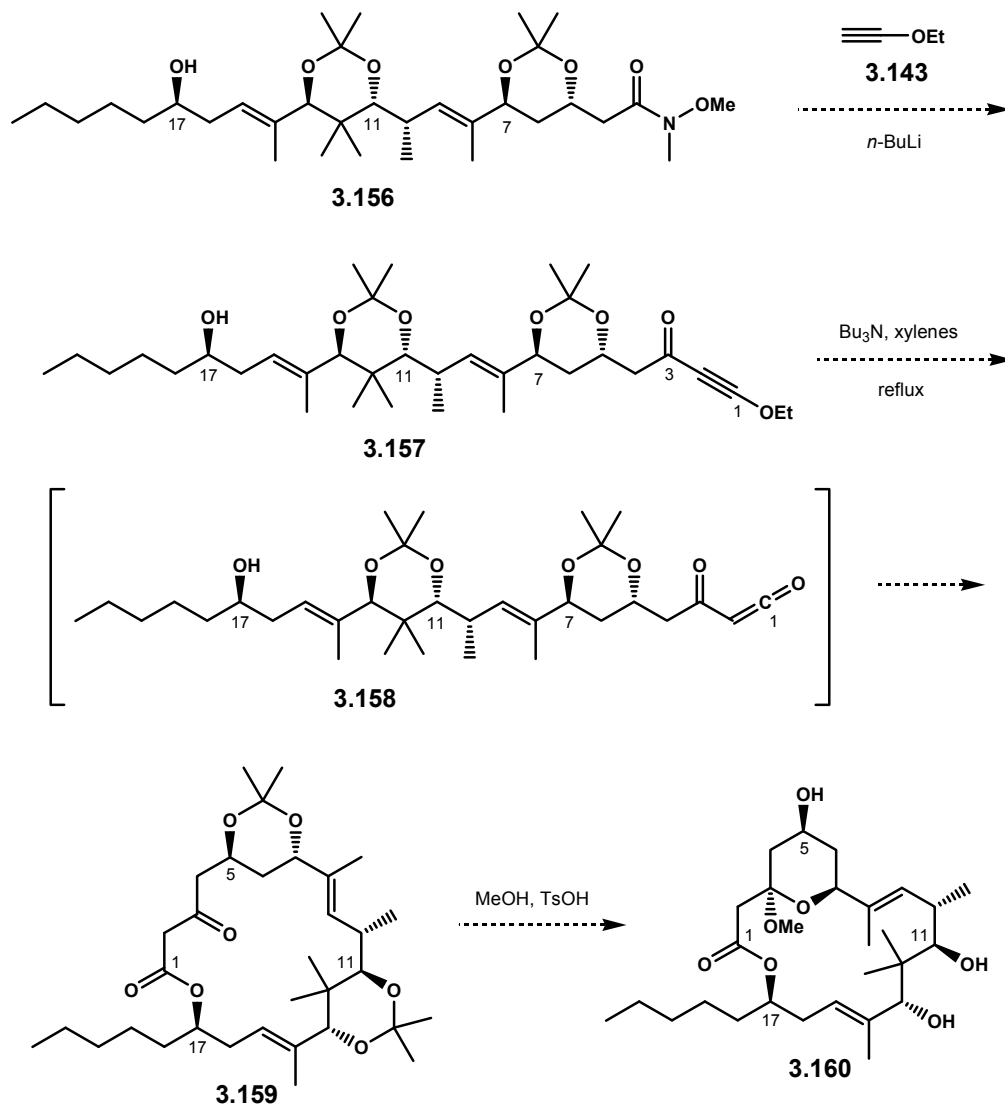
Scheme 3.58

### 3.13.2. Jamison Macrolactonization Strategy

Advanced intermediate **3.156** will be subjected to the key macrolactonization by utilizing a strategy previously demonstrated by Jamison. Addition of the lithium salt of ethoxyethyne anion to the Weinreb amide should install ketone **3.15**. The ensuing



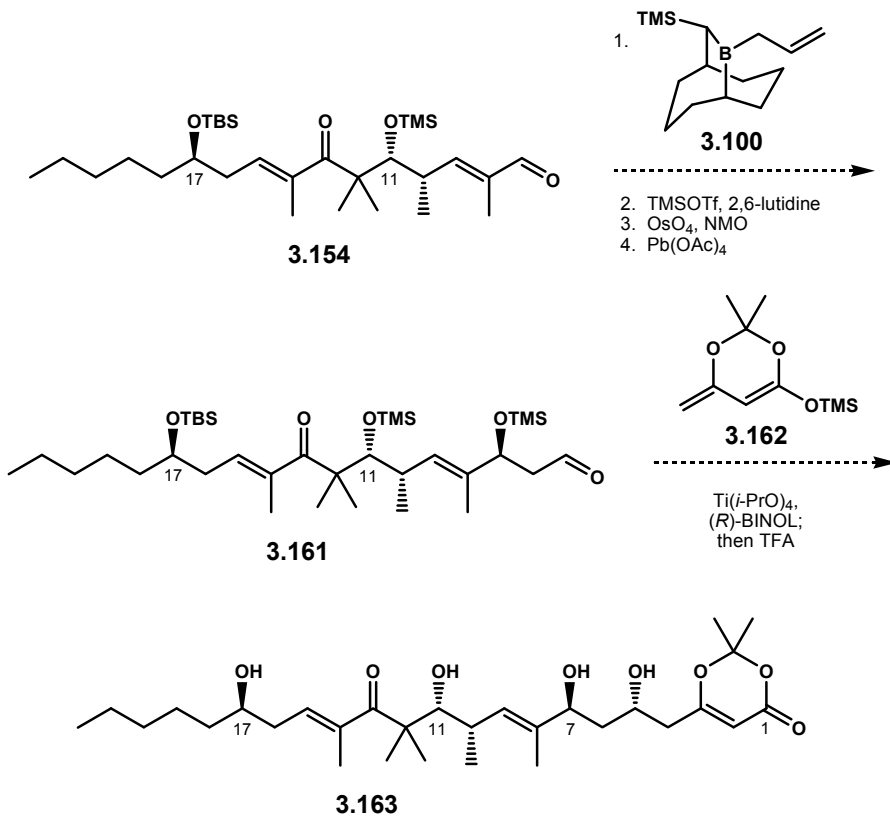
thermal retro-ene process should give ketene **3.158**, and subsequent *in situ* intramolecular trapping with remote C7 hydroxy group will afford macrolactone **3.159**.<sup>179, 180</sup> Removal of the acetonides followed by spontaneous cyclization to methyl pyranoside **3.160** will be affected by PPTS in methanol.



Scheme 3.59

### 3.13.3. Boeckman Macrolactonization Strategy

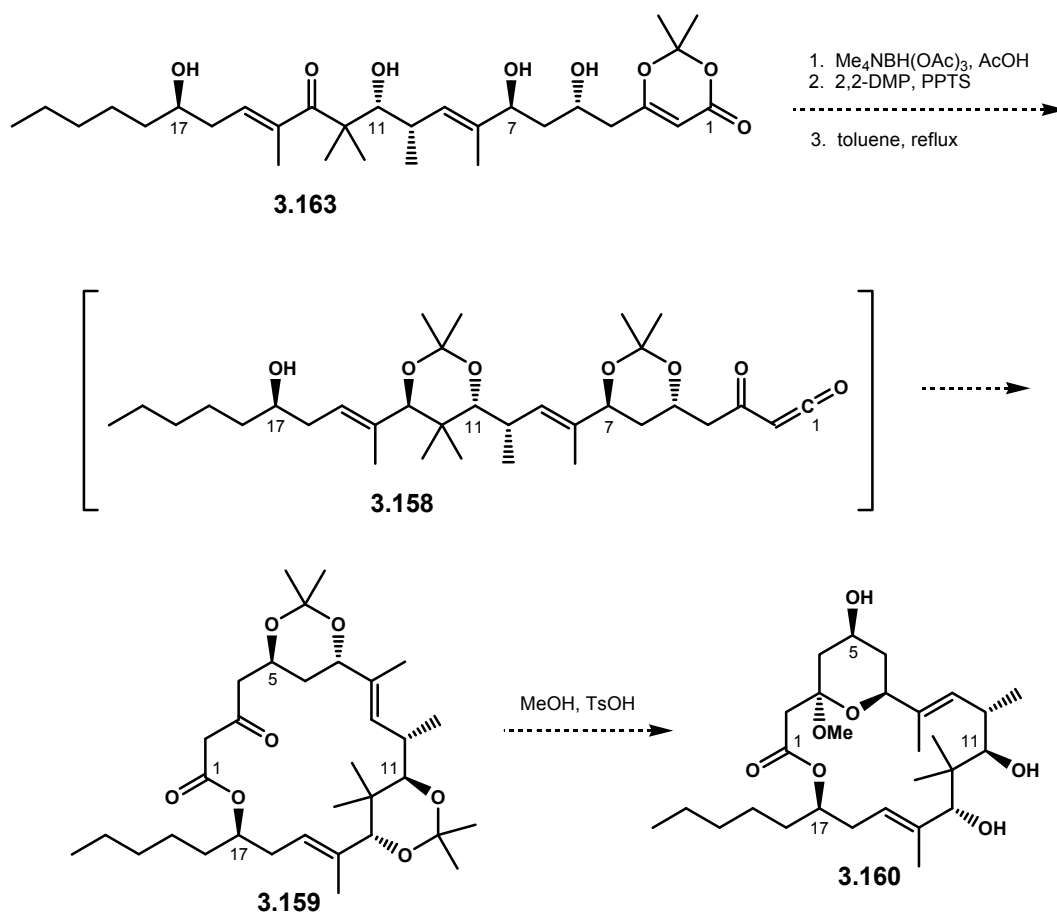
Alternatively, the macrolactonization strategy that employs ketene as a reactive intermediate can also be envisioned using a methodology developed by Boeckman and co-workers. The utilization of dioxinone functionality as shown in **3.163** as the macrolactonization precursor was demonstrated in their total synthesis of (-)-kromycin.<sup>276</sup> This strategy has also been further explored and optimized by Chen<sup>277</sup> and further exploited by Trost and co-workers in their total synthesis of cytotoxic macrolide callipeltosides.<sup>32, 33</sup>



Scheme 3.60

As shown in Scheme 3.60, to construct this dioxinone precursor, we will expose aldehyde **3.154** to asymmetric allylation with Soderquist's reagent **3.100**.<sup>261</sup> The ensuing protection and oxidative cleavage then should install the requisite acetate aldol adduct **3.161**. Treatment of this aldehyde in asymmetric Mukaiyama aldol reaction with diene **3.162** using the method of Soriente should readily afford the target dioxanone **3.163**.<sup>60, 256, 257</sup>

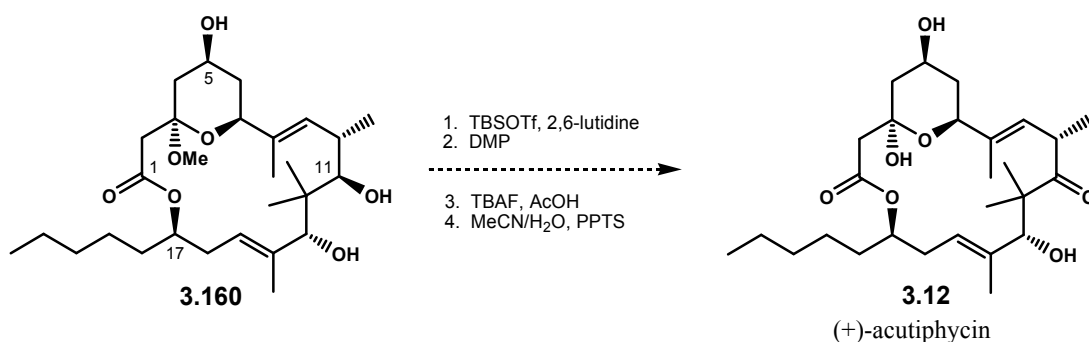
The subsequent reduction of C13 ketone in an *anti* fashion by the method of Evans<sup>72</sup> followed exposure of the corresponding pentaol with 2,2-DMP in the presence of PPTS should protect C5 – C7 and C11 – C13 diols as acetonides. The key macrolactonization will be then realized by exposing the material under refluxing toluene in which the dioxinone moiety will undergo a thermal retro-hetero-Diels-Alder reaction to give ketene **3.158**.<sup>276, 277</sup> This reactive intermediate should be readily trapped intramolecularly by C17 hydroxy group to give macrolactone **3.159**. Acidic methanolysis of this macrolactone will remove the acetonides and at the same time construct the requisite methyl pyranoside **3.160**, Scheme 3.61.



**Scheme 3.61**

#### 3.13.4. Endgame Strategy

The straightforward endgame strategy to acutiphycin will commence with selective protection of the sterically less encumbered C5 and C9 hydroxy groups as TBS ethers. The remaining C11 hydroxyl will be then oxidized with Dess-Martin reagent<sup>87</sup> to the requisite ketone functionality. Removal of the TBS ethers followed by acidic hydrolysis of the methyl pyranoside to the corresponding hemiketalpyran should finish the total synthesis of acutiphycin, Scheme 3.62.



**Scheme 3.62**

### 3.14. Conclusion

This chapter details synthetic studies of cytotoxic macrolide (+)-acutiphycin. These investigations began with a development of synthetic methodology for the production of acetate aldol adduct highlighted by the Beak's homoaldol reaction using auxiliary **3.21** and **3.51** and their subsequent ozonolysis study. Eventually, the construction of C12 – C22 fragment **3.13** was accomplished in just a few steps by employing a vinylogous Mukaiyama aldol reaction developed by Kobayashi. This strategy exploited a remote 1,7-asymmetric induction effect that directed installation of the requisite stereochemistry. For the construction of C1 – C11 fragment **3.14**, two alternative strategies were presented; one of which entailed a detailed analysis of the Evans' polar model with Chan's diene as the nucleophilic partner.

Unfortunately, the coupling of fragments **3.13** and **3.14** was not successful. As suggested by experimental evidence, the reduced reactivity of enol silane **3.133** coupled with the steric congestion imposed by the C10 methyl center in aldehyde **3.14** practically shut down the intended aldol reaction. For this reason, we envisioned a revised strategy

to acutiphycin that involved early construction of the problematic, sterically congested C9 – C14 region. This revision also included underutilized ketene-mediated macrolactonization originated from two alternative advanced intermediate **3.157** or **3.163**.

## CHAPTER FOUR

### PELORUSIDE A AND ELECTROPHILE-INDUCED ETHER TRANSFER

#### 4.1. Purpose

The purpose of this chapter is to detail literature reviews pertinent to a classic challenge in the construction of 1,3-*syn* diol monoether, a common oxygenation pattern in polyketide natural products, such as peloruside A. The chapter will then continue with a description of our novel methodology, electrophile-induced ether transfer, which readily solves this problem by installing such functionality in one step from a simple homoallylic alkoxymethyl ether. Detailed discussions on the reaction mechanism and the scope of reactions will also be presented.

#### 4.2. Peloruside A

As an integral part of our research program, our group has been investigating the role of highly cytotoxic polyketide natural products as potential anticancer drug candidates through systematic studies toward their total syntheses, thorough biological

evaluations, complete structure-activity-relationship study, and detailed conformational analyses. A particular polyketide that has recently caught our interest is peloruside A **4.1**.

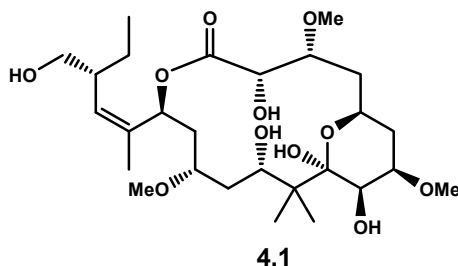


**Figure 4.1**

In 2000, Northcote and co-workers reported the isolation of peloruside A from a marine sponge, *Mycale* sp., collected from Pelorus Sound on the north coast of the South Island, New Zealand.<sup>278</sup> A further biological study of this natural product revealed that peloruside A was a potent cytotoxic agent with the mode of action of microtubules-stabilizer like that of paclitaxel.<sup>279</sup> However, it was later established that peloruside A and paclitaxel in fact did not bind to the microtubules at the same site.<sup>280, 281</sup> Due to this unexpected mode of action, peloruside A has attracted significant interests from the synthetic community. There are three total syntheses of peloruside A completed up to date;<sup>282, 283</sup> one of which was reported by our group in 2005.<sup>228, 284</sup> In addition, numerous efforts towards the total synthesis of this molecule have also been documented.<sup>285-293</sup>

This chapter would not detail our successful approach towards the total synthesis of peloruside A, but we would rather describe a significant synthetic challenge that arose from the structural complexity of the natural product itself and the solution that we



provided in the form of a novel synthetic methodology development, the electrophile-induced ether transfer reaction.

#### **4.2.1. Peloruside A as a Polyketide Natural Product**

When one considers the seco-acid form of peloruside A as depicted in structure **4.2**, one may immediately recognize the unique characteristic of any polyketide natural products: the repeating patterns of acetate and propionate subunits specifically with oxygenation at odd-numbered carbons and possible substitution at even-numbered carbons, Figure 4.2. The origin of this distinctive pattern can be readily explained from the manner in which polyketides are synthesized by the producing microorganisms through the complex machinery of the polyketide synthase (PKS) enzyme. It is well understood that the acetate and propionate subunits are biosynthetically installed through a Claisen condensation reaction from respectively acetyl or malonyl Co-A and methylmalonyl malonyl Co-A. There are several known domains in PKS: acyltransferase, acyl carrier protein, ketosynthase, ketoreductase, dehydratase, enoylreductase, and thioesterase. These domains are responsible for the sequential chain elongation and termination, thus providing the structure of polyketides.

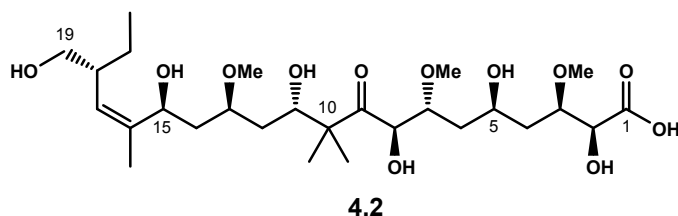


**Figure 4.2**

Other functionalization, such as oxygenation at even-numbered carbons at C2 and C8, is most likely a result of post-PKS oxidation. In addition, the *gem*-dimethyl group at C10 is unlikely to have been produced by two successive methylations, but instead, it has been proposed that one of the methyl groups is derived from the typical propionate extender subunit, whereas the second methyl is introduced via *C*-methyl transferase domain embedded within the PKS sequence.<sup>294</sup> Likewise, the methyl ether functionality at C3, C7, and C13 carbons may have been integrated in the natural product via two possible pathways: *O*-methyl transferase domain or a methoxymalonyl extender subunit.

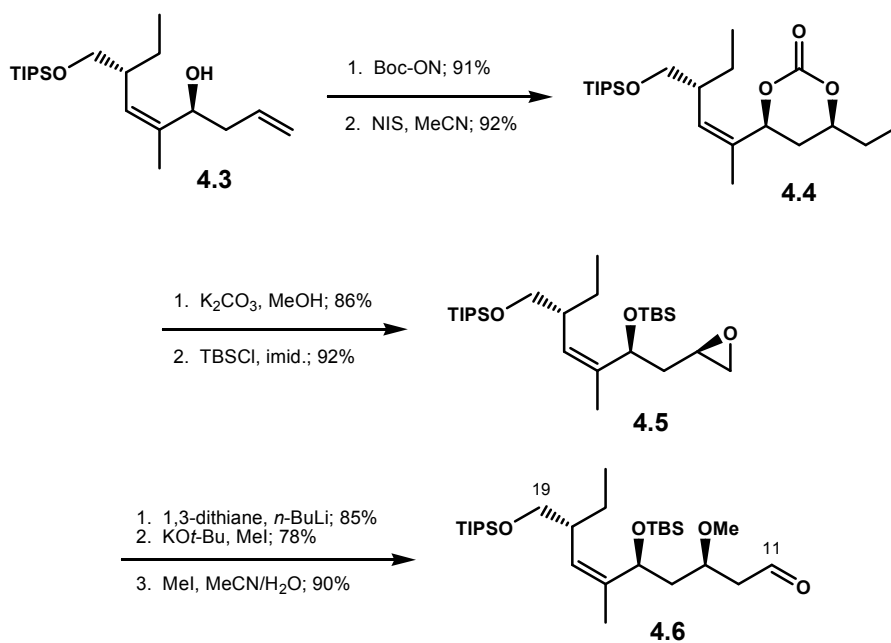
#### **4.3. Peloruside A and 1,3-*syn* Diol Monoether**

A particularly interesting structural feature unique to peloruside A is the 1,3-*syn* diol monoether functionality which resides in the C3 – C5 and C13 – C15 segments. Although 1,3-*syn* diol monoether seems to be a relatively simple functionality to construct, current synthetic methods do not support the stereoselectivity and efficiency of the evolved proteins. In order to access this 1,3-*syn* diol core, several discreet steps must be executed. More importantly, the subsequent mono methylation must be selective, and thus laborious protecting group manipulations become unavoidable.

This significant problem clearly emerges in several published synthetic works towards peloruside A. The following sections describes several established strategies which successfully accessed the key 1,3-*syn* diol monoether functionality en route to peloruside A.

#### 4.3.1. Carbonate Cyclization

In their work in peloruside A, Taylor and Jin reported an efficient generation of the C11 – C19 fragment highlighted by an electrophilic carbonate cyclization reaction which successfully installed the 1,3-*syn* diol monoether core.<sup>284</sup> As shown in Scheme 4.1, protection of homoallylic alcohol **4.3** as a *tert*-butyl carbonate followed by exposure to NIS produced cyclic carbonate **4.4**.<sup>295-297</sup> Basic methanolysis and TBS protection then yielded epoxy ether **4.5**. Addition of dithiane anion to **4.5** fragmented the epoxide at the less sterically hindered carbon, and subsequent methylation and hydrolysis thus afforded C11 – C19 fragment **4.6**.



**Scheme 4.1**

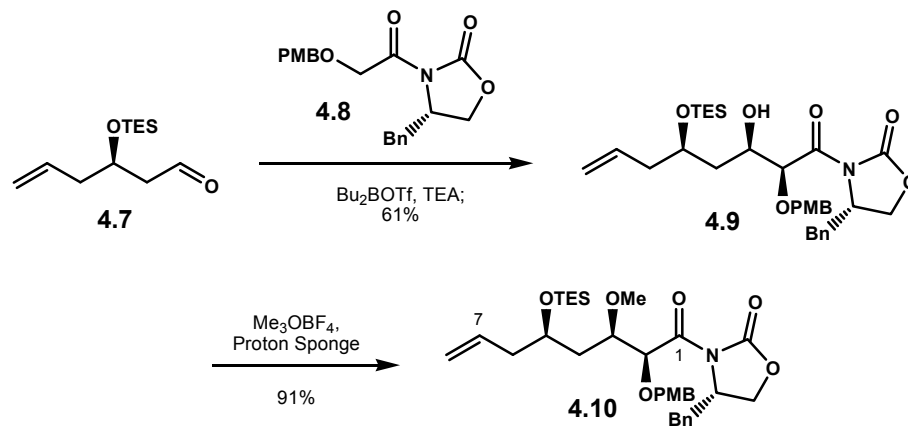
### 4.3.2. Chiral Auxiliary Promoted Aldol Reactions

The use of chiral auxiliaries has been documented in efforts towards the total synthesis of peloruside A. These auxiliaries are particularly used in an aldol reaction typically with a protected  $\beta$ -hydroxy aldehyde as the coupling partner. The chiral auxiliary will dictate stereochemistry such that the newly generated secondary alcohol is *syn* to the  $\beta$ -hydroxy group.

#### 4.3.2.1. Taylor's Approach

The utilization of such a strategy was demonstrated by the work of Taylor and Jin.<sup>228</sup> As shown in Scheme 4.2, the reaction of TES-protected  $\beta$ -hydroxy aldehyde **4.7**

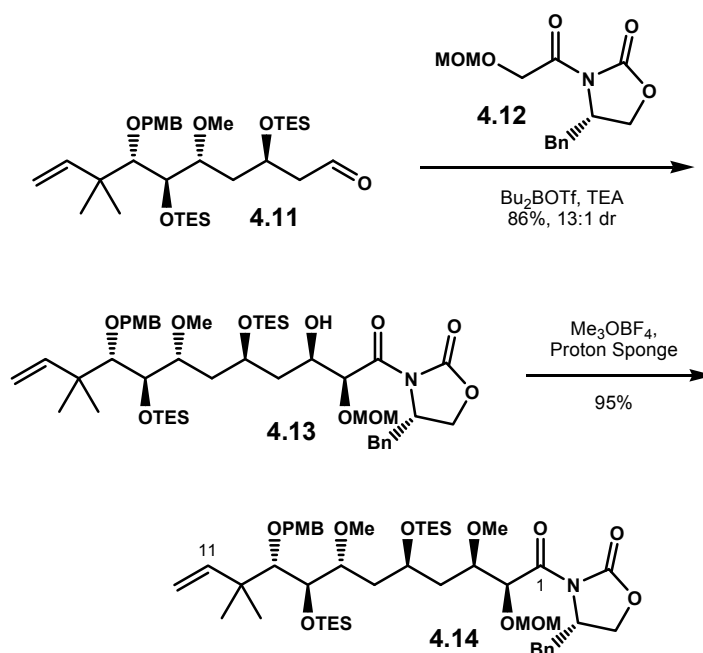
with oxazolidinone **4.8** upon enolization with dibutylboron triflate and triethylamine afforded aldol adduct **4.9**.<sup>298, 299</sup> The newly generated stereocenter at C3 was *syn* to that of C5 as controlled by the chiral auxiliary. Subsequent *O*-methylation<sup>92</sup> thus produced the 1,3-*syn* diol monoether **4.10** which represented the C1 – C7 fragment of peloruside A.



Scheme 4.2

#### 4.3.2.2. Roush's Approach

The work of Roush and co-workers in their total synthesis of peloruside A also exemplified the use of chiral auxiliary to access the 1,3-*syn* diol monoether functionality.<sup>286</sup> Advanced aldehyde **4.11** was coupled with oxazolidinone **4.12** which proceeded very smoothly to produce aldol **4.13** under the Evans enolization conditions.<sup>300</sup> Once again, this reaction established the requisite *syn* C3 – C5 stereochemistry. Subsequent *O*-methylation using Meerwein's reagent<sup>92</sup> then produced C1 – C11 fragment **4.14**, Scheme 4.3.



**Scheme 4.3**

### 4.3.3. Chiral Reagents

In recent documents detailing synthetic efforts towards peloruside A, chiral reagents have been employed to install the 1,3-*syn* diol monoether functionality. Such reagents included Brown's allyl(Ipc)<sub>2</sub>borane and the Corey-Bakshi-Shibata (CBS) oxazaborolidine for the asymmetric allylation and ketone reduction, respectively.

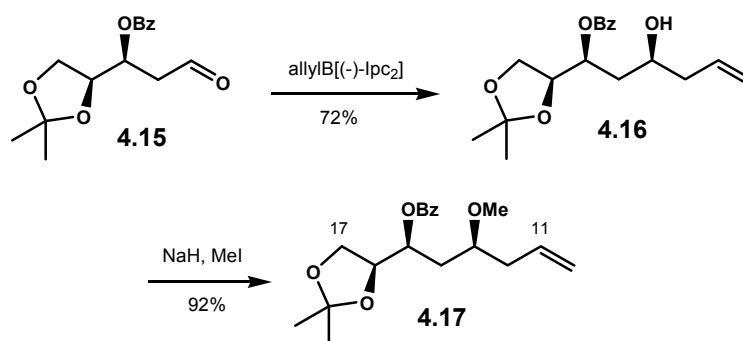
#### 4.3.3.1. Brown's Allyl(Ipc)<sub>2</sub>borane

The highly stereoselective installation of homoallylic alcohol mediated by chiral reagents, particularly the Brown's (Ipc)<sub>2</sub>allylborane reagents, has arguably evolved as one of the most important tools in asymmetric synthesis. The use of this reagent in the

construction of the 1,3-*syn* diol monoether functionality towards the total synthesis of peloruside A has been reported independently by Zhou<sup>290</sup> and De Brabander.<sup>282</sup>

#### 4.3.3.1.1. Zhou's Approach

Zhou reported a reaction of  $[(-)\text{-Ipc}]_2\text{allylborane}$  with  $\beta$ -benzoate aldehyde **4.15** which afforded homoallylic alcohol **4.16** containing the 1,3-*syn*-diol core as controlled by the chiral allylborane reagent.<sup>142, 290</sup> Subsequent strong base-induced methylation thus provided C11 – C17 fragment **4.17**, Scheme 4.4.

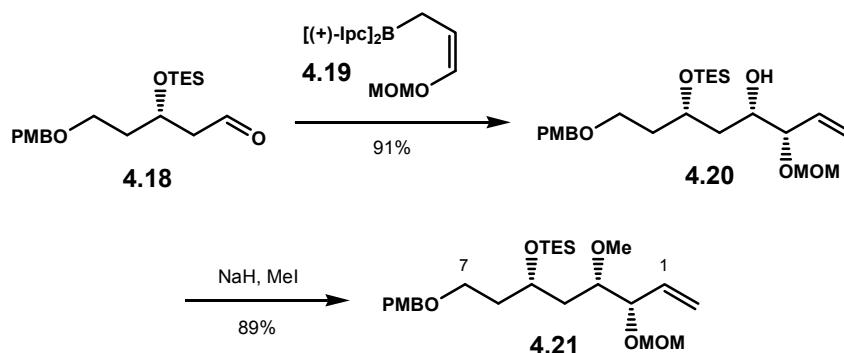


Scheme 4.4

#### 4.3.3.1.2. De Brabander's Approach

Similarly, the De Brabander's total synthesis to peloruside A also utilized the Brown allylation method to construct their C1 – C7 fragment **4.21**.<sup>282</sup> This route included a reaction of TES-protected  $\beta$ -hydroxy aldehyde **4.18** with chiral *Z*-alkoxyallylborane

**4.19** that yielded homoallylic alcohol **4.20**.<sup>301</sup> *O*-Methylation of the resulting hydroxy group provided 1,3-*syn* diol monoether fragment **4.21**, Scheme 4.5.

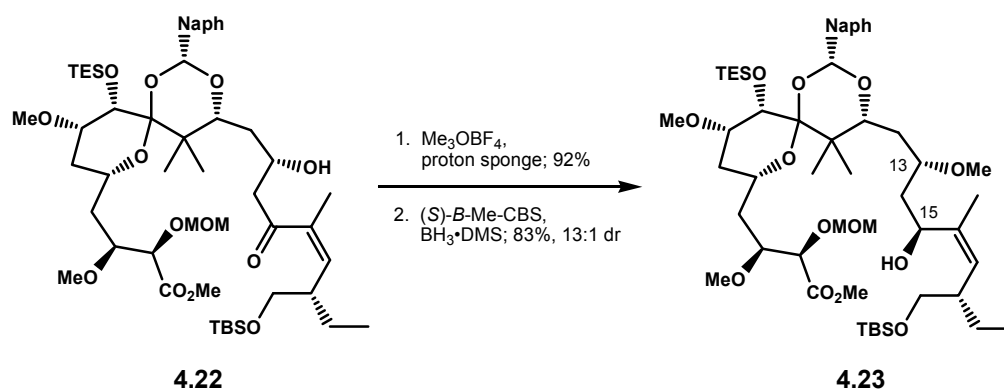


**Scheme 4.5**

#### 4.3.3.2. Ketone Reduction with the CBS Reagent

In order to install the C13 – C15 *syn* diol core, De Brabander utilized the CBS reaction to asymmetrically reduce a  $\beta$ -methoxy-ketone to its corresponding 1,3-*syn* diol monoether. As shown in Scheme 4.6, starting with advanced  $\beta$ -hydroxy ketone **4.22**, exposure of this compound upon methylation to excess CBS reagent provided **4.23** in 83% yield with the diastereomeric ratio of 13:1 favoring the desired 1,3-*syn* diol monoether.<sup>302</sup>





**Scheme 4.6**

#### 4.3.4. Substrate Controlled

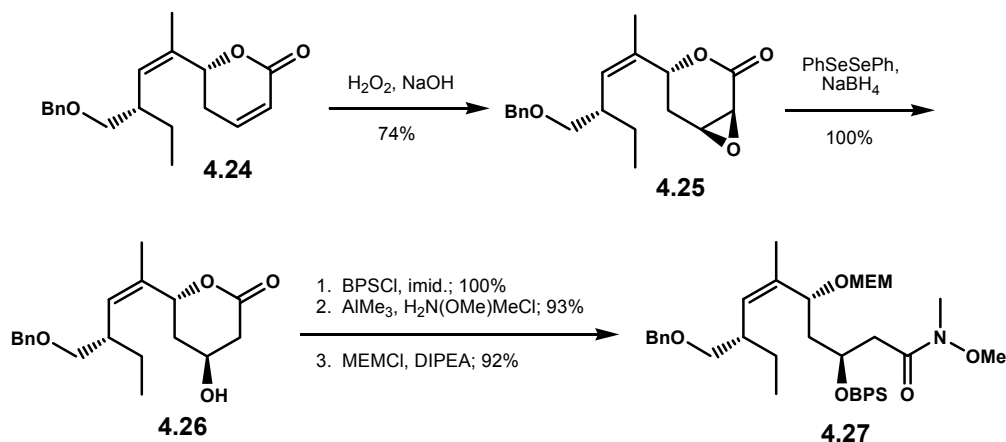
A stereocenter that is already present in the starting material could be potentially utilized to direct a generation of another stereocenter in a selective fashion. This basic concept has been successfully implemented in the installation of 1,3-*syn* diol monoether functionality in peloruside A, exemplified by the works of Ghosh,<sup>291</sup> Pagenkopf,<sup>288</sup> Gurjar,<sup>289</sup> and Paterson.<sup>293</sup>

##### 4.3.4.1. Epoxidation – Ring Opening

In his work towards peloruside A,<sup>291</sup> Ghosh utilized a synthetic scheme which accessed the C15 – C17 *syn* diol monoether core via substrate-controlled asymmetric epoxidation and ring opening reactions. As described in Scheme 4.7, stereoselective epoxidation of  $\delta$ -lactone **4.24** with hydrogen peroxide in an alkaline solution furnished epoxide **4.25** in 74% yield as a single diastereomer. Treatment of the resulting epoxide with diphenyldiselenide and sodium borohydride afforded exclusively  $\beta$ -hydroxy lactone

**4.26** which now contained the desired C15 – C17 *syn* diol stereochemical relationship.<sup>303</sup>

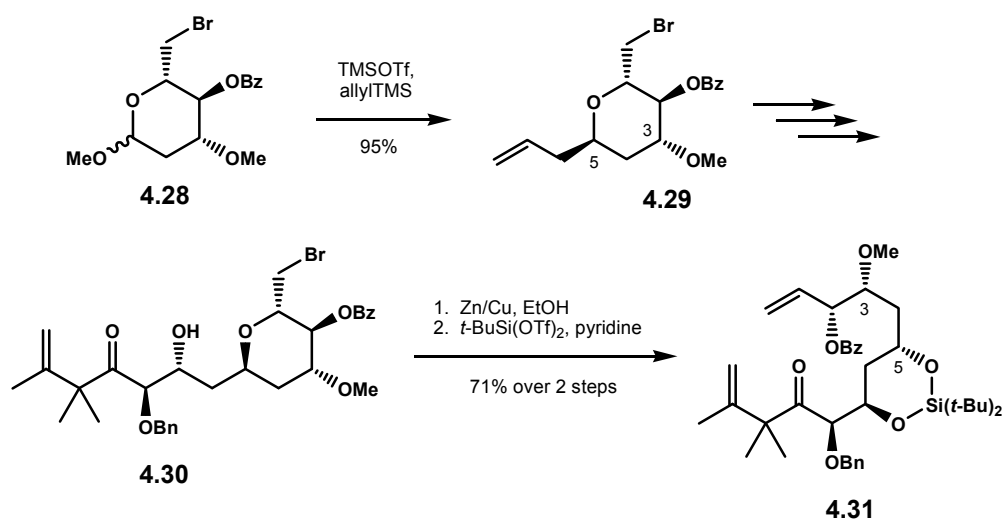
Subsequent protection of the alcohol as a BPS ether, followed by conversion of the lactone to the Weinreb amide<sup>260</sup> and protection of the newly exposed alcohol as a MEM ether produced orthogonally protected 1,3-*syn* diol **4.27**.



**Scheme 4.7**

#### 4.3.4.2. Allylation – Tetrahydropyran Ring Opening

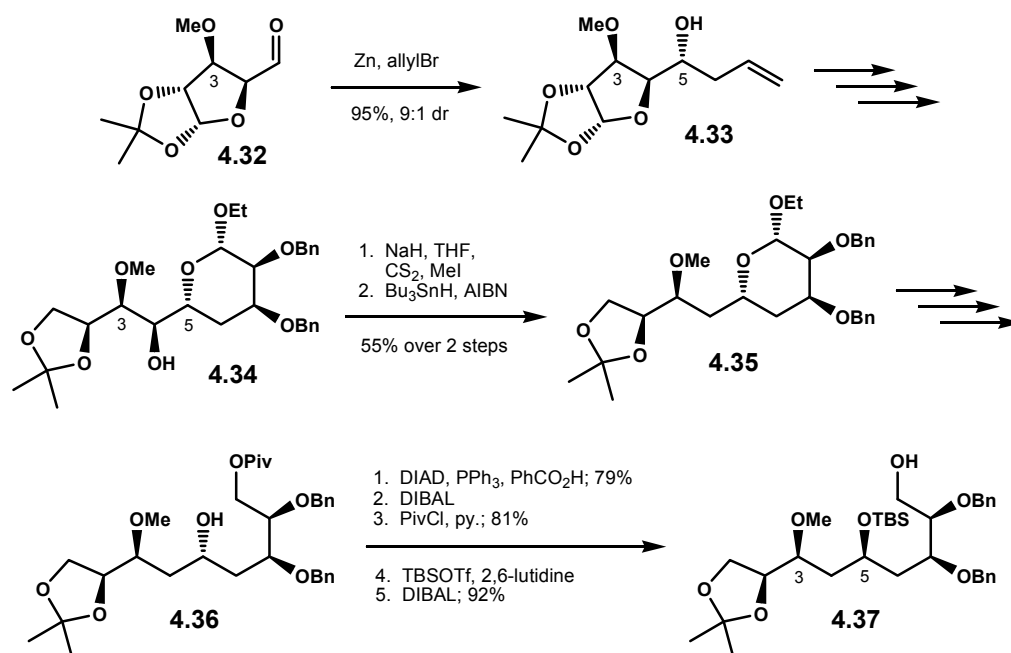
In 2004, Pagenkopf and co-workers reported their elegant synthetic route towards the preparation of advanced fragment **4.31**.<sup>288</sup> This work was highlighted by stereoselective allylation of methyl pyranoside **4.28** mediated by TMSOTf which set up the C3 – C5 *syn* stereochemistry shown in stereochemically rich tetrahydropyran **4.29**.<sup>304</sup> Further synthetic manipulations led to tetrahydropyran **4.30**, and subsequent Vasella ring opening<sup>305</sup> and protection yielded C1 – C12 fragment **4.31**, Scheme 4.8.



Scheme 4.8

#### 4.3.4.3. Mitsunobu Inversion

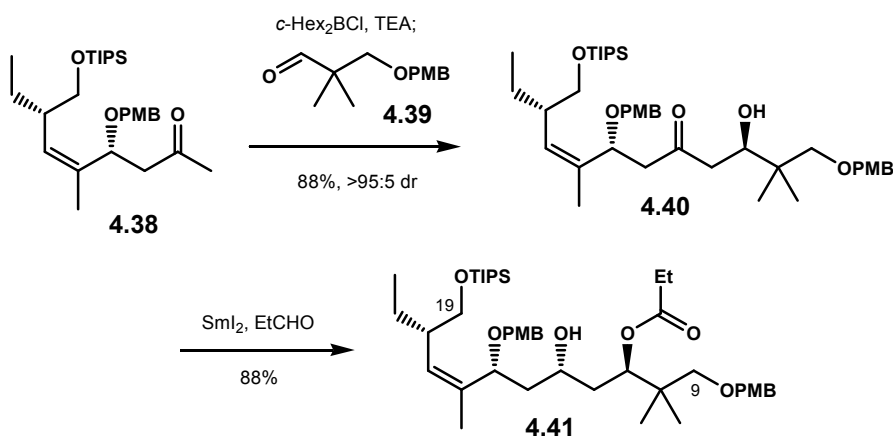
Gurjar and co-workers reported their work in peloruside A in 2004.<sup>289</sup> As shown in Scheme 4.9, their synthetic endeavor was approached from the chiral pool method that allowed installation of the stereogenic centers within fragment **4.37** as directed by the preexisting stereocenters contained within aldehyde **4.32**. Unfortunately, there are several drawbacks associated with this strategy. First, the synthetic sequence to their final target fragment was extremely laborious; second, Barton deoxygenation<sup>306</sup> (**4.34** → **4.35**) and Mitsunobu inversion<sup>307</sup> (**4.36** → **4.37**) became necessary to install the required 1,3-*syn* diol monoether moiety; and third, only the unnatural enantiomer of peloruside A was accessible due to the commercially available enantiomer of the corresponding sugar from which aldehyde **4.32** was prepared.



**Scheme 4.9**

#### 4.3.4.4. Evans-Tishchenko Reduction

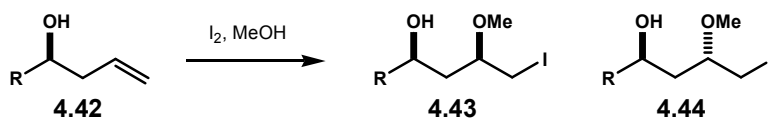
In one of the earliest published works towards the total synthesis of peloruside A, Ian Paterson and co-workers utilized their remote 1,5-asymmetric induction aldol methodology to construct the C9 – C19 fragment **4.41**.<sup>157, 158</sup> This methodology involved addition of boron enolate of ketone **4.38** to prochiral aldehyde **4.39** which then resulted in the generation of 1,5-*anti* aldol adduct **4.40** in excellent yield and stereoselectivity. The ketone functionality was sequentially reduced under the Evans-Tishchenko conditions to afford alcohol **4.41**.<sup>91</sup> The newly generated alcohol C13 carbon center now contained the required 1,3-*syn* diol C13 – C15 core of peloruside A, Scheme 4.10. Additionally, C11 hydroxy group was readily protected as a propionate ester with this approach, which allowed differentiation of this orthogonally protected tetraol system.



**Scheme 4.10**

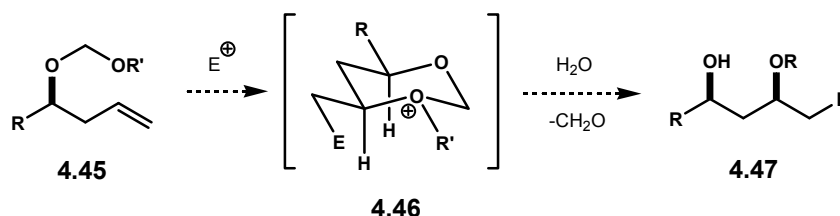
#### 4.4. Electrophile-Induced Ether Transfer

The examples as depicted in Schemes 4.1 – 4.10 are of clear precedents which support the need for the development of a more efficient method in generating 1,3-*syn* diol monoether functionality. One blatant solution to this problem can be imagined through an iodoetherification reaction starting with homoallylic alcohol **4.42** and methanol as the coupling partner, Scheme 4.11. However, this intermolecular process will not be stereoselective as diastereomeric products **4.43** and **4.44** will most likely arise from this simple reaction.



**Scheme 4.11**

However, inspired by our previous successful utilization of Smith's carbonate cyclization as shown in Scheme 4.1, we envision that the methyl ether functionality may be installed across the double bond in a stereo- and regioselective fashion via an intramolecular delivery as directed by the stereochemistry of homoallylic alcohol center. This general concept is depicted in Scheme 4.12. We propose that activation of homoallylic alkoxyethyl ether **4.45** under an electrophilic condition should lead to the generation of six-membered oxonium ion intermediate **4.46** in a chair-like fashion, thus leading to the 1,3-*syn* stereochemical relationship. Subsequent hydrolysis of this intermediate should then unmask the target 1,3-*syn* diol monoether functionality **4.47** in just one step from **4.45**. We termed this overall process as the *Electrophile-Induced Ether Transfer* reaction.<sup>236</sup>

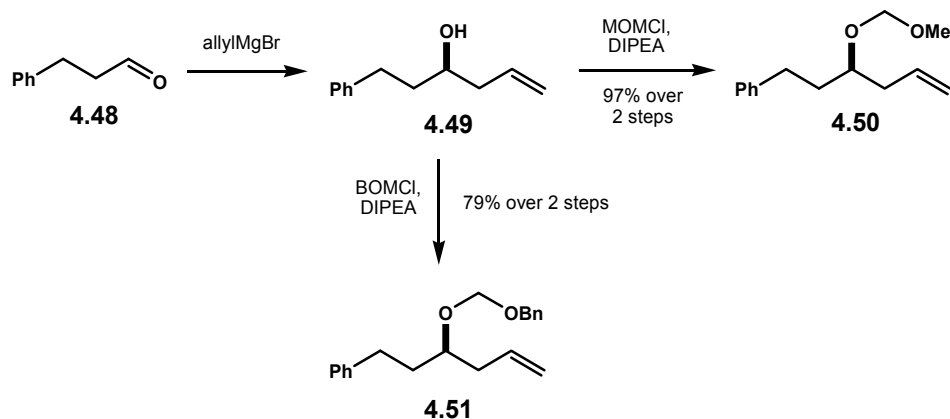


**Scheme 4.12**

#### 4.4.1. The Proof of Concept

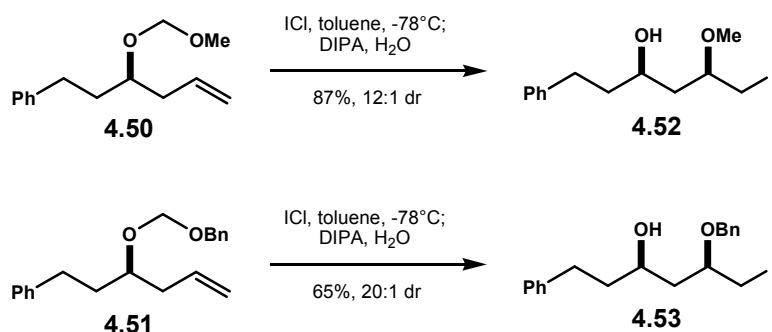
We first investigated this methodology quest with model substrates methoxymethyl ether (MOM) and benzyloxymethyl ether (BOM) protected homoallylic alcohol **4.50** and **4.51** respectively. These materials were readily accessible as a racemic mixture in just two simple steps: allylation of hydrocinnamaldehyde **4.48** followed by

subsequent protection of homoallylic alcohol **4.49** independently with MOMCl or BOMCl in the presence of DIPEA.



**Scheme 4.13**

With the materials in hand, we then focused our attention to screen the proper reaction conditions. Upon comprehensive optimizations, Kai Liu, a co-worker in our laboratories, found that treatment of homoallylic methoxymethyl ether **4.50** with commercially available iodine monochloride solution at  $-78^{\circ}\text{C}$  in toluene for 10 minutes followed by basic aqueous workup remarkably produced the desired 1,3-*syn* diol monoether **4.52** in 87% yield with diastereoselectivity of 12:1. Similarly, when homoallylic benzyloxymethyl ether **4.51** was subjected under identical reaction conditions, 1,3-*syn* diol monoether **4.53** was produced in 65% yield with diastereomeric ratio of 20:1.<sup>236</sup> The capability of the benzyloxymethyl ether to undergo ether transfer significantly expanded the scope of the methodology as this resulting benzyl ether served as an orthogonally protected 1,3-*syn* diol and may be removed under reductive conditions.



**Scheme 4.14**

#### 4.4.2. Mechanistic Insights

We were intrigued by the unexpected efficiency of our newly developed ether transfer reactions. Not only did the initial reactions afford our target 1,3-*syn* diol monoether adduct in high yields and excellent diastereoselectivity, but these reactions also essentially reached to completion as soon as a stoichiometric amount of iodine monochloride had been completely introduced to the reaction mixture. Therefore, the next logical question that needs to be addressed would surround the reaction mechanism. Considering the fact that the ether transfer reaction proceeds rapidly, a probably more interesting piece of the puzzle would be the type of experimental setups required to carry out this mechanistic study since kinetic experiments would be unbeneficial.

Fortunately, *in situ* observations of reactive intermediates by NMR techniques have evolved in past several decades as an integral tool in determining reaction mechanisms. For example, pioneered by his mentor, the 1994 chemistry Nobel Prize winner George Olah, Douglas Klumpp and co-workers at the Northern Illinois University have regularly utilized the *in situ* NMR experiments in depicting reaction mechanisms.



Particularly illustrated by their ongoing study of the role of superelectrophiles in the electrophilic aromatic substitution reactions, with this NMR technique, Klumpp and co-workers often successfully observed long-lived, reactive cationic or even much more reactive dicationic intermediates at low temperature.<sup>308</sup> For the investigation of the ether transfer reaction, we carefully designed our *in situ* NMR experiments with the following expectation. If the reaction mechanism indeed proceeds as proposed in Scheme 4.12, based on Klumpp's work, oxonium ion **4.54** should be observable by NMR, assuming the intermediate is stable and long-lived, Figure 4.3.

The *in situ* NMR experiment simply began by premixing starting material **4.50** and ICl solution in d<sub>8</sub>-toluene at -78°C directly in the NMR tube, and the sample was then inserted to an NMR probe precooled to -60°C. After allowing the NMR probe to slowly warm up to and equilibrate at -20°C, the <sup>1</sup>H and <sup>13</sup>C NMR spectra were then acquired. Our sample only indicated a single new compound by NMR, and the data are tabulated in Table 4.1 along with the <sup>1</sup>H and <sup>13</sup>C NMR observation from 1,3-*syn* diol monoether **4.52** as for comparison. These crucial NMR experiments were repeated three times to ensure reproducibility of the acquired data.

When both <sup>1</sup>H and <sup>13</sup>C chemical shifts collected from the *in situ* NMR experiments were compared to those of **4.52**, the chemical shifts between these two compounds are very similar. Consequently, we deduced that the structure of the intermediate generated in the ether transfer reaction must be in a very close resemblance to product **4.52**. In fact, the only signals that distinguish the ether transfer intermediate from **4.52** are a pair of doublets in the <sup>1</sup>H NMR at 5.08 and 5.01 ppm with coupling constant of 5.5 Hz, and each signal corresponds to 1 proton. For the <sup>13</sup>C NMR, the

distinct signal appears at 81.35 ppm. We found that these peculiar  $^1\text{H}$  and  $^{13}\text{C}$  signals are typical to those of chloromethyl ether functionality. The support for this analysis was based on direct observation of MOMCl in  $d_8$ -toluene, which at 4.90 ppm for  $^1\text{H}$  NMR and 84.80 ppm for  $^{13}\text{C}$  NMR. Thus, it is reasonable to suggest that the actual long-lived intermediate in our ether transfer reaction is chloromethyl ether **4.55**, but not the proposed oxonium ion **4.54**! In addition, the chemical shift of the methoxy group observed in the *in situ* NMR experiments (2.84 ppm for  $^1\text{H}$  and 55.91 ppm for  $^{13}\text{C}$ ) correlates very closely to those of **4.52** (2.84 ppm for  $^1\text{H}$  and 55.97 ppm for  $^{13}\text{C}$ ). This comparison further supports the intermediacy of chloromethyl ether **4.55** as such oxonium ion **4.54** will most likely induce the methoxy signal to move significantly downfield in terms of NMR chemical shifts.

**TABLE 4.1**

<sup>1</sup> H NMR		<sup>13</sup> C NMR	
4.55	4.52	4.55	4.52
7.14 - 6.97 (5H, m)	7.18 - 7.01 (5H, m)	141.87	142.61
5.08 (1H, d, J = 5.5 Hz)	---	--- <sup>[a]</sup>	129.00
5.01 (1H, d, J = 5.5 Hz)	---	128.57	128.56
3.61 (1H, q, J = 6.0 Hz)	3.56 (1H, dddd, J = 8.5, 8.5, 4.0, 2.5 Hz)	126.10	125.99
---	2.98 (1H, d, J = 13.0 Hz)	81.35	---
2.93 (2H, d, J = 4.0 Hz)	2.82 (1H, dd, J = 16.5, 5.5 Hz)	75.62	79.48
	2.87 (1H, dd, J = 17.0, 8.0 Hz)	75.17	69.32
2.84 (3H, s)	2.84 (3H, s)	55.91	55.97
2.65 (1H, m)	2.77 - 2.71 (2H, m)	38.52	41.99
2.57 - 2.42 (2H, m)	2.64 (1H, ddd, J = 13.5, 9.5, 7.0 Hz)	35.57	39.84
1.66 (1H, m)	1.66 (1H, m)	31.36	32.05
1.59 - 1.49 (3H, m)	1.59 - 1.50 (2H, m)	10.46	9.01
	1.42 (1H, ddd, J = 14.5, 4.0, 3.0 Hz)		

[a] One aromatic signal missing, presumably buried under the strong d<sub>8</sub>-toluene signals

Additionally, we also believed that the conversion of chloromethyl ether **4.55** to oxonium ion **4.54** is not a reversible process. This is supported by the fact that the variable temperature NMR experiments of intermediate **4.55** ranging from -78°C to room temperature did not indicate any spectral change in the both of <sup>1</sup>H and <sup>13</sup>C NMR.

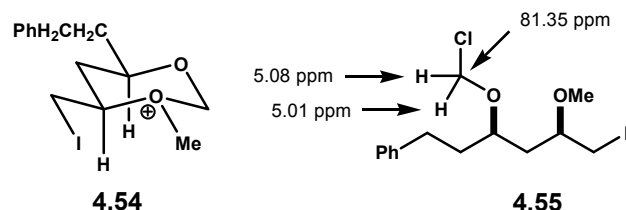
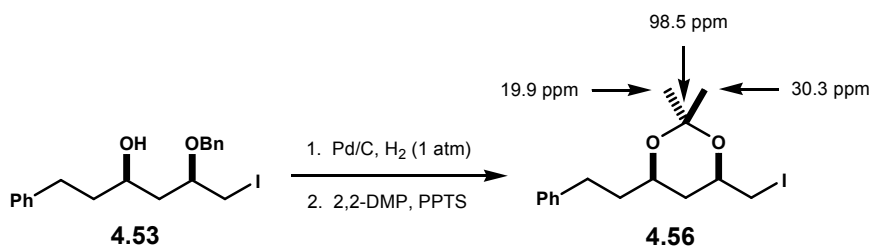


**Figure 4.3**

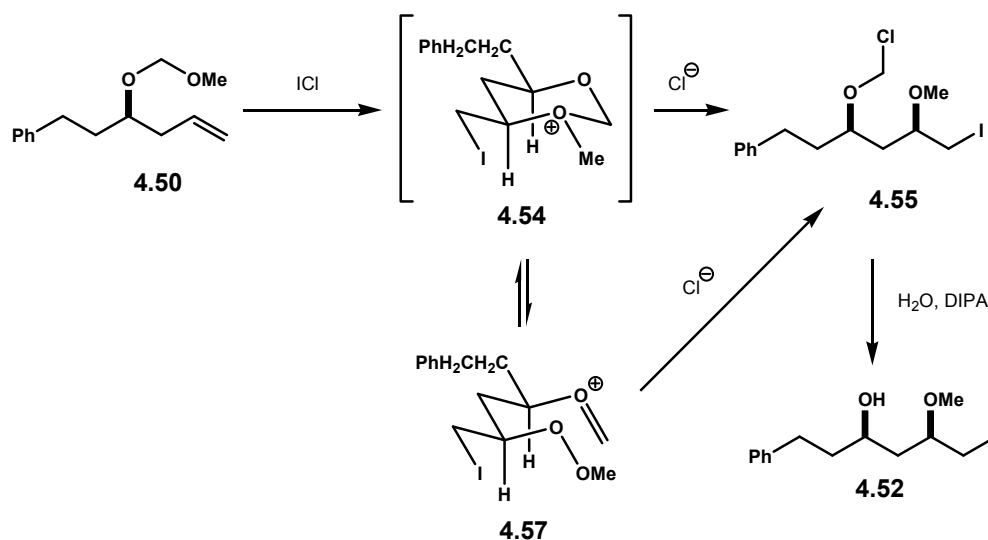
The stereochemical relationship of the 1,3-*syn* diol monoether adduct was established according to protocol developed by Rychnovsky.<sup>259</sup> Ether transfer adduct **4.53** was converted to the corresponding acetonide **4.56** upon hydrogenolysis of the benzyl ether and subsequent protection of the resulting diol with 2,2-dimethoxypropane in the presence of a catalytic amount of PPTS. The <sup>13</sup>C NMR spectroscopic analysis particularly at the acetonide carbon centers revealed chemical shifts that were assigned by Rychnovsky as a strong indication for the 1,3-*syn* diol stereochemical relationship.



**Scheme 4.15**

Based on these experimental evidence, our reaction mechanism for the electrophile-induced ether transfer reaction is proposed as shown in Scheme 4.16. Electrophilic activation of homoallylic alkoxyethyl ether **4.50** with iodine monochloride induces an intramolecular delivery of the alkoxy group across the double

bond in a chair-like fashion, providing six-membered oxonium ion **4.54**. This chair-like delivery thus establishes the 1,3-*syn* stereochemistry. Nucleophilic attack of the chloride ion to the acetal carbon ultimately yields the NMR observable chloromethyl ether **4.55**.



**Scheme 4.16**

The rapid addition of the chloride ion to oxonium ion **4.54** is presumably accentuated by a contact-ion pair system which should readily predominate in a non-polar reaction medium. The manner in which the chloride ion adds to the acetal carbon, however, remains unclear. There are two possible alternatives for the chloride addition: first, a direct attack of the chloride ion to the electrophilic acetal carbon in an  $\text{S}_{\text{N}}2$ -like mechanism, or second, a collapse of oxonium ion **4.54** to oxocarbenium ion **4.57** followed by the subsequent nucleophilic addition of the chloride ion. Finally, hydrolysis decomposes chloromethyl ether **4.55** to the alcohol functionality, thus providing the 1,3-*syn* diol monoether **4.52**.

#### 4.5. Ether transfer and Structural Diversity

The elucidation of chloromethyl ether **4.55** as a stable, long-lived intermediate in our ether transfer reaction proves to be an extremely valuable piece of information. In fact, this study became a pivotal point which led to the successful projects described in Chapters Five and Six. We envisioned that trapping of this intermediate with a variety of nucleophiles would offer additional opportunities for further synthetic creativity. In fact, as shown in Table 4.2, a co-worker in our laboratories, Kai Liu, has successfully generated a library of structurally diversified 1,3-*syn* diethers from simple homoallylic alkoxymethyl ether starting materials using the ether transfer activation followed by a variety of workup conditions.

For example, as shown in entries 1 and 2, activation of alkoxymethyl ether **4.50** and **4.51** with ICl followed by methanolic workup generated MOM-protected 1,3-*syn* diethers **4.58** and **4.59** in good yields and diastereoselectivity. Diether **4.59** represents a complete orthogonally protected 1,3-*syn* diol. In addition, as shown in entries 3 and 4, benzyl alcohol and acidic acid workups successfully afforded respectively BOM-ether **4.60** and alkoxyacetate **4.61**. A reductive workup such as hydride quench was also found suitable for this reaction. Such a workup provided *bis*-methyl ether **4.62** and benzylmethyl diether **4.63**, entries 5 and 6. To expand the methodology to the synthesis of more complex polyketide-like structures, substrates **4.64** and **4.66** as shown in entries 7 and 8 became essential test reactions as competitive cyclization events might occur. However, with appropriate protecting groups such as a BPS ether or benzoate ester,<sup>309</sup> only the expected ether transfer took place, and the alternative cyclization products were

not observed. Finally, with propionate-like structures such as substrates **4.68** and **4.70**, it was found that the allylic substitution regardless its stereochemistry did not affect the overall ether transfer reaction, entries 9 and 10.

**TABLE 4.2**

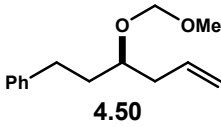
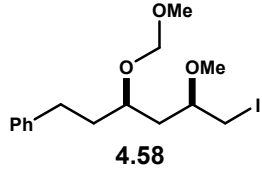
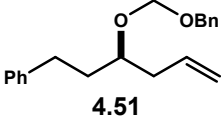
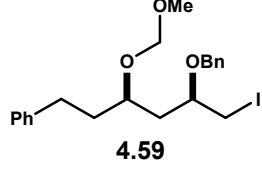
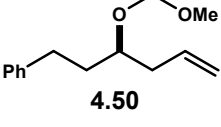
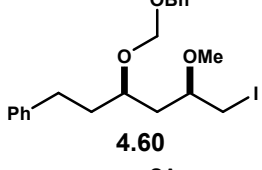
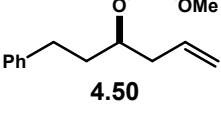
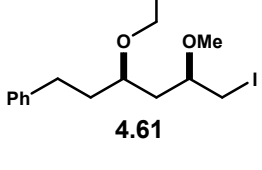
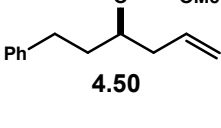
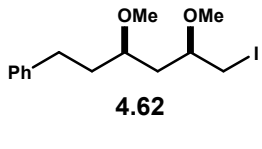
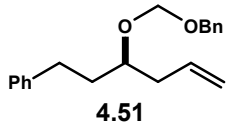
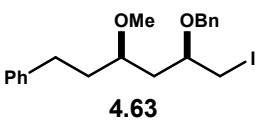
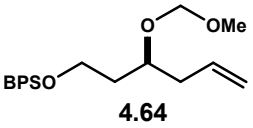
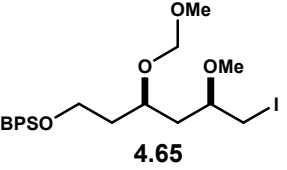
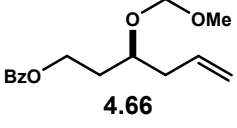
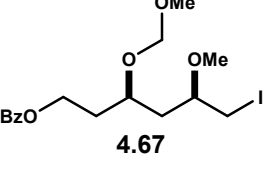
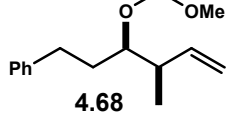
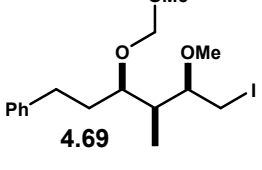
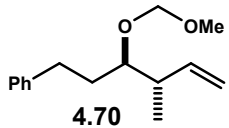
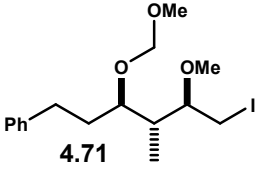
Entry	Starting Material	Workup	Product	Yield <sup>[a]</sup>	dr <sup>[b]</sup>
1	 <b>4.50</b>	MeOH, DIPEA	 <b>4.58</b>	75%	13:1
2	 <b>4.51</b>	MeOH, DIPEA	 <b>4.59</b>	56%	25:1
3	 <b>4.50</b>	BnOH, DIPEA	 <b>4.60</b>	80%	13:1
4	 <b>4.50</b>	AcOH, DIPEA	 <b>4.61</b>	88%	13:1
5	 <b>4.50</b>	LiBH <sub>4</sub>	 <b>4.62</b>	91%	12:1

TABLE 4.2 – continued

Entry	Starting Material	Workup	Product	Yield <sup>[a]</sup>	dr <sup>[b]</sup>
6	 4.51	LiBH <sub>4</sub>	 4.63	67%	25:1
7	 4.64	TMSOMe	 4.65	73%	25:1
8	 4.66	TMSOMe	 4.67	62%	15:1
9	 4.68	TMSOMe	 4.69	89%	25:1
10	 4.70	TMSOMe	 4.71	56%	10:1

[a] Yield isolated as a mixture of diastereomers. [b] Diastereomeric ratio was measured by <sup>1</sup>H NMR integration.

## 4.6. Conclusion

This chapter details peloruside A and the 1,3-*syn* diol monoether functionality contained within this cytotoxic polyketide natural product. Literature reviews demonstrated that 1,3-*syn* diol monoether was a daunting functionality to construct, and it typically required lengthy elaboration of protecting group.



Our group has provided a solution to this synthetic challenge with our newly developed methodology, the electrophile-induced ether transfer reaction. This tactic allowed for the production of 1,3-*syn* diol monoether **4.52** in just one step by exposing simple, readily accessible homoallylic alkoxymethyl ether **4.50** to iodine monochloride. By using *in situ* NMR observations, the reaction mechanism was proposed through an intermediacy of chloromethyl ether **4.55**. This chloromethyl ether species was then successfully subjected to various workup conditions which ultimately built a library of synthetically valuable, structurally diversified 1,3-*syn* diethers.

## CHAPTER FIVE

### STEREOSELECTIVE SYNTHESIS OF OXYGEN HETEROCYCLES VIA ELECTROPHILE-INDUCED ETHER TRANSFER

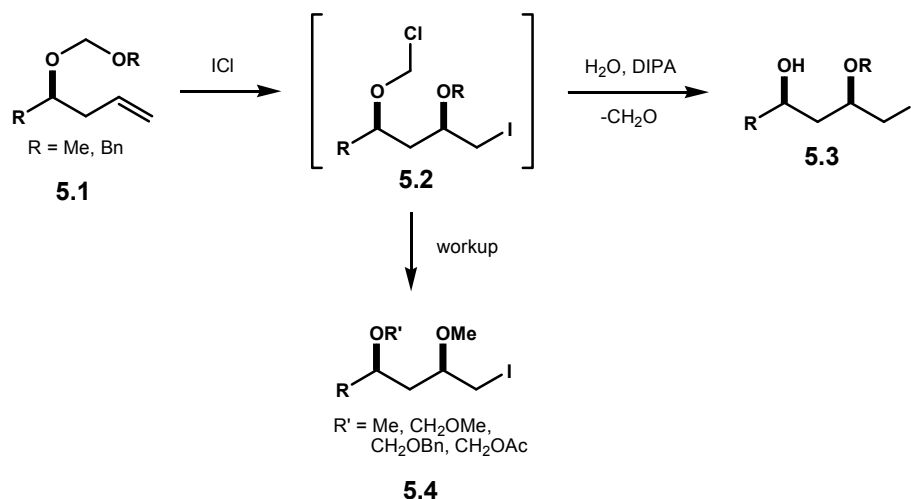
#### 5.1. Purpose

The purpose of this chapter is to describe a novel extension of the electrophile-induced ether transfer to stereoselective productions of six-membered oxygen heterocycles, which include 2,4,6-trisubstituted tetrahydropyrans and 2,6-disubstituted 3,4-dihydropyrans. A general three-step sequence: ether transfer, cyclization, and functionalization, will be executed to access these oxacycles which are common to biologically significant polyketide natural products. Successful applications of the method to complex molecule syntheses will be highlighted by the construction of synthetic fragments containing the oxygen heterocycle cores of phorboxazole A and swinholide A.

## 5.2. Ether Transfer and Oxacycle Methodology

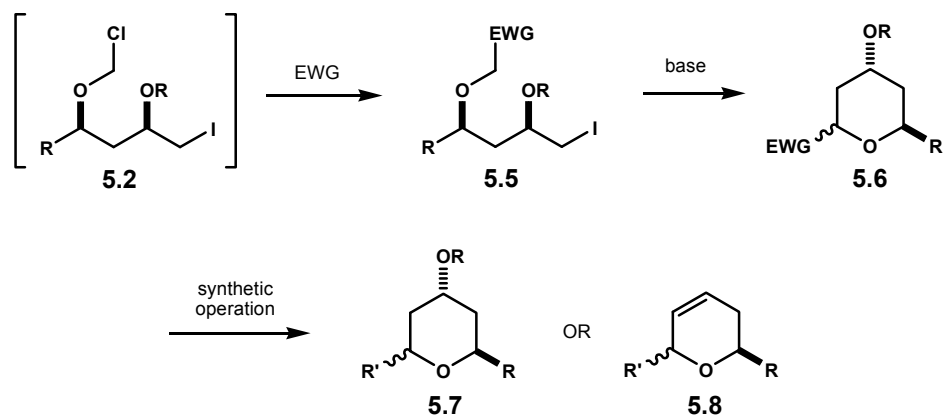
As previously stated in this dissertation, our research interests lie in the synthetic methodology development and total synthesis of biologically active polyketide natural products. The total synthesis project towards (+)-acutiphycin was described in Chapter Three, and Chapter Four discussed our newly explored tactic which accessed polyketide synthetic fragment 1,3-*syn* diol monoether **5.3** from a simple alkoxymethyl ether protected homoallylic alcohol **5.1**. This methodology was then termed as the electrophile-induced ether transfer reaction.

The mechanism of the ether transfer reaction has been proposed through the intermediacy of chloromethyl ether **5.2** based on the observation made by *in situ*  $^1\text{H}$  and  $^{13}\text{C}$  NMR experiments, Scheme 5.1. We then discovered that the chloromethyl ether **5.2** could be readily quenched with a variety of nucleophiles depending upon workup conditions, which gave rise to a library of structurally diverse compounds **5.4** containing the 1,3-*syn* diol structural core.<sup>236</sup>



**Scheme 5.1**

Based on the successful trapping experiments, we envisioned that the ether transfer reaction could be further utilized to access oxygen heterocycles with the following rationale. Displacement of chloromethyl ether **5.2** with an electron-withdrawing group (EWG) should provide ether transfer adduct **5.5**. The introduction of this group will result in the increased acidity of the corresponding  $\alpha$ -proton. Such an effect should then allow deprotonation and cyclization to tetrahydropyran scaffold **5.6**. A variety of synthetic manipulations at the anomeric center are well-established, and this will provide a convenient access to several stereochemically rich oxygen heterocycles such as tetrahydropyran **5.7** and 3,4-dihydropyran **5.8**, Scheme 5.2. In this chapter, a detailed description of the utilization of the cyano and sulfone functionalities as electron-withdrawing groups and their respective synthetic manipulations to the intended oxygen heterocycles methodology quest will be supplied.<sup>310</sup>



**Scheme 5.2**

Our interests in the development of the abovementioned methodology originated from the numerous polyketide natural products containing these oxygen heterocycles. Oxygen heterocycles are the most common ring system found in polyketides. Their presence adds a significant degree of conformational rigidity and is thus likely to be critical to the pharmacophore of biologically active natural products. As a small representative, phorboxazole A **5.9**,<sup>41</sup> leucascandrolide A **5.10**,<sup>94</sup> hydrangenoside E **5.11**,<sup>311</sup> and apicularen A **5.12**<sup>312</sup> all contain stereochemically complex tetrahydropyran rings, Figure 5.1. In addition, polyketides such as swinholide A **5.13**<sup>313</sup> and ambruticin **5.14**<sup>230</sup> both possess highly substituted tetrahydropyran as well as 3,4-dihydropyran rings, Figure 5.2.

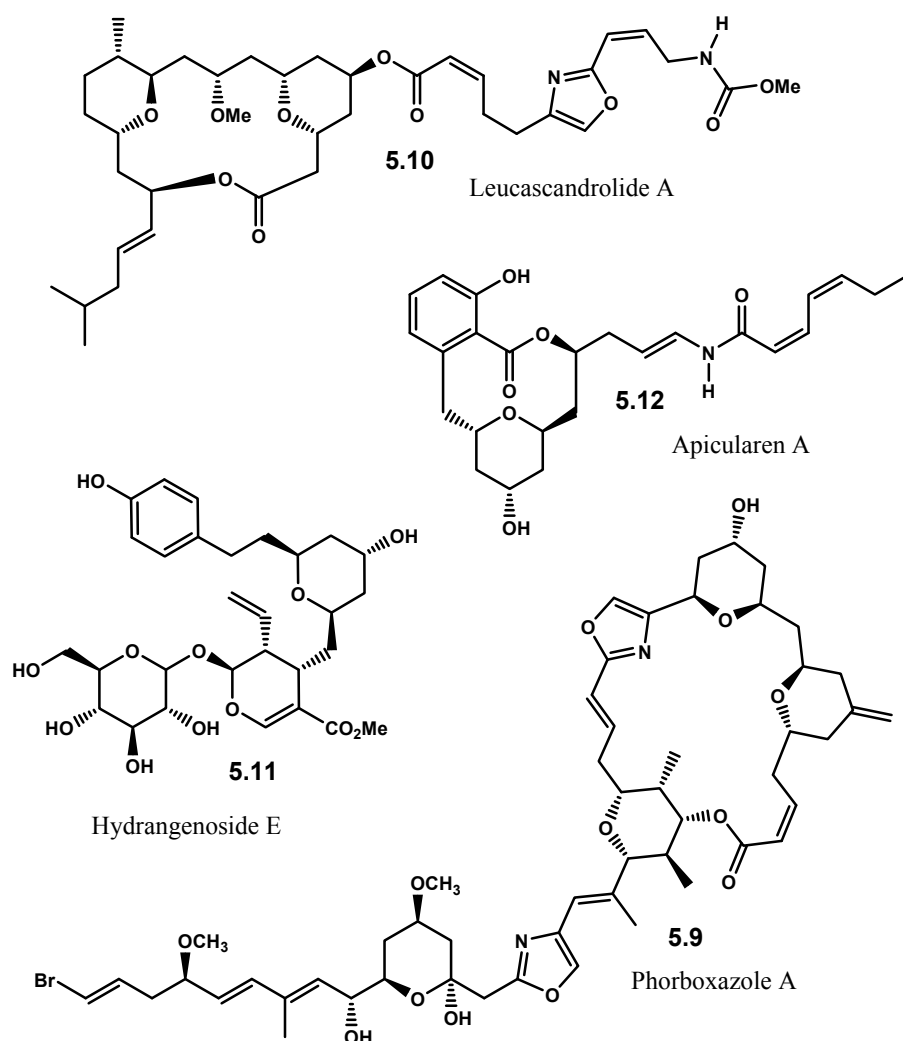


**Figure 5.1**

Numerous synthetic approaches to these oxygen heterocycles have been developed, and their utilization in total syntheses of complex molecules have been recently reviewed.<sup>310</sup> However, we believe that our strategy will provide an attractive alternative to these established methods. As demonstrated previously, the ether transfer reaction only requires a very simple, readily accessible homoallylic alkoxymethyl ether starting material. In addition, the reaction is reliable in terms of reproducibility, product yield, and diastereoselectivity. Furthermore, synthetic manipulations of anomeric

cyanide or sulfone are well preceded, thus warranting the likelihood of our methodology development to be successful.

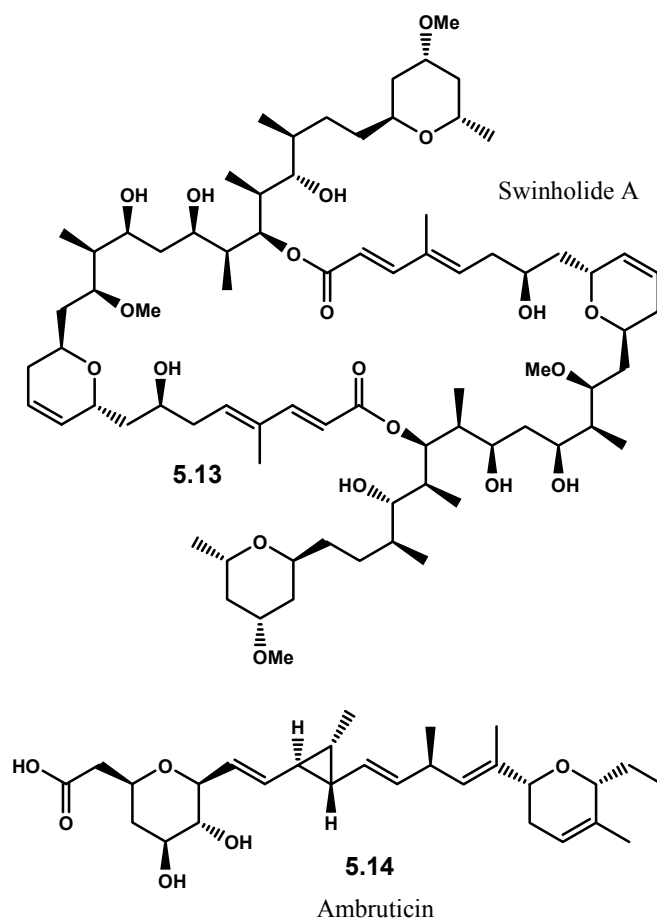


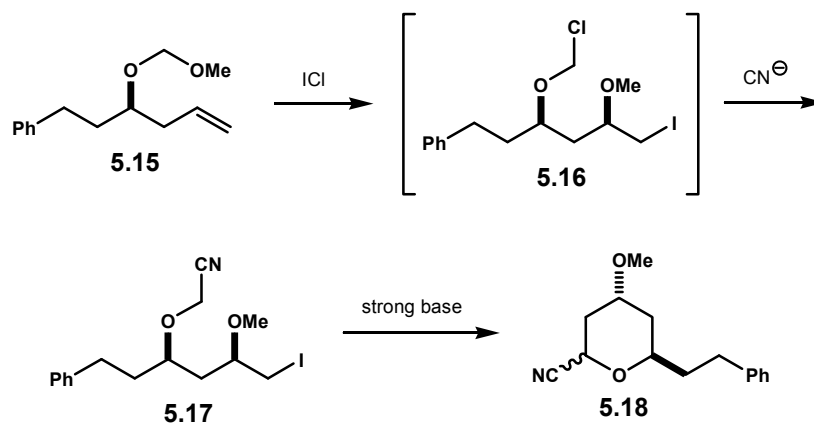
**Figure 5.2**

### 5.3. An Expedient Route to 2-Cyano Tetrahydropyran

We began the aforementioned oxygen heterocycle project by investigating the production of 2-cyano tetrahydropyran via our electrophile-induced ether transfer reaction.<sup>237</sup> The use of anomeric cyanide as a key synthetic intermediate for tetrahydropyran production has tremendously increased in recent years,<sup>314-316</sup> particularly

demonstrated by the work of Rychnovsky and co-workers at the University of California, Irvine. Rychnovsky and co-workers have developed an elegant synthetic manipulation of 2-cyano tetrahydropyran to several structurally complex fragments of natural products. This strategy was highlighted particularly through their highly versatile reductive decyanation process.<sup>317-319</sup>

Our strategy to 2-cyano tetrahydropyran is described in Scheme 5.3. Upon activation of homoallylic alkoxyethyl ether **5.15** with iodine monochloride, trapping of the resulting chloromethyl ether intermediate **5.16** with cyanide ion is expected to produce cyanoether adduct **5.17**.<sup>320, 321</sup> The introduction of a cyanide functionality will then allow deprotonation with a strong base, which should lead to subsequent favorable intramolecular six-atom cyclization through displacement of the primary iodide. This overall process should readily afford 2-cyano tetrahydropyran **5.18**.



**Scheme 5.3**

Choosing the appropriate source of cyanide ion is an important task that needs careful thought as toxicity, solubility, nucleophilicity, and cost-effectiveness of the



cyanide source must be taken into consideration. Cyanotrimethylsilane (TMSCN) would arguably be an excellent source of cyanide ion for its strong nucleophilicity and high solubility in various organic solvents, but TMSCN is unattractive in practice, particularly for a larger scale reaction, due to its substantial toxicity. There are several alternative and more reasonable sources of cyanide ion, which include potassium cyanide (KCN), diethylaluminum cyanide ( $\text{Et}_2\text{AlCN}$ ), copper cyanide ( $\text{CuCN}$ ), tributyltin cyanide ( $\text{Bu}_3\text{SnCN}$ ), and tetraethylammonium cyanide ( $\text{Et}_4\text{NCN}$ ). The result of the selection process is presented in Table 5.1.

After screening a variety of cyanide sources, it appeared that only the use of  $\text{Et}_2\text{AlCN}$  and  $\text{Et}_4\text{NCN}$  efficiently produced the desired cyanoether adduct **5.17**. Not surprisingly, the conditions in which MOM-protected homoallylic alcohol **5.15** was activated with iodine monochloride played a profound role in dictating the diastereoselectivity outcome of the ether transfer reaction. It is clear that diastereoselectivity eroded significantly when activation was performed in more polar solvents, entries 2 – 4 and 8 – 9. This further supports our mechanistic hypothesis described in the previous chapter, which is proposed through a cationic cyclization process as polar solvents are known to stabilize cationic species, thus potentially loosening the transition state for *syn*-methoxy delivery. Furthermore, activation temperature was also found crucial. As shown in entries 8 and 10, the diastereoselectivity of the ether transfer slightly improved from 9:1 at  $-30^\circ\text{C}$  to 12:1 at  $-78^\circ\text{C}$ . Interestingly, the temperature at which  $\text{Et}_4\text{NCN}$  was introduced to the reaction mixture did not considerably affect the overall quality of the cyanide incorporation process, entries 10 – 12. The optimized reaction conditions were established with

exposure of MOM-protected homoallylic alcohol **5.15** to ICl in toluene at -78°C, followed by warming up the reaction mixture to -30°C prior to the addition of Et<sub>4</sub>NCN. Et<sub>4</sub>NCN was introduced as a solution of 1:2 toluene / acetonitrile, and the reaction was stirred at -30°C for 18 hours.

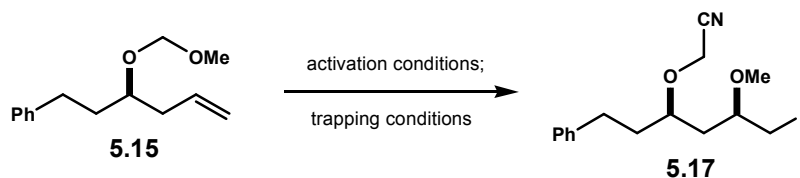


**TABLE 5.1**

Entry	Activation <sup>[a]</sup>		Cyanide Source	Quench		Yield <sup>[d]</sup>	dr <sup>[e]</sup>
	Solvent	Temp (°C)		Solvent <sup>[b]</sup>	Temp <sup>[c]</sup> (°C)		
1	toluene	-78	KCN <sup>[f,g]</sup>	---	-78 → rt	trace	---
2	toluene	-78	Et <sub>2</sub> AlCN	toluene	-78 → rt	37%	>20:1
3	1:1 tol / MeCN	-30	Et <sub>2</sub> AlCN	toluene	-30 → 0	74%	9:1
4	MeCN	-30	Et <sub>2</sub> AlCN	toluene	-30 → 0	57%	2:1
5	toluene	-78	Bu <sub>3</sub> SnCN	toluene	-78 → rt	trace	---
6	1:1 tol / MeCN	-30	Bu <sub>3</sub> SnCN	toluene	-30 → 0	trace	---
7	toluene	-78	CuCN <sup>[f]</sup>	---	-78 → 0	decomposition	---
8	toluene	-30	Et <sub>4</sub> NCN	1:1 tol / MeCN	-30 → rt	62%	9:1
9	1:1 tol / MeCN	-30	Et <sub>4</sub> NCN	1:1 tol / MeCN	-30 → 0	78%	5:1
10	toluene	-78	Et <sub>4</sub> NCN	1:1 tol / MeCN	-78 → 0	63%	12:1
11	toluene	-78	Et <sub>4</sub> NCN	1:1 tol / MeCN	-78 → rt	62%	12:1
12	toluene	-78 → -30	Et <sub>4</sub> NCN	1:2 tol / MeCN	-30	70%	12:1

[a] Conditions in which starting material **10** was activated with ICl. [b] Solvent used to dissolve the cyanide source. [c] Temperature at which cyanide source was introduced to the reaction mixture. [d] Yield isolated as a mixture of diastereomers. [e] Diastereomeric ratio was measured by <sup>13</sup>C NMR integration. [f] Cyanide source as added as powder. [g] 18-Crown-6 was employed as an additive.

After finding working, reliable conditions for the production of cyanoether **5.17**, we then focused our attention on optimization of the subsequent cyclization to cyanopyran **5.18**. As represented in Table 5.2, we found that the choice of solvent and base highly influenced the result of cyclization. For example, deprotonation with NaH in DMF or KO*t*-Bu in THF only led to elimination of the primary iodide to vinyl ether **5.19**; whereas, amide **5.20** was formed upon treatment of **5.18** with KO*t*-Bu in *t*-BuOH. LDA, with or without HMPA, was found unsuitable in this cyclization reaction due to decomposition of the starting material being observed. However, the desired cyanopyran **5.18** was readily generated in the presence of lithium hexamethyldisilazide and HMPA. As shown in entries 10 and 11, cyanopyran **5.18** was successfully prepared in high yields when cyanoether **5.17** was treated with excess LiHMDS – HMPA mixture at -78°C. Interestingly, some degrees of stereochemical induction at the newly formed anomeric center arose from relatively simple reaction conditions, as the 2-cyanopyran **5.18** was produced as a 4:1 mixture of diastereomers favoring the β-anomer.

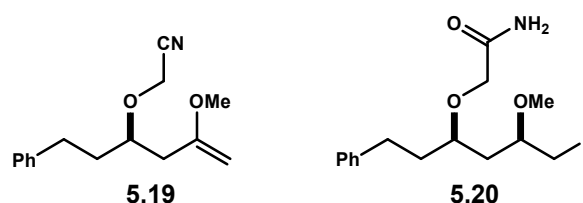


**Figure 5.3**

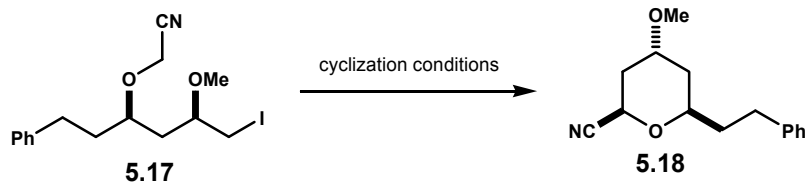


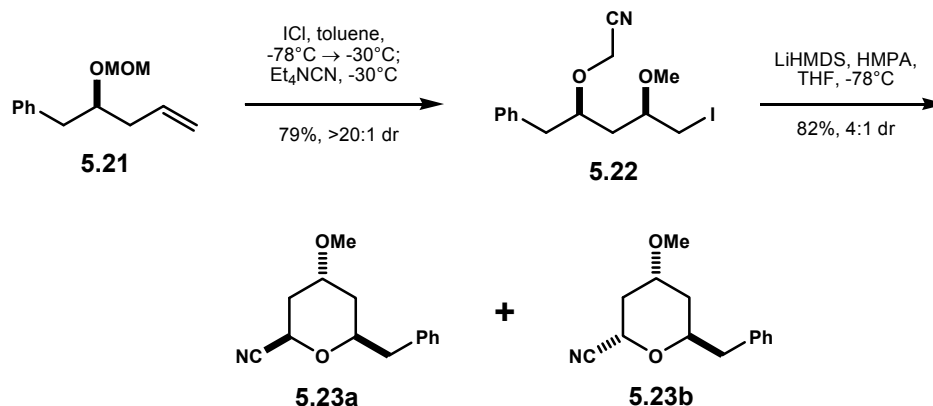
**TABLE 5.2**

Entry	Base	Additive	Solvent	Temp (°C)	Yield <sup>[a]</sup>	dr <sup>[b]</sup>
1	NaH	---	THF	0 → rt	no reaction	---
2	NaH	---	DMF	0 → rt	elimination <sup>[c]</sup>	---
3	KOt-Bu	---	DMF	0	decomposition	---
4	KOt-Bu	---	<i>t</i> -BuOH	0 → rt	hydration <sup>[d]</sup>	---
5	KOt-Bu	---	THF	-78 → -20	elimination <sup>[c]</sup>	---
6	LDA	---	THF	-78	decomposition	---
7	LDA	HMPA	THF	-78	decomposition	---
8	NaHMDS	---	THF	-78	trace	1:1
9	LiHMDS	---	THF	-78 → -20	30%	3:1
10	LiHMDS <sup>[e]</sup>	HMPA <sup>[e]</sup>	THF	-78	92%	4:1
11	LiHMDS <sup>[f]</sup>	HMPA <sup>[f]</sup>	THF	-78	85%	4:1

[a] Yield isolated as a mixture of diastereomers. [b] Diastereomeric ratio was measured by <sup>1</sup>H NMR integration. [c] Elimination led to vinyl ether **5.19**. [d] Hydration led to amide **5.20**. [e] 4.0 eq. of LiHMDS and 5.0 eq. of HMPA were employed. [f] 1.5 eq. of LiHMDS and 3.0 eq. of HMPA were employed.

To demonstrate the scalability of this 2-step reaction, MOM-protected homoallylic alcohol **5.21** was subjected to the optimized conditions for both ether transfer and cyclization reactions in a multigram-scale quantity. As shown in Scheme 5.4, starting with 4.39 grams of **5.21**, cyanoether product **5.22** was isolated in 79% yield (5.97 grams) with a diastereomeric ratio >20:1. In addition, cyclization of 5.23 grams of **5.22** proceeded in 82% yield (2.76 grams) to give cyanopyran **5.23a** and **5.23b** once again as a

4:1 mixture of diastereomers favoring  $\beta$ -anomer **5.23a**. These two diastereomers were separable by column chromatography, and their relative stereochemistry was unambiguously assigned based on  $^1\text{H}$  NMR coupling constant determination of the relevant protons.

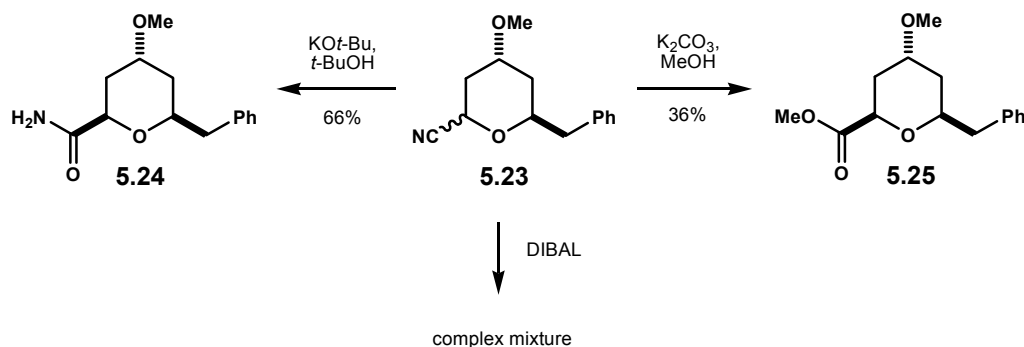


Scheme 5.4

### 5.3.1. Functional Group Interconversions

The cyano group contained in pyran **5.23** could potentially serve as a versatile functionality that could be subjected to a variety of functional group interconversions, thus providing access to valuable synthetic intermediates for tetrahydropyran-containing natural products. For example, one-pot hydration and epimerization of cyanopyran **5.23** readily occurred in wet  $t\text{-BuOH/KO-}t\text{Bu}$  to provide amide **5.24** in respectable yield as a single diastereomer. In addition, exposure of **5.23** to basic methanolysis readily afforded methyl ester **5.25**. An attempt to convert **5.23** to **5.25** under the Pinner conditions only resulted in decomposition. In addition, an attempt to convert the cyano group to the

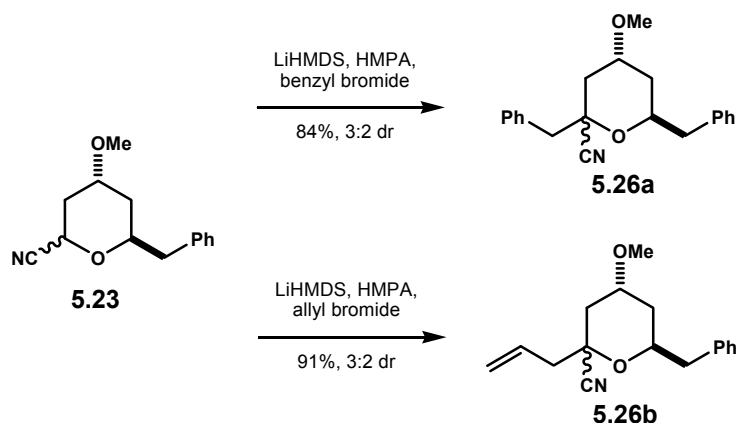
corresponding aldehyde under DIBAL reduction unfortunately was not particularly fruitful as the reaction yielded only a complex mixture.



**Scheme 5.5**

### 5.3.2. Reductive Decyanation Study

In addition to the above described transformations at the cyano group, at this point, we envisioned that cyanopyran **5.23** may also be subjected to further synthetic operations particularly at the anomeric carbon center. Such operations will include alkylation at the anomeric center followed by reductive decyanation process. This overall sequence should afford 4-alkoxy-2,6-*cis*-tetrahydropyran **5.27**. As shown in Scheme 5.6, when cyanopyran **5.23**, as a mixture of diastereomers, was treated with a mixture LiHMDS and HMPA followed by addition of activated electrophiles such as benzyl bromide and allyl bromide, alkylated pyrans **5.26a** and **5.26b** were produced in good yields.



**Scheme 5.6**

We also found that pyrans **5.26a** and **5.26b** were conveniently accessible from cyanoether **5.22** via a one-pot cyclization – alkylation reaction. This process included treatment of cyanoether **5.22** with large excess of LiHMDS followed by direct addition of electrophiles. The presence of excess base would allow for two sequential deprotonation steps: the first for cyclization and the second for alkylation. In fact, with this strategy, an introduction of benzyl bromide and allyl bromide produced **5.26a** and **5.26b**, both as a 3:2 mixture of diastereomers, in 82% and 95% yields, respectively.

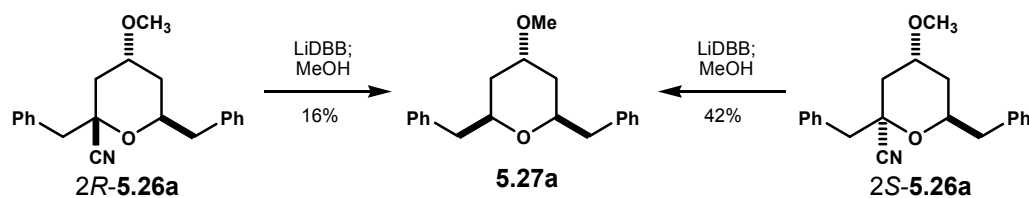




mixture of unidentifiable compounds. The relative stereochemistry of the ring was determined by  $^1\text{H}$  NMR coupling constant analysis.

Although Rychnovsky claimed that the stereochemistry of cyanide group does not bear consequences to the reduction process,<sup>326, 327</sup> it seemed that in these 4-alkoxy systems, the two diastereomers of cyanopyran **5.26** might possess a difference in reactivity toward reduction. To justify this postulation, the two diastereomers of cyanopyran **5.26a** were then carefully separated by chromatography and then individually exposed to the reducing conditions. The stereochemical assignment of each diastereomer was deduced from detailed NMR analyses including a ROESY experiment.

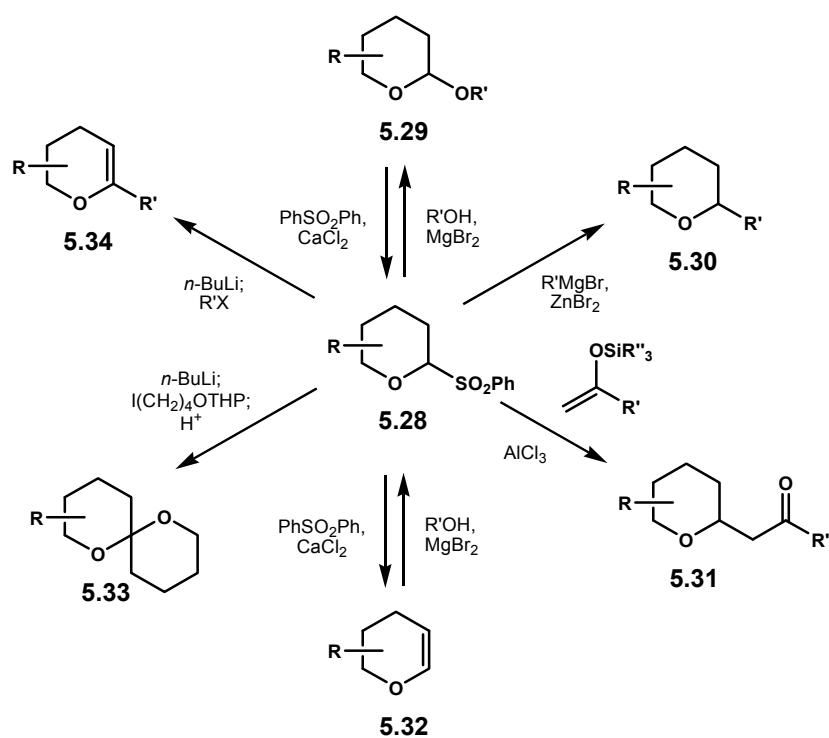
Indeed, we found that the reductive decyanation of the less polar diastereomer *2R*-**5.26a** and the more polar diastereomer *2S*-**5.26a** did not proceed with equal quality. Upon exposure to LiDBB, *2R*-**5.26a** and *2S*-**5.26a** produced **5.27a** in 16% and 42% yields respectively, Scheme 5.7. The origin of this observation is not clear to us. Although the conformational stability and reactivity of an anomeric radical in simple tetrahydropyrans and carbohydrates has been thoroughly investigated,<sup>328-330</sup> to our knowledge, the stability of 2-tetrahydropyranyl radical bearing 4-alkoxy substituent is not yet well understood. Furthermore, we found that based on  $^1\text{H}$  NMR coupling constant measurement and NOE experiment, *2R*-**5.26a** existed in twist-boat conformation, whereas *2S*-**5.26a** existed in chair conformation. The relationship between conformation of cyanopyran **5.26** and their reactivity toward reduction has not yet been established, and a further investigation is thus necessary.



**Scheme 5.7**

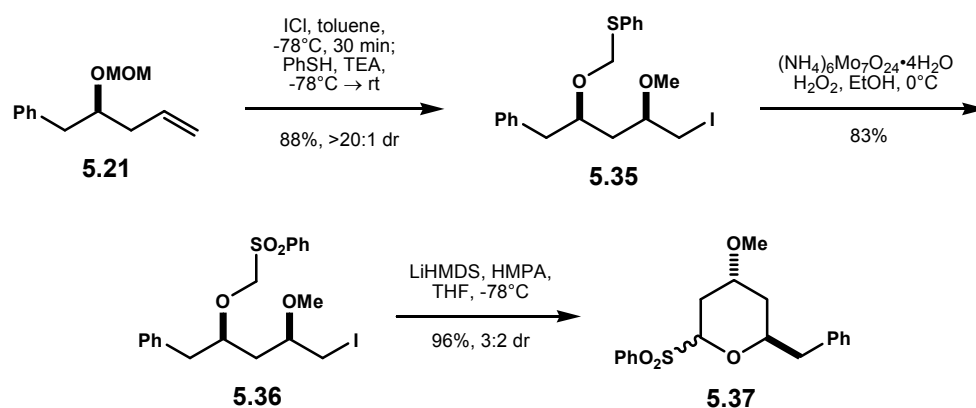
#### 5.4. Preparation of Highly Versatile 2-Sulfone Tetrahydropyran

Since our synthetic methodology to 4-alkoxy tetrahydropyrans was hindered by the key, problematic reductive decyanation step, we had to consider an alternative functionality, which might potentially have similar reactivity patterns to those of anomeric cyanide. A particular functionality that immediately caught our attention was the anomeric sulfone. In late 1980's, Steven Ley and co-workers pursued a detailed study on the chemistry involving anomeric sulfone functionality.<sup>331-334</sup> As summarized in Scheme 5.8, sulfonylpyran **5.28** could be readily transformed to various functional groups, such as alkyl pyranoside **5.29**, tetrahydropyrans **5.30** and **5.31**, glycals **5.32** and **5.34**, as well as spiroketal **5.33**. Although these studies demonstrated that alkyl substitutions at sulfonylpyran may or may not potentially influence the stereochemical outcome particularly in the substitution reaction, it is important to note that our 4-alkoxy pyran systems had not been included in this investigation. Sparked by our curiosity in further studying the relationship between conformation and reactivity patterns of these 4-alkoxy pyran systems, we felt that our exploration of Ley's chemistry is strongly warranted.



**Scheme 5.8**

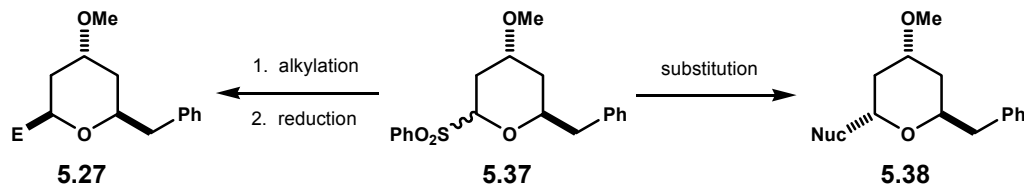
Our synthetic approach to sulfonylpyran **5.37** is fairly straightforward and reminiscent of that of cyanopyran **5.23**. We began with installing the sulfone functionality directly in the ether transfer reaction. Treatment of MOM-protected homoallylic alcohol **5.21** with ICl in toluene at  $-78^{\circ}\text{C}$ , followed by quenching of the chloromethyl ether intermediate with a thiophenol – TEA mixture afforded ether transfer adduct **5.35** in 88% yield as a single diastereomer. Subsequent sulfide oxidation using a mixture of ammonium molybdate –  $\text{H}_2\text{O}_2$  provided sulfonylether **5.36**, which was then readily cyclized under LiHMDS to anomeric sulfone **5.37** as a 3:2 mixture of diastereomers. Both steps proceeded in high yield, Scheme 5.9. It is important to note that direct trapping of the chloromethyl ether intermediate with sodium benzenesulfinate did not produce sulfonyl ether **5.36**.<sup>238</sup>



Scheme 5.9

## 5.5. Stereoselective Synthesis of 2,4,6-Trisubstituted Tetrahydropyrans

With the anomeric sulfone **5.37** in hand, we proposed that this valuable synthetic intermediate could be further transformed to either 4-alkoxy-2,6-*trans*- or 2,6-*cis*-disubstituted tetrahydropyrans **5.38** or **5.27**, respectively. The 2,6-*trans*-tetrahydropyran **5.38** should be readily accessible via a substitution reaction; whereas, the stereocomplementary 2,6-*cis*-tetrahydropyran **5.27** should be accessible via an alkylation – reduction sequence, similar to those described in Table 5.3.



Scheme 5.10

#### 5.5.1. 4-Alkoxy-2,6-*trans*-Disubstituted Tetrahydropyran

In order to access the 2,6-*trans*-tetrahydropyran **5.38**, we proposed a substitution reaction which would require a direct ionization of anomeric sulfone **5.37** followed by trapping the resulting oxocarbenium ion with nucleophiles.<sup>238</sup> In fact, Ley has previously demonstrated a successful ionization of cyclic benzenesulfonyl ethers using aluminium chloride.<sup>331</sup> In these 4-alkoxy substrates, we found upon optimization that treatment of sulfonylpyran **5.37** with slight excess of AlCl<sub>3</sub> and a variety of nucleophiles in toluene at -78°C, followed by warming up to -40°C over one hour cleanly afforded 2,6-*trans*-disubstituted tetrahydropyrans **5.38** in high yields and excellent diastereoselectivity, Table 5.4. The 2,6-*trans* relative stereochemistry was readily deduced based on <sup>1</sup>H NMR coupling-constant analysis.

The nucleophiles screened in this substitution reaction included allyl silanes (entries 1 and 2), enolsilanes (entry 3), silyl ketene acetals (entries 4 – 5 and 7 – 8), and allylstannanes (entry 6). Although generally these nucleophiles afforded tetrahydropyran **5.38** with high degree of 2,6-*trans* stereocontrol, an attempt to generate an additional methyl center, a common substitution pattern to polyketide natural products, in a stereoselective fashion turned out to be unfruitful. For example, with methyl substituted silyl ketene acetals shown in entries 7 and 8, products **5.38g** and **5.38h** were obtained as a complete mixture of diastereomers at the methyl center. Interestingly, with allylstannane as shown in entry 6, cyclopropyl tetrahydropyran **5.38f** was obtained as the major product.<sup>335</sup>

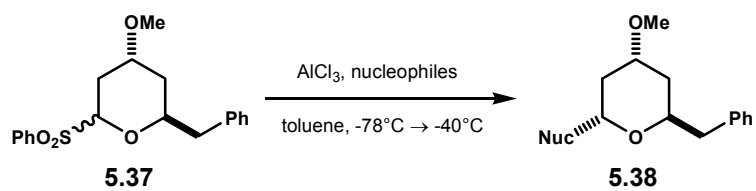


TABLE 5.4<sup>[a]</sup>

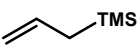
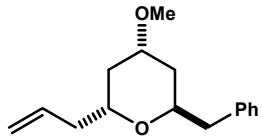
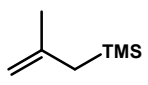
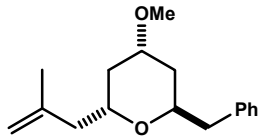
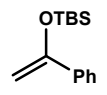
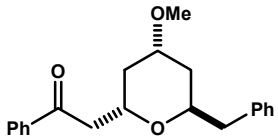
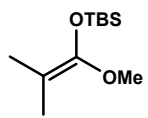
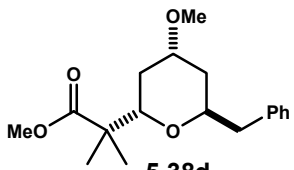
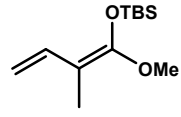
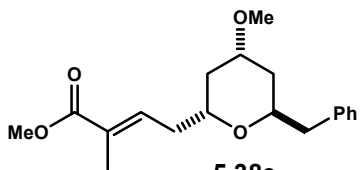
Entry	Nucleophile	Substitution Product	Yield
1		 <b>5.38a</b>	80% <sup>[b]</sup>
2		 <b>5.38b</b>	86% <sup>[b]</sup>
3		 <b>5.38c</b>	82% <sup>[b]</sup>
4		 <b>5.38d</b>	80% <sup>[b]</sup>
5		 <b>5.38e</b>	70% <sup>[b]</sup>

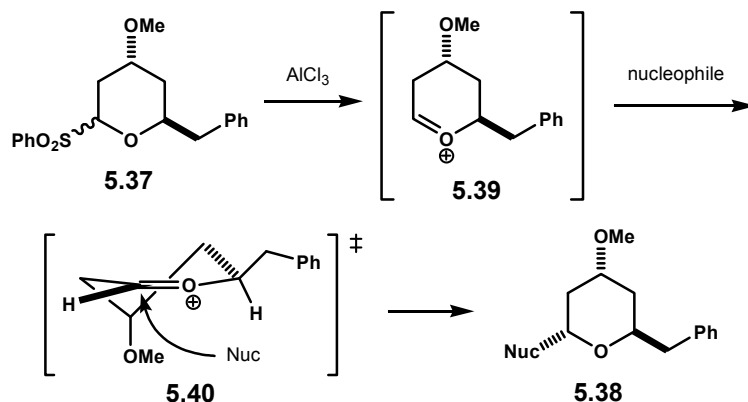
TABLE 5.4 – continued

Entry	Nucleophile	Substitution Product	Yield
6			26% <sup>[b,c]</sup>
7			82% <sup>[d]</sup>
8			62% <sup>[d]</sup>

[a] Typical reaction conditions: 1.5 eq. of  $\text{AlCl}_3$  and 3 eq. of nucleophiles. [b] Yield isolated as a single diastereomer.  $^1\text{H}$  NMR analysis of the crude mixture indicated >20:1 dr. [c] The relative stereochemistry of the cyclopropane ring to the tetrahydropyran was not determined. [d] Yield isolated as a mixture of diastereomers.  $^1\text{H}$  NMR analysis of the crude mixture indicated 1:1 dr.

The mechanism for the above substitution reaction is proposed as follows. The complexation of  $\text{AlCl}_3$  to sulfonylpyran **5.37** results in the ionization of the anomeric sulfone functionality to oxocarbenium ion **5.39**. Judged by the remarkable diastereoselectivity, the intermediate oxocarbenium ion **5.39** must be assumed to have an exceptional conformational stability. In fact, Woerpel and co-workers argued that the conformational stability of cyclic oxocarbenium ion containing an alkoxy substituent such as **5.39** might have been attributed by the axial orientation of the C4-alkoxy group

via the favorable through-space electrostatic interactions.<sup>336-338</sup> The subsequent nucleophile delivery to this intermediate exclusively occurs via preferential axial attack as depicted in transition state **5.40**, thus providing the 2,6-*trans* relative stereochemistry.<sup>339</sup>



Scheme 5.11

### 5.5.2. 4-Alkoxy-2,6-*cis*-Disubstituted Tetrahydropyran

For the stereocomplementary 2,6-*cis*-disubstituted tetrahydropyran **5.27**, we proposed a two-step sequence: alkylation followed by reduction.<sup>238</sup> Our efforts were initially focused on screening the alkylation reaction conditions including finding the proper choice of base and solvent. We immediately found that our 4-alkoxy sulfonylpyran was not suitable for conditions reported by Ley.<sup>332-334</sup> When sulfonylpyran **5.37** was subjected to deprotonation under *n*-BuLi, the decomposition of starting material was immediately observed. Decomposition of the starting material also occurred with LDA.



Moving onto the weaker amide base series, such as the hexamethyldisilazides, the choice of alkaline metal counterparts was found to play significant roles in dictating the outcome of the alkylation reaction. When LiHMDS or KHMDS was charged into a cold solution of sulfonylpyran **5.37**, a noticeable color change immediately took place, and this observation could have been a strong indication that the corresponding anion most likely was generated. However, an introduction of reactive electrophiles, such as benzyl bromide, did not result in alkylation. Interestingly, with NaHMDS, alkylation of sulfonylpyran **5.37** produced a mixture of glycal **5.41** and 2-hydroxypyran **5.42**. More importantly, further solvent optimization revealed that toluene resulted in the cleanest alkylation of sulfonylpyran **5.37**.

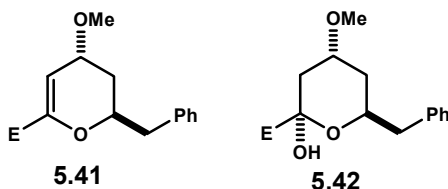


**Figure 5.4**

Actually, glycal **5.41** was the expected alkylation product. In his work summarized in Scheme 5.8, Ley described that the sulfonyl group would be cleanly eliminated in the alkylation reaction most likely during the aqueous workup.<sup>332-334</sup> However, much to our surprise, with our 4-alkoxy systems, glycal **5.41** turned out to have been readily hydrated upon aqueous workup to the corresponding 2-hydroxypyran **5.42**. More importantly, the hydration process seemed favorable as **5.42** was found to be the major product. An attempt to individually isolate these two products with column

chromatography proved extremely difficult. This prompted us to take the products mixture and transform them to their corresponding methyl pyranoside **5.43** under acidic methanolysis which then allowed simple chromatographic purification.

Methyl pyranoside **5.43** then served as our substrates for the subsequent reduction. Indeed, exposure to a mixture of TMSOTf and Et<sub>3</sub>SiH in CH<sub>2</sub>Cl<sub>2</sub> at -78°C conveniently reduced the methyl pyranoside **5.43** to exclusively 2,6-*cis*-tetrahydropyran **5.27**.<sup>304, 340</sup> Once again, <sup>1</sup>H NMR coupling-constant determination of the relevant protons was utilized to deduce the relative stereochemistry of the ring. Several electrophiles were screened, including benzyl bromide, allyl bromide, BOMCl, and methyl iodide, and the sequential alkylation – reduction process generally produced the desired 4-alkoxy-2,6-*cis*-disubstituted tetrahydropyran **5.27** in good yields with excellent diastereoselectivity, Table 5.5.

The reaction mechanism which accounts for the 2,6-*cis* relative stereochemistry is reminiscent of that of substitution reaction for anomeric sulfone **5.37**. The ionization of methyl pyranoside **5.43** with TMSOTf is assumed to produce conformationally stable oxocarbenium ion **5.44**. The conformational stability of this intermediate once again may be argued from the favorable through-space electrostatic interaction between the pseudoaxial 4-alkoxy substituent and the newly formed cationic center.<sup>336, 337</sup> The hydride delivery presumably takes place via preferential axial attack, which set up the 2,6-*cis* stereochemistry.

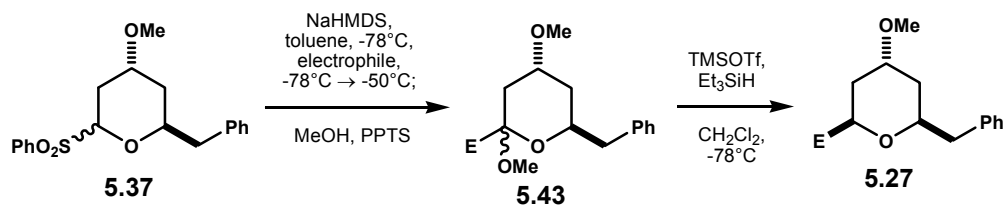
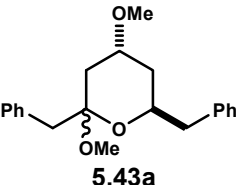
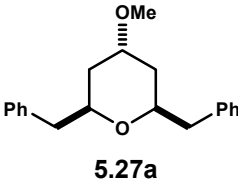
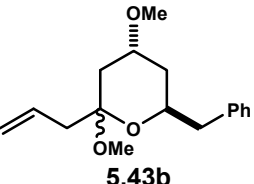
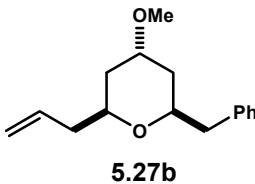
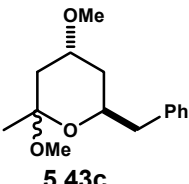
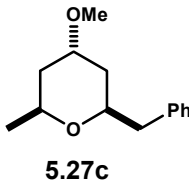
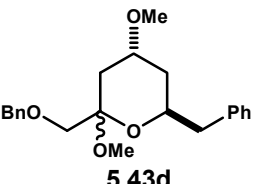
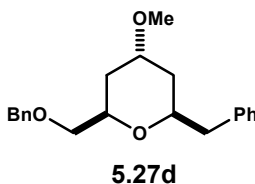
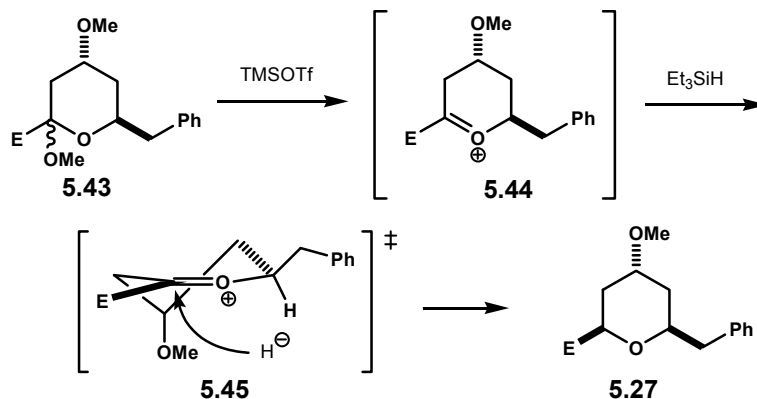


TABLE 5.5

Entry	Electrophile	Alkylation Product <sup>[a]</sup>	Yield <sup>[b]</sup>	Reduction Product <sup>[c]</sup>	Yield <sup>[d]</sup>
1	benzyl bromide	 <b>5.43a</b>	79%	 <b>5.27a</b>	91%
2	allyl bromide <sup>[e]</sup>	 <b>5.43b</b>	85%	 <b>5.27b</b>	82%
3	methyl iodide	 <b>5.43c</b>	97%	 <b>5.27c</b>	72%
4	BOMCl <sup>[f]</sup>	 <b>5.43d</b>	82%	 <b>5.27d</b>	66%

[a] Typical alkylation conditions: 3 eq. of NaHMDS and 4 eq. of alkylating agent. [b] Yield isolated as a mixture of diastereomers. [c] Typical reduction conditions: 3 eq. of TMSOTf and 2 eq. of Et<sub>3</sub>SiH. [d] Yield isolated as a single diastereomer. <sup>1</sup>H NMR analysis of the crude mixture in all cases indicated >20:1 dr. [e] PPTS was not added during methanolysis. [f] Alkylation reaction was warmed up to -40°C.



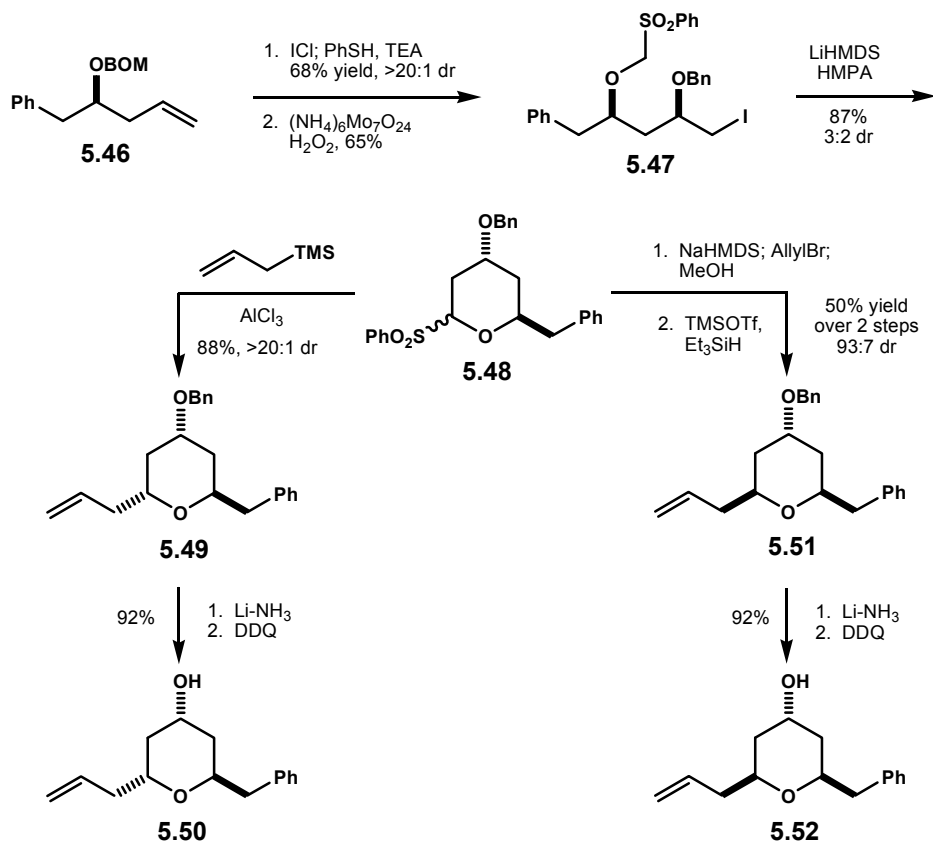
Scheme 5.12

### 5.5.3. 4-Hydroxy-2,6-Disubstituted Tetrahydropyrans

As briefly described in Chapter Four, we have disclosed that benzyloxymethyl ether efficiently undergoes the ether transfer reaction. This finding significantly expands the scope of our ether transfer methodology since the resulting benzyl ether can be deprotected and thus unmasking the secondary alcohol. For our tetrahydropyran methodology, the use of benzyloxy transfer opens up an opportunity for an efficient production of stereocomplementary 4-hydroxy-2,6-disubstituted tetrahydropyran.

Starting with BOM-protected homoallylic alcohol **5.46**, the previously discussed ether transfer, oxidation, and cyclization sequence provided sulfonylpyran **5.48** in respectable yield, Scheme 5.13. Sulfonylpyran **5.48** was then subjected to either the substitution reaction or the alkylation – reduction sequence, which then afforded respectively 2,6-*trans* and 2,6-*cis*-disubstituted tetrahydropyran **5.49** and **5.51**, once again in good yields and excellent diastereoselectivity. Individual exposure of the 4-benzyloxy tetrahydropyrans to reductive conditions such as Li-NH<sub>3</sub> mixture cleanly removed the

benzyl ether and yielded the target stereocomplementary 4-hydroxy tetrahydropyrans **5.50** and **5.52**.



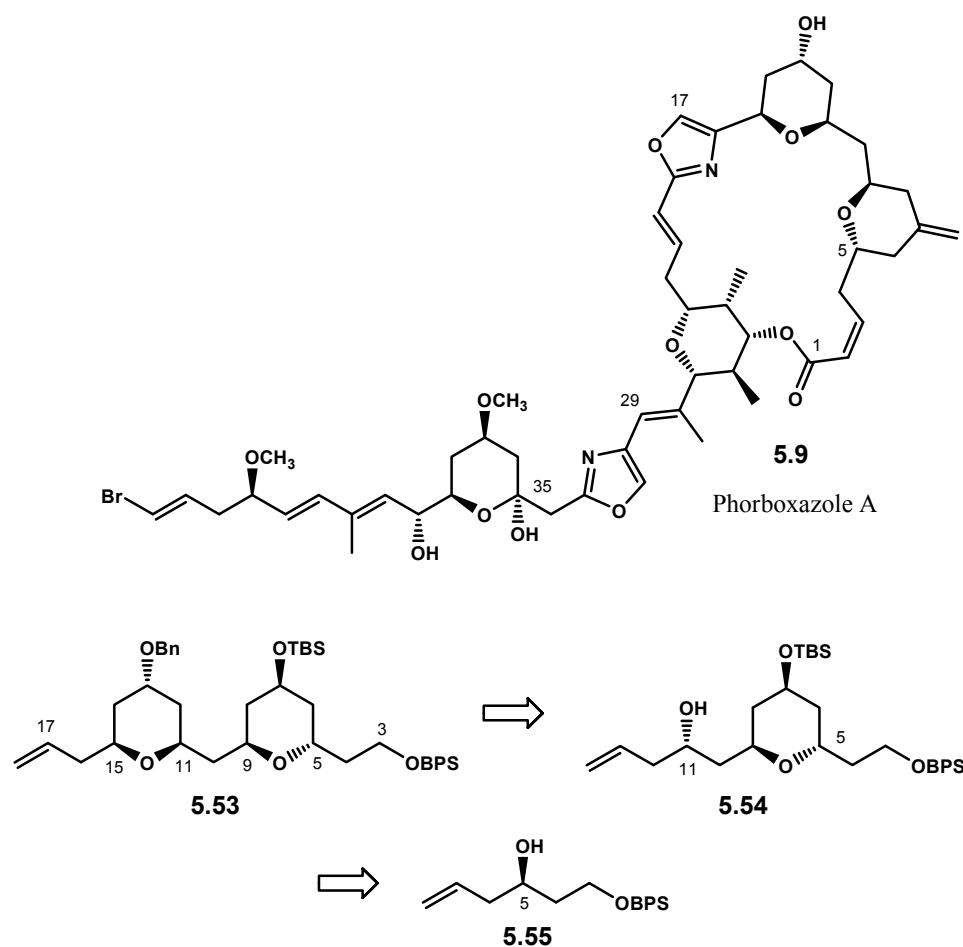
Scheme 5.13

#### 5.5.4. Stereoselective Synthesis of C3 – C17 Fragment of Phorboxazole A

With the methodology to access stereocomplementary 4-alkoxy-2,6-*cis*- and 2,6-*trans*-disubstituted tetrahydropyrans in hand, phorboxazole A **5.9**, particularly its C5 – C15 *bis*-tetrahydropyran region, caught our interest.<sup>41</sup> This natural product is an ideal target which would demonstrate the applicability of our method in complex molecule syntheses.<sup>238</sup> The phorboxazoles have become a popular target among synthetic chemists

for their unique and diverse biological activities. Total syntheses of these complex structures have been accomplished by several groups.<sup>145, 341-352</sup> Furthermore, the development of synthetic methods for the construction of their *bis*-tetrahydropyran C5 – C15 region, are well documented.<sup>353-357</sup> Typically, different cyclization strategies were employed to install each of the stereocomplementary rings within this fragment.

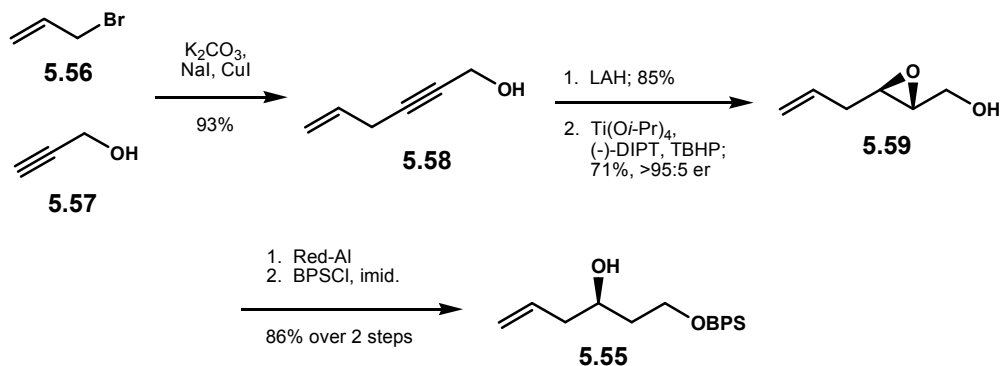
Our synthetic goal to the C5 – C15 *bis*-tetrahydropyran of phorboxazole A is represented as advanced intermediate **5.53**. This intermediate will be assembled through two successive common strategies: ether transfer, cyclization, and functionalization reactions from two sequential homoallylic alcohols **5.54** and **5.55**. Our successfully implemented strategy is described as follows.



**Scheme 5.14**

We began our synthesis to *bis*-tetrahydropyran **5.53** with a large-scale preparation of homoallylic alcohol **5.55** by exploiting a protocol developed by Yadav and co-workers.<sup>358</sup> As shown in Scheme 5.15, a coupling reaction between allyl bromide **5.56** and propargyl alcohol **5.57** cleanly provided enyne **5.58**. The crude material was then subjected to LAH reduction, and the corresponding allylic alcohol was immediately subjected to the Sharpless asymmetric epoxidation reaction. Exposure of the resulting enantiomerically enriched epoxy alcohol **5.59** to Red-Al resulted in the reductive epoxide ring opening to 1,3-diol, and the ensuing kinetically controlled protection of the primary

alcohol with BPSCl furnished homoallylic alcohol **5.55**. The Mosher ester analysis of this alcohol confirmed its enantiomeric purity being greater than 95:5.<sup>196</sup> This route was highly robust such that we were able to prepare more than 20 grams of enantiomerically pure homoallylic alcohol **5.55**.

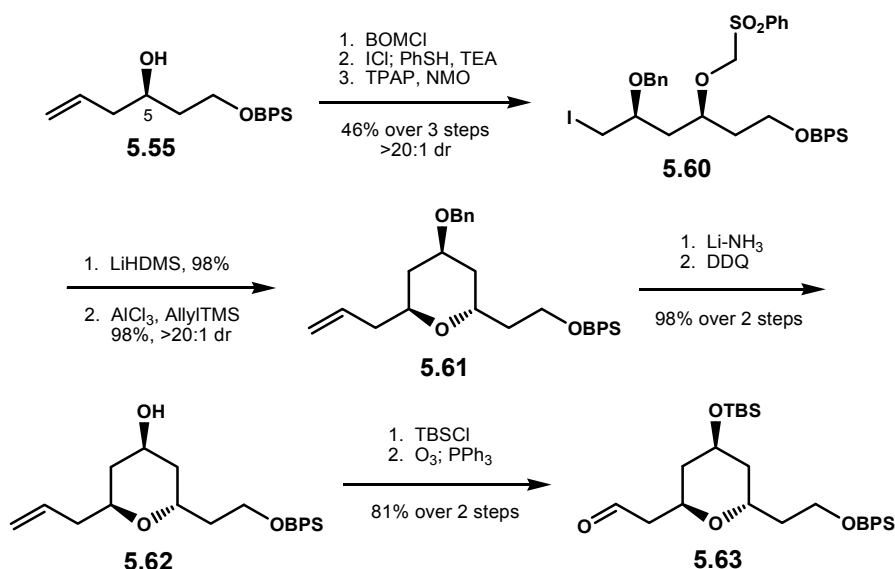


**Scheme 5.15**

The first implemented common strategy to *bis*-tetrahydropyran **5.53** commenced with BOM protection of **5.55** followed by the ether transfer and subsequent sulfide oxidation reactions. This sequence provided sulfonylether **5.60** in 46% yield over three steps as a single diastereomer. TPAP – NMO was found a more suitable oxidant in this particular substrate as sulfide oxidation with ammonium molybdate –  $H_2O_2$  proved low yielding,<sup>359</sup> presumably due to the limited solubility of starting material in the reaction medium. LiHMDS-mediated cyclization of **5.60** followed by cationic allylation of the resulting sulfonylpyran set up the first tetrahydropyran ring **5.61** in excellent yield and diastereoselectivity. This ring represents the 2,6-*trans* stereochemistry of C5 – C9 segment. The benzyl group was then removed with a Li-NH<sub>3</sub> mixture. Under these conditions, the phenyl groups within the BPS ether were converted to cyclohexadienes.

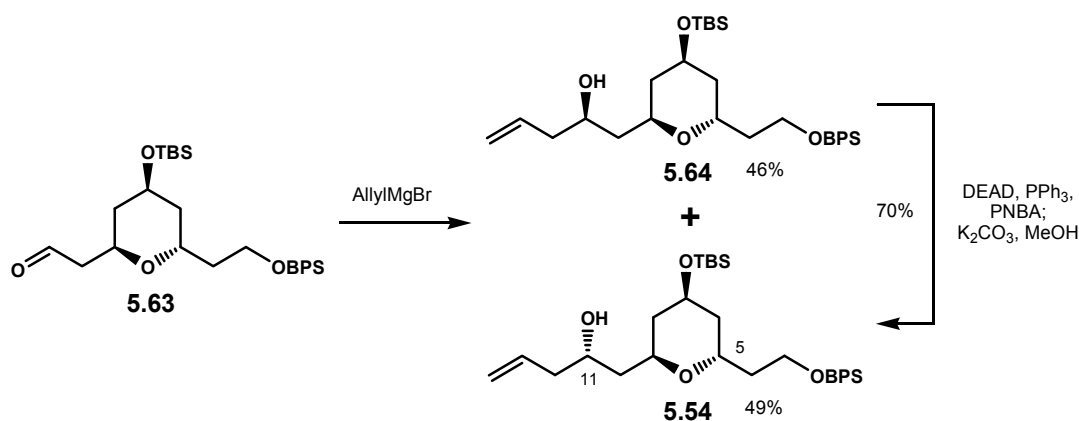


However, after exposure to DDQ, 4-hydroxy tetrahydropyran **5.62** was afforded in essentially quantitative yield for the two steps. After TBS protection, oxidative cleavage of the terminal olefin gave aldehyde **5.63** in 81% yield over two steps.



**Scheme 5.16**

Addition of allylmagnesium bromide to aldehyde **5.63** then afforded a diastereomeric mixture of homoallylic alcohols **5.64** and **5.54** in near quantitative yield. These two alcohols were easily separated by column chromatography. The stereochemistry of alcohol **5.64** was then converted by Martin-modified Mitsunobu inversion to that of **5.54**.<sup>139</sup> The absolute stereochemistry of the desired homoallylic alcohol **5.54** was determined by the Mosher's ester analysis.<sup>196</sup>

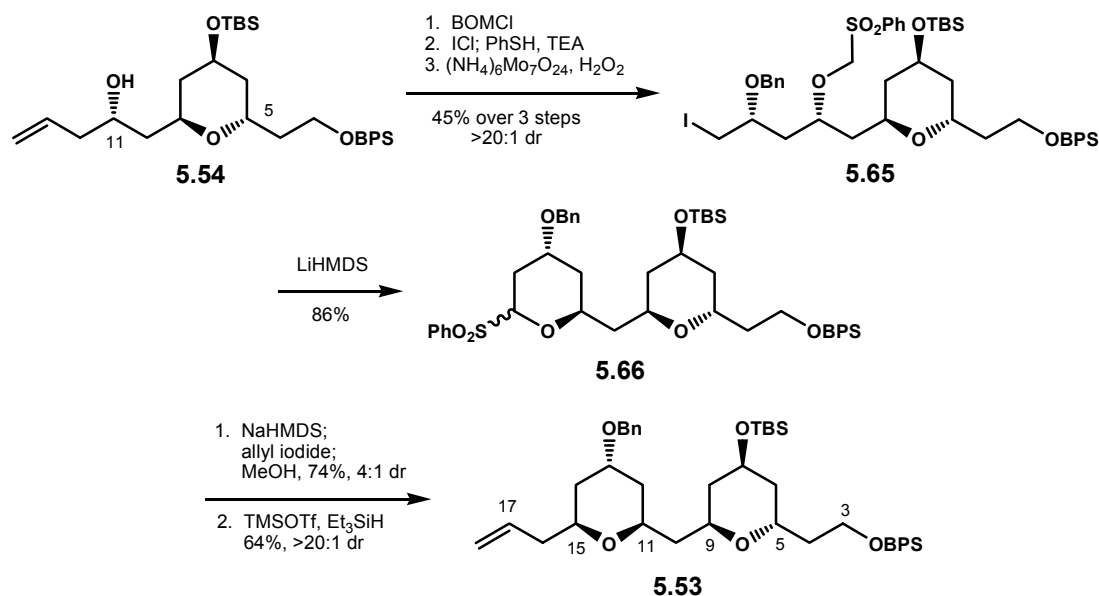


**Scheme 5.17**

Attempts to direct the aldehyde addition facial selectivity with a reagent-controlled allylation were unproductive. For example, when aldehyde **5.63** was subjected to Soderquist allylation method,<sup>261</sup> only a complex mixture was produced. Whereas the Roush's tartrate-allylborane reagent<sup>248</sup> afforded homoallylic alcohols **5.64** and **5.54** as a 1:2 mixture of diastereomers, Brown's allyl(Ipc)<sub>2</sub>borane<sup>142</sup> produced homoallylic alcohol **5.54** and **5.64** in the ratio of 5:1. Unfortunately, removal of Ipc alcohol byproduct turned out to be problematic with these conditions.

Homologation to the second tetrahydropyran fragment was then accomplished on homoallylic alcohol **5.54**. BOM protection, ether transfer, and oxidation reactions gave sulfonylether **5.65** in 45% yield over three steps as a single diastereomer, Scheme 5.18. The strength of the methodology is now clearly demonstrated by its applicability to complex substrates. Furthermore, the ether transfer reaction proceeded very smoothly, and remarkably, no material decomposition was detected despite the reactive nature of iodine monochloride. LiHMDS-promoted cyclization of **5.65** afforded the corresponding sulfonylpyran **5.66**, which was then subjected to the alkylation – reduction sequence. In

this complex substrate, alkylation of the intermediate sulfone anion proved slow under our initial conditions. However, after optimization, the alkylation product was isolated in 74% yield as a mixture of diastereomers. The completion to the synthesis of *bis*-tetrahydropyran fragment **5.53** was accomplished by a stereoselective reduction using TMSOTf and Et<sub>3</sub>SiH.



Scheme 5.18

#### 5.5.4.1. Optimizing The Alkylation Step

As mentioned earlier, alkylation of sulfonylpyran **5.66** proved problematic under the initial reaction conditions. Consequently, we were prompted to once again carry out another systematic reaction optimization. As shown in Table 5.6, entry 1, with our standard alkylation conditions, i.e. 3 eq. of NaHDMS and 4 eq. of allyl bromide, methyl pyranoside **5.67** was isolated only in 28% yield, and the remainder of the crude mixture

was unreacted starting material **5.66**. It is important to note that alkylation of sulfonylpyran **5.66** needed to be carried out in degassed toluene; otherwise, the sulfonylpyran anion **5.68** seemed to be readily oxidized in the presence of oxygen to conjugated carboxylic acid **5.69**. With a more reactive electrophile, allyl iodide, the yield moderately improved to 42%, entry 4. As expected, the use of LiHMDS and KHMDS did not lead to the production of the alkylation product, entries 2 – 3 and 4 – 5. Surprisingly, combined with much excess allyl iodide and 10 equivalents of NaHMDS, the alkylation of sulfonylpyran **5.66** afforded methyl pyranoside **5.67** in 74% yield.

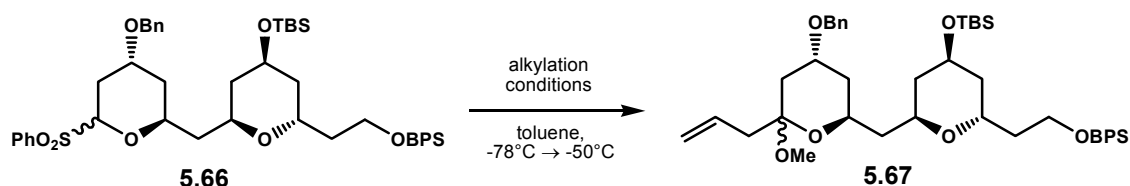


**TABLE 5.6**

Entry	Base	Eq.	Electrophile	Eq.	Yield
1	NaHMDS	3	allyl bromide	4	28%
2	LiHMDS	3	allyl bromide	4	no reaction
3	KHMDS	3	allyl bromide	4	no reaction
4	NaHMDS	3	allyl iodide	4	42%
5	LiHMDS	3	allyl iodide	4	no reaction
6	KHMDS	3	allyl iodide	4	no reaction
7	NaHMDS	3	allyl iodide	30	38%
8	NaHMDS	6	allyl iodide	30	42%
9	NaHMDS	10	allyl iodide	30	74%

One postulation that may explain this chemical behavior is the sulfonyl anion aggregation state. It is reasonable to propose that the corresponding anion resulting from deprotonation of sulfonylpyran **5.66** may have existed as an intramolecular aggregate as depicted in structure **5.68**. Henderson and co-workers have demonstrated from their elegant X-ray crystallography methods that the sodium salt of anomeric sulfone anion preferentially exists with the sodium cation tightly bound to the sulfonyl oxygen, thus leaving the anion as a true lone pair at the anomeric carbon center.<sup>360</sup> The sodium cation is known to possess strong chelating affinity to oxygen atoms, and this chelation effect is even more pronounced in non-polar solvents, such as toluene. Therefore, it is reasonable to suggest that in our sulfonylpyran anion system, under our initial reaction conditions, the sodium cation may have potentially chelated to the two tetrahydropyran rings and created aggregate **5.68** that may have prevented the alkylation to occur. This thought is further supported by the fact that the alkylation readily proceeded in the presence of much excess NaHMDS. It seems that the excess hexamethyldisilazide anion may have readily competed for aggregation with the bound sodium cation, and thus potentially breaking up aggregate **5.68**.

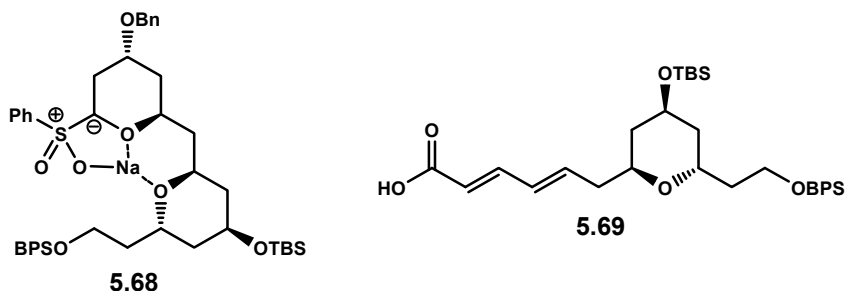
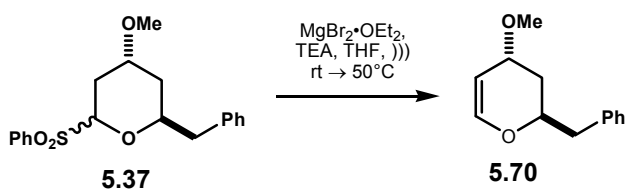


**Figure 5.5**

## 5.6. Stereoselective Synthesis of 2,6-*trans*-Disubstituted 3,4-Dihydropyran

So far, we have described our novel approach to tetrahydropyrans via a common three-step sequence. The first step includes our newly developed electrophile-induced ether transfer which produces either the cyanoether or sulfonylether; the second step is base-induced cyclization of the ether transfer adducts; and the final step involves functionalization of the corresponding anomeric cyanide or sulfone to the target tetrahydropyrans.

We imagined once again the utilization of this strategy to another class of oxygen heterocycles common to polyketides, 2,6-disubstituted 3,4-dihydropyran, by simply manipulating the functionalization sequence.<sup>239</sup> As described in Scheme 5.8, Ley and co-workers have shown that treatment of anomeric sulfone with  $\text{MgBr}_2 \cdot \text{OEt}_2$  and TEA mediated by ultrasound cleanly eliminated the sulfone functionality to the corresponding glycal.<sup>331</sup> In fact, when these conditions were applied to our sulfonylpyran **5.37**, glycal **5.70** was cleanly produced in 95% yield.



Scheme 5.19

Glycal **5.70** then served as our substrate to the target 2,6-disubstituted 3,4-dihydropyran **5.71** via Ferrier carbon rearrangement.<sup>361</sup> As demonstrated in Table 5.7, the

ionization of glycal **5.70** with TMSOTf in CH<sub>2</sub>Cl<sub>2</sub> at -78°C followed by addition of nucleophiles provided Ferrier rearrangement products **5.71** in excellent yields and diastereoselectivity. A variety of nucleophiles were tolerated in this reaction. When allylic silanes were used as nucleophiles, dihydropyrans **5.71a** and **5.71b** were produced in excellent yields and as a single diastereomer under both catalytic and stoichiometric amounts of TMSOTf (entries 1 – 3). Other nucleophiles such as organozinc, organotin (entries 4 – 6), and enol silanes (entries 7 and 8) also provided products **5.71c** – **5.71g** in high yields and diastereoselectivity. Interestingly, slight erosion in diastereoselectivity was observed with a bulkier nucleophile (entry 6).

However, when a silyl ketene acetal was employed, we were surprised to find that dihydropyran **5.71h** was produced in a 1:1 mixture of 2,6-*trans* and 2,6-*cis* diastereomers. Interestingly, when the activation was carried out with BF<sub>3</sub>•OEt<sub>2</sub> in toluene, diastereoselectivity slightly improved to 3.6:1 favoring the 2,6-*trans* stereochemistry (entries 9 and 10). The exact origin of this unexpected stereoselectivity is unclear to us, but it appears the high reactivity of enol silane clearly affects stereoselectivity. Similar observation has also been reported by Paterson and co-workers.<sup>362</sup> It is also important to note that with enol silanes and ketene acetals, three equivalents of Lewis acid were required for the reaction to achieve completion (entries 7 – 10). We speculated that the stronger Lewis basicity of the newly generated carbonyl group compared to that of ether readily competed for activation with the Lewis acid, thus preventing the ionization pathway.

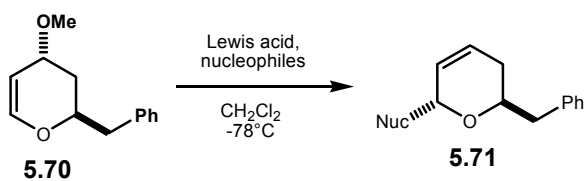


**TABLE 5.7**

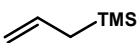
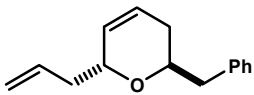
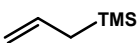
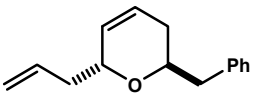
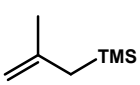
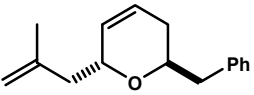
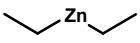
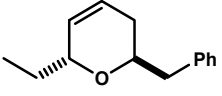
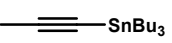
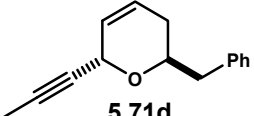
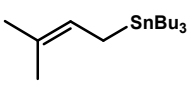
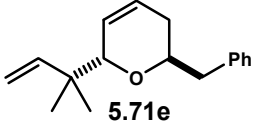
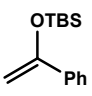
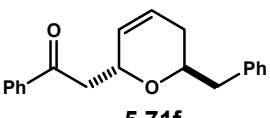
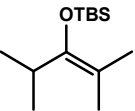
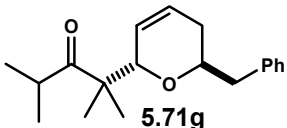
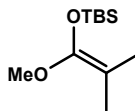
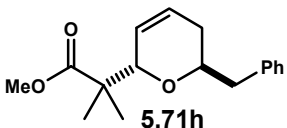
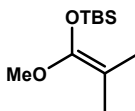
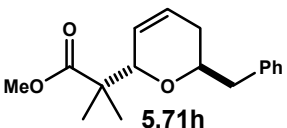
Entry	Lewis Acid	Eq.	Nucleophile	Product	Yield <sup>[a]</sup>	dr <sup>[b]</sup>
1	TMSOTf	2		 <b>5.71a</b>	91%	>20:1
2	TMSOTf	0.1		 <b>5.71a</b>	90%	>20:1
3	TMSOTf	2		 <b>5.71b</b>	91%	>20:1
4	TMSOTf	2		 <b>5.71c</b>	89%	>20:1
5	TMSOTf	2		 <b>5.71d</b>	96%	>20:1
6	TMSOTf	3		 <b>5.71e</b>	78%	10:1
7	TMSOTf	3		 <b>5.71f</b>	96%	>20:1



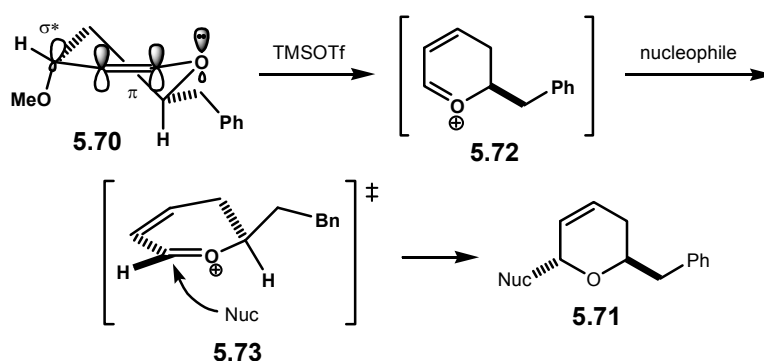
TABLE 5.7 – continued

Entry	Lewis Acid	Eq.	Nucleophile	Product	Yield <sup>[a]</sup>	dr <sup>[b]</sup>
8	TMSOTf	3		 <b>5.71g</b>	95%	>20:1
9	TMSOTf	3		 <b>5.71h</b>	41% <sup>[c]</sup>	1:1
10	BF <sub>3</sub> •OEt <sub>2</sub> <sup>[d]</sup>	3		 <b>5.71h</b>	67% <sup>[e]</sup>	3.6:1

[a] Yield was reported from the isolation of major diastereomer. [b] Diastereomeric ratio was determined by <sup>1</sup>H NMR integration of the crude reaction mixture. [c] The minor 2,6-*cis* diastereomer was isolated in 40% yield. [d] The reaction was carried out in toluene. [e] The minor 2,6-*cis* diastereomer was isolated in 15% yield.

In the classic Ferrier rearrangement, an allylic acetate, mesylate, or tosylate is typically employed as the functionality for activation. In fact, to our knowledge, the use of a secondary allylic ether for this purpose is not preceded most likely due to its poor leaving group ability and the fact that its relatively weak Lewis basicity may cause slow, inefficient ionization. However, surprisingly in our case, it appeared glycol **5.70** readily underwent rapid ionization. We observed that our Ferrier reaction essentially went to completion as soon as the Lewis acid was added to the reaction mixture. This unusually rapid ionization of the allylic ether may have been facilitated by the pseudoaxial orientation of the methoxy group where the C–OMe  $\sigma$  anti-bonding orbital is oriented relatively parallel to the rearranging  $\pi$  system. The conformation of dihydropyran **5.70**

was deduced by  $^1\text{H}$  NMR coupling-constant analysis. The 2,6-*trans* stereochemistry is presumably assembled via subsequent axial delivery of nucleophiles to the newly generated oxocarbenium ion **5.72** upon activation as depicted in transition state **5.73**. Based on the observation where diastereoselectivity eroded with bulkier nucleophiles, we proposed that a contact-ion pair system may have been involved which could potentially hinder axial delivery of such nucleophiles.

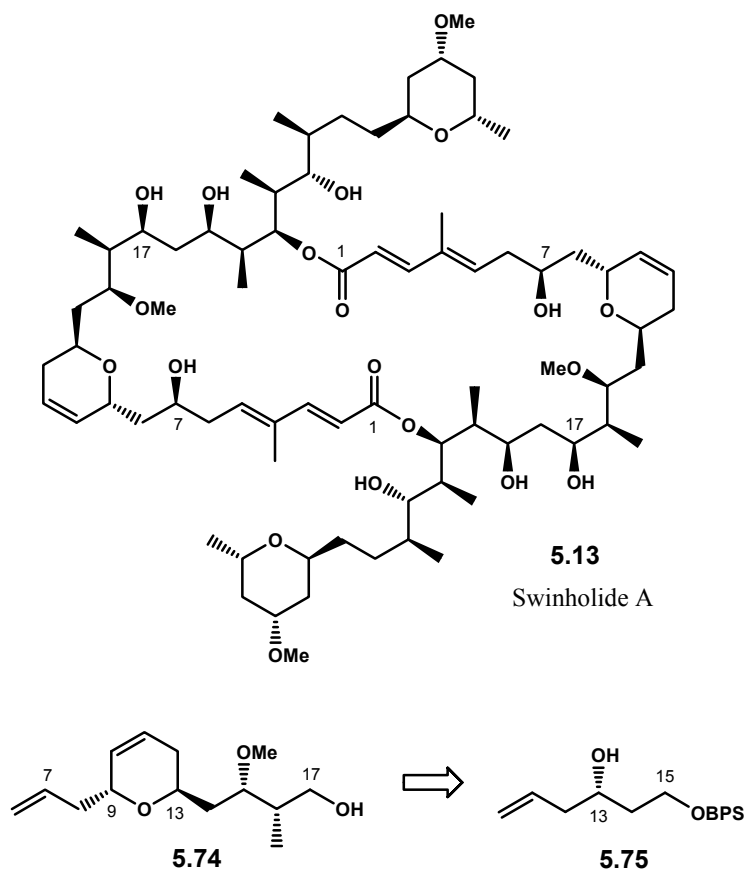


**Scheme 5.20**

### 5.6.1. Stereoselective Synthesis of C7-C17 Fragment of Swinholide A

Once again, to demonstrate that our method is applicable to complex molecule syntheses, we decided to pursue swinholide A **5.13**, particularly the C7 – C17 dihydropyran region. Swinholide A **5.13** is one of several examples of biologically important polyketides containing a 2,6-*trans*-disubstituted 3,4-dihydropyran ring.<sup>313, 363-366</sup> There are two completed total synthesis of this molecule independently reported by Paterson<sup>362, 367-375</sup> and Nicolaou<sup>376-379</sup> groups. Our target fragment is represented as structure **5.74**, a synthetic intermediate that was previously utilized in Nicolaou's route.

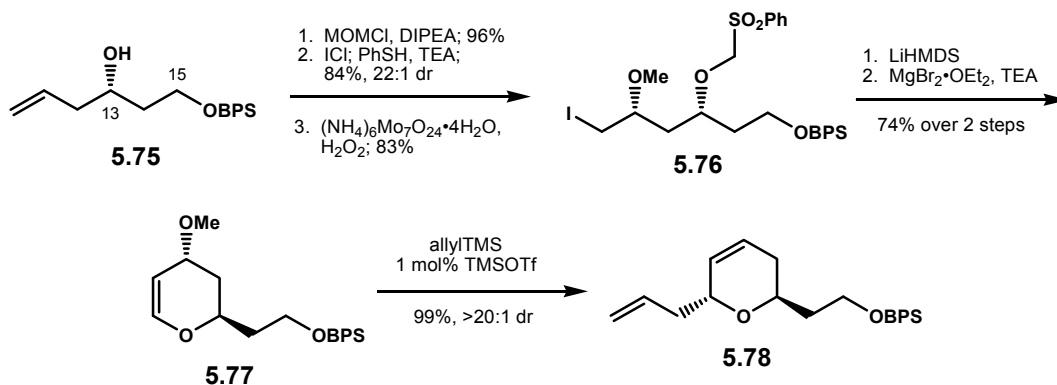
As shown in Scheme 5.21, as an alternative to Nicolaou's approach, our synthetic sequence to fragment **5.74** will begin with readily accessible, enantiomerically pure homoallylic alcohol **5.75**.<sup>358</sup>



Scheme 5.21

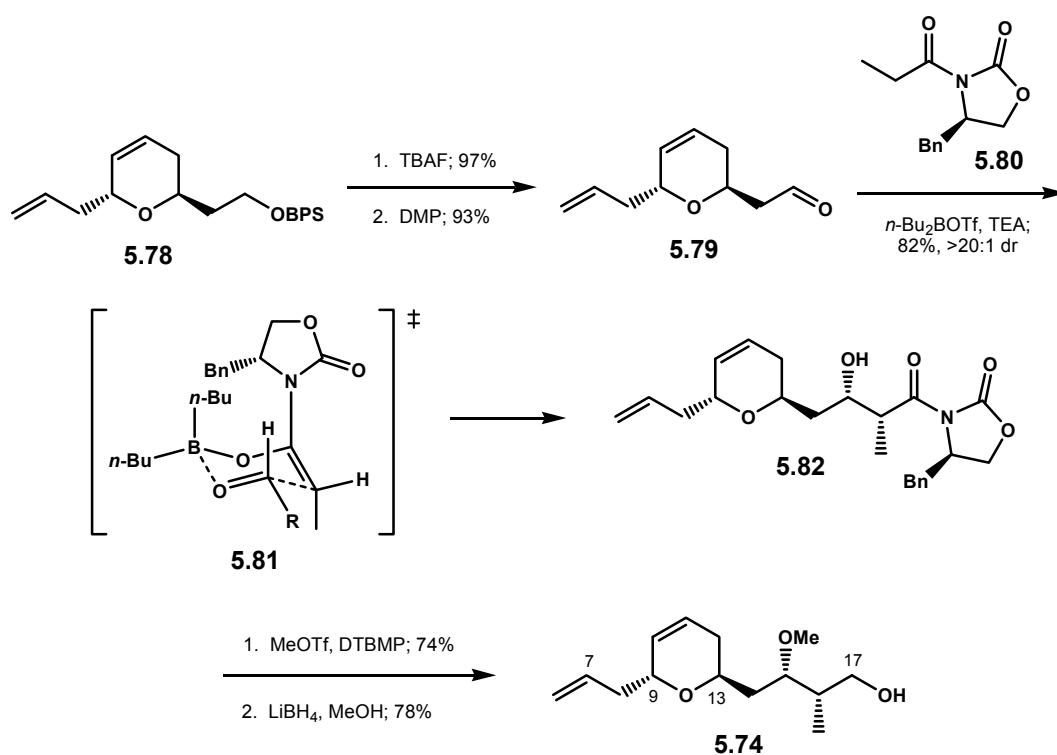
We began the synthesis of target molecule **5.74** with our familiar sequence, starting with protecting alcohol **5.75** as a MOM ether, the ether transfer reaction with thiophenol – triethylamine workup, and sulfide oxidation. As a result, sulfonylether **5.76** was produced in good yield with high 1,3-*syn* stereocontrol. LiHMDS-mediated cyclization followed by elimination of the anomeric sulfone under  $\text{MgBr}_2 \cdot \text{OEt}_2$  and TEA

afforded 2,3-dihydropyran **5.77** in 76% yield over two steps. Exposure of **5.77** to the optimized Ferrier reaction conditions with allyltrimethylsilane and very low catalyst loading of TMSOTf produced 3,4-dihydropyran **5.78** in essentially quantitative yield and as a single diastereomer.



**Scheme 5.22**

As shown in Scheme 5.23, the removal of the BPS ether with TBAF then unmasked the primary alcohol which was then oxidized with Dess-Martin periodinane<sup>87</sup> to aldehyde **5.79**. Both steps proceeded in high yields. Aldehyde **5.79** was then subjected to a boron-mediated aldol reaction with oxazolidinone **5.80** under the Evans' protocol which installed the requisite propionate functionality in 82% yield.<sup>380</sup> The transition state accounted for the observed stereoselectivity is proposed through a Zimmerman-Traxler model **5.81**. Subsequent *O*-methylation with MeOTf and DTBMP<sup>138</sup> followed by reductive removal of the auxiliary under  $\text{LiBH}_4$  conditions completed our concise synthetic route to dihydropyran **5.74**. The spectroscopic analyses of this molecule were in complete agreement to those reported by Nicolaou and co-workers.<sup>376</sup>



**Scheme 5.23**

## 5.7. Conclusion

This chapter details the production of oxygen-containing heterocycles, including 2,4,6-trisubstituted-tetrahydropyrans and 2,6-disubstituted-3,4-dihydropyrans via a common three-step sequence: ether transfer reaction, cyclization, and functionalization reactions. Installed in the ether transfer step, the roles of anomeric cyanide and sulfone were then investigated. We found that manipulation of the anomeric cyanide and sulfone could be exploited for the production of 4-alkoxy-2,6-*cis*-disubstituted tetrahydropyran via an alkylation – reduction sequence; whereas, the use of anomeric sulfone in a direct substitution reaction provided access to the stereocomplementary 4-alkoxy-2,6-*trans*-disubstituted tetrahydropyrans. Conversion of the sulfonylpyran to the corresponding

glycal then set up the 2,6-*trans*-disubstituted-3,4-dihydropyrans via an unprecedented Ferrier rearrangement of a secondary allylic ether. These strategies were then applied to the synthesis of complex molecules, such as the C3 – C17 fragment of Phorboxazole A and the C7 – C17 fragment of Swinholide A.

## CHAPTER SIX

### CONCISE ENANTIOSELECTIVE TOTAL SYNTHESIS OF NEOPELTOLIDE MACROLACTONE

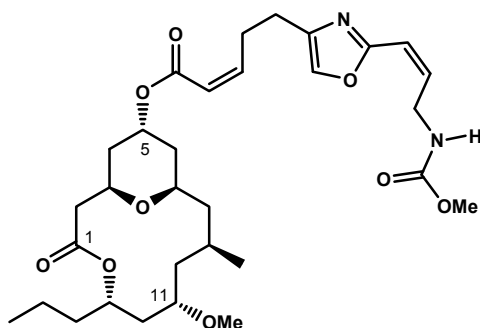
#### 6.1. Purpose

The purpose of this chapter is to detail the synthetic study towards cytotoxic macrolide neopeltolide, particularly its macrolactone core. The total synthesis will be approached from a linear strategy which employs the sequential electrophile-induced ether transfer, functionalization, and radical cyclization reactions to stereoselectively construct the requisite tetrahydropyran segment. The current strategy is highlighted by concisely 14 steps in the longest linear sequence, 15 steps overall, from commercially available materials. In addition, our route is free of discreet steps for protecting group manipulation, thus representing a rare example in polyketide synthesis

#### 6.2. Neopeltolide

Neopeltolide **6.1** is a cytotoxic macrolide, most likely of cyanobacterial origin, isolated from a deepwater sponge of the family Neopeltidae collected off the north

Jamaican coast, and the report was published by Wright and co-workers in 2007.<sup>121</sup> Neopeltolide was found to exhibit interesting biological activities. In addition to being antifungal against *Candida albicans* with an MIC value of 0.62  $\mu\text{g/mL}$ , the macrolide was cytotoxic against several cancer lines, including P388 murine leukemia, A-549 human lung adenocarcinoma, and NCI-ADR-RES human ovarian sarcoma, with their respective  $\text{IC}_{50}$  values of 0.56, 1.2, and 5.1 nM. Neopeltolide also showed strong cytostatic inhibitory effects against PANC-1 pancreatic and DLD-1 colorectal cell lines.<sup>121</sup> Because of this interesting wide array of biological properties, neopeltolide has been subjected to six total syntheses, independently by Panek,<sup>123</sup> Scheidt,<sup>124</sup> Lee,<sup>125</sup> Maier,<sup>126</sup> Sasaki,<sup>127</sup> and Kozmin.<sup>122</sup> The descriptions of these approaches are fully described in Chapter One, Section 1.10



**6.1**

neopeltolide

**Figure 6.1**



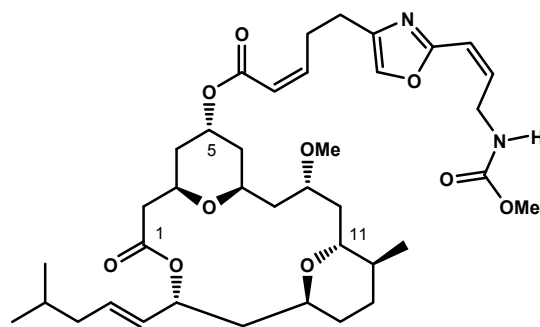
### 6.2.1. Mode of Action

Kozmin and co-workers have recently elucidated the mode of action of neopeltolide.<sup>122</sup> Through their systematic biochemical assays, neopeltolide appeared to inhibit electron transports in the mitochondrial ATP synthesis with cytochrome *bc*<sub>1</sub> as the primary molecular target. This proposal was supported by evidence which indicated that treatment of isolated mitochondria with neopeltolide resulted in dose-dependent inhibition of cytochrome *bc*<sub>1</sub> with an IC<sub>50</sub> value of 0.6 nM. Furthermore, with a purified bovine heart mitochondrial *bc*<sub>1</sub> complex, the inhibition was recorded at IC<sub>50</sub> 2.0 nM.

### 6.2.2. Structural Resemblance to Leucascandrolide A

Neopeltolide appears to share a close structural similarity to a completely unrelated macrolide, isolation-wise, leucascandrolide A **6.2**.<sup>94</sup> In addition to the 2,4,6-trisubstituted tetrahydropyran ring embedded within the C3 – C7 segment, neopeltolide is also decorated at the C5 position by an oxazole carbamate side chain, identical to that of leucascandrolide A. The major structural differences between these two macrolides lie in the functionality within the macrolactone ring; leucascandrolide A possesses an additional tetrahydropyran ring, which is absent in neopeltolide. The position of the methyl substitution is also noteworthy. In leucascandrolide A, the methyl group is located at C12, which represents a common propionate subunit typical in polyketide natural products. However, in neopeltolide A, this methyl substitution appears at C9; this exemplifies a unique variant to the common pattern in polyketide biogenesis. The

incorporation of methyl substitution at odd-number carbons has been proposed due to an HMG-CoA synthase embedded in the PKS gene cluster.<sup>423</sup> This unique structural feature presumably evolved to create additional conformational and structural diversity.



**6.2**

leucascandrolide A

**Figure 6.2**

### 6.2.3. Molecular Compartments Responsible for the Observed Biological Activities

As described in Chapter One, Section 1.9, leucascandrolide A possesses interesting biological properties. In addition to the natural product being cytotoxic and antifungal, further biological analyses revealed that the cytotoxicity and antifungal activity of leucascandrolide A may have been contributed respectively by the different molecular compartments of the natural product as suggested by the following experimental evidence.<sup>94</sup> Leucascandrolide A macrolactone **6.3** and oxazole carbamate methyl ester **6.4**, generated upon exposure of the natural product to base-promoted methanolysis, were proved cytotoxic at the level of 0.5 – 10  $\mu\text{g/mL}$ , only ten fold less

potent than the parent natural product. However, it appeared that only oxazole carbamate **6.4** was found active in the antifungal assays.

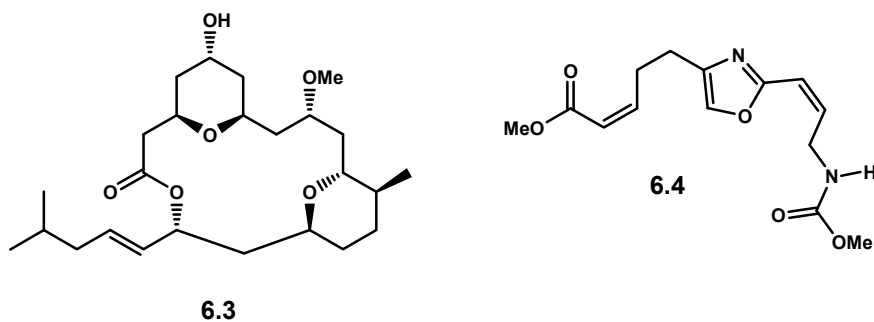


Figure 6.3

Based on the clearly similar structural and biological properties of leucascandrolide A and neopeltolide, we hypothesize that neopeltolide macrolactone **6.5** may be the cytotoxic compartment of the natural product. If this hypothesis is justified, the need for the oxazole carbamate side chain installed in the neopeltolide macrolactone would be insignificant, thus greatly simplifying neopeltolide's structural complexity planned for our future structure- and conformation-activity-relationship studies.

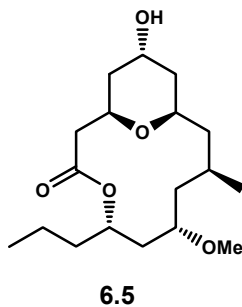
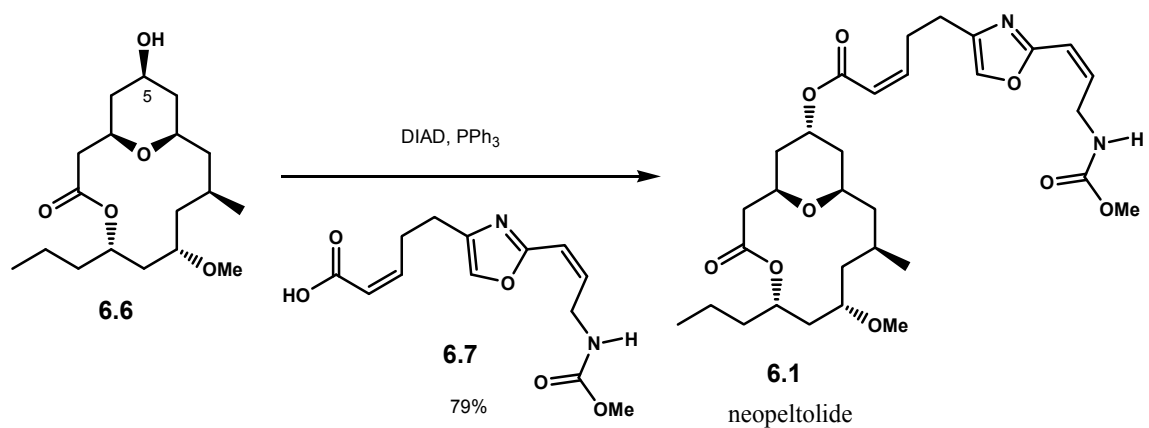


Figure 6.4

#### 6.2.4. Neopeltolide C5-Epimer

Despite the fact that six different routes have been established for the synthesis of neopeltolide, five of these approaches provided the equatorial C5-epimer macrolactone **6.6**.<sup>122, 124-127</sup> This hydroxyl stereochemistry was eventually inverted upon incorporation of oxazole carbamate acid **6.7** using the method of Mitsunobu. Obviously, neopeltolide C5-epimer macrolactone **6.6** would be an inappropriate substrate for the justification of our hypothesis.

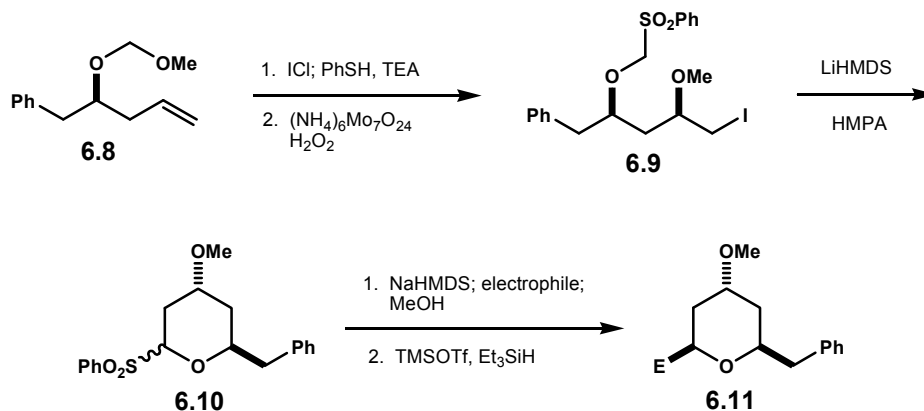


Scheme 6.1

The only strategy which directly accessed the natural stereochemistry of neopeltolide macrolactone **6.5** was developed by Panek.<sup>123</sup> However, this route was fairly lengthy; the longest linear sequence was 17 steps with 24 overall steps from commercially available starting materials.

### 6.3. Limitation of Sulfonylpyran-Based Methodology

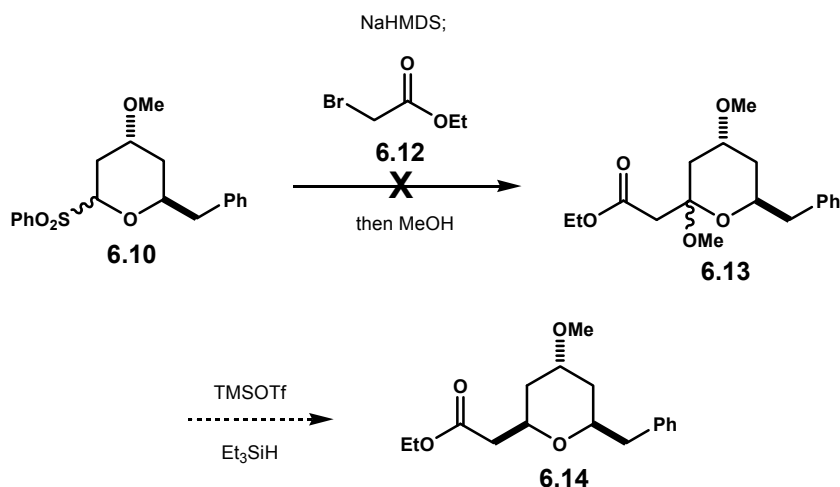
We initially planned to utilize our preexisting tetrahydropyran methodology as described in Chapter Five, Section 5.5.2, to construct neopeltolide's 2,4,6-trisubstituted tetrahydropyran ring.<sup>238</sup> This methodology was highlighted by the electrophile-induced ether transfer of simple homoallylic alkoxyethyl ether **6.8** to the corresponding sulfonyl ether **6.9**. Cyclization to sulfonylpyran **6.10** and subsequent functionalization which involved a sequence of alkylation – reduction reactions should provide 2,6-*cis*-4-alkoxy tetrahydropyran **6.11**.



Scheme 6.2

In order to directly install the requisite oxidation state at C1 in neopeltolide, methyl 2-bromo-acetate **6.12** needed to be employed as the electrophilic partner in the functionalization reaction. Unfortunately, in a model study as shown in Scheme 6.3, when this electrophile was added to a solution of the sodium salt of sulfonylpyran anion of **6.10**, the coupling reaction failed to produce the target methyl pyranoside **6.13** as only

starting material was quantitatively recovered upon workup. It was not clear whether the sulfonylpyran anion had failed to displace the bromide or readily undergone intermolecular proton transfer with the electrophile.

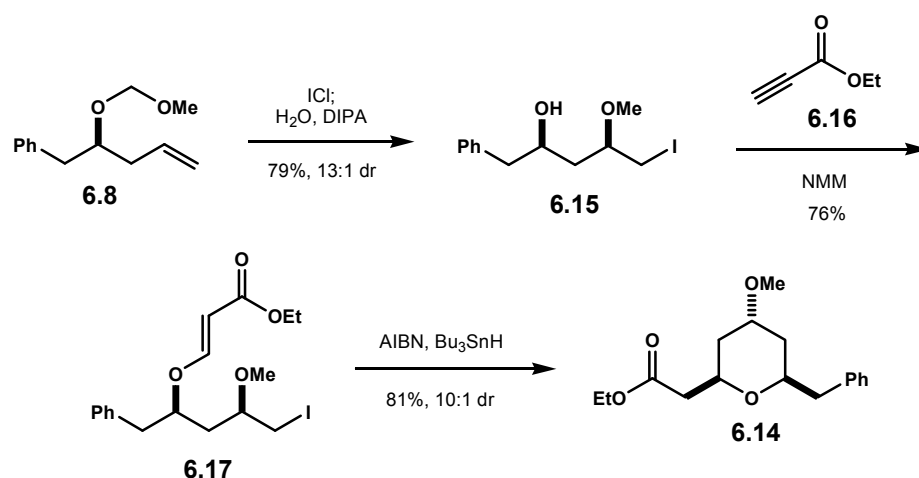


**Scheme 6.3**

### 6.3.1. Alternative Sequence to 2,6-*cis*-Tetrahydropyran

To circumvent the problematic alkylation step, we envisioned a possible solution by simply reorganizing the synthetic sequence for the production this stereochemically rich tetrahydropyran. The proposed sequence would begin with the ether transfer reaction which is followed by functionalization and then cyclization. As demonstrated by an undergraduate researcher in our laboratories, Thomas Gruffi, exposure of homoallylic MOM ether **6.8** to ICl successfully produced the intended ether transfer product **6.15** in 79% yield with a diastereomeric ratio of 13:1.<sup>236</sup> The functionalization step was then realized with the utilization of ethyl propiolate **6.16**. Under a catalytic amount of NMM,

ether transfer adduct **6.8** readily underwent Michael addition to ethyl propiolate which yielded  $\beta$ -alkoxyacrylate **6.17** in 76% yield.<sup>381</sup> Radical promoted cyclization of this material affected by AIBN and Bu<sub>3</sub>SnH in refluxing toluene successfully produced the target tetrahydropyran **6.14** in 81% as a 10:1 mixture of diastereomers, Scheme 6.5.<sup>382</sup> Based on the promising result with this model study, we then implemented the strategy to the construction of 2,4,6-trisubstituted tetrahydropyran core of neopeltolide.

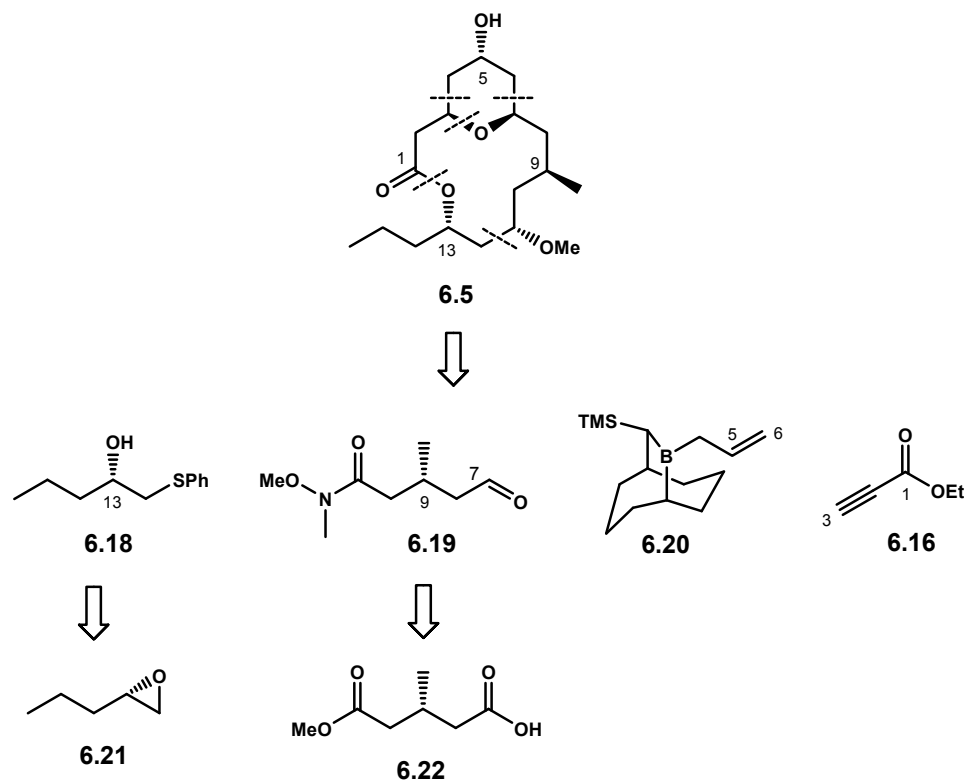


Scheme 6.4

#### 6.4. Retrosynthesis

Our retrosynthetic analysis to neopeltolide was designed such that the numbers of unavoidable oxidation – reduction sequences and protecting group manipulations were minimal. We proposed strategic bond disconnections as depicted in Scheme 6.2 which resulted in four synthetic segments:  $\beta$ -hydroxy sulfide **6.18**, aldehyde **6.19**, chiral allylborane **6.20**, and ethyl propiolate **6.16**.  $\beta$ -Hydroxy sulfide **6.18** and aldehyde **6.19**

should be readily accessible respectively from commercially available materials (*S*)-2-propyloxirane **6.21** and (*R*)-3-((methoxycarbonyl)methyl)butanoic acid **6.22**.



**Scheme 6.5**

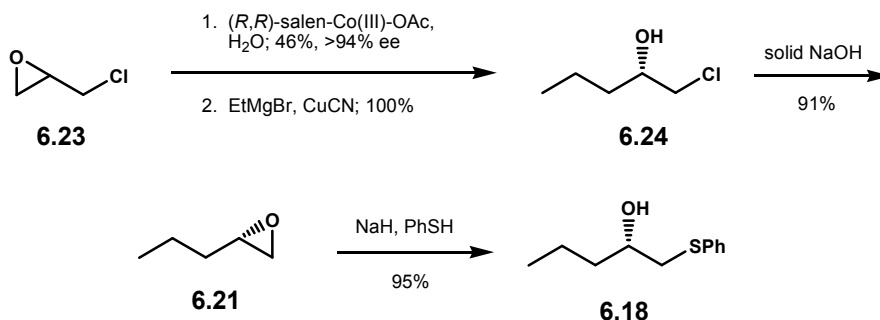
These fragments would be installed in a linear fashion with ethyl propiolate **6.16** serving as a lynchpin for the macrolactonization. The stereoselective construction of the tetrahydropyran segment would be highlighted by our electrophile-induced ether transfer strategy, similar to that presented in Scheme 6.4. Additionally, the installation of  $\beta$ -hydroxy sulfide **6.18** would be affected by a reductive method newly developed by Rychnovsky,<sup>383</sup> and late-stage Yamaguchi macrolactonization<sup>69</sup> would then complete the



total synthesis. Our route as outlined in this chapter would produce neopeltolide macrolactone **6.5** in just 14 steps in the longest linear sequence and 15 steps overall.

### 6.5. Preparation of $\beta$ -Hydroxy Sulfide **6.18**

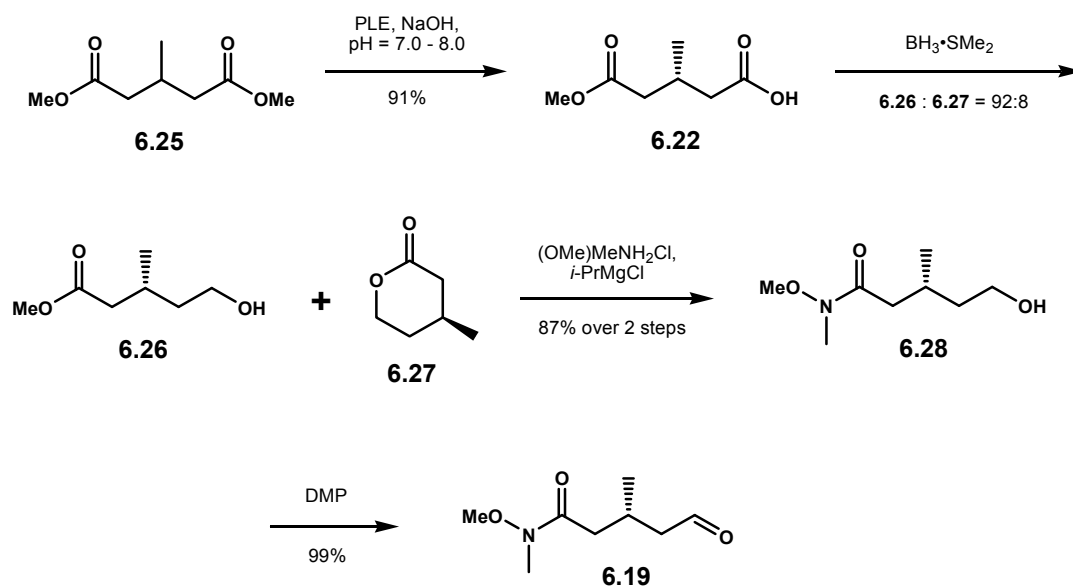
We began our synthetic endeavor to neopeltolide by preparing the requisite synthetic fragments. The synthesis of  $\beta$ -hydroxy sulfide **6.18** began with (*S*)-2-propyloxirane **6.21**. Although this epoxide is commercially available, multigram scale preparation of this material can be readily accessible very inexpensively from racemic epichlorohydrin **6.23** in just several steps.<sup>384</sup> As shown in Scheme 6.6, hydrolytic kinetic resolution of epichlorohydrin mediated by Jacobson's catalyst<sup>273</sup> followed by regioselective addition of ethylmagnesium bromide provided chlorohydrin **6.24**. Exposure to sodium hydroxide then yielded epoxide **6.21**. The ensuing regioselective addition of sodium thiophenoxide to this epoxide cleanly afforded  $\beta$ -hydroxy sulfide **6.18** in excellent yield.



Scheme 6.6

## 6.6. Preparation of Aldehyde 6.19

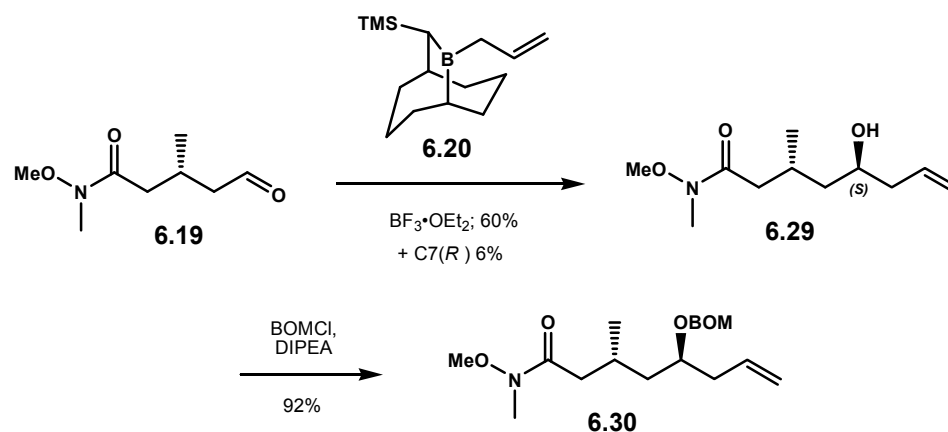
Aldehyde **6.19** was conveniently prepared from (*R*)-3-((methoxycarbonyl)methyl)butanoic acid **6.22**. Despite the commercial availability of this chiral pool, accessibility to this compound particularly in a large quantity was found more cost-efficient by employing stereoselective enzymatic hydrolysis of its precursor dimethyl-3-methylglutarate **6.25** with pig liver esterase (PLE).<sup>385</sup> Subsequent chemoselective reduction of acid **6.22** with borane dimethylsulfide complex produced a mixture of the desired alcohol **6.26** and the corresponding lactone **6.27** in a ratio of 92:8. This product mixture was found inconsequential for the ensuing installation of the Weinreb amide moiety as alcohol **6.28** was cleanly produced in 87% yield over two steps.<sup>136</sup> Finally, Dess-Martin oxidation of this alcohol then furnished aldehyde **6.19** in near quantitative yield, Scheme 6.7.<sup>87</sup>



Scheme 6.7

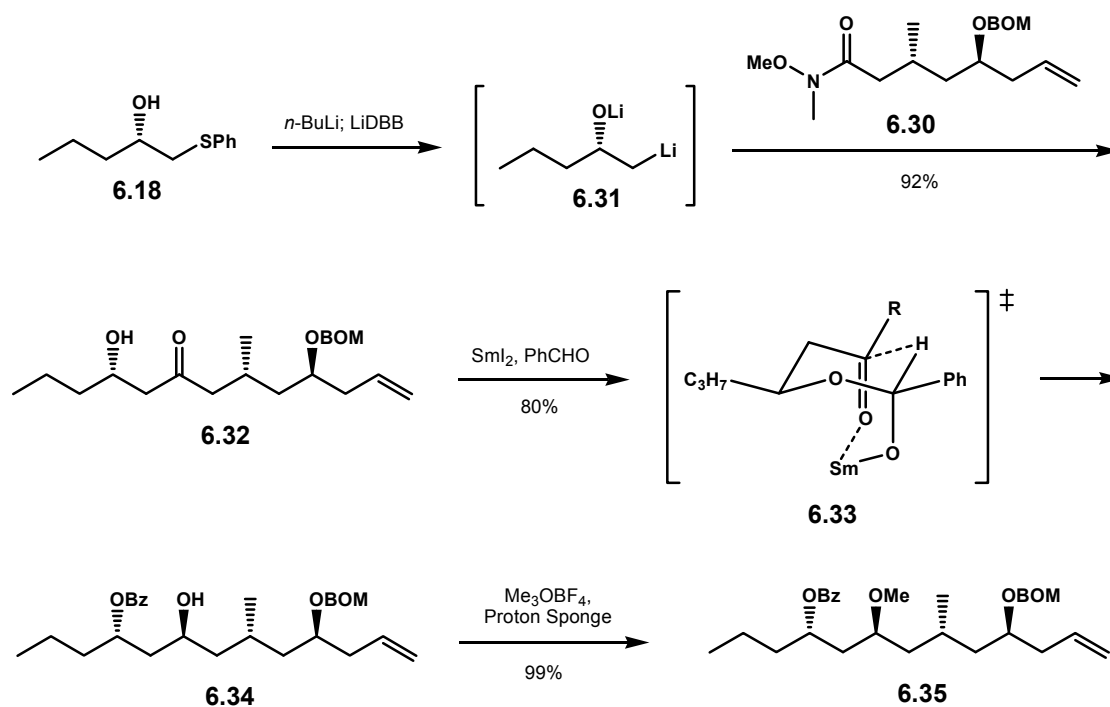
## 6.7. Segments Coupling

Amide-aldehyde **6.19** represents an interesting synthetic intermediate due to its dual electrophilic sites; however, they exhibit an appreciable difference in reactivity. By exploiting the more electrophilic aldehyde functionality, asymmetric allylation should set the C7 stereochemistry necessary for neopeltolide macrolactone. Upon screening a variety of allylation methods as performed by Thomas Gruffi, an undergraduate researcher in our laboratories, the transformation to homoallylic alcohol **6.29** was found most effective with Soderquist's chiral bicyclodecane-allylborane reagent **6.20**.<sup>261</sup> Under a modified reaction condition which included an introduction of  $\text{BF}_3 \cdot \text{OEt}_2$  in a stoichiometric amount, homoallylic alcohol **6.29** was readily isolated in 60% and its diastereomer C7(*R*) in 6% yield. This external Lewis acid was found necessary to sequester the much stronger Lewis basic Weinreb amide functionality. Homoallylic alcohol **6.29** was then readily converted to the corresponding benzyloxymethyl ether via treatment with BOMCl in the presence of DIPEA. Although this conversion appeared as a protecting group manipulation step, the BOM ether would actually serve as a substrate for the upcoming ether transfer reaction.



Scheme 6.8

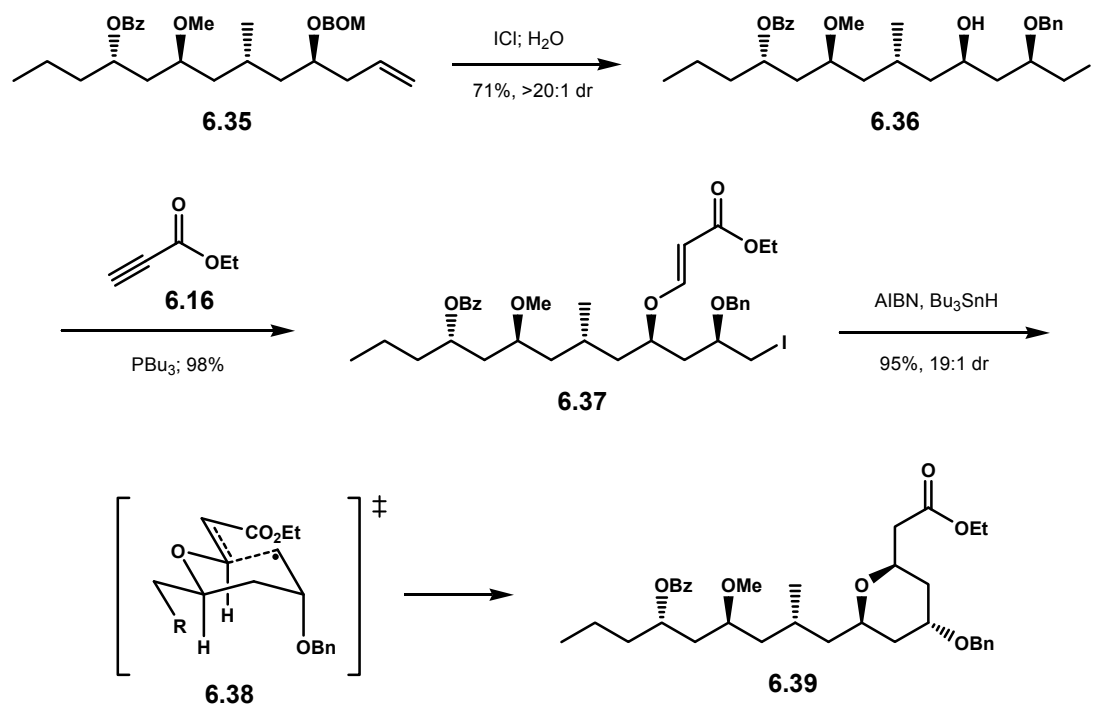
With homoallylic BOM ether **6.30** in hand, we then turned our attention to the incorporation of the C12 – C17 segment via the utilization of  $\beta$ -hydroxy sulfide **6.18**. Based on the methodology developed by Rychnovsky, deprotonation of **6.18** with *n*-BuLi followed by *in situ* reduction of the phenyl sulfide with LiDBB provided dilithium species **6.31** which added very smoothly to the Weinreb amide.<sup>383</sup> The utilization of this strategy allowed the generation of  $\beta$ -hydroxy ketone **6.32** in 92% yield without the necessity for protection at the C13 hydroxyl. Exposure of this adduct to SmI<sub>2</sub> in the presence of benzaldehyde successfully yielded the Evans-Tischenko 1,3-*anti* reduction product **6.34** in 80% yield with C13 hydroxyl readily differentiated as a benzoate ester.<sup>91</sup> The migration of C13 benzoate ester to C11 hydroxyl, however, was found facile, such that upon isolation of **6.34**, immediate methylation of the remaining C11 hydroxy group was necessary. With Meerwein's salt in the presence of Proton Sponge,<sup>92</sup> advanced intermediate **6.35** was produced in near quantitative yield, Scheme 6.9.



Scheme 6.9

## 6.8. Construction of 2,4,6-Trisubstituted-Tetrahydropyran Core

Advanced homoallylic BOM ether **6.35** served as our substrate for the key ether transfer, functionalization, and cyclization sequence to the intended tetrahydropyran ring. As expected, treatment of **6.35** with  $\text{ICl}$  readily produced the corresponding ether transfer adduct **6.36** in 71% yield as a single diastereomer fully elaborated with five contiguous stereogenic centers.<sup>236</sup> To complete the carbon skeleton of neopeltolide macrolactone, alcohol **6.36** was then subjected to a Michael reaction with ethyl propiolate **6.16** to yield  $\beta$ -alkoxyacrylate **6.37**.



Scheme 6.10

In contrast to what was observed with a model study as shown in Scheme 6.5, this conjugate addition reaction proved very challenging as the alternative five-membered cyclization event to tetrahydrofuran **6.40** was highly competitive under the established protocol with NMM.<sup>381</sup> Much to our annoyance, this undesired product was not separable from the intended  $\beta$ -alkoxyacrylate **6.37** by the means of chromatography. In addition, the use of other amine promoters, such as DMAP, DABCO, or TEA also resulted exclusively in the production of **6.40** as the major product regardless the choice of solvents. In fact, ether transfer adduct **6.36** in the absence of ethyl propiolate **6.16** underwent rapid cyclization to tetrahydrofuran **6.40** with these amines.

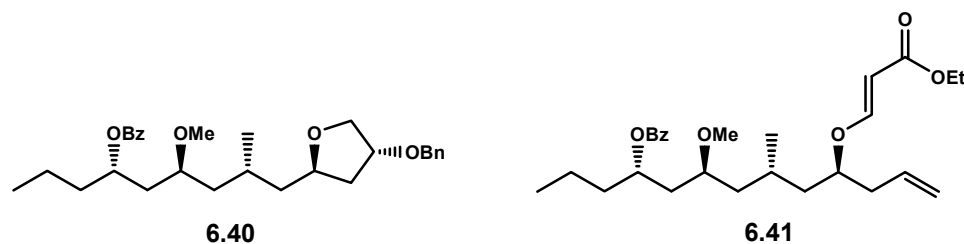


**Figure 6.5**

As an alternative Michael promoter, Inanaga and co-workers have reported the use of a catalytic amount of  $\text{PBU}_3$  for rapid conjugate addition of alcohols to propiolate ester.<sup>386</sup> However, when these conditions were applied to our substrate **6.36**, it appeared that the starting material was never completely consumed, suggesting that the catalytic cycle had been sequestered. This observation consequently led us to believe that the use of a stoichiometric amount of  $\text{PBU}_3$  might become necessary.

The first stage of the optimization process involved screening of solvents for the Michael reaction. As shown in Table 6.1, entries 1 – 3, the increasing solvent polarity induced predominantly the formation of tetrahydrofuran **6.40**. However, in non-polar solvents, such as toluene or methylene chloride, the formation of  $\beta$ -alkoxyacrylate **6.37** appeared favorable and competitive.

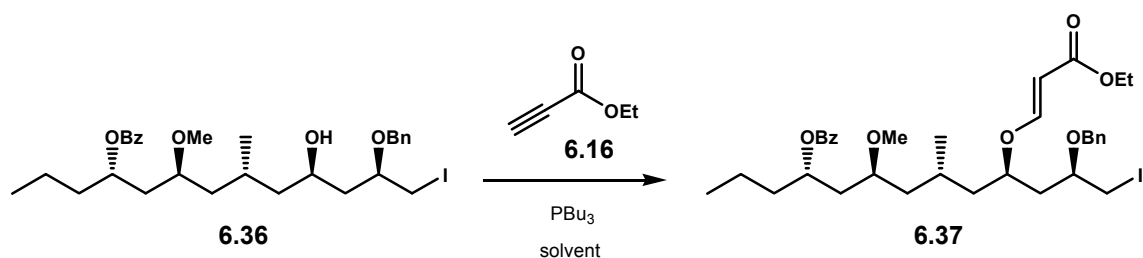


TABLE 6.1<sup>[a]</sup>

Entry	Solvent	6.37 : 6.40
1	ether	1:1
2	THF	1:2
3	DMF	0:1
4	toluene	1:1
5	CH <sub>2</sub> Cl <sub>2</sub>	2:1

[a] Typical reaction conditions: PBu<sub>3</sub> (3.0 eq., neat) was added in one injection to a solution containing ether transfer adduct **6.36** and ethyl propiolate **6.16** (3.0 eq.) and stirred until completion.

Having identified that methylene chloride might provide the best ratio for addition vs. cyclization products **6.37** and **6.40** respectively, the optimization process then continued with screening the order of addition of reagents, which was eventually proven significant. When a solution of PBu<sub>3</sub> (0.5 M in CH<sub>2</sub>Cl<sub>2</sub>) was added dropwise over 30 minutes to a solution containing ethyl propiolate and ether transfer product **6.36**, the reaction mixture gave predominantly tetrahydrofuran **6.40**. A similar result was observed when a premixed solution of ethyl propiolate and PBu<sub>3</sub> was added dropwise to a solution of starting material **6.36**. An introduction of ethyl propiolate (0.5 M in CH<sub>2</sub>Cl<sub>2</sub>) to a solution of **6.35** and PBu<sub>3</sub>, in contrast, produced primarily β-alkoxyacrylate **6.37** (50%) however, with significant contamination from retro-ether transfer **6.41** (35%) presumably



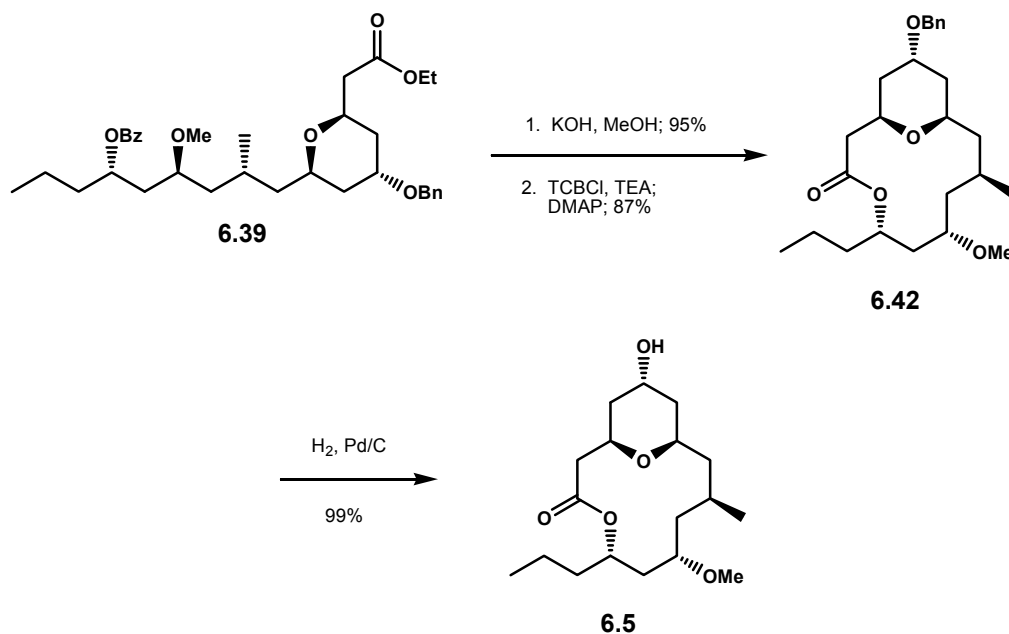
produced upon a competitive nucleophilic attack of excess  $\text{PBU}_3$  to the primary iodide. Fortunately, the product ratio significantly improved when separate solutions of ethyl propiolate and  $\text{PBU}_3$  were added simultaneously via a syringe pump into a solution of substrate **6.36** over 30 minutes. These conditions not only did minimize the formation of tetrahydrofuran **6.40**, but also retro-ether transfer **6.41** to give exclusively the desired  $\beta$ -alkoxyacrylate **6.37** in 98% yield.

With cyclization precursor **6.37** in hand, construction of the 2,6-*cis* tetrahydropyran moiety was realized under radical conditions. As preceded by Lee,<sup>387</sup> the utilization of EPHP and  $\text{Et}_3\text{B}$  in ethanol cleanly provided the corresponding 2,6-*cis* tetrahydropyran **6.39**, as a single diastereomer, presumably via a chair-like transition state **6.38**. However, this method yielded **6.39** in varying yields: 30 – 80%. Alternatively, the radical cyclization was also readily promoted by AIBN and  $\text{Bu}_3\text{SnH}$  in refluxing toluene.<sup>382</sup> These conditions gratifyingly afforded **6.39** in 95% yield as a 19:1 mixture of diastereomers, Scheme 6.10.

## 6.9. Endgame Strategy

The endgame strategy to neopeltolide macrolactone **6.5** was straightforward. Exposure of **6.39** to KOH in MeOH readily saponified the ethyl ester functionality and at the same time cleaved the C13 benzoate ester. The resulting seco acid was then activated with TCBCl in the presence of TEA to the corresponding mixed anhydride which readily underwent intramolecular cyclization to the macrolactone **6.42** upon introduction of DMAP in 87% yield.<sup>69</sup> Subsequent removal of the benzyl ether proceeded efficiently

under hydrogenolysis conditions which quantitatively unmasked the C5 hydroxyl group, thus completing the total synthesis of neopeltolide macrolactone **6.5**.

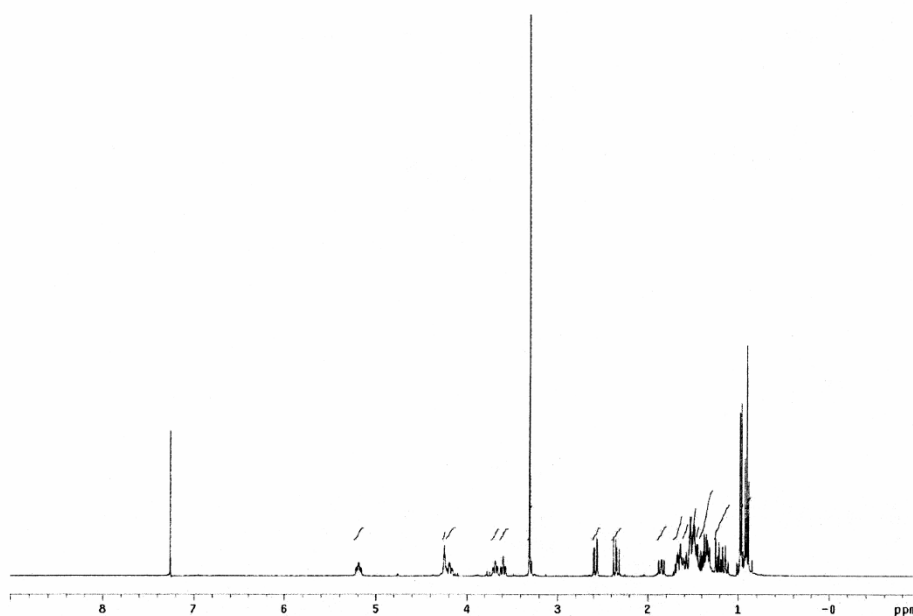


**Scheme 6.11**

## 6.10. Spectroscopic Comparison

As presented in Figure 6.6 and 6.7, the <sup>1</sup>H and <sup>13</sup>C NMR spectra of our synthetic neopeltolide macrolactone **6.5** matched perfectly when compared to those provided by the Panek's group. This evidence strongly supports the structural validity of our synthetic material.<sup>388</sup>

Panek's Neopeltolide Macrolactone **6.5** ( $^1\text{H}$  NMR, 400 MHz)



Taylor's Neopeltolide Macrolactone **6.5** ( $^1\text{H}$  NMR, 600 MHz)

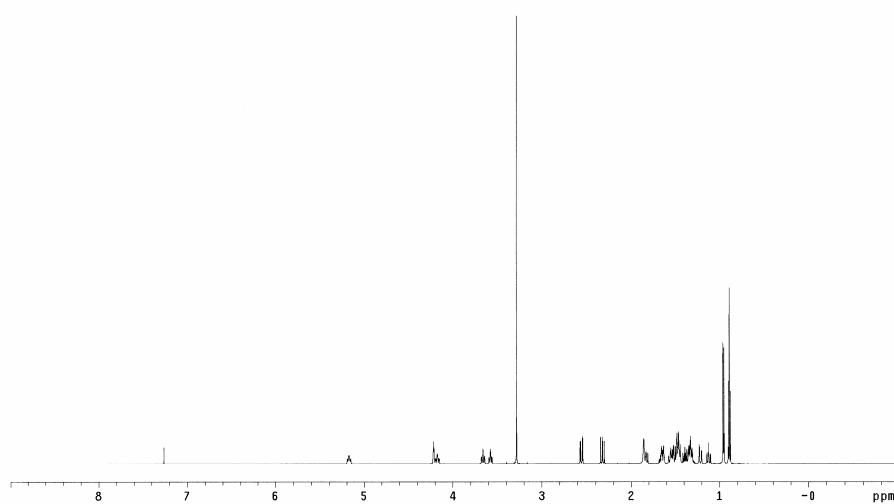
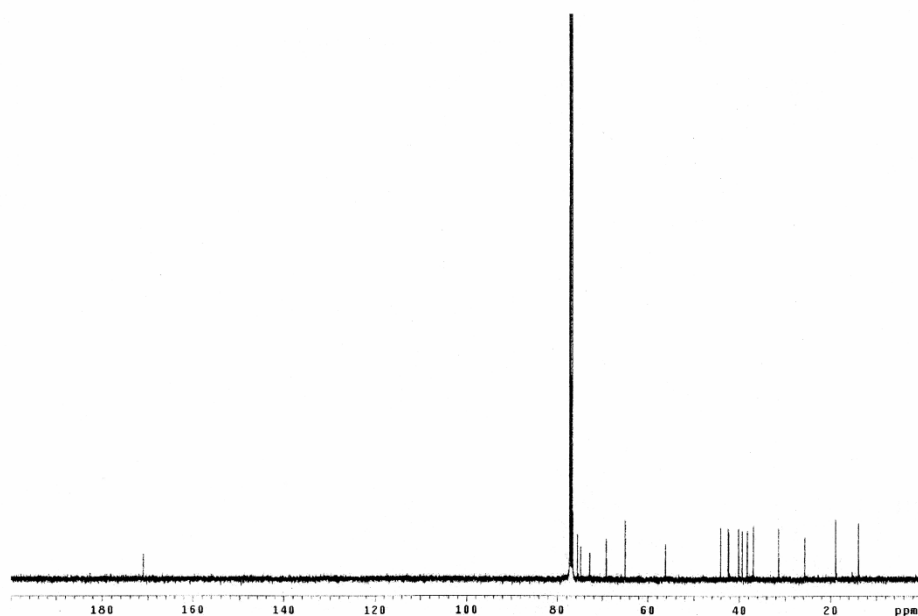


**Figure 6.6**

Panek's Neopeltolide Macrolactone **6.5** ( $^{13}\text{C}$  NMR, 100 MHz)



Taylor's Neopeltolide Macrolactone **6.5** ( $^{13}\text{C}$  NMR, 150 MHz)

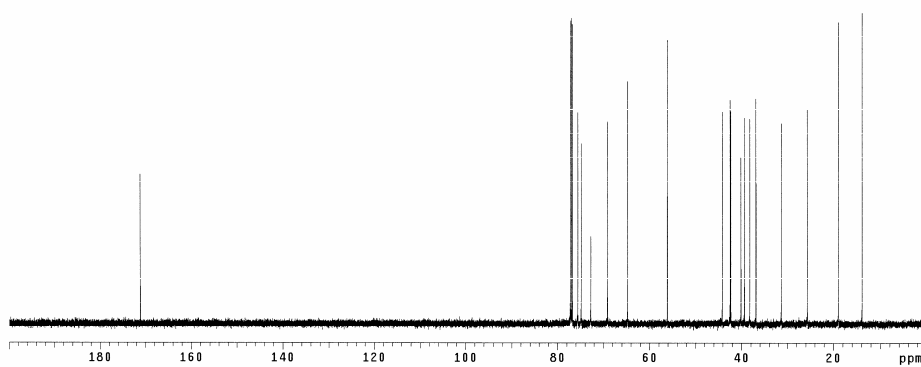


**Figure 6.7**

## 6.11. Conclusion

In summary, we have accomplished a concise total synthesis of neopeltolide macrolactone **6.5** in only 14 steps in the longest linear sequence and 15 steps overall (one additional step was required for preparation of  $\beta$ -hydroxysulfide **6.18**) from any commercially available materials. The route outlined in this communication successfully implemented a strategy which utilized our ether transfer methodology which directly installed the requisite C5 stereochemistry. In addition, our present route readily avoided discreet installation of protecting groups. In fact, the two apparent “protecting groups” (C5 benzyl ether and C13 benzoate ester) were produced simultaneously upon generation of a stereocenter and utilized primarily in the differentiation of the resulting 1,3-diol systems. During the submission of this dissertation, detailed biological evaluations of neopeltolide macrolactone **6.5** and subsequent extensive conformational analyses are currently underway. These preliminary studies will serve as a strong foundation for our future rationally designed, conformationally-biased neopeltolide analogues.

## CHAPTER SEVEN

### FUTURE DIRECTIONS

#### **7.1. Purpose**

The purpose of this chapter is to detail future directions of the research programs described in this dissertation. For acutiphycin, this chapter will outline a strategic structure-activity-relationship study to detect the biologically active conformers of the macrolide when bound to the target proteins. Meanwhile, for the synthetic methodology counterpart, this chapter will present a proposal on further expansion of the ether transfer methodology to other structurally novel compounds, such as spiroketals, oxepanes, oxepanones, and complex 1,3,6-triols.

#### **7.2. Synopsis of Previous Chapters**

This dissertation presents two major components: literature reviews pertinent to polyketide natural products and our detailed research description in the field of synthetic organic chemistry. The first chapter presents assessment on published articles relevant to a class of tetrahydropyran containing macrolides with common biosynthetic origin from

cyanobacteria. The literature presentation continues to Chapter Two which solely focuses on (+)-acutiphycin. The isolation, structural elucidation, and previous total syntheses of this cytotoxic natural product have been described in details in this chapter. The ensuing four chapters then detail our research efforts. As described in Chapter Three, we have made a significant progress towards the total synthesis of (+)-acutiphycin. Chapter Four explains our newly developed strategy, electrophile-induced ether transfer, which readily allows the production of 1,3-*syn* diol monoether, a functionality common to polyketides. The ether transfer methodology has been successfully extended further to other functionalities common to polyketides, such as the oxygen heterocycles. In fact, Chapter Five features our unique approach to stereoselective preparation of 2-cyano tetrahydropyran, 2,4,6-trisubstituted tetrahydropyrans, and 2,6-disubstituted-3,4-dihydropyran. The expansion of the ether transfer technology then continued in Chapter Six where applications toward the total synthesis of cytotoxic macrolide neopeltolide are discussed.

Based on these results, this chapter will be exclusively dedicated to proposals which describe our research directions in the near future. Once again, these proposals will further signify our deep interests in polyketides, not only in terms of total syntheses and synthetic methodology development, but also extensive structure – activity relationship studies to probe their biological profiles and true pharmacophores.

### 7.3. Structure – Activity Relationship Study

The structure – activity relationship (SAR) study has been extensively utilized by medicinal chemists in order to produce better drug candidates, in terms of potencies and efficiencies, and understand their pharmacophores by modifying their chemical structures. An excellent example of a natural product that has been subjected to probably the most extensive SAR studies is the epothilones.

#### 7.3.1. Conformation – Activity Relationship in Epothilones

A unique SAR approach that our group has undertaken with the epothilones is to probe the effect of conformation on biological activities. The relationship between conformational effects of macrocyclic polyketides to their biological activities have been often ignored and underappreciated. In fact, our group has recently established the biologically active conformation of epothilones B **7.1** and D **7.2** via detailed NMR analyses, computational methods, and total syntheses of rationally designed analogues.<sup>389-</sup>

391

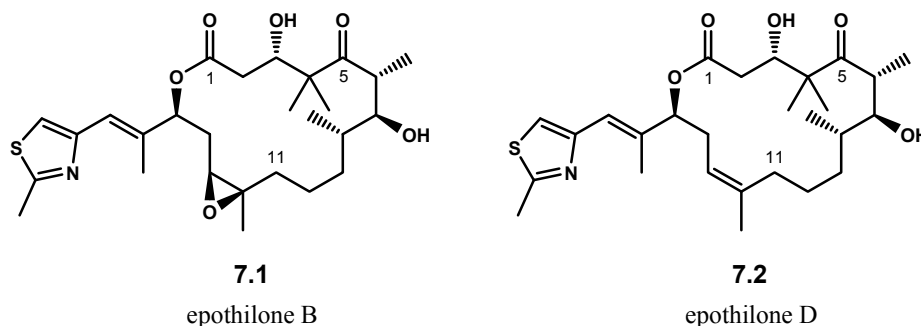
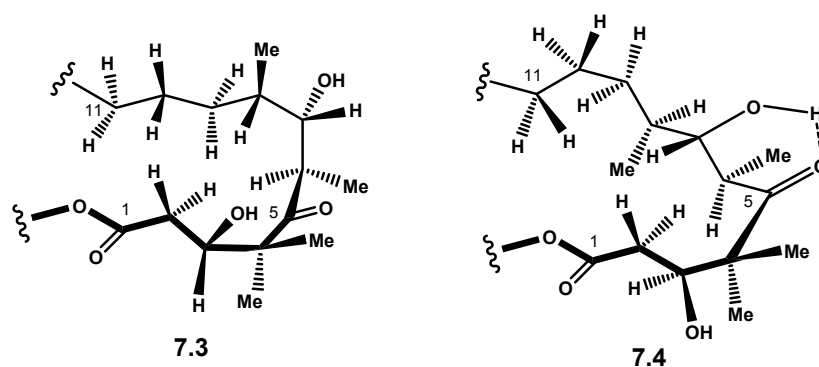


Figure 7.1



In 1999, our group reported the overall solution conformation of epothilones based on the observation made by high field NMR experiments and computational methods.<sup>391</sup> The flexibility of the macrolide ring was analyzed in two subregions: C1 – C11 and C12 – C1. These analyses found that the C1 – C11 region exists in two conformations. The major and minor conformations are depicted in structures **7.3** and **7.4** respectively.



**Figure 7.2**

Similarly, the C12 – C1 region also exists in two conformations: major **7.5** and minor **7.7**. As represented by their respective Newman projections **7.7** and **7.8**, conformer **7.5** is stabilized by a favorable C13 – C16 *anti* relationship, but destabilized by C13 – O gauche interaction; whereas, in conformer **7.6**, gauche relationship between C13 – O and C13 – C16 become the primary destabilizing effect.

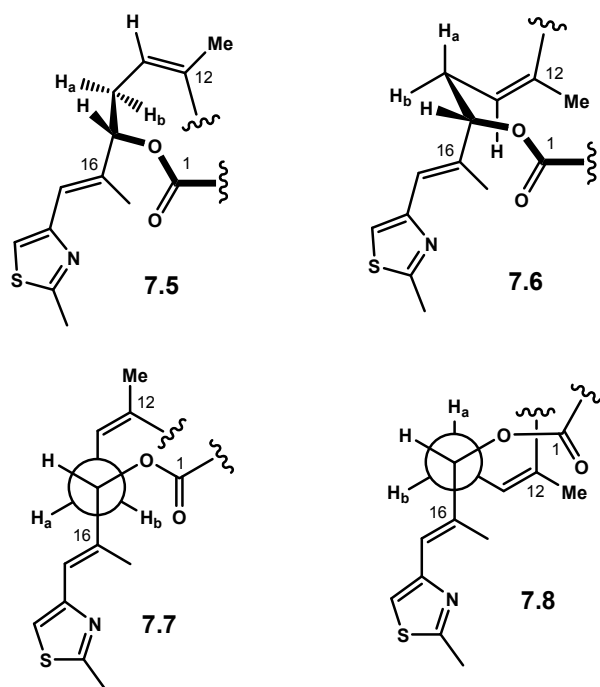


**Figure 7.3**

Based on the work of a previous graduate student in the group, Yue Chen, while focusing on the conformation in the C12 – C1 region, epothilone analogues were rationally designed with the anticipation that these analogues would deduce the biologically active conformer when bound to the target protein. In 2003, the total synthesis of the C14-methyl analogues of epothilone B and D, **7.9** – **7.11**, along with their biological studies were completed and subsequently published.<sup>390</sup>

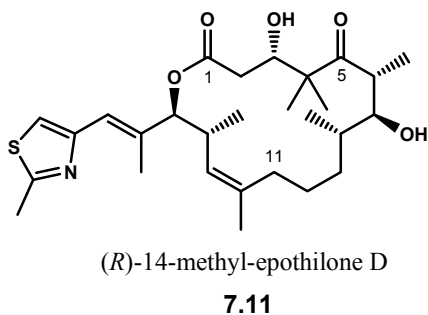
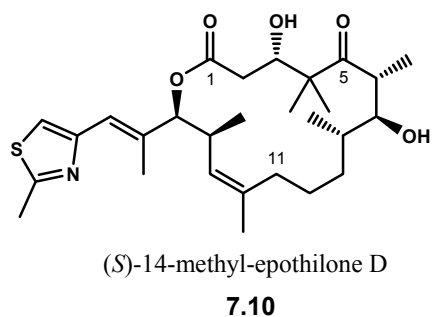
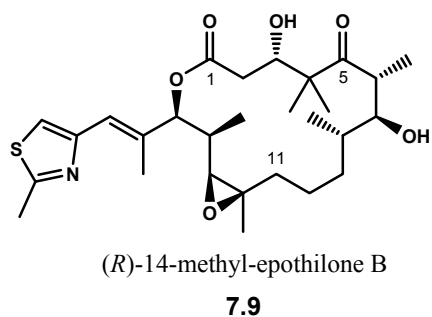


**Figure 7.4**

The biological evaluations of these analogues were astonishing. It was found that the stereochemistry of the newly introduced C14-methyl group significantly affected the biological activities. As demonstrated in Table 7.1, the (*R*)-14-methyl-epothilone B **7.9** and (*S*)-14-methyl-epothilone D **7.10** clearly retained significant cytotoxicity against a panel of human tumor cell lines. In marked contrast, the (*R*)-14-methyl-epothilone B **7.11** did not show any measurable cytotoxicity.

**TABLE 7.1**

Entry	Compound <sup>[a]</sup>	MCF-7	NCI/DR	H460	SF
1	<b>6.1</b>	1.5	3.6	1.7	0.7
2	<b>6.2</b>	5	26	20	7
3	<b>6.9</b>	3	23	3	3
4	<b>6.10</b>	35	238	42	42
5	<b>6.11</b>	>1000	>1000	>1000	>1000

[a] IC<sub>50</sub> was reported in nM concentration

This crucial biological data indeed confirms our initial hypothesis regarding the relationship between conformation and biological activity. The introduction of (*R*)-14-methyl substituent in analogues **7.9** and **7.10** destabilizes conformation **7.6**, thus forcing the equilibrium to shift to the major conformation **7.5**. Meanwhile, in analogues **7.11**, the minor conformation **7.6** becomes more favorable as the (*S*)-14-methyl group destabilizes conformation **7.5**. Thus, we concluded that conformation **7.5** appears to be the biologically active conformer of epothilones. In addition, we believe that the introduction of C14-methyl substituent does not impose significant structural modification to the natural product. In fact, the C14-methyl epothilone analogs are a mere representation of a switch in polyketide biogenetic patterns from acetate to propionate subunit.

### 7.3.2. Conformation – Activity Relationship in (+)-Acutiphycin

From our successful conformation – activity relationship study in epothilones, we plan to utilize this approach to analyze the biologically active conformation of acutiphycin **7.12**. Due to the lack of additional conformational data concerning this polyketide at the time when this dissertation was written, our proposal would extensively rely on the conformation proposed by Moore and co-workers.<sup>12</sup> Based on the detailed analyses presented in Chapter Two, Section 2.3.3, acutiphycin is proposed to have existed as conformer **7.13**.

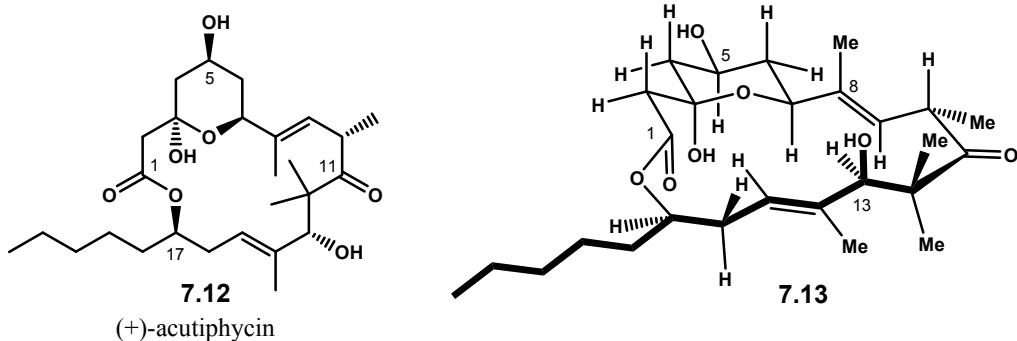
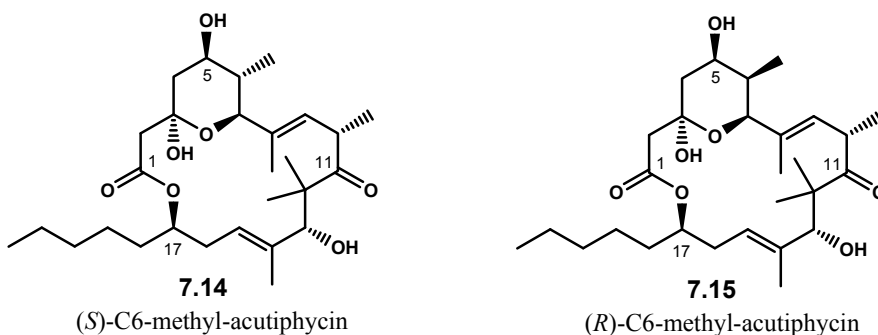


Figure 7.5

#### 7.3.2.1. Conformational Analysis about C5 – C13 Region

The first region that will be subjected under conformational scrutiny is the C5 – C13 segment. Judging from conformation **7.13**, it seems that the degree of conformational freedom about C10 – C13 region is dependent on the spatial arrangement of C8 methyl group. As previously described, the C8 methyl substituent is proposed to

be eclipsing with the C6 and C10 protons as well as C13 hydroxyl group. In order to investigate if this proposed conformation is responsible for the observed biological activity, we will prepare C6-methyl-acutiphyacin analogues **7.14** and **7.15**, Figure 7.6.



**Figure 7.6**

We envision that the introduction of (*S*)-C6 equatorial methyl as shown in analogue **7.14** will result in an increased population of conformation **7.16** as the eclipsing interaction between C8 methyl and C6 proton is further rigidified through minimization of the steric interaction between C6 equatorial methyl and C8 methyl groups. In contrast, the (*R*)-C6 axial methyl analogue **7.15** will destabilize conformation **7.16** and shift the equilibrium to potentially conformation **7.17**. In the presence C6 axial methyl, a rotation about C7 – C8 bond should readily occur to avoid unfavorable *syn*-pentane interaction between C6 axial methyl and C8 methyl groups.<sup>389</sup> This bond rotation will result in C8 methyl group being oriented *exo* to the macrolide ring. Consequently, distant spatial reorganization throughout C10-C13 region should follow. Based on the crude conformational analyses performed on a plastic model kit, we propose that C10 proton will remain nearly eclipsing with C8 methyl in order to minimize A<sub>1,3</sub>-strain between C8

methyl and C10 methyl groups. Thus, this new orientation of C10 methyl will most likely result in the reorientation of C13 hydroxy group. Obviously, detailed investigation of these proposed conformations will be executed via high-field NMR analyses and computational methods. These two analogues will be eventually subjected to biological evaluations, and the result should provide us more insight into the biologically active conformation about the C5 – C13 region.

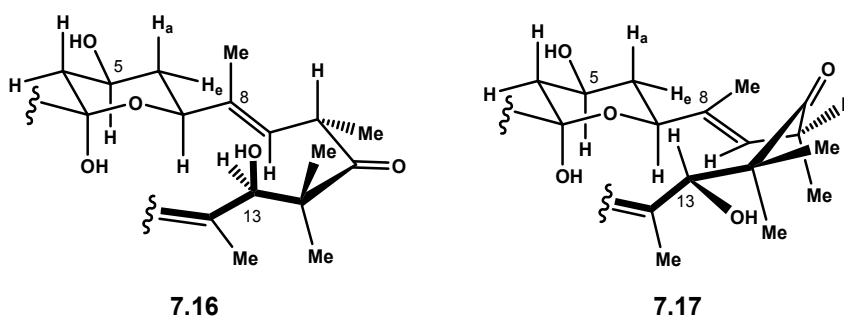
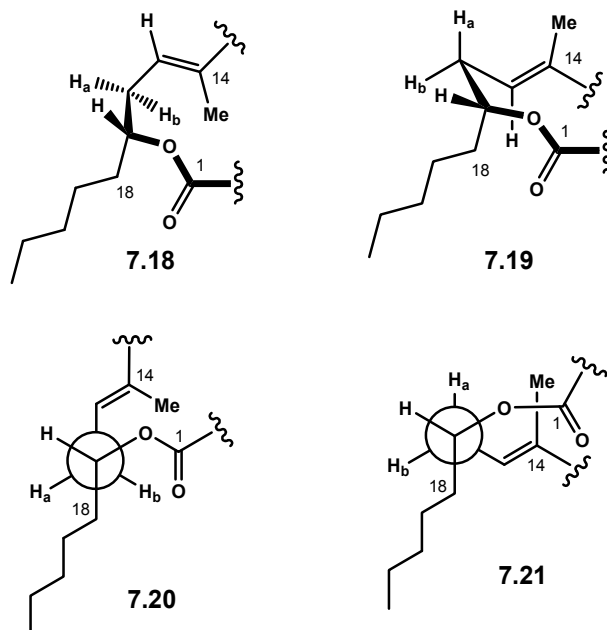


Figure 7.7

### 7.3.2.2. Conformational Analysis about C14 – C1 Region

We will continue our conformational analyses in acutiphycin to the next segment in the molecule, which is the C14 – C1 region. As described in the previous section in this chapter, the conformational analysis of C12 – C1 region of epothilone D suggested conformational flexibility.<sup>389</sup> Due to the structural similarity between the C12 – C1 region in epothilones and the C14 – C1 in acutiphycin, we propose that the C14 – C1 conformation in acutiphycin will be in resemblance to that observed in the C12 – C1 in epothilones. The two proposed extreme conformations, **7.18** and **7.19**, are presented in Figure 7.8. As represented by their respective Newman projections **7.20** and **7.21**,

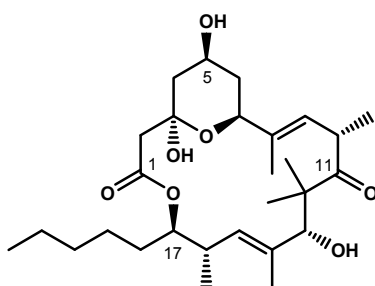
conformer **7.18** is characterized by a C15 – C18 *anti* relationship, whereas conformer **7.19** contains a gauche relationship between C15 and C18. Computational methods and high-field NMR experiments will be employed to confirm the existence of these two conformers as well as to determine the distribution of population in each conformer.



**Figure 7.8**

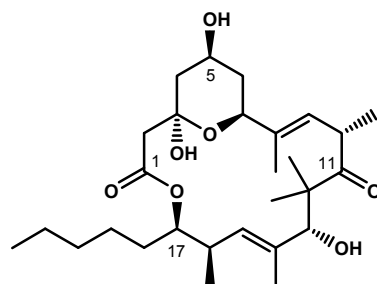
To determine which of the above conformers more closely resembles its biologically active conformation, C16-methyl-acutiphyecin analogs **7.22** and **7.23** will be prepared, Figure 7.9. With a similar rationale presented in epothilones, analogs **7.22** and **7.23** are expected to increase the population of conformations **7.18** and **7.19** respectively since the presence of C16-methyl group will destabilize the alternative conformation.





**7.22**

(*S*)-C16-methyl-acutiphycin



**7.23**

(*R*)-C16-methyl-acutiphycin

**Figure 7.9**

Once again, it is important to mention that the four proposed rationally designed analogues of acutiphycin **7.14**, **7.15**, **7.22**, and **7.23** should maintain their natural product-like structures as the polyketide pattern within these molecules is retained. In fact, the introduction of a methyl substitution at C6 or C16 only represents a switch from acetate to propionate in the polyketide biogenetic patterns.

#### 7.4. Electrophile-Induced Ether Transfer: Stereoselective Synthesis of Spiroketal

As described in Chapter Five, we have explored a new synthetic approach to the stereoselective synthesis of oxygen heterocycles.<sup>237-239</sup> This approach was highlighted by a common three-step sequence: electrophile-induced ether transfer, cyclization, and functionalization. Depending upon the functionalization step, we were able to access 2,4,6-trisubstituted tetrahydropyran or 2,6-disubstituted-3,4-dihydropyran. We envision that this strategy can be stretched even further to the stereoselective synthesis of spiroketal functionalities. Spiroketal are one of the commonly found functionalities in

polyketide natural products. For instance, milbemycin  $\beta_3$  **7.24**<sup>392</sup> and (+)-aigialospirol **7.25**<sup>393</sup> both contain a key spiroketal moiety, Figure 7.10.

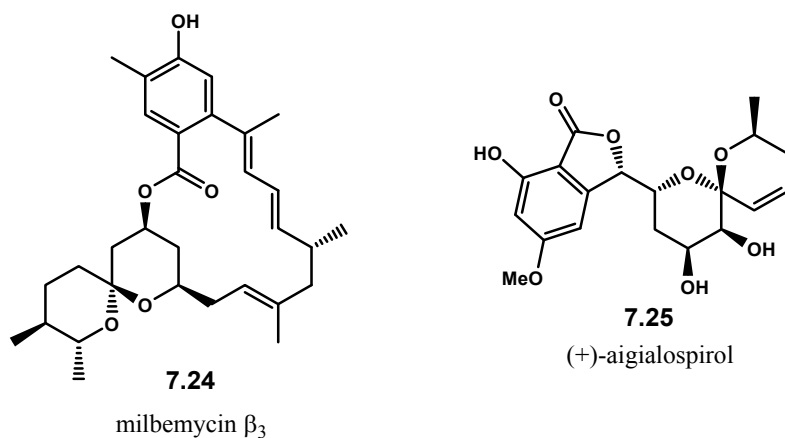
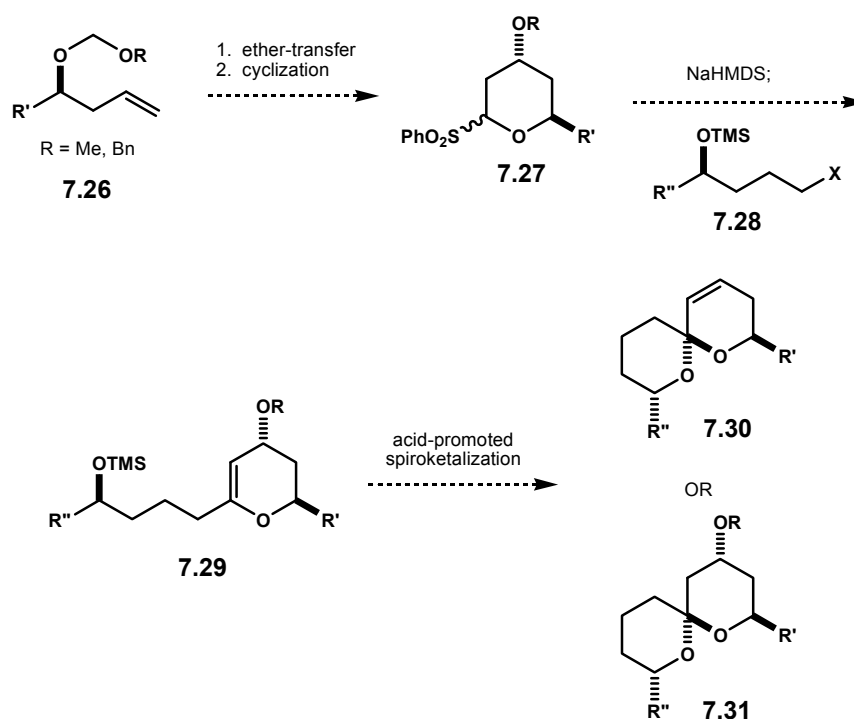


**Figure 7.10**

Our general approach to a spiroketal formation is presented in Scheme 7.1. The transformation of homoallylic alcohol **7.26** to its corresponding sulfonylpyran **7.27** should be readily achieved via ether transfer and cyclization reactions. Sulfonylpyran **7.27** will be then subjected to a base-mediated coupling reaction with fragment **7.28** to yield glycal **7.29**.<sup>238</sup> Exposure of glycal **7.29** to acid, depending upon conditions, should promote a spiroketalization process to either spiroketal **7.30** or **7.31**. To demonstrate the applicability to natural product syntheses, we envision the utilization of this spiroketalization approach to construct the spiroketal core in milbemycin  $\beta_3$  **7.24** as well as in (+)-aigialospirol **7.25**.



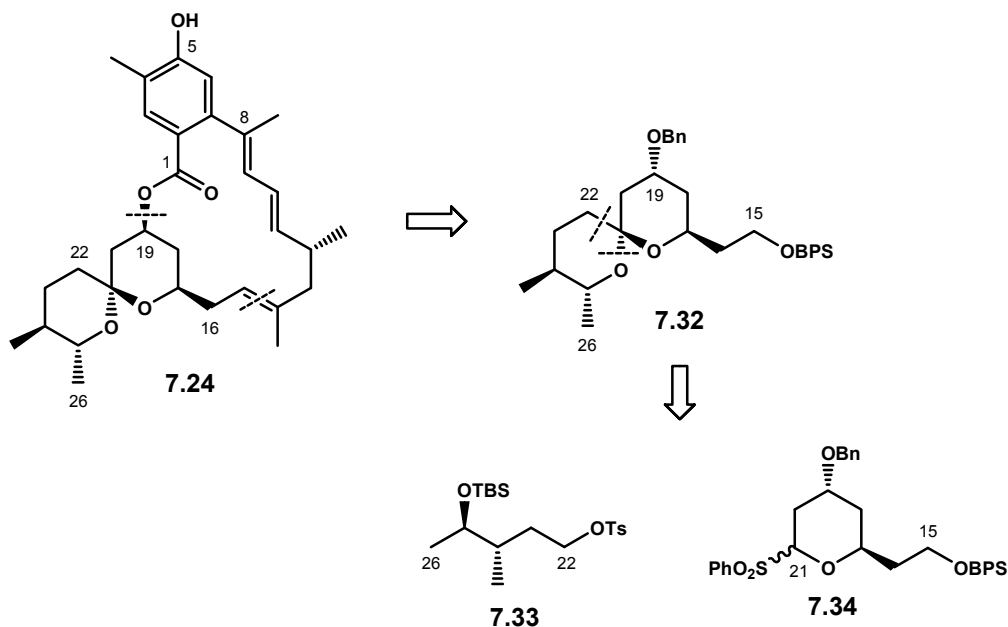
Scheme 7.1

#### 7.4.1. Preparation of Milbemycin $\beta_3$ Spiroketal Core

Milbemycin  $\beta_3$  **7.24** is a spiroketal containing polyketide natural product isolated from streptomyces B-41-146 strain.<sup>392</sup> In addition to its antibiotic activity, this class of natural products has been known to possess significant activity against agricultural pests and parasites while displaying low cytotoxicity towards plants and animals. Several total syntheses to this unique molecule have been reported,<sup>394-401</sup> most recently by O'Doherty and Li.<sup>402</sup>

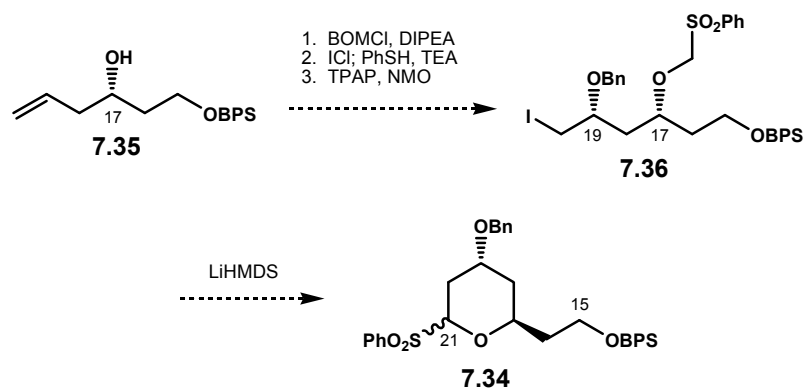
As shown in Scheme 7.2, our interests in this macrolide will be confined in the construction of C15 – C26 spiroketal fragment **7.32**. We envision that spiroketal **7.32**

should be readily accessible from sulfonylpyran **7.34** and tosylate **7.33** for the coupling partner.



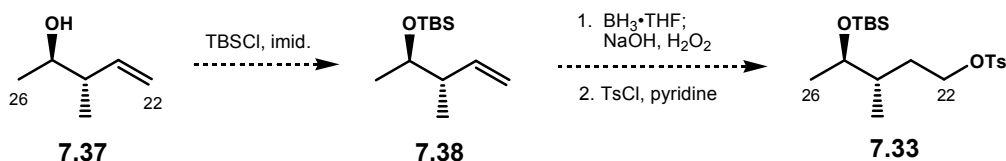
**Scheme 7.2**

The preparation to sulfonylpyran **7.34** should proceed smoothly starting with homoallylic alcohol **7.35**. Similar to the protocol described in Scheme 5.15, the protection of alcohol **7.35**<sup>358</sup> as BOM ether, followed by ether transfer and sulfide oxidation should provide sulfonylether **7.36**. The subsequent cyclization mediated by LiHMDS should furnish sulfonylpyran **7.34**, Scheme 7.3.



**Scheme 7.3**

As for the coupling partner, we will begin with protection of a known alcohol **7.37**<sup>261</sup> as TBS ether **7.38**. Hydroboration of **7.38** should install the required primary alcohol at C22, and the ensuing treatment with TsCl and pyridine should provide the corresponding tosylate **7.33**.

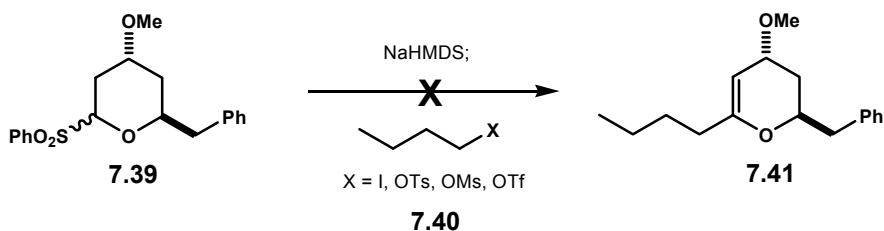


**Scheme 7.4**

#### 7.4.1.1. A Model Study in the Alkylation Reaction

Our plan for coupling of sulfonylether **7.34** with tosylate **7.33** is based on our initial result as presented in Chapter Five, Section 5.5.2. We have demonstrated that deprotonation of anomeric sulfone **7.39** with NaHMDS readily produced the corresponding anion which adds smoothly to activated electrophiles, such as benzyl

bromide, allyl bromide, methyl iodide, and BOMCl. However, a recent investigation revealed that this alkylation reaction was found unproductive with unactivated electrophiles. The utilization of butyl iodide, tosylate, mesylate, and even triflate as electrophiles under the optimized reaction conditions only resulted in the recovery of **7.39** upon workup.

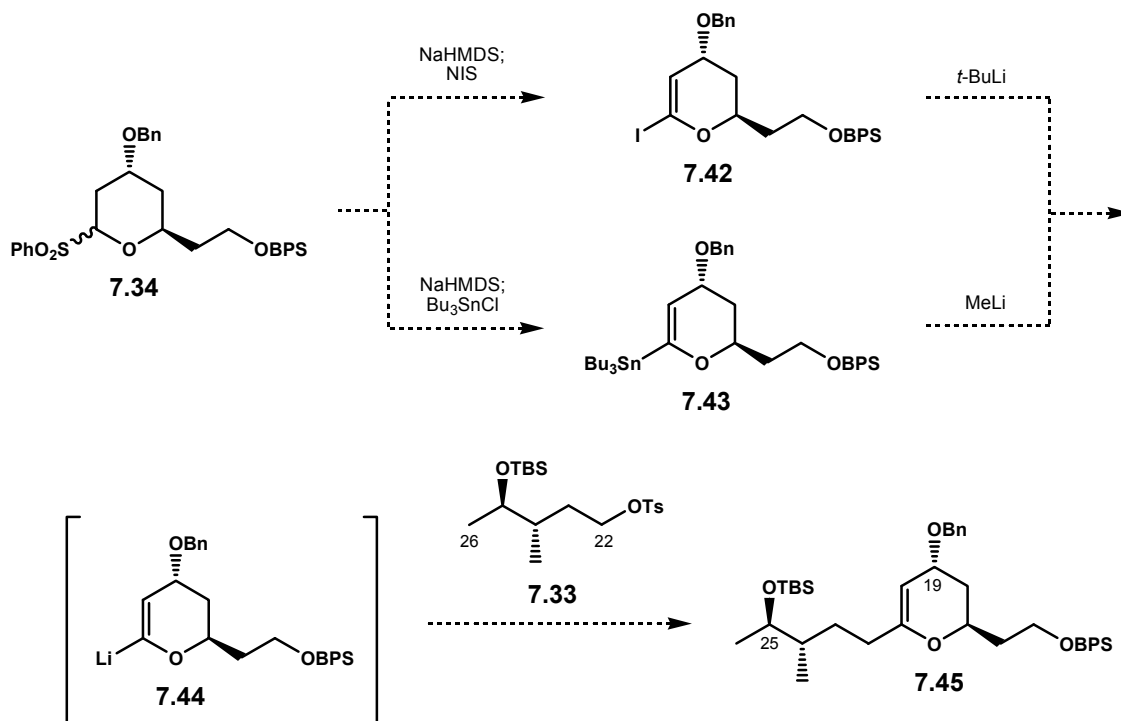


**Scheme 7.5**

#### 7.4.1.2. Alkylation via Vinyl Lithium

The failure to alkylate sulfonylpyran **7.39** with butyl tosylate in a model study as shown in Scheme 7.5 led us believe that a similar problem will be also observed with substrates **7.33** and **7.34**. As a result, it is reasonable to tackle this key coupling reaction via several different approaches. One alternative involves conversion of sulfonylpyran **7.34** to vinyl iodide **7.42** or vinyl tin **7.43** which should readily take place upon deprotonation with NaHMDS and quenching the corresponding anion with iodine or Bu<sub>3</sub>SnCl respectively. Spontaneous elimination of the sulfone functionality is expected to occur as previously observed in Chapter Five, Section 5.5.2. Treatment of vinyl iodide **7.42** or vinyl tin **7.43** with *t*-BuLi or MeLi,<sup>403</sup> respectively, should readily provide vinyl

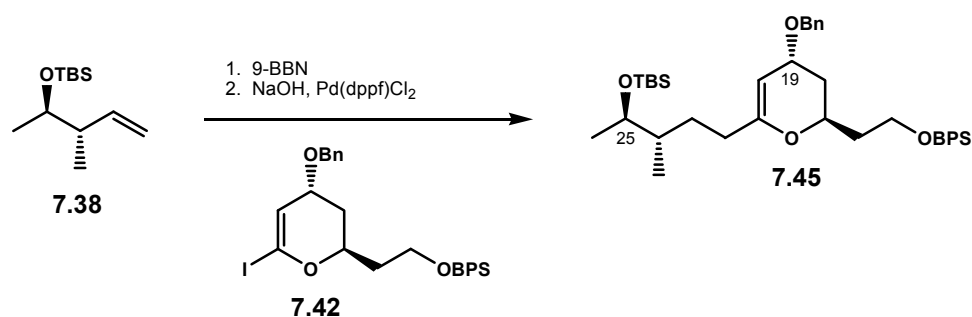
lithium **7.44** which will displace the tosylate group in **7.33** and thus setting the C21 – C22 connectivity.



Scheme 7.6

#### 7.4.1.3. Coupling via the Suzuki-Miyaura Reaction

If the above-described lithium-based coupling reaction also fails, Tan and Potuzak demonstrated that coupling of alkene **7.38** and vinyl iodide **7.42** should be accessible via *B*-alkyl Suzuki-Miyaura cross coupling reaction.<sup>404</sup> As shown in Scheme 7.7, treatment of **7.38** with 9-BBN followed by addition of **7.42** in an aqueous NaOH solution should readily produce glycal **7.45** as catalyzed by Pd(dppf)Cl<sub>2</sub>.

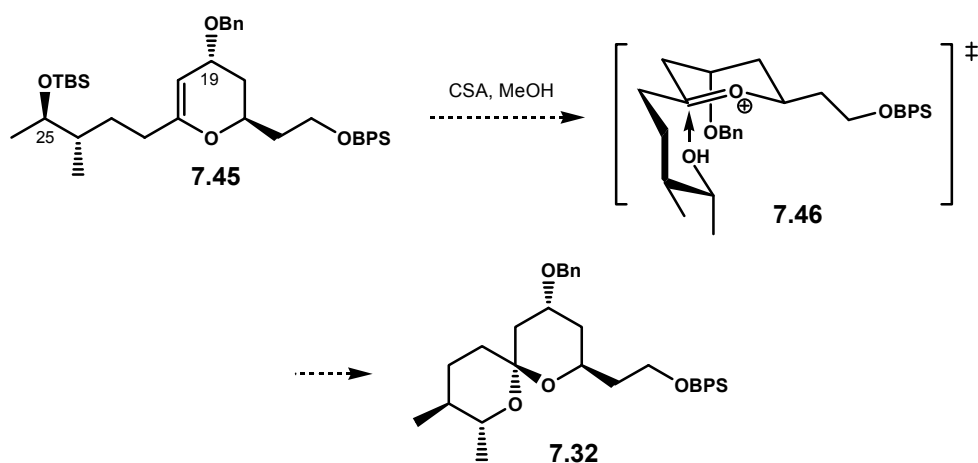


**Scheme 7.7**

#### 7.4.1.4. Acid Promoted Spiroketalization

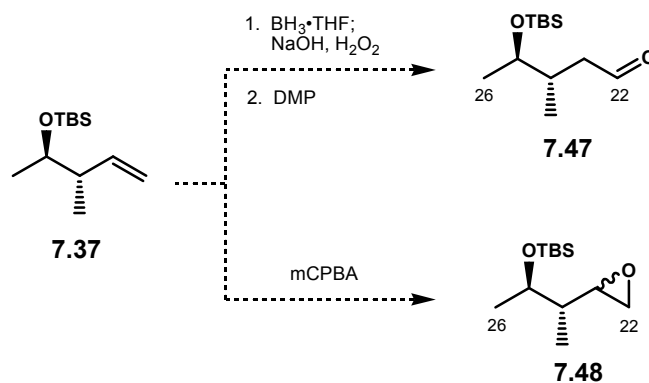
The formation of spiroketal **7.32** commences with exposure of glycal **7.45** to acidic methanol. These conditions should readily cleave the TBS ether, unmask the C25 hydroxy group, and promote cyclization to the target spiroketal **7.32**.<sup>333</sup> The absolute stereochemistry of the newly generated spiroketal center will be directed by the stereochemistry of C19 benzyl ether group. Upon ionization, the C19 benzyl ether is expected to orient pseudoaxially, thus stabilizing the conformation of oxocarbenium ion **7.46**.<sup>336, 337</sup> The approach of C25 hydroxy group will most likely proceed via preferential axial attack influenced by the anomeric effect.





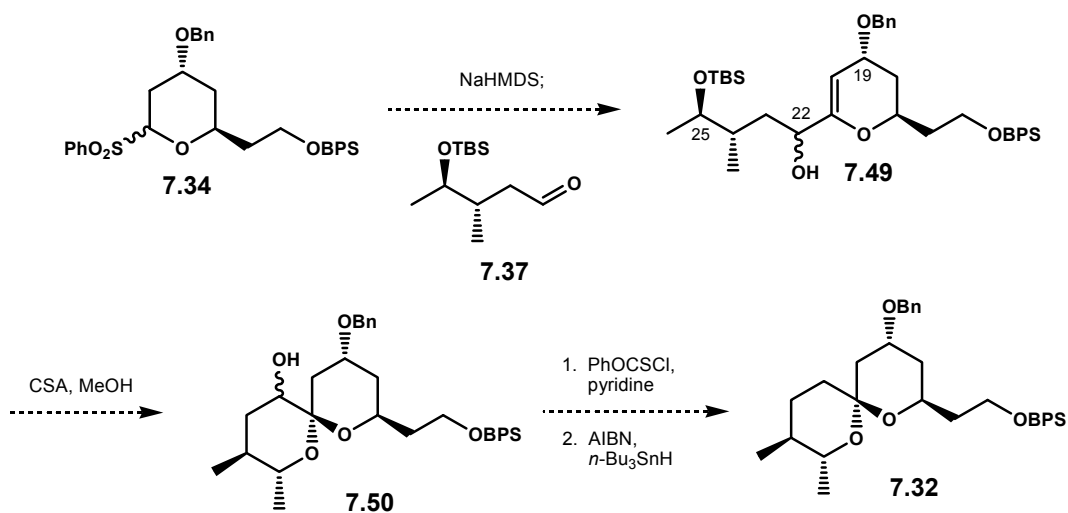
#### 7.4.1.5. Alternative Route via Barton-McCombie Deoxygenation

Another viable route to the production of milbemycin  $\beta_3$  spiroketal fragment **7.32** is described as followed. Although a reaction between the sodium salt of sulfonylpyran **7.34** and tosylate **7.33** is not expected to take place, activated electrophiles such aldehyde **7.47** or epoxide **7.48** should provide an alternative option as the coupling partner.<sup>332-334</sup> As shown in Scheme 7.9, aldehyde **7.47** should be readily accessible via a hydroboration and oxidation sequence from alkene **7.37**, whereas treatment with mCPBA should afford epoxide **7.48** as a mixture of diastereomers. This stereochemistry will be eventually inconsequential due to the deoxygenation reaction late in the sequence.



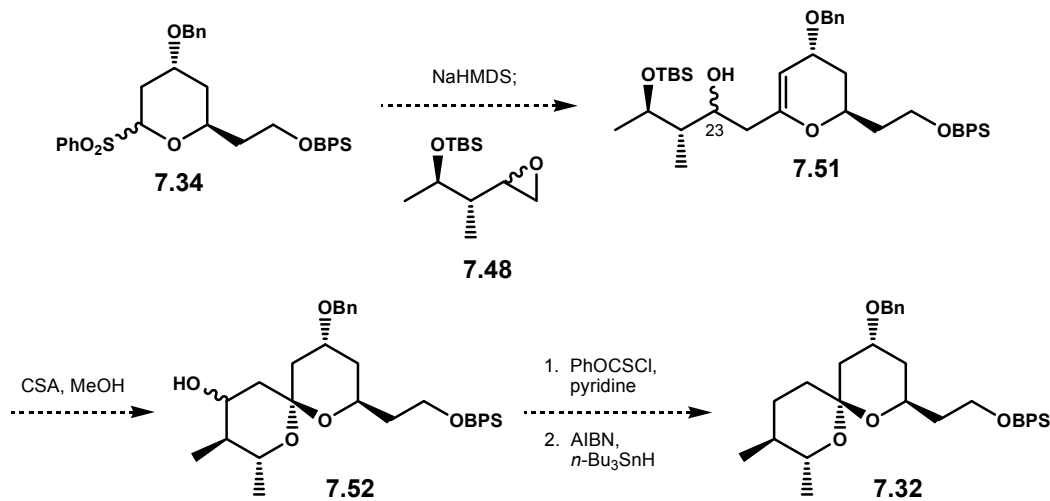
Scheme 7.9

Scheme 7.10 demonstrates a planned coupling strategy for sulfone **7.34** and aldehyde **7.37** which should give glycol **7.49** upon spontaneous elimination of the sulfone functionality. Treatment of this compound under acidic methanolysis conditions should induce stereoselective spiroketalization to **7.50** based on the transition state similar to **7.46**. Removal of the C22-hydroxy group under the Barton-McCombie deoxygenation protocol should furnish target spiroketal **7.32**.<sup>306</sup>



Scheme 7.10

Similarly, the utilization of epoxide **7.48** in the alkylation reaction should yield glycal **7.51**. Spiroketalization under acidic conditions to **7.52** and subsequent Barton-McCombie<sup>306</sup> deoxygenation of the C23-hydroxyl should complete the synthesis of spiroketal **7.32**, Scheme 7.11.

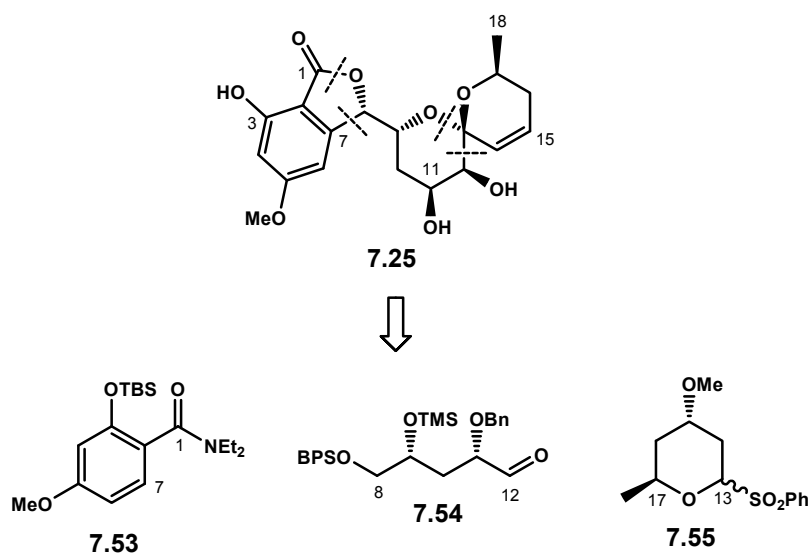


**Scheme 7.11**

#### 7.4.2. Total Synthesis of (+)-Aigialospirol

(+)-Aigialospirol **7.25** is a secondary metabolite produced by *Aigialus parvus* BCC 5311.<sup>393</sup> The isolation and structural elucidation of this molecule was reported in 2004, and to date, there is only one total synthesis to this natural product which was reported in 2007 by Hsung and co-workers.<sup>405</sup> Aigialospirol belongs to the class of polyketide natural products with several unique structural features, such as the spiroketal core, five-membered lactone, and oxidation at C8 and C12 which are most likely introduced by post-PKS modification enzymes.

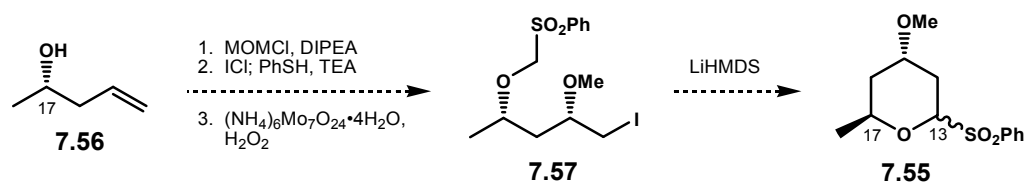
Our retrosynthesis to aigialospirol is described in Scheme 7.12. We envision a highly convergent approach via four bond disconnections to the natural product: C7 – C8, C12 – C13, the lactone, and the spiroketal bonds. These disconnections will lead to three major fragments: aromatic amide **7.53**, orthogonally protected diol aldehyde **7.54**, and sulfonylpyran **7.55**. Extensive utilization of our ether transfer reaction highlights the installation of the requisite stereochemistry contained within each synthetic fragment.



Scheme 7.12

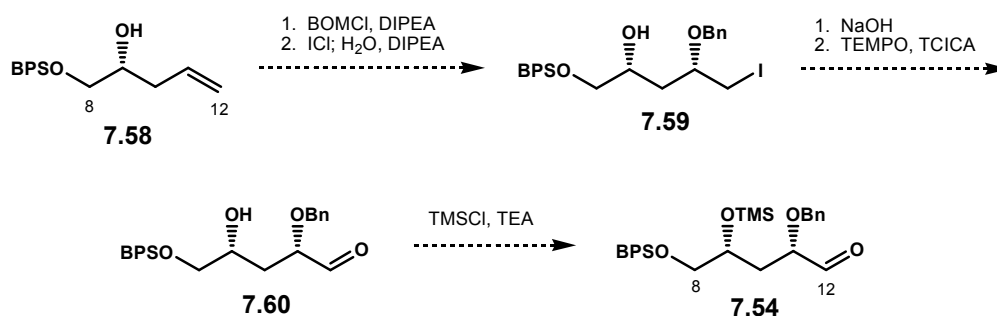
#### 7.4.2.1. Preparation of Fragments **7.54** and **7.55**

The preparation of sulfonylpyran **7.55** will follow our standard sequence. Protection of homoallylic alcohol **7.56**<sup>261</sup> as MOM ether followed by the ether transfer and oxidation reactions should afford sulfonylether **7.57**. The ensuing cyclization will produce sulfonylpyran **7.55**, Scheme 7.13.



Scheme 7.13

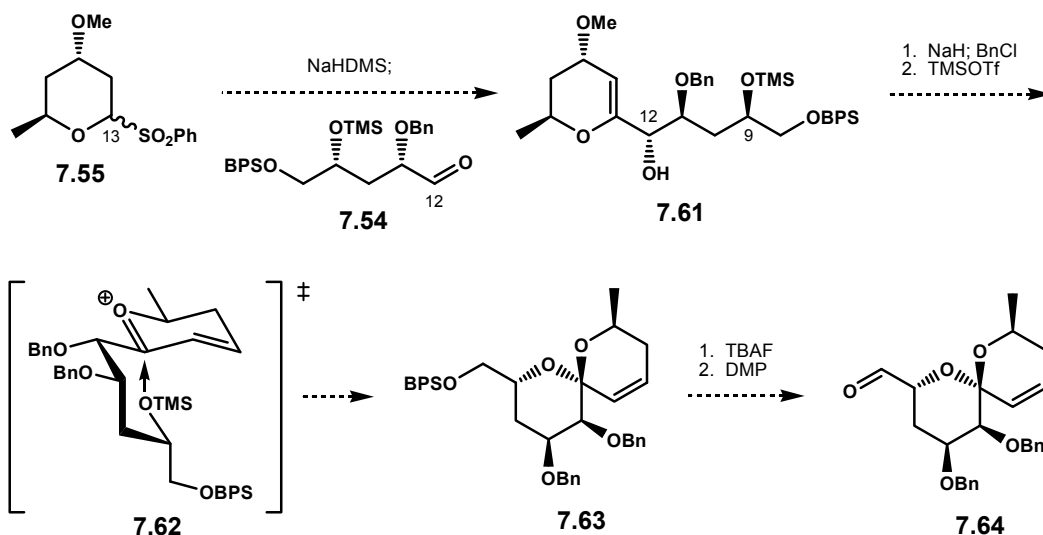
For the synthesis of aldehyde fragment **7.54**, we will begin with homoallylic alcohol **7.58**.<sup>406</sup> Protection of **7.58** as a BOM ether followed by exposure to ICl should provide ether transfer product **7.59**.<sup>236</sup> The displacement of primary iodide to the corresponding primary alcohol followed by a chemoselective oxidation with TEMPO and trichloroisocyanuric acid should readily produce hydroxy aldehyde **7.60**.<sup>407, 408</sup> The ensuing protection of the hydroxyl group as a TMS ether will finish the sequence to aldehyde **7.54**.



Scheme 7.14

#### 7.4.2.2. Ferrier-Like Spiroketalization

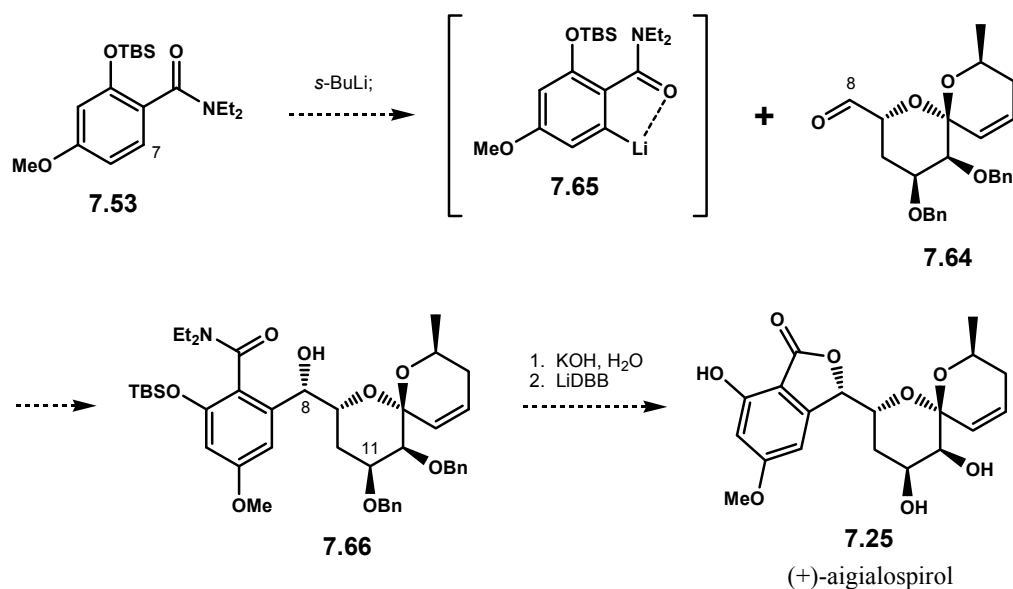
The coupling reaction of sulfonylpyran **7.55** and aldehyde **7.54** is envisioned via the utilization of NaHMDS. The facial addition of sulfonate anion of **7.55** to aldehyde **7.54** is proposed to be stereoselective based on the Felkin-Anh asymmetric induction model,<sup>268</sup> and this should set up the hydroxyl stereochemistry at C12. Protection of alcohol **7.61** as a benzyl ether followed by exposure to catalytic amount of TMSOTf should furnish spiroketal **7.63**. The reaction mechanism for the spiroketalization is proposed through a Ferrier-like ionization process.<sup>409</sup> As shown in transition state **7.62**, preferential axial attack of C9 OTMS group, influenced by the anomeric effect, should install the requisite stereochemistry at the spiroketal center. Removal of the BPS ether and subsequent oxidation of the primary alcohol with Dess-Martin periodinane should furnish aldehyde **7.64**, Scheme 7.15.



Scheme 7.15

### 7.4.2.3. Endgame Strategy

Scheme 7.16 presents the endgame strategy to (+)-aigialospirol. Ortho-lithiation<sup>410, 411</sup> of known aromatic amide **7.53**<sup>412</sup> followed by addition of advanced aldehyde **7.64** should stereoselectively produce alcohol **7.66** based on the Felkin-Anh model.<sup>268</sup> KOH promoted lactonization followed by a mild reductive debenzylolation with LiDBB should conclude our highly convergent synthetic route to (+)-aigialospirol **7.25**.<sup>405</sup>

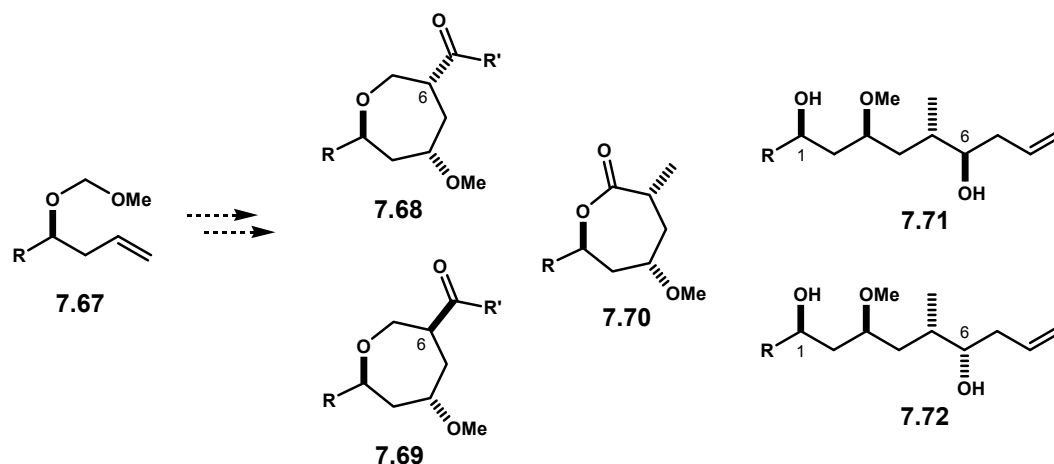


Scheme 7.16

## 7.5. More Structural Novelty from the Ether Transfer Reactions

Chapter Five clearly shows versatility of the ether transfer reaction to access several chemical moieties beyond our initial target 1,3-*syn* diol monoether. We plan to

extend our synthetic creativities to a stereoselective approach to several novel structures previously not readily accessible, such as stereocomplementary 2,4,6-trisubstituted oxepane **7.68** and **7.69** and oxepanone **7.70**. We will also propose a novel non-aldol approach to post-PKS modified-like polyketide structures, such as 1,3,6-trioxygenated synthetic fragments **7.71** and **7.72**.



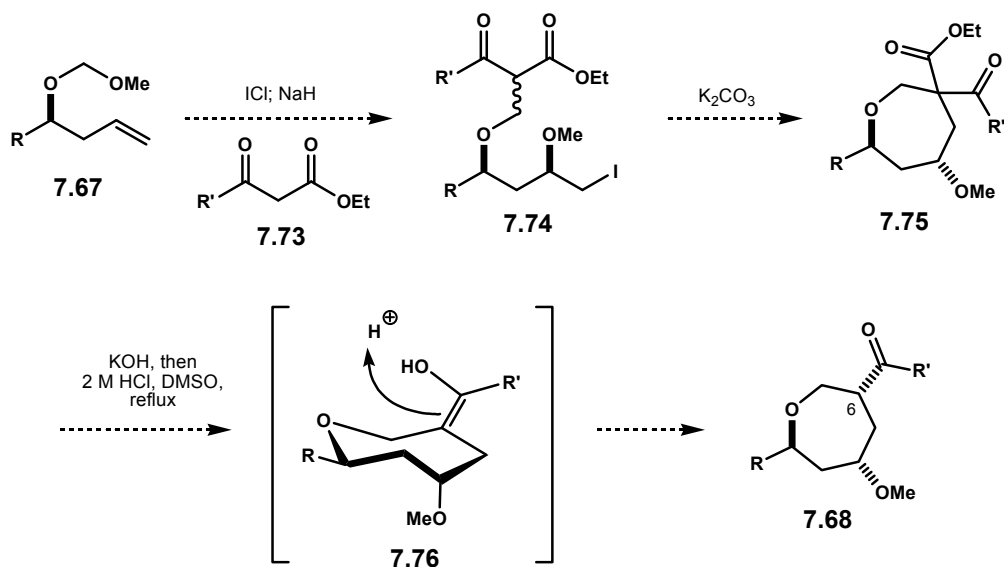
Scheme 7.17

### 7.5.1. Novel Approach to 2,4,6-Trisubstituted Oxepane

Our initial results in the ether transfer reaction as presented in Table 4.2 indicated that the ether transfer reaction can be quenched with various nucleophiles to produce structurally unique 1,3-*syn* diether compounds.<sup>236</sup> Hence, it is reasonable to expect that introduction of a carbon nucleophile, such as the sodium enolate of  $\beta$ -ketoester **7.73**, in the ether transfer reaction should give adduct **7.74**. Stereoselectivity is not expected in this addition reaction, and it will be inconsequential in the subsequent transformation. Cyclization to **7.75** promoted by  $K_2CO_3$ , followed by saponification and acid-promoted

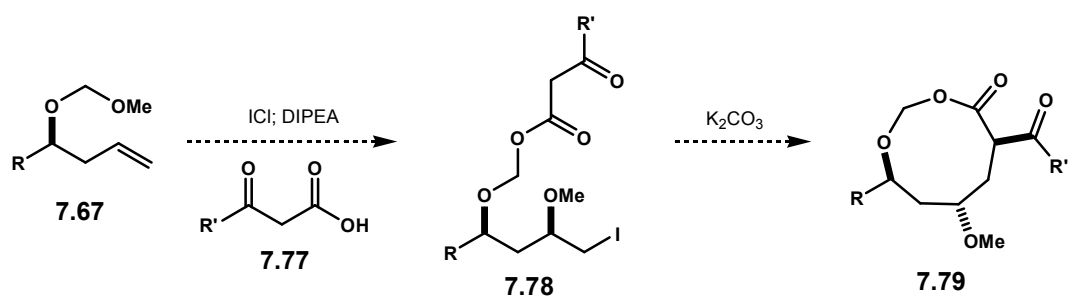


decarboxylation should produce 2,4,6-trisubstituted oxepane **7.68**. The selectivity of the newly generated C6 stereocenter is predicted by kinetic protonation as depicted in transition state **7.76**.



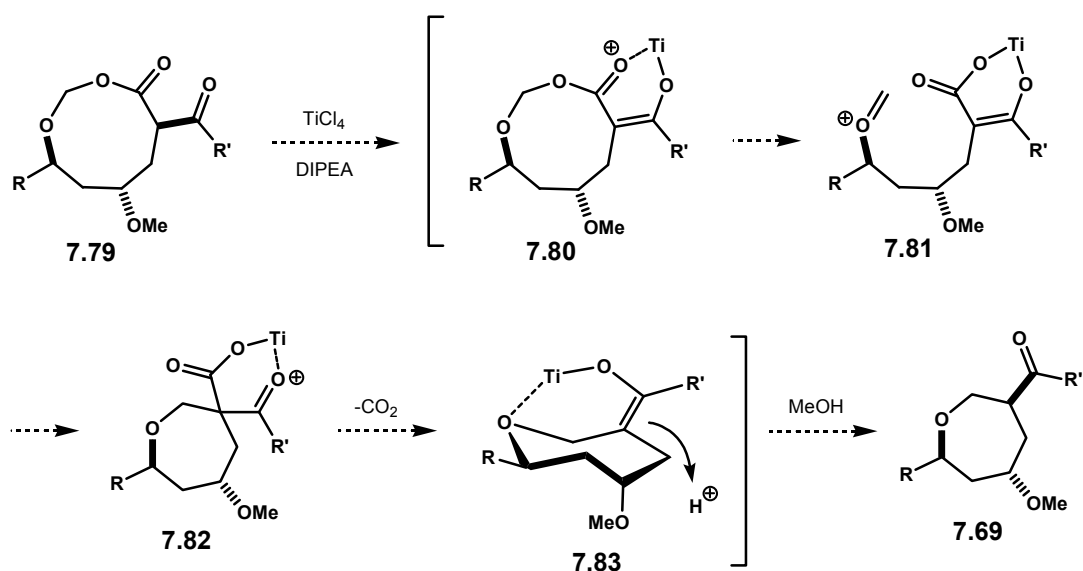
Scheme 7.18

For the production of C6 stereocomplementary oxepane **7.69**, the utilization of  $\beta$ -ketoacid **7.77** as the quenching agent upon activation of homoallylic methoxymethyl ether **7.67** with  $\text{ICl}$  is needed, and this should produce  $\beta$ -ketoester ether **7.78**. Exposure of this adduct to  $\text{K}_2\text{CO}_3$  should then result in the deprotonation and cyclization to dioxonanone **7.79**.<sup>413</sup> Once again, although we do not expect stereoselectivity in the cyclization reaction, the stereochemistry of the newly generated stereocenter will be inconsequential to the production of our target oxepane **7.69**.



**Scheme 7.19**

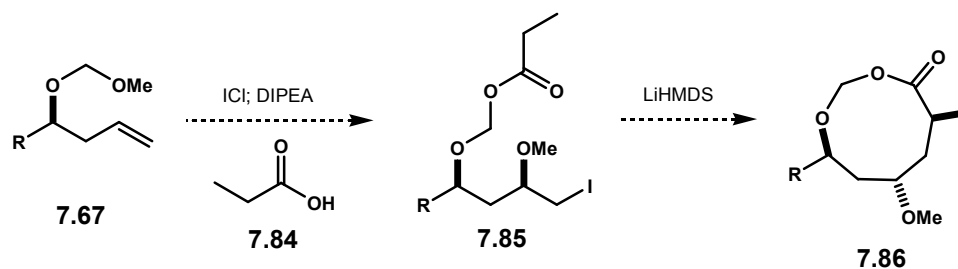
Treatment of dioxonanone **7.79** with Lewis acids, such as  $\text{TiCl}_4$ , in the presence of DIPEA should readily fragment and contract the nine-membered ring to 2,4,6-trisubstituted oxepane **7.69**. The reaction mechanism for this novel transformation is described in Scheme 7.20. The presence of  $\text{TiCl}_4$  and DIPEA should readily promote enolization of **7.79** to **7.80** which then is then followed by ring fragmentation to oxocarbenium ion **7.81**. An intramolecular ring closure of the titanium enolate to the electrophilic oxocarbenium ion furnishes the seven-membered intermediate **7.82**. We expect spontaneous decarboxylation to titanium enolate **7.83** based on the well-established precedents for metal-mediated decarboxylation of  $\beta$ -ketoester.<sup>414, 415</sup> The conformation of the resulting titanium enolate is presumably rigidified via intramolecular chelation such that kinetic protonation from the sterically less encumbered  $\alpha$ -face should set up the proposed stereochemistry in oxepane **7.69**.



Scheme 7.20

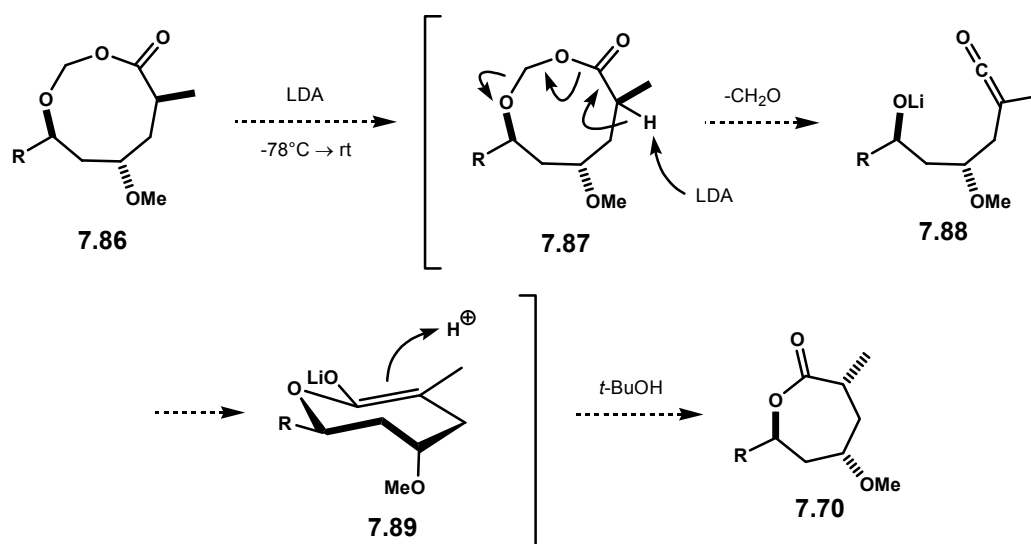
### 7.5.2. A Unique Access to 2,4,6-Trisubstituted Oxepanone

To access our target 2,4,6-trisubstituted oxepanone **7.70**, we will employ propiolic acid **7.84** as the quenching agent in the ether transfer reaction.<sup>236</sup> Cyclization of the resulting ether transfer adduct **7.85** to dioxonanone **7.86** will be promoted by LiHMDS. Although the ground conformational preference of a nine-membered lactone is known to remotely provide asymmetric stereochemical induction,<sup>416</sup> the stereochemistry of the newly generated stereocenter will be inconsequential to the production of our target oxepanone **7.70**. Lactone **7.86** will also serve as a common precursor to the target fragments **7.71** and **7.72**. However, for this transformation, a single diastereomer from **7.86** will become necessary. Just in case the cyclization of **7.86** to **7.72** is not stereoselective, the resulting methyl stereocenter or its epimer should be readily accessible through epimerization, *vice versa*.



**Scheme 7.21**

Scheme 7.22 describes our plan for a straightforward production of 2,4,6-trisubstituted oxepanone **7.70** from common precursor **7.86** in just one step. Based on a precedent by Schultz,<sup>417</sup> we expect deprotonation of **7.86** with LDA at -78°C followed by warming up to room temperature should readily fragment the nine-membered ring to ketene alkoxide **7.88**. A spontaneous intramolecular ring closure followed kinetic protonation then should yield the target oxepanone **7.70**. The facial selectivity of the protonation should be directed by the axial orientation of the methyl ether. If necessary, a bulkier proton source, such as *tert*-butanol will be utilized to further influence this steric effect.



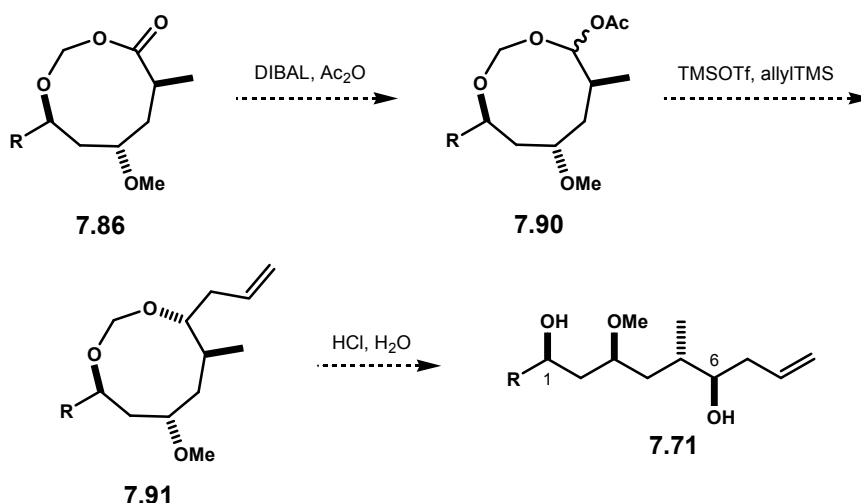
**Scheme 7.22**

The preparation of oxepanone would typically require a Baeyer-Villiger rearrangement of cyclohexanones. However, to access the 2,6-disubstituted variants, this classic method is usually limited to the use of symmetrical cyclohexanone since unsymmetrical substrates would potentially lead to regioisomers.<sup>418, 419</sup> Nevertheless, our above outlined strategy would provide a new, attractive solution to the problem as these substitution patterns are independently installed throughout the synthetic sequence. Furthermore, with the benzyloxy ether transfer, the 4-hydroxy variant should also be accessible.<sup>236</sup>

### 7.5.3. Preparation of Post-PKS Modified-Like Polyketide Synthetic Fragments

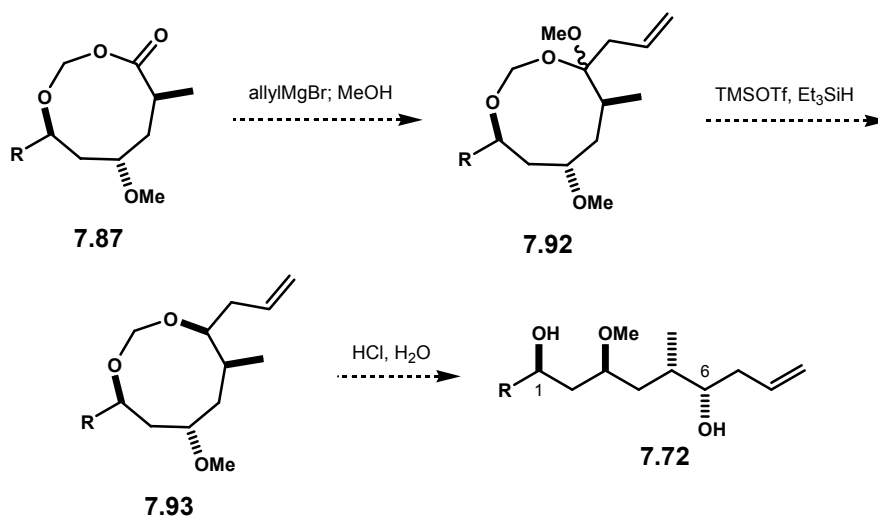
We also plan to exploit the transformation of dioxonanone **7.86** to a pair of post-PKS modified-like polyketide 1,3,6-triol synthetic fragments **7.71** and **7.72**. Scheme 7.23

describes our approach to target fragment **7.71**. We will begin with reduction of lactone **7.86** to mixed acetal **7.90** using a protocol developed by Rychnovsky.<sup>420</sup> Exposure of mixed acetal **7.90** to TMSOTf and allyl silane should provide cyclic acetal **7.91** in a stereoselective fashion. Selectivity of ionization towards the acetate group is directed by its strong Lewis basicity and should be entropically favorable. Hydrolysis of **7.91** under acidic conditions will then unmask the target 1,3,6-trioxygenated fragment **7.71**.



**Scheme 7.23**

To access the C6-diastereomer **7.72**, dioxonanone **7.86** will be carefully treated with one equivalent of allylmagnesium bromide. Subsequent methanolic workup should lead to mixed acetal **7.92**. A stereoselective reduction of **7.92** with TMSOTf and Et<sub>3</sub>SiH should then afford acetal **7.93**. Once again, hydrolysis of the acetal functionality under acidic conditions will then furnish target fragment **7.72**, Scheme 7.24.



**Scheme 7.24**

The key feature for a successful installation of C6 stereochemistry relies on conformational stability of the resulting oxocarbenium ion upon ionization of mixed acetals **7.90** and **7.92**. Woerpel and co-workers have published a systematic study which observed conformational stability of oxocarbenium ion in five,<sup>421</sup> six,<sup>336-338</sup> and eight-membered rings<sup>422</sup> containing an alkoxy substituent. Their results revealed that regardless the ring size, the preferential pseudoaxial orientation of the alkoxy substituent stabilized the conformation of the oxocarbenium ions via favorable through space electrostatic interactions. Although the study in a nine-membered ring system has not yet been reported, we propose that a similar phenomenon will be observed. As shown in Figure 7.11, conformation of oxocarbenium ion **7.94** and **7.95** will be stabilized by the pseudoaxial orientation of the methoxy group, and the subsequent delivery of nucleophile via preferential axial attack sets the stereochemistry as depicted in products **7.91** and **7.93**.

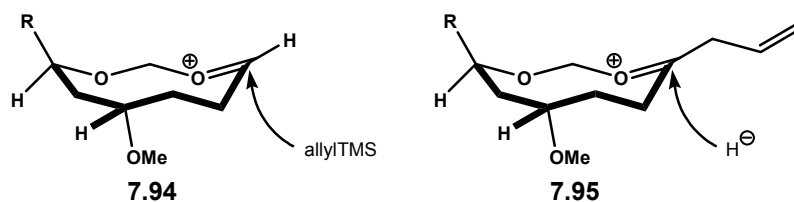


**Figure 7.11**

## 7.6. Conclusion

This chapter details our future research directions both in total synthesis as well as synthetic methodology development based on the foundation laid by our current results. For acutiphycin, our short-term goals include: first, a complete biological testing of the synthetic material including the determination of mode of action through collaborations; second, detailed conformational analyses using high-field NMR and computational methods; and third, preparation of four synthetic analogues: C6-methyl-acutiphycin **7.14** and **7.15** as well as C16-methyl-acutiphycin **7.22** and **7.23**. The biological evaluation of these analogs will probe the actual binding conformation responsible for the observed biological activity.

Meanwhile, for synthetic methodology development, we plan to further explore several synthetic creativities instilled by our exciting ether transfer reaction. First, we will continue our exploration in sulfonylpyran technology particularly for the stereoselective construction of spiroketal functionality. This spiroketal methodology will be applied to the total synthesis of complex polyketides, such as milbemycin  $\beta_3$  **7.24** and (+)-aigialospirol **7.25**. Additionally, we will investigate the utilization of  $\beta$ -ketoester and carboxylic acids for the quench reagents in the ether transfer reaction. We envision that



the corresponding ether transfer products can be further transformed to several structurally novel compounds such as 2,4,6-trisubstituted oxepane **7.68** and **7.69**, oxepanone **7.70**, and post-PKS modified-like polyketide subunits **7.71** and **7.72**.